ISIS 2001

ISIS Facility Annual Report 2000-2001

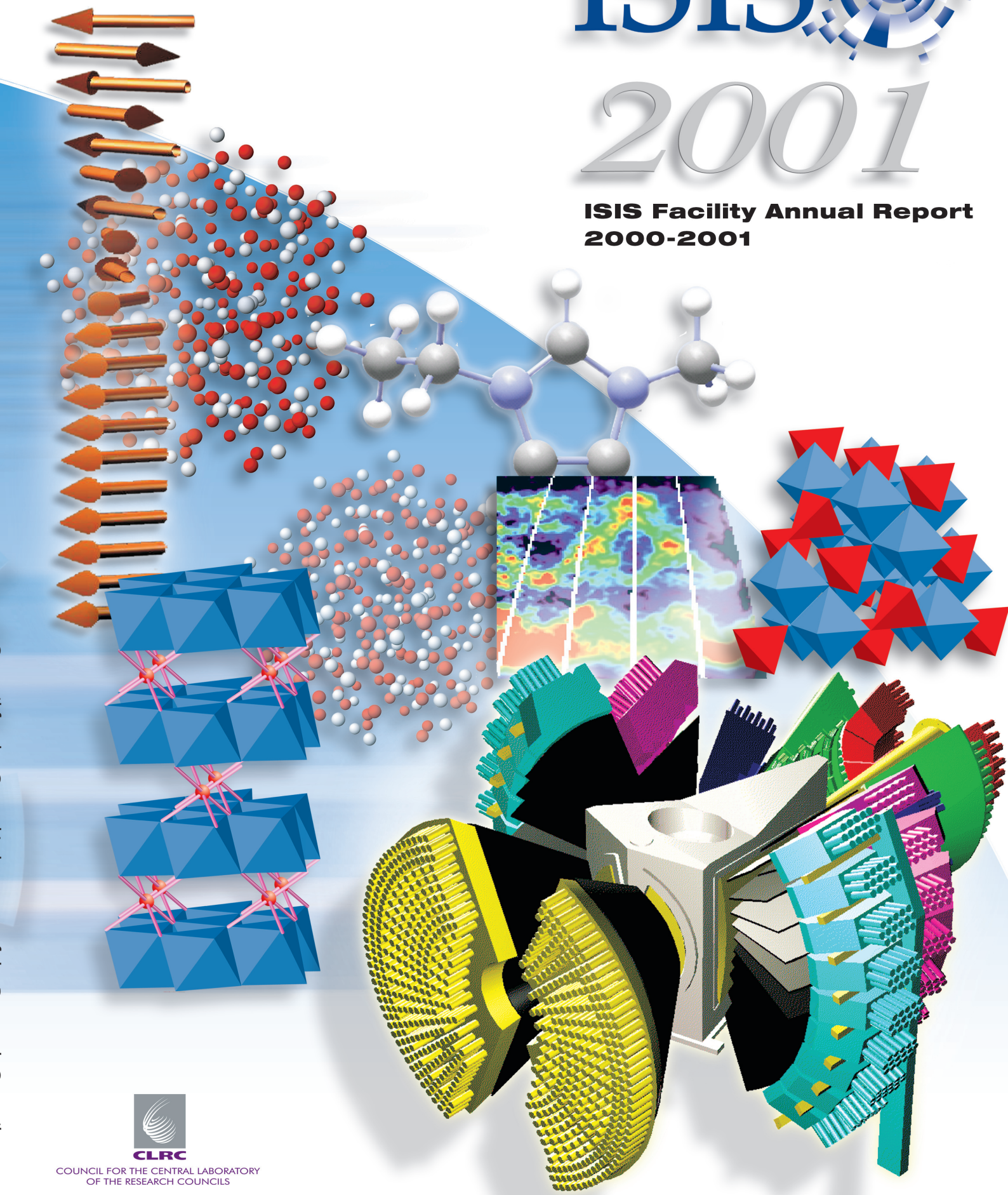

CLRC
COUNCIL FOR THE CENTRAL LABORATORY
OF THE RESEARCH COUNCILS

ISIS 2001

ISIS 2001 was prepared for the ISIS Facility, CLRC Rutherford Appleton Laboratory, Chilton, Oxfordshire, OX11 0QX, UK

ISIS Director, Dr Andrew Taylor (01235) 446681
User Office (01235) 445592
Fax: (01235) 445103
e-mail: isisuo@rl.ac.uk
Web: www.isis.rl.ac.uk

ISIS 2001 Production Team:
Philip King, Freddie Akeroyd, Roger Bennet, Rob Bewley, Mark Daymond, Nigel Diaper, Sam Foster, Vanessa Fox, Chris Frost, Spencer Howells, Bill Marshall.

Printed by CLRC Photographic and Reprographic Services and ESP, Swindon. Design and artwork by Ampersand Design Ltd, Abingdon.

September 2001

Contents

Highlights of ISIS Science (pages 18 - 71)

Top left: Lord Sainsbury, Minister for Science and Innovation (centre), learns about neutron diffraction under pressure from Richard Nelmse (ISIS/Edinburgh, right) during his tour of the Facility with John Wood, CCLRC Chief Executive (01RC3281). Top Right: Prof T Ogawa (Executive Director, RIKEN) signing a new ten-tear partnership agreement between CCLRC and RIKEN with Gordon Walker, acting CCLRC chief Executive. The RIKEN-RAL muon facility at ISIS is the first large-scale scientific partnership between the UK and Japan (00RC4375). Left: Brian Fender, Chairman of the Higher Education Funding Council, opens the OSIRIS spectrometer (00RC4460). Lower left: Chris Henshall and Frances Saunders (OST) touring ISIS with Jeff Penfold (ISIS) (01RC2611). Lower right: Gavin Williams (ISIS) describing the facility to Professor Hiroo Imura (Executive Member, Prime Minister's Council for Science and Technology, Japan) (00RC4353).

Foreword

In July we welcomed Lord Sainsbury, the Minister for Science and Innovation, to RAL and to ISIS. The timing of his visit could not have been more appropriate with the Diamond project gathering momentum and the decision about the ISIS Second Target Station expected in the autumn. Being successful in our bid to build a Second Target Station will enable us to make full use of the opportunities that will arise from a symbiotic relationship with Diamond: RAL is well placed to become a world centre for condensed matter research. Lord Sainsbury was fully cognisant of our achievements to date, and of the future potential of ISIS.

This annual report demonstrates once again that the ISIS science programme is world-class and, in many areas, world leading. This year saw MAPS joining the instrument suite and producing data of outstanding quality. GEM continues to impress all those fortunate enough to be awarded beamtime. Upgrades to SXD, HRPD, PRISMA, TOSCA and eVS have been completed and during the next twelve months ENGIN-X will be commissioned. At the same time, accelerator developments are progressing which will increasing the ISIS current to 300 μA. These developments expand the envelope of neutron scattering research and set the standards by which new sources in the US and Japan will be judged.

ISIS continues to go from strength to strength, thanks to the commitment of all our stakeholders – particularly our vigorous user community and our dedicated facility staff.

My thanks to all.

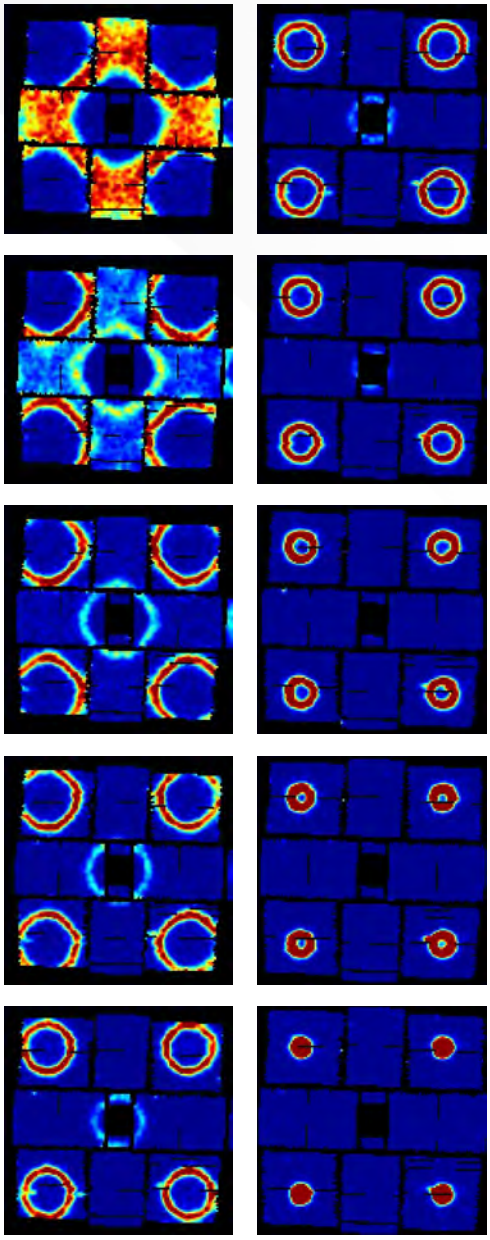

Spin Fluctuation in Rb_2MnF_4 measured on MAPS (R Cowley, Oxford).

Top left: EPSRC programme managers learnt about ISIS from Andrew Taylor in September (00RC4262). Top right: Congratulations from ISIS to Dame Julia Higgins FRS, FREng, who received her DBE honour in June. Julia is Professor of Polymer Science at Imperial College London, and has had a long association with ISIS and CCLRC (photo courtesy of James Hunkin). Left: Members of the Chinese Academy of Sciences learning about ISIS from Andrew Taylor (00RC3446). Lower left: Professor Teck-Seng Low and Professor Tow-Chong Chong (National University of Singapore and Data Storage Institute) touring ISIS with Sean Langridge (ISIS) (01RC2589). Lower right: The KARMENfest meeting celebrated 10 years of neutrino science at ISIS - delegates are pictured here (01RC3216).

1 Science at ISIS

ISIS is the world's most powerful pulsed spallation neutron source. The facility provides beams of neutrons and muons that enable scientists to probe the structure and dynamics of matter in areas encompassing Physics, Chemistry, Earth Science, Materials Science, Engineering and Biology. An overview of ISIS science is given here; specific highlights can be found in the next chapter, and reports describing the experiments performed in the last year can be found on the accompanying CD.

Introduction to ISIS

ISIS is the world's most intense pulsed neutron and muon source and the major facility at CLRC's Rutherford Appleton Laboratory. First neutrons were produced in 1984, and over the past seventeen years the facility has developed into a major international force in condensed matter research and attracted substantial international investment.

Why neutrons and muons?

The neutron is a powerful probe for the study of the microscopic structure and dynamics of condensed matter, having significant advantages over other forms of radiation. Detailed information obtained from neutron scattering has had a major impact on our understanding of the microscopic nature of materials, from magnetism and superconductivity to chemical surfaces and interfaces. Muons are an alternative probe of condensed matter, giving complementary information on structure and dynamics.

The ISIS experimental hall (99RC5752).

Neutron production

Neutrons are produced at ISIS by the spallation process. A heavy metal target is bombarded with pulses of highly energetic protons from a synchrotron accelerator, driving neutrons from the nuclei of the target atoms. This results in an extremely intense neutron pulse, delivered with only modest heat production in the neutron target. The neutrons produced have very high energies, and are slowed to speeds (wavelengths) useful for condensed matter research by an array of hydrogenous moderators around the target. They are then directed to some 20 neutron instruments, each optimised to explore different properties of the microscopic structure of materials.

Other radiation

ISIS also produces intense pulsed beams of muons, via the insertion of a thin graphite intermediate target into the extracted proton beam; these are fed to six experimental areas for condensed matter investigations and other muon physics studies. In addition, the KARMEN experiment has exploited the rich neutrino flux from the neutron target to investigate problems in fundamental Physics.

A user facility

ISIS is a User Facility, providing a fully supported instrument suite to enable visiting teams to exploit the neutron and muon techniques. Experiments carried out at ISIS typically complement work programmes performed at home laboratories. Researchers come from over 30 different countries, and include both academic and industrial scientists. Experiments are selected by a peer review process. In the last year, 634 user experiments were performed at the facility by some 1600 visiting researchers. ISIS also proves an excellent training ground for young researchers, with a large number of visiting scientists being aged 30 or under.

ISIS Instruments

MAPS
Single Crystal Excitations
Toby Perring, ext. 5428, T.G.Perring@rl.ac.uk

VESUVIO
Electron Volt Spectroscopy
Jerry Mayers, ext. 5882, J.Mayers@rl.ac.uk

SXD
Single Crystal Diffraction
Matthias Guttmann, ext. 6397,
m.j.guttmann@rl.ac.uk

KARMEN
Neutrino Facility
Peter Plischke, ext. 5738
peter@karm6.nd.rl.ac.uk

MARI
S(Q,ω) Vibrational
& Magnetic Spectroscopy
Steve Bennington, ext. 5193
S.M.Bennington@rl.ac.uk

GEM
General Purpose Diffraction,
Liquids and Amorphous Structures
Paolo Radaelli, ext. 5685
P.G.Radaelli@rl.ac.uk
Alex Hannon, ext. 5358
A.C.Hannon@rl.ac.uk

HRPD
High Resolution Powder Diffraction
Richard Ibberson, ext. 5871
R.M.Ibberson@rl.ac.uk

PEARL
Engineering & High Pressure Instrument
Mark Daymond & Bill Marshall, ext. 5414
M.R.Daymond@rl.ac.uk, W.G.Marshall@rl.ac.uk

DEVA
Muon Development Beam
James Lord, ext. 5674, J.S.Lord@rl.ac.uk

MuSR, EMU
Implanted Muon Spectroscopy
Stephen Cottrell, ext. 5352, S.P.Cottrell@rl.ac.uk
Adrian Hillier, ext. 6001, A.D.Hillier@rl.ac.uk
Francis Pratt, ext. 5135, F.L.Pratt@rl.ac.uk

Moderators

liquid hydrogen, 20K

liquid methane, 100K

water, 316K

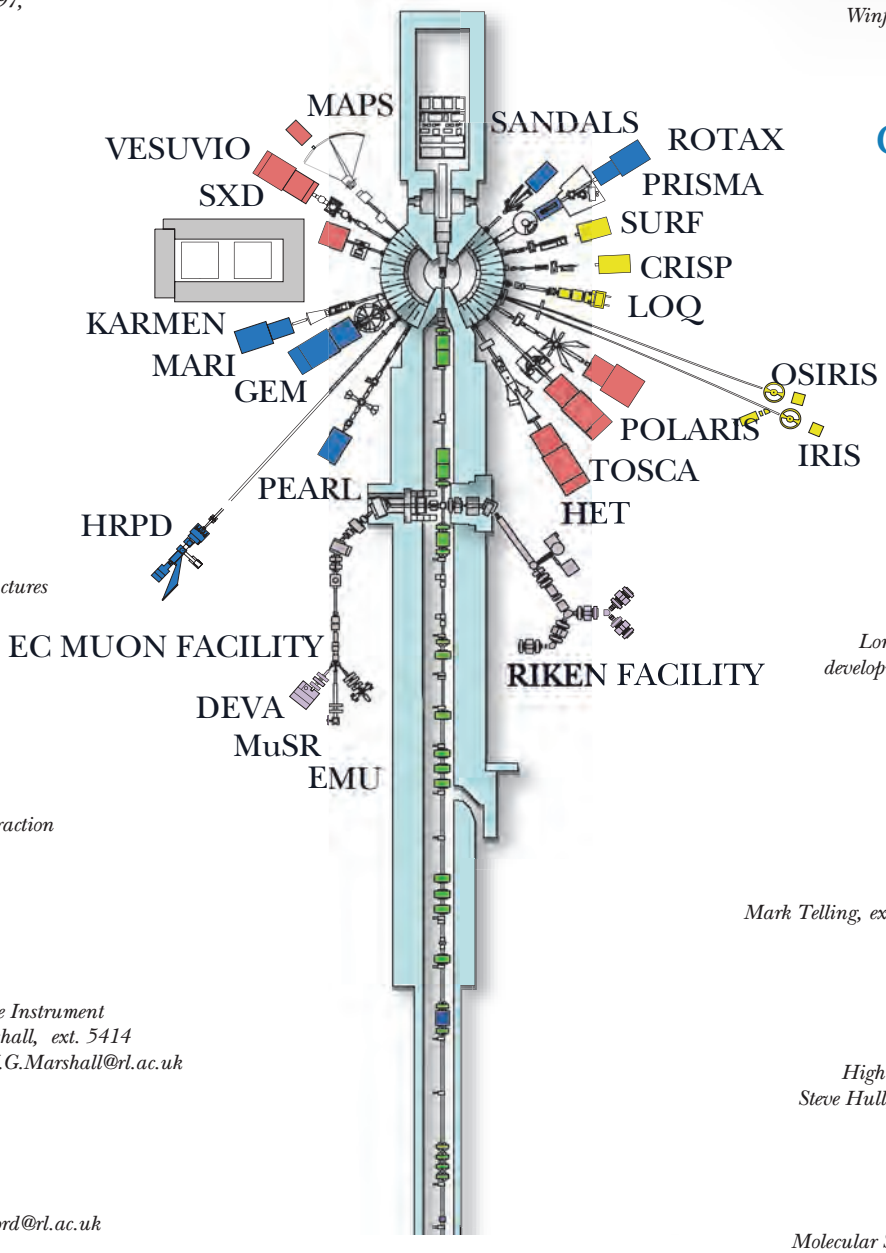

SANDALS
Small Angle Liquids & Amorphous Diffraction
Daniel Bowron, ext. 6397, D.T.Bowron@rl.ac.uk

PRISMA
Coherent Excitations & Critical Scattering
Martyn Bull, ext. 5805, M.Bull@rl.ac.uk

ROTAX
Multiple Purpose Diffractometer
Winfried Kockelmann, ext. 6731
W.Kockelmann@rl.ac.uk

CRISP, SURF
Neutron Reflectometry
Sean Langridge, ext. 5269
S.langridge@rl.ac.uk
John Webster, ext. 6381
J.R.P.Webster@rl.ac.uk

LOQ
Small Angle Scattering
Richard Heenan, ext. 6744
R.K.Heenan@rl.ac.uk

OSIRIS
Long wavelength diffractometer;
development of polarisation analysis
Ken Andersen, ext. 6731
K.H.Andersen@rl.ac.uk

IRIS
Low Energy Spectroscopy
Long d-spacing Diffraction
Mark Telling, ext. 5529, M.Telling@rl.ac.uk

POLARIS
High Intensity Powder Diffraction
Steve Hull, ext. 6628, S.Hull@rl.ac.uk

TOSCA
Molecular Spectroscopy & Crystal Fields
Stewart Parker, ext. 5797, S.F.Parker@rl.ac.uk

RIKEN
Surface & Decay Line Muon Facility
Katsu Ishida, ext. 6802, K.Ishida@rl.ac.uk

HET
Excitations at Low Momentum Transfer
Rob Bewley, ext. 5797, R.I.Bewley@rl.ac.uk

Crystallography

GEM
HRPD
POLARIS
SXD
HiPr/PEARL

The Crystallography instruments POLARIS, HRPD, GEM, SXD and HiPr/PEARL all operate busy user programmes straddling the areas of Chemistry, Materials and Physics, and offer a very diverse portfolio of structural science.

Contact:
Chick Wilson
c.c.wilson@rl.ac.uk
01235 445137

The high resolution powder diffractometer HRPD provides a powerful tool for studies of phase transitions, subtle structural effects and studies of low melting point molecular systems. Recently, this work has been combined with advanced computational methods with strong input into the interpretation of tunnelling measurements. The new detector capability at 90° has already shown its potential for enhancing the programme in magnetic diffraction, and will also benefit ongoing studies of other forms of complex materials such as loaded zeolites (pages 26-27)

The high intensity powder diffractometer POLARIS delivers vigorous programmes in solid state chemistry (see the highlight on page 24) and materials science. Recent trends include measurement of hydrogen-loaded metallic systems, brought about by their potential applications in producing environmentally-friendly fuels. Complex sample environment is also strongly emphasised, for example by work at high pressure and combined high p/high T. The potential for neutron diffraction studies of complex chemical reactions has been demonstrated through use of the chemical reaction and hydrothermal cells.

The strengths of the programme on SXD, the single crystal diffractometer, lie both in the study of molecular systems and in areas such as diffuse scattering, quasicrystals and incommensurate structures. The newly established single crystal high pressure programmes are developing well, including use of variable temperature and variable pressure methods in looking at systematic changes in organic structure (see page 20). The ideas of supramolecular chemistry, and the associated weak interactions, also feature strongly.

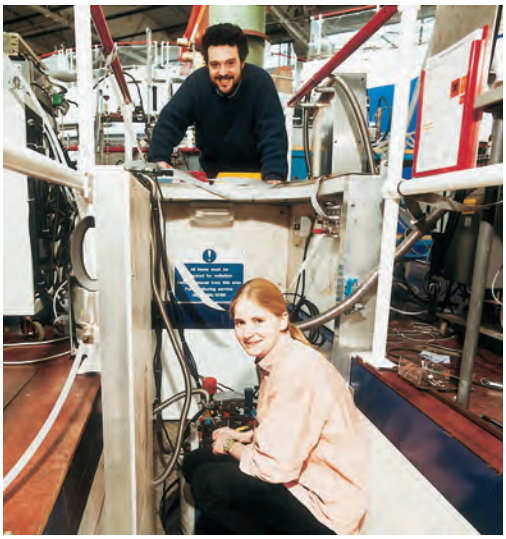

Paolo Radaelli (ISIS) and Wiebke Lohstroh (Oxford) using GEM for investigations of CeB_6(01RC1624).

The high pressure programme is principally carried out on the HiPr high pressure instrument on the PEARL beamline exploiting the Paris-Edinburgh cell, though with some ambient temperature work in this cell still carried out on POLARIS (see page 22). Highlight areas include studies of novel phases of small molecule systems and extensive work in mineralogy, with increasingly complex and low symmetry systems being opened up to study.

The general materials diffractometer GEM offers short counting times coupled with high resolution, making rapid scanning diffraction and studies of small samples routine. Its user programme is strong in a range of areas in materials science and solid state chemistry, along with studies of disordered materials. The area of total scattering (measuring and modelling Bragg and diffuse scattering together) is very well suited to the GEM set-up and work in this area is developing rapidly.

Disordered Materials

Disorder is present to a greater or lesser extent in all materials. For the disordered materials most often studied by this Group, however, long range crystalline order is absent. The example in Fig. 1.1 conveys many of the ideas of the work that encompasses the Group's work.

Neutrons are ideal for studying the disordered states of matter for a number of reasons. They are complementary to X-rays because they are scattered strongly by important light atoms, such as hydrogen, carbon, nitrogen and oxygen. In addition, in a number of cases it is possible to extract the individual site-site correlations from a diffraction pattern (see Fig. 1.1) by the technique of *isotope substitution.*

However there are many instances of liquids or other disordered materials where the appropriate isotopic contrast is not available, and the complementary X-ray experiment (such as EXAFS or anomalous dispersion) may not be possible. This is especially true of molecular systems, where a complete specification of the local structure will never be obtained by experiment. In these cases especially, it is imperative that the available diffraction data and other evidence (such as the molecular structure if this is known) are compared to a realistic model of the structure. In recent years there has been a great deal of effort within the Group to develop ways of achieving this structure refinement.

Water over a wide range of temperature and pressure, aqueous solutions and mixtures, and a range of non-aqueous liquids, have featured strongly in many recent investigations. Highlights include the first neutron diffraction experiment on liquid alumina, and very important work on the structure of high and low density amorphous ice, with its direct relevance to ongoing debate about the nature of the water phase diagram at low temperatures. SANDALS has been the main focus for most of this work. On GEM, the Disordered Materials programme has concentrated mostly on glasses and amorphous materials where the resolution required is higher than for liquids. This programme will receive a boost when the new low angle detectors, now funded, become available in the next year or so.

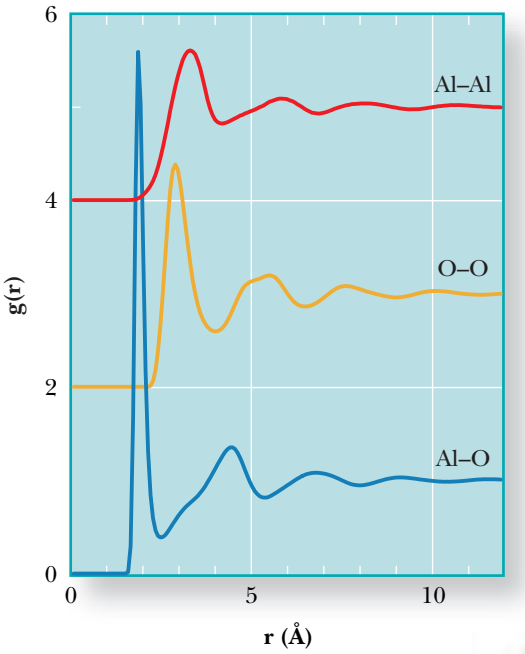

Fig. 1.1. Shown on the right is an apparently random array of white and red atoms (representing aluminium and oxygen respectively in molten alumina at ~2500 K). However on closer inspection we find that strong local *correlations exist. This is seem on the plot above, where the positions of the atoms are correlated. Aluminium atoms associate preferentially with oxygen atoms, whereas the O-O and Al-Al correlations occur at greater distances, in spite of the much smaller ionic size of Al compared to O. In all cases the oscillations are damped at larger distances, showing that the correlations can only be short or medium ranged.*

GEM SANDALS

The ISIS Disordered Materials Group provides neutron scattering facilities for characterising the atomic scale structure of fluids, liquids, glasses, and amorphous materials. In addition it supports an extensive suite of data analysis programs and is developing novel techniques for the interpretation of neutron scattering data from disordered systems in terms of three-dimensional atomic models.

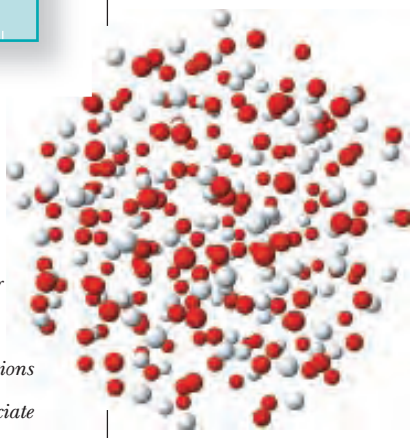

Contact:
Alan Soper
a.soper@rl.ac.uk
01235 445543

Large Scale Structures

LOQ
SURF
CRISP

Small Angle Neutron Scattering, SANS, (LOQ) and Neutron Reflectometry (SURF, CRISP) are key techniques for the study of the microscopic structure of important and technologically relevant systems in Soft Matter, Advanced Materials and Bio-molecular Science. SANS probes meso-scale structures, in the size range 20 to 1000 Å. Specular reflectivity provides structural information orthogonal to surfaces or interfaces on a length scale of 10 to 4000 Å, and off-specular scattering probes in-plane structural correlations on a length scale of microns.

Contact:
Jeff Penfold
j.penfold@rl.ac.uk
01235 445681

Small Angle Neutron Scattering

Binary mixtures of long n-alkanes co-crystallise even when the chain lengths differ by up to 100 CH_2 groups. The solid solutions form two different phases – the semi-crystalline form (SCF) at high temperatures and the triple layer super-lattice at low temperatures – and structural models have been proposed on the basis of SAXS data. Ungar and Spells have studied mixtures of the hydrogenous n-alkanes, $C_{162}H_{326}$ and the longer, partially-deuterated n-alkane, $C_{12}D_{25}C_{192}H_{384}C_{12}D_{25}$. They find structural models consistent with those proposed from X-ray data, with the high temperature SCF phase being made up of alternating crystalline and amorphous layers. Subtle differences between the SANS and small angle X-ray scattering (SAXS) data (Fig. 1.2) are associated with the uneven distribution of deuterated chain ends within the amorphous layer, and enable quantification of the overcrowding effect and dissipation of order at the crystalline–amorphous interface in polyethylene.

Understanding surfactant mixing in micelles and at interfaces is important in the context of their domestic and technological applications. The surfactant composition can have a profound effect on micelle structure; this was well illustrated in the recent work by Penfold et al from SANS data on the binary anionic/nonionic surfactant mixture of sodium dodecyl sulphate (SDS) and hexaethylene glycol monododecyl ether ($C_{12}E_6$). Their results show that the micelle aggregation number has a pronounced maximum at a solution composition rich in $C_{12}E_6$. At these concentrations $C_{12}E_6$ forms small spheroidal

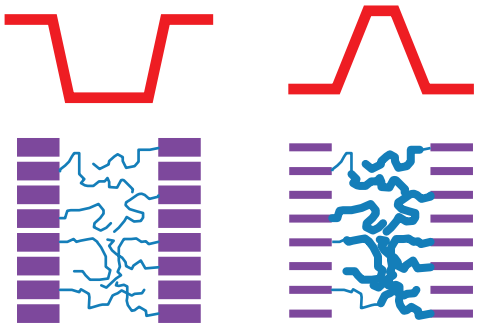

Fig. 1.2 SANS (A) and SAXS (B) profiles, showing SCF phase structure for $C_{162}H_{326}$ and a partially deuterated n-alkane.

micelles. The addition of small amounts of SDS relaxes the steric constraints of bulky E_6 headgroup of the nonionic surfactant, resulting in micellar growth. Eventually as sufficient SDS is added the electrostatic contribution to the free energy of micellisation is more dominant, and small micelles are again energetically favourable. The addition of hexadecane, solubilised into the pallisade layer for micelles rich in $C_{12}E_6$, perturbs the delicate balance between the steric and the electrostatic contributions to the free energy of micellisation, resulting in suppression of the micelle growth regime for micelles rich in $C_{12}E_6$ seen in the absence of hexadecane.

Neutron Reflectometry

The factors affecting the extent to which a protein may change its structure in solution or at an interface, through protein-protein and protein-surface interactions, are of much current interest, because of the role of unfolding in fibril-related diseases, fouling and bio-compatibility. Holt and White used neutron reflectometry to show for the first time thermally-induced denaturation of proteins in the first 100 Å of the air-solution

interface for lysozyme and β-lactoglobulin. The data (see Fig. 1.3) for the globular protein hen egg white lysozyme show a dramatic increase in thickness in the temperature range 25 to 70 °C. This change is related to the unfolding of the protein at the interface and the subsequent penetration of solvent into the protein layer, reducing the protein fraction.

Wetting phenomena are of crucial importance in a range of applications, including paints, coatings, lubricants, detergents and cosmetics. Zarbakhsh and Webster have used reflectivity to investigate a model system, an n-alkane on silicon. Surface Force Apparatus measurements have shown a transition in the structure of adsorbed n-C_{16} films a few degrees above their melting temperature. Zarbakhsh et al have measured the thickness of an n-C_{16} adsorbed film on both hydrophilic and hydrophobic surfaces. For the latter, the transition in alkane film thickness occurs at a slightly lower temperature on cooling than on heating, suggesting a first-order phase transition.

The interfacial width between two immiscible polymers is not atomically sharp. Measured interfacial widths (by neutron reflection) are larger than calculations would suggest due to a contribution from capillary waves. For thin films the capillary wave contribution has a logarithmic dependence derived from dispersion forces acting across the film. These forces either stabilise the interface against capillary wave fluctuations, or lead to capillary wave amplification and spinodal de-wetting, depending on the sign of the Hamaker constant. Bucknall and Sferrazza have measured the interfacial width between two immiscible polymers (deuterated polystyrene (dPS) and high density polyethylene (HDPE)) subject to mechanical confinement. The measured interfacial roughness is ~15 Å for thicker films and ~11 Å for thin films, larger than numerical predictions. In contrast to the prediction that the long-ranged van der Waals forces would destabilise this system, it is stable within the time-scale of the measurements. This suggests that mechanical confinement suppresses the de-wetting process.

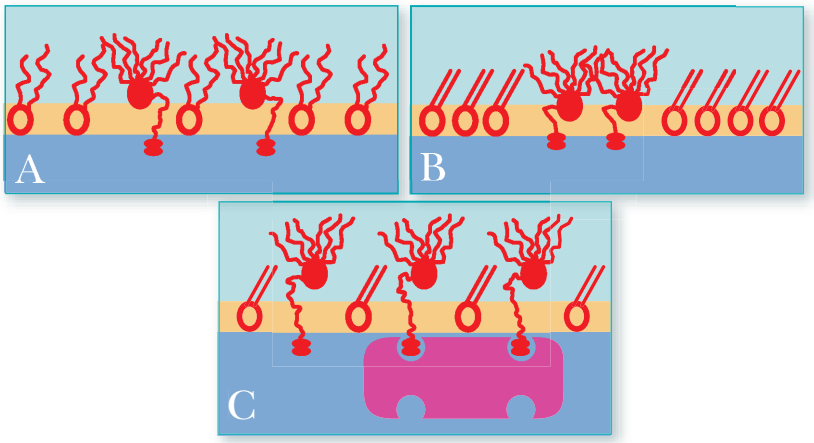

Fig.1.4. Model of the BF / DPPC monolayer. (A) LE phase showing a homogeneous distribution in the monolayer, (B) LC phase showing BF aggregation, and biotin anchor partially retracted into the lipid headgroup region, and (C) coupling of streptavidin to the biotin anchor.

Bayerl et al have used a combination of techniques to demonstrate how lateral pressure can be used to control receptor binding to a ligand-containing monolayer. Streptavidin was shown to bind to biotinylated amphiphilic fullerenes (BF) and dipalmitoylphosphatidyl choline (DPPC) mixed monolayers at low pressures (see Fig. 1.4). Upon compression, the BF aggregates and is partially squeezed out of the layer. The biotin anchor is retracted into the lipid headgroup region, and streptavidin binding is inhibited. Streptavidin coupled to the monolayer remains bound during compression, and prevents the biotin anchor retraction.

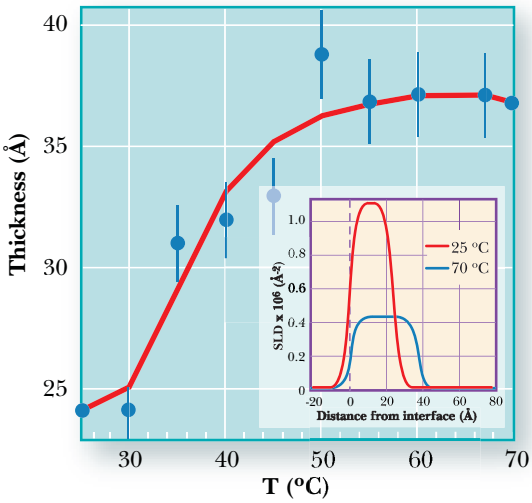

Fig.1.3. Variation of lysozyme film thickness with temperature at the air-water interface. Inset shows scattering length density distributions of the protein at 25 and 70 °C.

Excitations

MAPS
HET
MARI
PRISMA
ROTAX
ALF

The Excitations Group operates the three chopper spectrometers, HET, MARI and MAPS, the single crystal spectrometer PRISMA, the diffractometer ROTAX and the single crystal alignment facility ALF. The scientific programme of the group spans a wide range of disciplines from the investigation of model magnetic systems to the dynamics of disordered materials and quantum fluids.

Contact:
Steve Bennington
s.m.bennington@rl.ac.uk
01235 445193

The first full year of MAPS operation has brought outstanding results from experiments on a range of systems including high temperature superconductors, low dimensional magnets and CMR materials. Most of the experiments have focused on magnetic excitations, but studies of lattice dynamics have also been highly successful. A review of some of the highlights from the MAPS scientific programme is presented starting on page 48.

The programme on HET has developed as a consequence of the reduction in the proportion of experiments on single crystals. Experiments on GMR materials and Heavy Fermion systems under pressure have been successful. Small changes in the energy of crystal field excitations in $TbCu_2$ were measured at pressures of up to 25 Kbar. Another interesting addition to the programme has been the study of biological systems. Both bones and fish proteins have been studied successfully, and such experiments may represent the start of an ongoing programme.

The wide angular coverage, excellent resolution and good flux on MARI make it an ideal tool for experiments in a wide range of fields. The last year has seen the continuation and development of programmes on quantum fluids, vibrational density-of-states measurements and low-dimensional magnetism. A significant fraction of the work focuses on the dynamics of disordered materials, with the aim of understanding the universal properties of glasses at the microscopic level (page 46).

The upgrade to PRISMA (see page 74 for more details) has delivered a flux increase of up to a factor of ten and greater flexibility for conditioning the incident beam. As a consequence, experiments under difficult sample environment conditions have benefited greatly. Measurements on magnetic structures in Erbium under pressure, in non-fermi liquid systems under pressure and at very low temperatures, and studies of frustrated magnetic systems at mK temperatures and in a magnetic field have all been very successful. The spectroscopy programme has included measurements of low dimensional systems and high T_c materials.

The flux available on ROTAX has been enhanced by a factor of two due to the PRISMA guide. The sharp pulse shape from the methane moderator and the high flux of long-wavelength neutrons make ROTAX ideal for magnetic diffraction, but it also has an active programme looking at the provenance of archaeological specimens.

The crystal alignment facility, ALF, is now being upgraded, with the installation of position sensitive detectors, a new goniometer and more user-friendly control software.

Funding has been sought to construct a new spectrometer, MERLIN, which will offer high flux at medium resolution. Merlin's design specification can be found on page 77.

Tom Fenneu (UCL/RI)analysing his $Dy_2Yi_2O_7$ data from PRISMA (01RC1617).

Molecular Spectroscopy

The scientific backbone on IRIS remains predominantly that of quasi-elastic neutron scattering from 'soft' matter, namely polymeric and biological systems. However, there also continues a growing interest in low energy magnetic excitations. Such studies have been greatly enhanced by the improved background on the instrument, a consequence of the pyrolytic graphite analyser upgrade project. In addition, accurate alignment of single crystal magnetic material has been aided by the investment in a high precision rotation stage, designed for use with the dilution refrigerator.

The science on TOSCA continues to span many areas, but catalysis has been a major theme. This year has seen work on hydrogen adsorption and spillover on fuel cell catalysts, the observation of an intermediate in the synthesis of methyl chloride, as well as studies of the effect of different templates on zeolite formation. Hydrogen-bonded systems are another area of active study: from water-splitting protein photosystem II (where the interest is in how the water is accommodated in the protein) to co-crystals where the hydrogen bonding defines the structure. Such studies are essential in order to be able to exploit crystal engineering more effectively.

With a view to supporting the work of TOSCA across the board, a new analysis programme has been written, a-CLIMAX. This takes ab initio output and generates the TOSCA spectrum of a molecule selected as a model compound (see: http://www.isis.rl.ac.uk/molecularSpectroscopy/aclimax/) in order to aid identification of the central structural elements of the systems under study.

VESUVIO measures single atom momentum distributions in condensed matter systems by scattering neutrons of sufficiently high energies that the impulse approximation can be used to interpret data - neutron Compton scattering. The scientific program on VESUVIO this year has included the first experimental determination of single-particle mean kinetic energies in the solid, bcc and hcp phases of ^{3}He (page 60). The results were in excellent agreement with recent diffusion Monte Carlo simulations.

Also important was the first reconstruction of the proton momentum distribution n(**p**) in the hydrogen bonded KDP system, both above and below the ferroelectric transition (Fig. 1.5). The high temperature n(**p**) suggests a spatial wavefunction that is coherent over two sites owing to quantum tunneling. The experiments are certainly sensitive enough to see the effect of the surrounding ions on the hydrogen bond, and include many body effects that are difficult to calculate with existing methods.

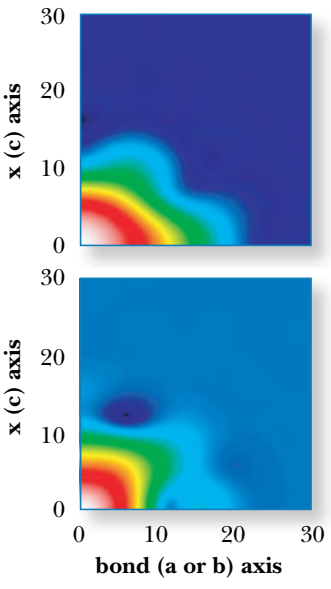

Fig. 1.5. The momentum distribution in the ac plane of KDP for a single hydrogen bond below (T= 90 K, top) and just above (T= 130 K) the ferroelectric transition at T= 124 K. The overall narrowing of the distribution in the T= 130 K data shows that the transition involves a large scale change in the distance along the bond axis over which the proton motion is coherent.

IRIS
OSIRIS
TOSCA
VESUVIO

The Molecular Sciences Group hosts experiments across the board from biology to quantum fluids, via many aspects of chemistry. The group operates four spectrometers: IRIS and OSIRIS, addressing diffusional problems and long characteristic times with very high-energy resolution; TOSCA, addressing vibrational problems and short characteristic times with good energy resolution; and VESUVIO, addressing Compton scattering studies and very short characteristic times with modest energy resolution.

Contact:
John Tomkinson
j.tomkinson@rl.ac.uk
01235 446686

Muons

EMU
MuSR
DEVA
RIKEN

The µSR instruments MuSR, EMU, ARGUS and DEVA run a very diverse science programme, using implanted positive muons both as magnetic probes, in magnetism and superconductivity, and as proton analogues in chemical physics, including molecular dynamics, charge transport in conducting polymers, hydrogen behaviour in semiconductors and light particle diffusion. Muon catalysed fusion studies and fundamental muon physics investigations are also carried out at the RIKEN-RAL muon facility.

Contact:
Philip King
p.j.c.king@rl.ac.uk
01235 446117

In magnetism, muon spin rotation is sensitive to weak moments and to ordering which is short range, or of spin-glass character, as well as to long-range ferro- or antiferromagnetism. Muon spin relaxation is sensitive to relatively slow correlations and fluctuations. In both these respects, muon studies ideally complement neutron scattering. Examples this year have included characterisation of fluctuations in low dimensional and frustrated magnetic structures, investigation of giant and colossal magnetoresistive, magnetostrictive and magnetocaloric materials, mesoscale magnetic systems, high spin molecules and superparamagnetic clusters.

In superconductivity, muon studies have continued to probe the interplay with magnetism as well as to characterise the flux line lattices of the vortex state, in systems including cuprates, intercalated fulleride materials, heavy fermions, the novel superconductor MgB_2 and, in the low critical current superconductor PbIn, a flowing flux line lattice in the presence of a transport current.

Muons mimicking the chemical behaviour of protons have been used in studies of ionic conductors and battery materials, and investigation of hydrogen spillover on heterogeneous catalysts. Spin labelling of molecules by muonium has enabled studies of guest molecule reorientation in zeolite voids.

Particularly fruitful this year has been the modelling of hydrogen defect centres, using their muonium counterpart, in wide band-gap semiconductors. Particularly significant was the confirmation of a predicted shallow donor hydrogen state in ZnO. Similar shallow states have now been identified also in CdS, CdSe and CdTe. With hydrogen a significant impurity in all these compounds – materials which are on the verge of important blue-light and UV optoelectronic applications – these ISIS experiments are providing an invaluable guide to its behaviour and electrical activity.

Muon catalysed fusion (µCF) results from the RIKEN-RAL facility over the past year have included the discovery of anomalous temperature-dependent phenomena in solid D-T mixtures; the first observation of D_2 molecule ortho-para dependence in (ddµ) molecular formation; and the discovery of an anomalous fusion neutron energy spectrum in (ttµ) fusion. Condensed matter research highlights from the RIKEN ARGUS spectrometer include the discovery of magnetic stripe structure in the LaSrCuO high T_c superconductor with a hole-concentration of 0.21; the first real-time observation of microscopic magnetic structure change associated with recovery of remnant magnetism in the cluster spin-glass $FeMnTiO_4$; and the observation of electron transport along base-pairs in DNA. In addition, technical developments have included the generation of ultra-slow μ^+ by laser ionization of thermal muonium and the production of muonic atoms with implanted He ions via muon transfer in solid H_2/D_2 thin layers.

Slava Storchak and Dmitri Eschenko condensing noble gases on EMU for muon investigations (01RC2687).

Engineering

The Engineering team at ISIS has continued to deliver a successful and heavily oversubscribed programme, whilst simultaneously preparing for the installation of the new Engin-X beamline (see page 75).

Experiments over the last year have broadly fallen into two categories: investigations into manufacturing or fabrication processes, often carried out by academic groups in collaboration with industrial partners; and a number of fundamental materials properties studies. The former category has included investigations into novel welding techniques and studies of fabrication stresses in a range of samples from complex aerospace engine parts to steel wires. *In situ* loading experiments have been conducted on a wide range of materials including ferroelectrics, shape memory alloys and metal-metal composites. The growing interactions with the geological community have also proved highly successful (see Highlight article on page 18).

This year has also seen the final stages of a successful research collaboration to produce and use a two dimensional pixellated detector making use of the transmitted neutron beam (see Highlight article on page 66).

The final measurements at ISIS within the Versailles Project on Advanced Materials and Standards (VAMAS) Technical Working Area 20 were conducted this year. VAMAS TWA-20 constitutes an international group of academic and facility experts who have been working to define an international standard for strain measurement using neutrons, in order to ensure compatibility and uniformity in achievable results across laboratories. A putative standard has been submitted to the International Standards Organisation for publication. This publication will serve to strengthen the interest and confidence of industry in the technique, just as improved data acquisition rates will be provided by the Engin-X instrument.

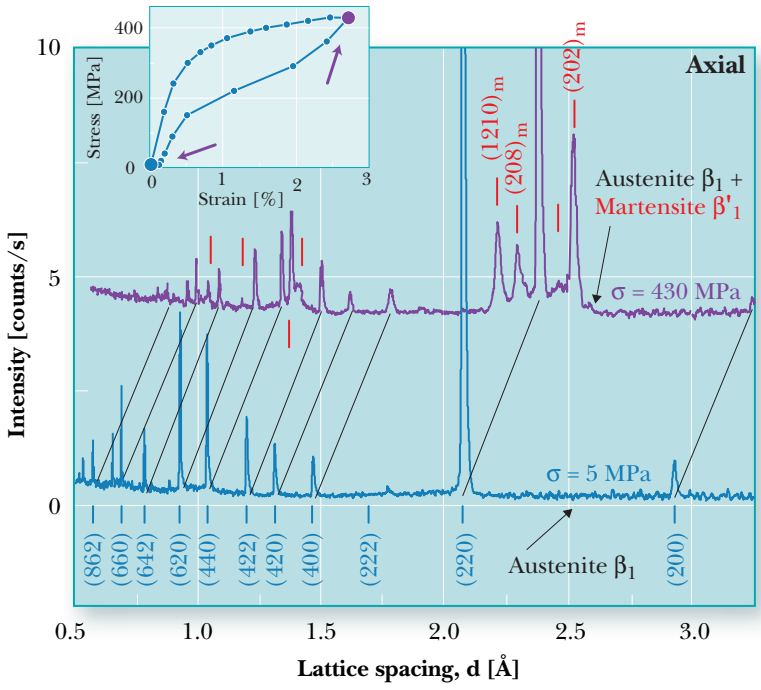

Fig. 1.6. Neutron diffraction spectra from a CuAlZnMn shape memory alloy polycrystal recorded in situ during a pseudoelastic tensile test (inset), parallel to the stress axis. The original cubic austenite reflections shift and new reflections corresponding to stress-induced monoclinic martensite appear at elevated stresses. The martensite has a strong texture due to lattice correlation between austenite and martensite phases, and selective transformation (P. Šittner et al).

ENGIN

The engineering program at ISIS is at present based around the ENGIN instrument, utilising approximately half the available time on the PEARL beamline. Bragg diffraction measurements yield information on the distortion of the atomic lattice, typically as a function of position, or applied thermal and/or mechanical loads. This information is used to shed light on deformation mechanisms, processing and manufacturing routes and failure mechanisms in real components and test samples.

Contact:
Mark Daymond
m.r.daymond@rl.ac.uk
01235 445414

Data Analysis

The Data Analysis and Visualisation Group develops algorithms and software in a number of areas that impact upon science performed at ISIS, especially in the area of powder diffraction.

The ISIX project, which aims to produce an object oriented Rietveld analysis package for neutron and X-ray diffraction data, has resumed after a year long interruption. Base classes for fundamental symmetry operations are in place, and simulated patterns may now be generated for TOF neutron diffraction data. Meanwhile, existing CCSL based refinement programs continue to be supported. Recent developments include PC versions of refinement programs, a program for determining extinction symbols directly from Pawley fitted diffraction profiles and a robust algorithm for background fitting.

The DASH project, performed in collaboration with the Cambridge Crystallographic Data Centre, has yielded a commercial software product for crystal structure solution of organic materials from powder diffraction data. Whilst the commercial version is targeted at X-ray diffraction, the underlying methodology and code has been used successfully to solve numerous structures from neutron diffraction data (Fig. 1.7). Ongoing development plans include closely linking DASH to the Cambridge Structural Database and the development of more efficient global optimisation algorithms. Full details of DASH and how to obtain it are available at http://www.ccdc.cam.ac.uk/prods/dash.

With data analysis and visualisation increasingly being performed on personal computers running the ubiquitous Windows operating system, porting of the many existing programs developed on VMS/UNIX workstations onto this platform is an important goal. The development of a 'Winteracter' driver for the widely used PGPLOT graphics library now provides a straightforward route for this particular aspect of porting.

Amongst other developments has been the maximum entropy Fourier implementation of recent ideas on Bayesian phase extension. The computer code has now been tested more fully, with a related enhancement in the user-friendliness of the program. Work on improving the visualisation and basic data analysis tools for SXD has also been undertaken, and has already demonstrated significant gains.

The group is also acting as the focus for E-science projects within ISIS. Work on a CLRC 'Data Portal' has so far utilised mainly ISIS data, and the project is set to move forward as a collaboration between ISIS and the E-science centre, ensuring that ISIS is in a strong position to exploit recent developments in GRID based technology.

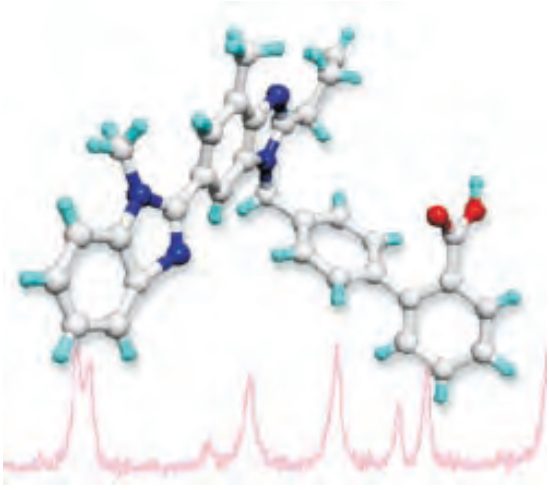

Fig. 1.7: The molecular conformation of a polymorph of the angiotensin II receptor antagonist telmisartan, as determined directly from powder diffraction data using DASH.

Contact:
Kenneth Shankland
k.shankland@rl.ac.uk
01235 446381

Condensed Matter Theory

The Theory Division support experimental work using neutrons, muons and X-rays, developing models to explain experimental results and propose new experimental work.

Experimental data on magnetically ordered V_2O_3 obtained by neutron and X-ray diffraction have been combined to infer the orbital magnetization of a V ion. This material is regarded as an archetypal Mott-Hubbard insulator; above about 160 K, V_2O_3 assumes the corundum structure and it is both metallic and paramagnetic, and below this temperature the material is monoclinic, insulating and a collinear antiferromagnet.

It has been shown that the structure factor for resonant X-ray Bragg diffraction contains a new type of selection rule that acts to limit contributions from electric-dipole events, and the selection rule stems from the established chemical and magnetic structure. On the strength of this finding, and complete success in an interpretation of azimuthal-angle scans executed at several Bragg reflections, it is possible to infer the V ion orbital magnetization displayed in Fig. 1.8. The orbital and quantities derived from it provide tests to be met by ab initio theories of magnetically ordered V_2O_3.

The effect of spin exchange has been studied between electrons bound in defect states in semiconductors and colliding conduction electrons. A new formulation of this problem, expressing the indistinguishability of the localised and delocalised electrons, is being developed leading to numerical simulations of the observable effects of spin-flip encounters, notably a generalised Korringa relation between spin relaxation and the modification of Larmor precession frequency. The new approach will be tested on experimental data on muon depolarization and frequency shift, for muonium centres in silicon at high temperature.

Aiming at an accurate density-functional theoretical description of molecular dynamics under strong laser illumination, two variational approaches have been developed based on the stationary-action principle: first, a mean-field treatment of the electron-nuclear interaction and, secondly, an explicitly correlated ansatz for the molecular wavefunction. The two methods have been tested on a simplified, non-trivial one-dimensional model of H_2^+, which can be solved exactly. The correlated approach significantly improved the mean field result, describing the correct qualitative picture even for lasers strong enough to lead to substantial photo-dissociation.

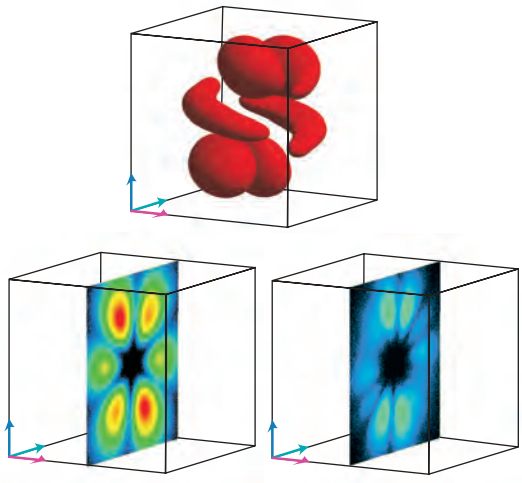

Fig. 1.8. Top: the orbital magnetic moment is contained in the plane spanned by the blue and green axes and it is inclined at an angle ~ 70° from the blue axis. The orbital is inferred from X-ray diffraction data enhanced by the V ion K-shell resonance (Paolasini et al.); the X-ray scattering is by V orbital magnetic moments whereas neutron diffraction is by the V magnetic moments, $\underline{L} + 2\underline{S}$. Lower left: an equivalent colour-contour slice through the 3-dimensional density; lower right: the corresponding one-sigma uncertainties displayed on the same scale.

Contact:
Stephen Lovesey
s.lovesey@rl.ac.uk
01235 446359

KARMEN

ISIS provides the world's most intense pulsed source of low energy neutrinos from the decays of pions and muons produced by the 800 MeV proton beam in the spallation target. The KARMEN (KARlsruhe Rutherford Medium ENergy) experiment has exploited the unique features of the neutrino source to investigate the interaction between neutrinos and nuclei and to search for neutrino oscillations.

The topics investigated by KARMEN over the past 10 years are closely related to particle astrophysics. The neutrino-nuclei investigations reveal insights into the dynamics of supernovae, whereas the search for neutrino oscillations can answer the question of whether neutrinos have mass and if they contribute to Dark Matter.

The ISIS neutrino source distinguishes itself by the purity of neutrino flavours and by the precisely defined expectations of the neutrino beam in time and energy. The KARMEN detector is a 56 ton liquid scintillation calorimeter located 17.7 m from the beam stop in a massive 7000 ton iron blockhouse which provides, in combination with three layers of anti-counters, shielding against the spallation neutron background and suppression of cosmic-induced background.

The neutrinos produced at ISIS are very similar in their energy distribution to those expected from a supernova. The measured neutrino cross sections in the laboratory are thus extremely helpful in making reliable estimates of the frequency of elements generated by neutrinos in stars. KARMEN has measured the charged current interactions of electron neutrinos on ^{12}C,^{13}C,^{13}N and ^{56}Fe with an accuracy of a few percent. Furthermore, neutrino-induced neutral currents on ^{12}C were observed for the first time (Fig. 1.9), a reaction which can help to detect directly all types of neutrino flavours emitted during a supernova.

Of special interest are the KARMEN results in the search of neutrino oscillations for muon anti-neutrinos to electron anti-neutrinos. As electron anti-neutrinos are not produced by the ISIS source, their appearance would be evidence for neutrino oscillations and thus evidence for neutrino mass. In 1995 the LSND experiment at Los Alamos (USA) claimed evidence for such oscillations. KARMEN has been able to test this finding, and the results are unequivocal: there are no hints of an oscillation signal in the KARMEN data. KARMEN sets the most stringent upper limit for the probability of muon antineutrino to electron antineutrino oscillations with $P<0.65\times10^{-3}$, in contradiction to the claimed neutrino oscillation probability of $P=(2.2\pm0.67)\times10^{-3}$ by LSND.

The KARMEN experiment has been based at ISIS from the facility's start, and has seen during its life 18579 Coulombs of protons on target, or 5.3×10^{21} produced neutrinos. As KARMEN has successfully completed its scientific programme the data capture was ended in March 2001 and the dismantling of the detector has begun. The experiment and neutrino physics have considerably benefited not only from the unique physical characteristics of the ISIS neutrino source but also from its performance and reliability.

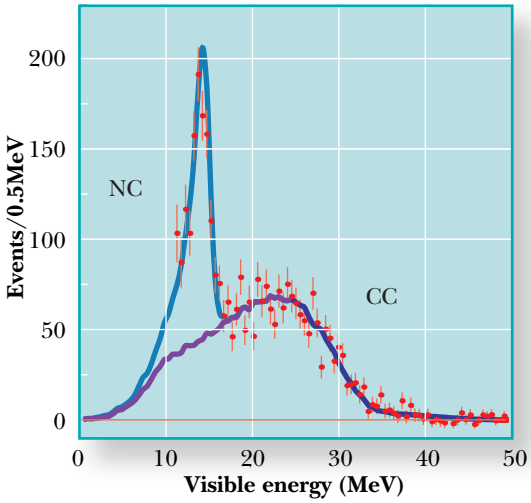

Fig. 1.9. KARMEN measured over 3300 neutrino-nucleus interactions. The peak excess at 15 MeV energy is due to the neutral current excitation $^{12}C(\nu,\nu')^{12}C$ (15.1 MeV).

ISIS Scheduling Panel Meeting, June 2000

The quality and timeliness of the science to be performed at ISIS is assessed by the 70 international scientists who form the 7 ISIS Scheduling Panels. These panels meet twice per year to review all the proposals that have been submitted and to allocate beamtime. Full details of the panels can be found on page 86. Shown here are photos from the June 2000 panel dinner.

Above: Roberto De Renzi (Parma), Pierre Dalmas de Réotier (CEA Grenoble), Pietro Carretta (Pavia) and Kosmos Prassides (Sussex) (00RC2969). Below: Bjorn Winkler (Kiel) and Amparo Navarro (University of Jean, Spain) (00RC2961).

Above: John Tomkinson (ISIS) and Bob Delapane (Uppsala) (00RC2960). Middle: Bill Clegg (Newcastle) and Andrew Taylor (ISIS) (00RC2962). Below: Mike Johnson (ISIS), Deborah Jones (Montpellier), Winfried Petry (Munich) and Uschi Steigenberger (ISIS) (00RC2967).

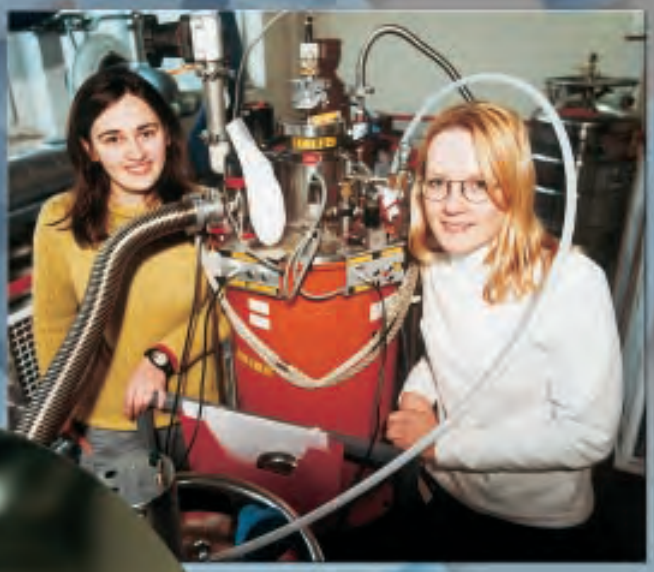

Above: Henry Glyde (University of Delaware) and Reinhard Scherm (Braunschweig) studying quantum liquids on Mari (01RC1455). Below: Steve Cottrell (ISIS) and Adrian Hillier (now ISIS, formerly ILL) preparing the MuSR orange cryostat (01RC1448).

Above: Anna Lashtabeg and Angela Kruth (St Andrews) working on a HRPD experiment (01RC1542). Middle: Joao Cabral examining a polybutadiene blend to be studied on LOQ (01RC1561). Below: Ilias Michalarias (UMIST) operating the gas handling panel on TOSCA whilst studying anti-freeze proteins (01RC1557).

The partitioning of strain during rock deformation

Deformation at the Earth's surface, such as occurs during major earthquakes, is ultimately driven by solid-state convection within the Earth's mantle. A detailed understanding requires knowledge of the structure of the Earth's interior and the way in which mantle rocks deform. Our knowledge of deformation derives largely from measurements of the seismic (elastic) properties of geological materials. These properties are affected by grain-scale variations in composition and microstructure influences; experiments on ENGIN are exploring this, providing unique information on deformation accommodation within rocks with a wide range of compositions and microstructures.

I C Stretton *(Bayerisches Geoinstitut),* ***S J Covey-Crump*** *(University of Manchester),* ***P F Schofield*** *(Natural History Museum),* ***M R Daymond***, ***K S Knight*** *(ISIS)*

The rocks that make up the Earth's crust and mantle (Fig H1.1) generally comprise two or more minerals, each with different mechanical properties. During the deformation of such materials, the different minerals experience different strains. The key to understanding what controls the resulting whole rock mechanical properties is to measure the extent of this strain partitioning and how it varies with rock composition and microstructure. In normal deformation experiments, such information is not obtainable because only whole rock properties can be measured and not the contribution that each mineral phase makes to those properties. However, the penetrating power of neutrons circumvents this problem. By conducting the deformation experiment in the neutron beam, the change in the crystal lattice dimensions of the component minerals may be monitored as a function of applied load, and from this information it is straightforward to calculate the average elastic deformation experienced by each individual mineral as a function of load.

On the ENGIN beamline, entire diffraction patterns are collected simultaneously by two fixed-angle detector banks located, one on either side of the specimen, at 90° to the incident beam. With the sample oriented at 45° to the beam, one of the detector banks only detects neutrons with scattering vectors from lattice planes oriented parallel to the loading direction, and the detects other only neutrons with scattering vectors from lattice planes oriented perpendicular to the loading direction (Fig. H1.2). Consequently, both the axial and the radial strains in each mineral present in the rock may be measured simultaneously at each applied load (Fig. H1.3).

Fig. H1.1. Structure of Earth's interior.

We have performed experiments on several different rocks, both synthetic and natural. Typical results for an isotropic olivine+magnesiowüstite rock, two important minerals within the Earth's mantle, are shown in Fig. H1.3. These particular results reveal that the measured strain partitioning falls within the bounds predicted by the widely used Hashin-Shtrikman variational method of

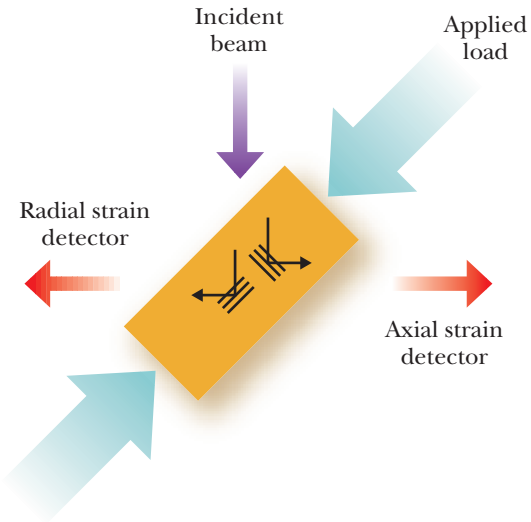

Fig. H1.2. A schematic representation of the specimen, incident beam, detector geometry and applied load. Lattice planes oriented to represent the radial and axial directions are indicated.

calculating the elastic properties of isotropic composites from the properties of the component minerals. The Hashin-Shtrikman bounds are extremely close for this material and the fact that the experimental results fall within the bounds (Fig. H1.4) provides strong confirmation of the experimental technique.

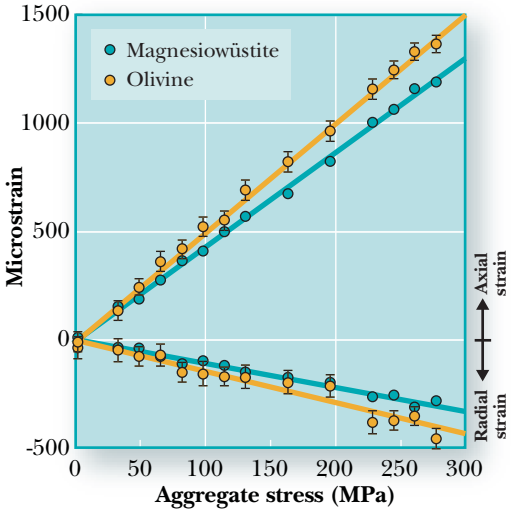

Fig. H1.3. The axial and radial microstrains of both phases in the aggregate are measured simultaneously at incremental aggregate stresses.

Having demonstrated the technique for isotropic materials, we are currently using it to investigate how strain partitioning varies in samples which are strongly textured and where the mineral phases are non-randomly distributed through the rock. Encouraged by the success of the experiments, we have also used them to investigate how strain partitioning changes between the phases when one or more phases starts to deform permanently by intracrystalline plasticity. The principle behind this is that if we know the elastic strain in a phase, we can calculate the stress in that phase, and then if we know the stress/plastic strain curve for that phase, we can obtain information about the plastic strain. Knowledge of this gives us the second key ingredient referred to above for understanding mantle convection, that is, information for establishing the way in which mantle rocks deform. So far our experiments have been on synthetic calcite+halite (Fig. H1.5) and garnet+halite samples. We find that within uncertainty the elastic strain partitioning between the two phases is unaffected by the plastic yielding of the weak phase (halite at 350 μstrain in Fig. 1.5) but that when the second phase starts to yield (calcite at 550 μstrain) there is a major change in the strain partitioning behaviour which reflects the onset of load transfer between the phases.

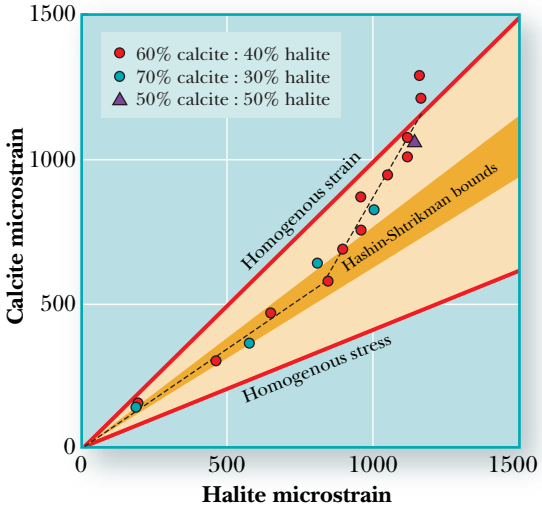

Fig. H1.5. Divergence of strain partitioning behaviour from the Hashin-Shtrikman bounds as the calcite undergoes plastic deformation, reflecting the onset of load transfer.

The application of neutron diffraction to the measurement of strain partitioning in polymineralic rocks is providing clear insights into the mechanical properties of deforming rocks. The implementation of ENGIN-X will greatly enhance this work by providing much tighter constraints on deformation induced textural changes as well as permitting work on common, but crystal chemically complex minerals.

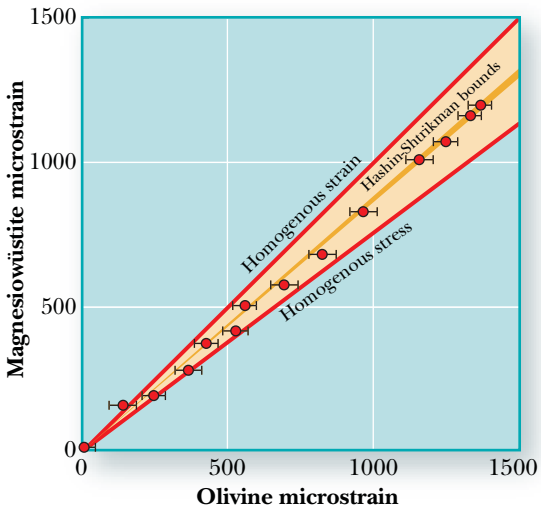

Fig. H1.4. The Hashin-Shtrikman bounds are extremely close for this material (dark orange shaded region) and the fact that the experimental results fall within the bounds provides strong confirmation of the experimental technique.

Migrating protons in organic crystal structures

Recent developments in applying rapid data collection methods on SXD to the study of hydrogen atoms in interesting chemical and crystal environments have included studies of protons in short, strong hydrogen bonds. The aim is to investigate possible proton migration (or disorder) in these systems by measuring a structure over a range of temperatures. This approach can reveal extra information regarding the behaviour of these hydrogen atoms and the potentials in which they sit.

C C Wilson, K Shankland *(ISIS),* ***N Shankland*** *(University of Strathclyde),* ***T Steiner*** *(FU Berlin),* ***I Majerz*** *(Wroclaw)*

There is great current interest in short, strong hydrogen bonds (HB), both in the chemical and the biological field. In contrast to 'normal' and weak HB, which are primarily electrostatic interactions X^{-}-$H^{+}\cdots Y^{-}$, strong HB have a quasi-covalent character. On SXD we have undertaken the first systematic investigations of homonuclear (O···H···O) and heteronuclear (O···H···N) HB systems in which the proton position is tuned by temperature.

Urea has been widely used as a complexing agent for organic acids in investigations of hydrogen bonding phenomena. It is well-known that the acidic H-atom in these complexes shows a varying degree of 'transfer' from one compound (the acid) to the other (urea). Earlier neutron diffraction analyses of urea-phosphoric acid (UPA) have shown a situation intermediate between the two extremes of hydrogen atom transfer. At room temperature, a near-symmetrical O···H···O arrangement can be observed, while low-temperature data suggest a greater degree of asymmetry.

Fig. H2.1 shows the refined structures of UPA at 150 K and 350 K. The geometry of the short O···H···O HB is summarised in Fig. H2.2. Over the temperature range studied, the O···O distance (≈2.4 Å) does not change significantly, nor does the O···H···O angle. The most striking finding is the systematic increase in the $O_{urea}\cdots H$ distance with increasing temperature. At 150 K, the O···H···O geometry is markedly asymmetric, with $O_{urea}\cdots H$ = 1.168(4) Å and $H\cdots O_{acid}$ = 1.252(4) Å. At ~ 300 K, however, the H-atom becomes essentially centred between the two O-atoms, and remains so up to 350 K. The slight (≈0.04 Å), but systematic, shift in position of the H-atom with temperature implies that the position of the potential minimum also shifts slightly with temperature. It may be postulated that such a shift might arise as a consequence of the effect of crystal packing due to changes in the local environment with temperature. However, there also remains the possibility that this is caused at least in part by the effect of temperature on molecular motion.

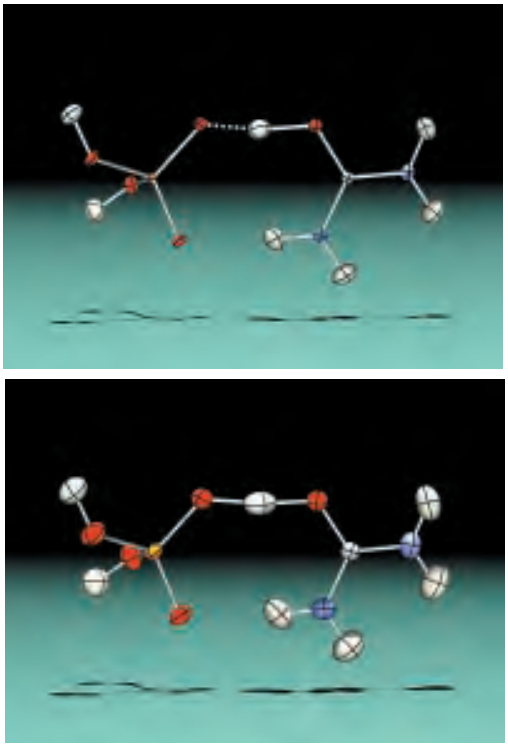

Fig. H2.1. The hydrogen atom in urea-phosphoric acid migrates from being closer to the urea oxygen atom at 150 K (top) to being essentially centred at 350 K (bottom). The magnitude of the displacement ellipsoid for atom H4, and its elongation along the hydrogen bond direction, increases systematically with increasing temperature and is fairly pronounced at 350 K. There is no evidence in the refinements to support the notion that atom H4 is disordered.

The second example of thermally-induced proton migration involves complexes

of methylpyridines (MePy) with pentachlorophenol (PCP). The proton position in the very short N-H···O (or O-H···N!) hydrogen bond can be tuned both chemically (by changing the position of the Me substituent) and by temperature. For example, a previous SXD study of the low temperature structure of 2-MePy:PCP showed that the H atom in the short HB is closer to the O atom, while an initial study of the complex 4-MePy:PCP at 25 K showed that the hydrogen atom in the N···H···O HB is slightly closer to N (Fig. H2.3). However, a room temperature X-ray experiment for the same material indicated that the hydrogen atom appeared to be closer to O. The possibility of tuning the proton migration within this system is exciting, and a variable temperature study on SXD was undertaken following the original 25 K work.

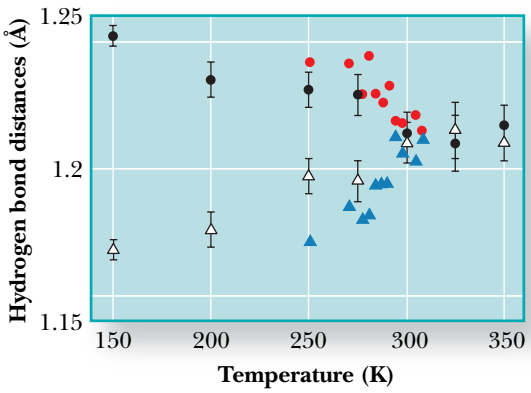

Data were collected using a crystal of 22 mm^3 volume, at seven temperatures in the range 45-200 K. The same well-ordered structure is found at all temperatures and the proton position is indeed found to alter with temperature, gradually migrating from being closer to N (at low T) to being closer to O (at high T). Such a phenomenon has not been observed before in a heteronuclear HB. At 100 K, the HB is found to be very close to geometrically centered, with the O···H and the H···N distances differing by less than one standard uncertainty (Fig. H2.4). This is a highly significant observation which has great importance for the understanding of strong hydrogen bonding interactions. There is no obvious way in which this effect could be caused by changing thermal population of a constant hydrogen bond potential. The proton migration is most likely a consequence of the changing crystal field of the contracting lattice. Indeed, it is well known that, in general, hydrogen bond potentials can respond strongly to changes in the environment – the same explanation as advanced in the related work on UPA.

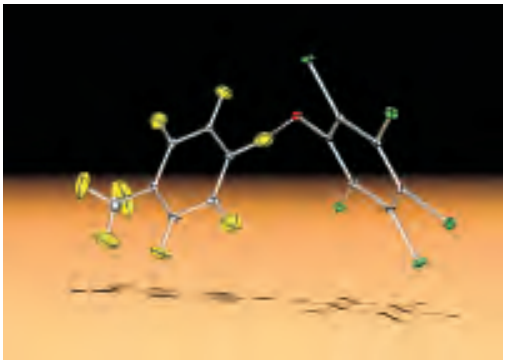

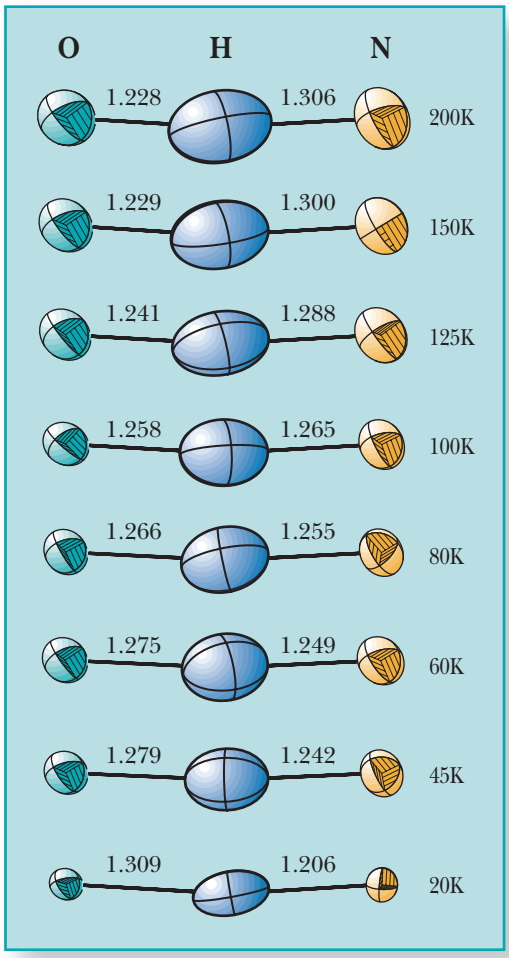

Fig. H2.2. The 'migration' of the H-atom in the short, strong hydrogen bond in urea-phosphoric acid. As temperature increases, the O5···H4 (triangles) and O4···H4 (circles) distances converge to 1.21 Å. The results from the multi-crystal experiment at finer T steps are also shown (red, blue).

Fig. H2.4. The H atom in 4-methylpyridine-pentachlorophenol migrates by ~ 0.1 Å between 20 K and 200 K.

Fig. H2.3. The H atom in the short HB in the low temperature structure of 4-methylpyridine-pentachlorophenol is closer to the N atom, but is found to migrate with increasing temperature (Fig. H2.4).

Development of sample encapsulation for the Paris-Edinburgh cell: sharper peaks under pressure

By means of a straightforward modification to the gasket configuration of the Paris-Edinburgh cell it is now possible to utilise truly hydrostatic pressure transmitting media up to at least 9 GPa. This important breakthrough ensures that high-quality, essentially resolution-limited, diffraction data may now be collected over the standard 0-10 GPa pressure range of the P-E cell without the need for sample heating. A very clear demonstration of the general improvement in compression conditions was provided by the discovery of two hitherto unknown structural phases of urea during what was supposed to be a simple high-compressibility sample test.

W G Marshall, D J Francis (ISIS)

Early in the development program of the Paris-Edinburgh (P-E) pressure cell it was found that the standard anvil profile and gasketting arrangement (Fig. H3.1) did not permit the use of the preferred pressure transmitting fluids such as mixtures of methanol/ethanol or pentane/iso-pentane. Any attempt to compress a sample beyond ~2 GPa led to anvil failure as a result of progressive propagation of microcracks in the anvil material. Until recently, therefore, the pressure transmitting fluid used for most experiments was Fluorinert, a mixture of fluorinated hydrocarbons which freezes at ~1.8 GPa at room temperature. Beyond this pressure, however, the sample is subject to significant non-hydrostatic stresses and, hence, reflection peak broadening. Fig. H3.2 illustrates the typical extent of the pressure-induced broadening for cell loadings utilising the standard P-E cell gasket setup and Fluorinert for the cases of α-quartz, OD-chlorite and OD-chondrodite.

This highlight describes a recent straightforward and effective resolution of this limitation, which now permits the use of truly hydrostatic media up to 9 GPa, the freezing pressure for the standard methanol-ethanol mixture. For the limiting case of a single small crystallite the compression conditions would indeed be truly hydrostatic, but the very nature of the packed sample volume of the P-E cell inevitably implies the possible presence of stresses induced by crystallite bridging.

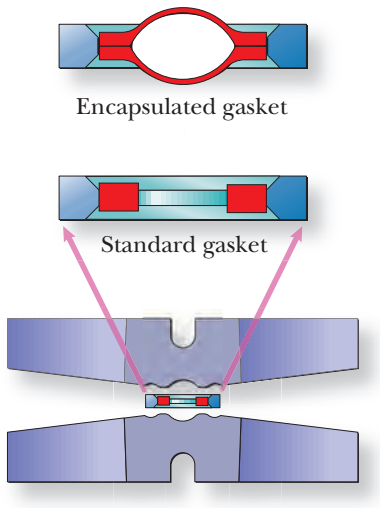

Fig. H3.1. P-E cell anvil and gasket assemblies.

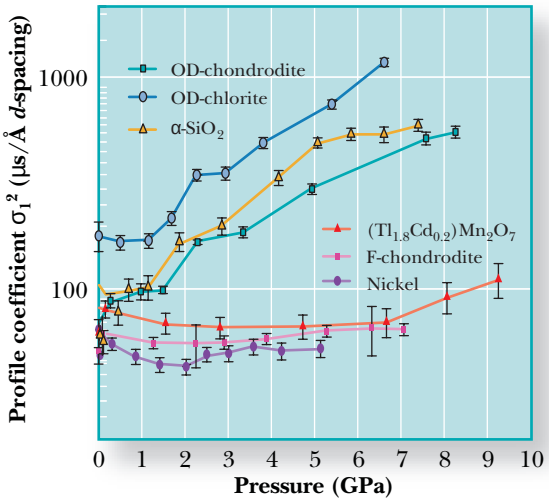

Fig. H3.2. Pressure variation of the profile parameter σ_1^2 for typical sample loadings using the earlier gasket design and Fluorinert (open symbols) and the new encapsulated gaskets and methanol-ethanol mixture (filled symbols).

Fig. H3.1 shows the prototype design of encapsulated gasket, machined from TiZr, that was eventually chosen for initial testing. A series of offline trials showed that the new gasket design actually trapped fluid and generated pressure. The first online test – using a mixed phase sample of powdered Ni and NaCl and deuterated methanol-ethanol – also established that the gaskets behaved as well as the standard gaskets in terms of pressure-load performance. Rietveld refinements of the neutron time-of-flight diffraction patterns indicated no significant increase in the nickel lineshape parameters as a function

of pressure. The filled circles in Fig. H3.2 illustrate the variation with pressure of the refined nickel lineshape parameter σ_1^2 – the dominant linear (as a function of *d*-spacing) Gaussian contribution of the sample to the overall diffraction peak lineshape. Also shown are the corresponding results for F-chondrodite and Cd-doped $Tl_2Mn_2O_7$ pyrochlore.

A further impressive demonstration of the improved compression conditions was provided by an online test using deuterated urea. Fig. H3.3 illustrates some earlier room temperature PEARL/HiPr results obtained using the standard gasket setup and Fluorinert. As the cell load increases the diffraction peaks broaden progressively due to the familiar non-hydrostaticity of Fluorinert above ~ 2 GPa. Beyond 45 tonnes load (~ 3.6 GPa) a weak new reflection appears at ~ 3.9 Å *d*-spacing accompanied by a redistribution of intensity amongst the reflections of the phase III pattern, suggestive of a possible transition to a new phase. Fig. H3.4 shows the corresponding results obtained on POLARIS using the new encapsulated gaskets and methanol-ethanol. The differences between the new and old results are quite striking and unexpected. As in the earlier tests, the reflections remained sharp for all pressures up to the maximum of 8.5 GPa. However, the POLARIS results clearly indicate the presence of *two* new high-pressure phases of urea at room temperature. Clearly, the key effect of improving the compression conditions in this case has been to eliminate the inhibiting effect of non-hydrostatic stresses imposed by the solidified Fluorinert transmitting medium.

Even in the prototype form, it is evident that the technique of sample encapsulation has exceeded all initial expectations. In addition to offering improvements in diffraction data quality by permitting the use of hydrostatic fluid transmitting pressure media, the new gaskets perform as well as if not better, in terms of pressure versus load, than the previous gasket configuration. Further possibilities are being explored: i) capsules of reduced wall thickness, so as to increase available sample volume once again, ii) the preparation and testing of scaled-down gaskets suitable for use in sintered diamond anvils to permit access to the 10-20 GPa pressure range; and iii) use of encapsulation for the offline preparation of chemically reactive or volatile samples.

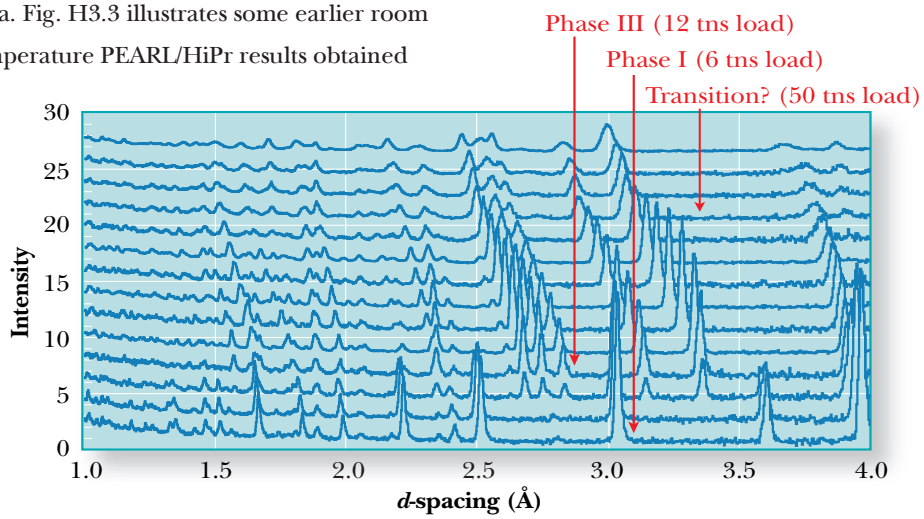

Fig.H3.3. PEARL/HiPr high-pressure/RT data for d_4-urea using the earlier gasket geometry and Fluorinert. Cell load increases from the bottom to the top of the figure. Note the progressive broadening of the peaks with increasing pressure.

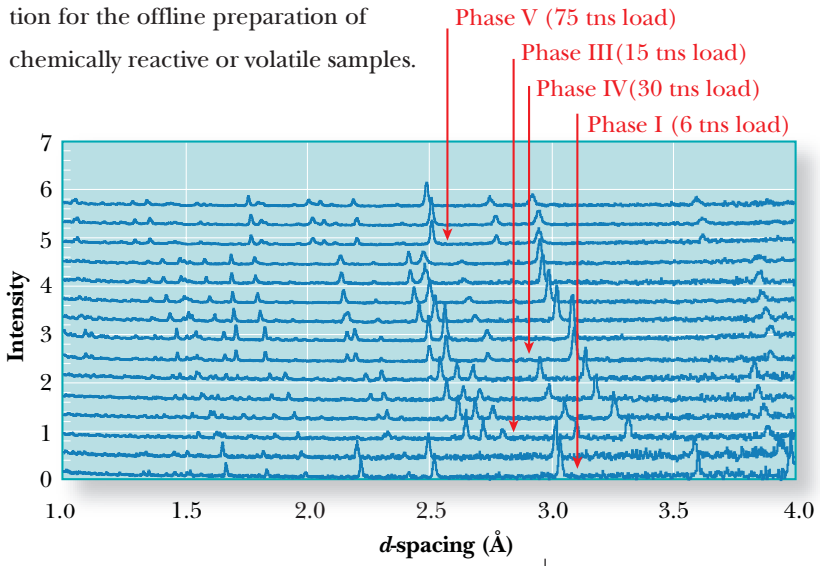

Fig.H3.4. POLARIS high-pressure/RT data for d_4-urea using the new encapsulated gaskets and methanol-ethanol mixture. Cell loads range from 6 tonnes (bottom) to 90 tonnes (top). Note the effective absence of peak broadening and the sharp phase-pure patterns of two hitherto unknown phases of urea.

Structural transformations in sulphides at elevated temperatures and pressures

The capacity of neutrons to discriminate between cations of similar atomic number has been exploited in a series of studies of metal sulphides containing elements from the first transition series. These materials exhibit pressure and temperature induced structural transformations that are accompanied by changes in magnetic and electronic properties. Diffraction studies carried out on POLARIS under high temperatures and pressures have allowed major structural reorganisation and more subtle atomic rearrangements to be investigated. The results demonstrate that both chemical composition and processing conditions influence the structural behaviour and hence physical properties.

A V Powell, P Vaqueiro
(Heriot-Watt University)

Transition metal sulphides of stoichiometry AB_2S_4 may, depending on the identity of the cations A and B, adopt either the Cr_3S_4 or the spinel structure (Fig. H4.1). The former is an ordered defect structure related to that of NiAs, containing layers of edge-sharing MS_6 octahedra of overall stoichiometry MS_2, separated by a cation deficient layer in which 50% of the available octahedral sites are occupied in an ordered manner. In a ternary phase, two limiting arrangements of A and B cations may be identified, corresponding to the normal, (A)$[B_2]S_4$ and inverse (B)$[AB]S_4$ structures, where parentheses and square brackets represent sites in the vacancy and dichalcogenide layers respectively. The degree of cation partitioning, which strongly influences the transport and magnetic properties, is seldom complete and is dependent both on the identity of the A and B ions and on the mode of preparation. Cations drawn from the early part of the transition series exhibit a marked preference for sites in the dichalcogenide layer, whereas the later transition-series cations favour sites in the vacancy layer.

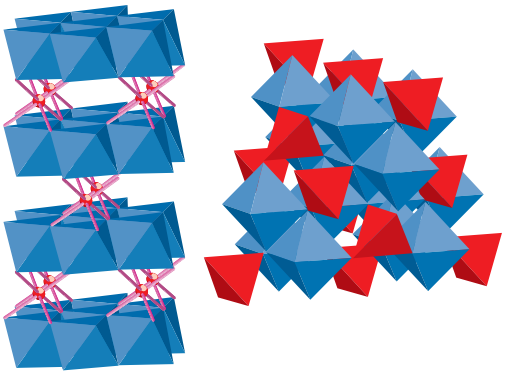

Fig. H4.1. The Cr_3S_4 (left) and spinel (right) structures, for sulphides of stoichiometry AB_2S_4 containing A and B cations from the first transition series.

In a recent POLARIS experiment, *in-situ* powder neutron diffraction was used to study the behaviour of $NiCr_2S_4$ on heating to the high temperatures used in synthesis. At 835 °C, the material undergoes a first-order transition from the monoclinic Cr_3S_4 structure to a hexagonal cation-deficient NiAs structure. As the transition temperature is approached, intralayer disordering of vacancies within the half-occupied layer occurs, although in contrast to the binary sulphides this remains incomplete. At the transition temperature, cation vacancies become statistically distributed between all cation layers and a first-order phase change to the cation-deficient NiAs structure occurs. These structural changes are illustrated in Fig. H4.2. The cation disorder introduces additional short-range cation-cation interactions that are not present in the ideal $NiCr_2S_4$ structure and are the cause of the pronounced magnetic history dependence of the magnetic susceptibility of phases prepared by quenching from high temperature.

The spinel structure, in which one-third of the cations occupy tetrahedral sites, provides an alternative to that of Cr_3S_4 for AB_2S_4 materials. It has a lower density than the Cr_3S_4 structure and therefore should transform to the latter at high pressures. Heating ACr_2S_4 (A= Mn, Fe, Co) spinels at elevated temperatures and pressures allows isolation of defect NiAs-type phases by rapid quenching, although the extent of defect ordering has not been established unambiguously. The penetrating nature of the neutron, together with the fixed scattering geometry available on a pulsed source, permits the use of bulky sample cells to perform *in-situ* studies of such processes under extremes of temperature and

pressure, providing data of high quality, relatively uncontaminated by background scattering from the sample cell. Initial experiments revealed that $CoCr_2S_4$ transforms to a defect NiAs phase at 1.3 GPa and 800 °C. However, even under these conditions, which are close to the operating limits of the high-p/T cell, the phase change is incomplete.

Fig. H4.1 reveals that the structure of ACr_2S_4 at ambient temperature and pressure changes from spinel to Cr_3S_4 when the Co cation is replaced by Ni. Therefore a series of materials, $Co_{1-x}Ni_xCr_2S_4$ in which nickel progressively substitutes for cobalt, was prepared. The limiting substitution for retention of the spinel structure was identified as x=0.35. Rietveld refinement using room temperature powder neutron diffraction data (Fig. H4.3a) established that substitution occurs exclusively at the tetrahedral sites. Neutron diffraction measurements made at high temperatures and pressures reveal a phase transition at 0.4 GPa and 750 °C. Remarkably, this represents a reduction in the transformation pressure to less than one-third that of the undoped material. Rietveld refinement (Fig. H4.3b) demonstrates that the transition is to a hexagonal CdI_2-like phase with a structure in which the cobalt and nickel cations are confined to the vacancy layer between CrS_2 layers and there is complete intralayer disordering of cobalt and nickel over the octahedral sites (Fig. H4.2b). Slow-cooling of the sample cell under the applied pressure results in an ordering transition to produce the Cr_3S_4 structure in which a statistical distribution of nickel and cobalt cations occupy 50% of the sites in the vacancy layer in an ordered fashion (Fig. H4.3c). The phase transition results in a collapse in the magnetisation, which becomes effectively temperature independent. This is indicative of a change from a localised to an itinerant electron system, as a result of increased cation-cation interaction between octahedra which now share faces. The dramatic reduction in the transformation pressure is a consequence of the strong octahedral site preferences of Ni^{2+} and Cr^{3+}, which lead to a marked stabilisation of NiAs-related structures, in which only octahedral cations are present.

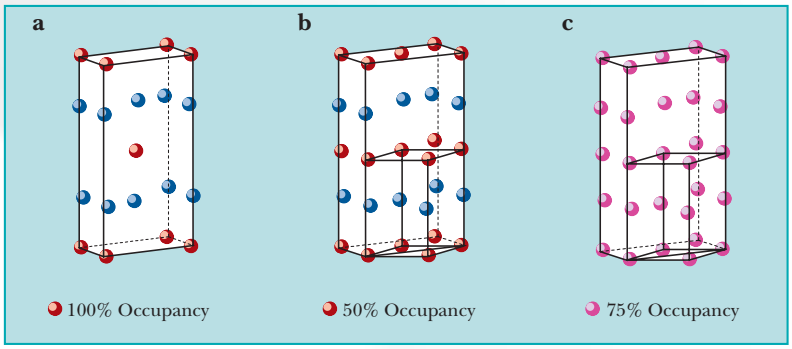

Fig. H4.2. Relationship between (a) the ordered-defect Cr_3S_4 structure, (b) the CdI_2 structure, in which there is intralayer disordering of defects and (c) the cation-deficient NiAs structure, in which there is interlayer disordering. Blue circles represent cations in the dichalcogenide layer.

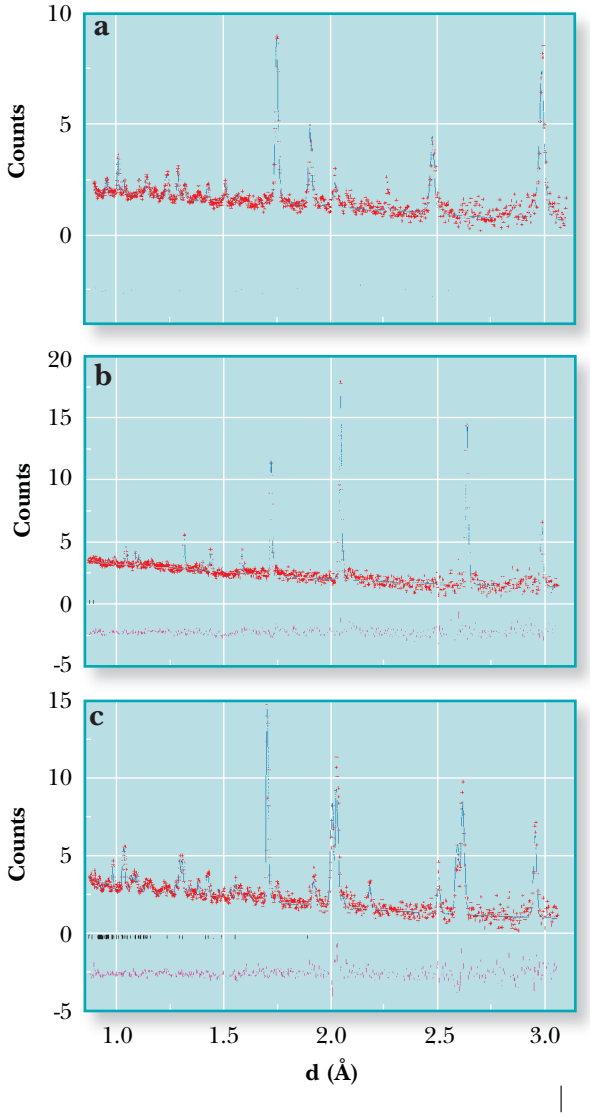

Fig. H4.3. Powder neutron diffraction data for $Co_{0.65}Ni_{0.35}Cr_2S_4$ collected at 0.4 GPa and (a) 140 °C (spinel); (b) 750 °C (CdI_2); and (c) after cooling to 25 °C (Cr_3S_4). A reflection from the platinum sample can is evident at ca. *2.2 Å in (a).*

Location of the active Ti sites in the MFI framework of Ti-silicalite-1 catalyst by high resolution powder diffraction

Direct evidence that Ti atoms are not equi-distributed over the 12 crystallographically-independent T sites of the MFI framework has been highlighted by neutron diffraction data collected using HRPD. The fact that defective silicalite exhibits the same preferential sites for Si vacancies strongly suggests that the incorporation mechanism of the Ti atoms occurs via the insertion into defective sites of silicalite. This implies that Ti has a mineralising effect on the MFI framework.

G L Marra, G Spanò (Istituto G. Donegani), G Artioli (University of Milan), A Zecchina, S Bordiga (University of Turin), C Lamberti (University of Turin and INFM UdR of Turin)

The microporous titanosilicate *Ti-silicalite* (TS-1), discovered in the early eighties, has become one of the most relevant heterogeneous industrial catalysts in the last twenty years due to its remarkable high efficiency and molecular selectivity in oxidation reactions employing H_2O_2 under mild conditions. As an example, Fig. H5.1 describes the role of TS-1 in the industrial production of Nylon 6. The precise structural role played by the Ti atoms in TS-1 was the subject of lively debate up until the middle of the nineties: titanyl groups, extraframework defect sites or TiO_2 nanoclusters, monomeric and dimeric Ti species, or Ti species incorporated in edge sharing units forming bridges across the zeolite channels, had all been proposed by various authors.

Much of the initial confusion was a result of difficulties in synthesizing high-quality samples of TS-1. This requires the use of extremely pure reagents and stringent control of the synthesis conditions, and cannot be achieved if the Ti loading exceeds 2-3 wt%. In the period 1989-1994, experiments based on XRD, IR, Raman, UV-Vis, EXAFS and XANES (most of them supplied by our group), proved definitively that the Ti atoms substitute for silicon atoms in the MFI framework at $[TO_4]$ sites. It was also shown that the catalytic yield of TS-1 is related to the fraction of tetrahedrally incorporated Ti atoms. Subsequent theoretical studies supported this picture.

As part of our ongoing programme to understand the role played by the microporous nature of the MFI framework hosting the active Ti sites, it was shown that Ti-free silicalite is a defective material showing a high density of bulk Si vacancies (•) resulting in

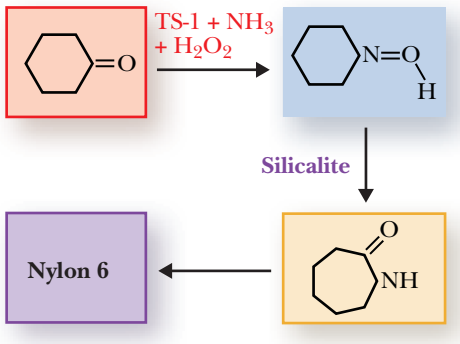

Fig. H5.1. Schematic representation of the industrial path followed for the synthesis of Nylon 6, where the role of both TS-1 (cyclohexanone ammoximation) and defective silicalite (Beckman rearrangement) catalysts has been evidenced.

hydroxylated nests: $[Si(\text{-}O\text{-}Si\equiv)_4] \rightarrow [\bullet(HO\text{-}Si\equiv)_4]$. The defectivity of the MFI matrix is also observed for TS-1 and it has been demonstrated by IR and microcalorimetry that the insertion of Ti heteroatoms in the MFI lattice has a mineralising effect causing the progressive reduction of the internal defects. Fig. H5.2 (inset) reports the IR spectra, in the OH stretching region, of TS-1 samples, with increasing Ti content, from 0 (silicalite) to 2.64 atoms per unit cell. This IR study indicates that the progressive incorporation of Ti atoms in the framework implies the parallel reduction of the OH band due to internal, defective, Si-OH groups.

Two fundamental questions remain open to debate for TS-1:

(*1*) Are the Ti atoms distributed randomly over the 12 independent T sites of the MFI framework or is there some preferential site occupation?

(*2*) What is the role of structural defects and the interplay between Si vacancies and Ti insertion?

To date, all direct structural information concerning TS-1 has been derived from powder diffraction. The relatively low electron density contrast between Si and Ti ($\Delta Z = 8$) and the low Ti content has not permitted us to locate unambiguously the Ti atoms even with high quality X-ray data collected at the ESRF. The success of the present work is based largely on the *qualitative* difference existing between the neutron coherent scattering lengths of Ti and Si, and on the excellent flux/resolution characteristics of HRPD. Simultaneous Rietveld refinement of the HRPD 90° and 168° detector bank spectra (Fig. H5.2) revealed T6, T7, T10 and T11 as the preferred substitution sites for three different TS-1 samples. This finding answers question (*1*). The fact that defective silicalite exhibits the *same* four preferential sites for Si vacancies (as determined in a previous HRPD experiment) allows us to hypothesise an answer for question (*2*) too.

The correspondence of the four sites preferentially hosting the Si vacancies in defective silicalite with those occupied by Ti atoms in TS-1 is striking and suggests that the incorporation mechanism of the Ti atoms in the MFI framework occurs via the insertion of titanium in defective sites of silicalite. In this regard, the theoretical work by Ricchiardi *et al.* has shown that the $[TiO_4]$ and the $[(OH)_4]$ units, substituting a regular $[SiO_4]$ unit in the MFI framework of silicalite, have a similar size. This can explain the tendency of the same sites to host either a defect (Si vacancy) or a Ti heteroatom, and why the amount of incorporated Ti increases to the detriment of internal OH species: $[\bullet(HO\text{-}Si\equiv)_4] \Leftrightarrow [Ti(\text{-}O\text{-}Si\equiv)_4]$ being the equilibrium displaced to the right hand term by increasing the synthesis Ti concentration. The fact that T7, T10 and T11 sites are adjacent to each other explains the formation of large hydroxylated cavities in silicalite, and implies that Ti heteroatoms in TS-1 have a non-negligible probability of being located close to a defective site. Fig. H5.3 pictorially represents the model emerging from this study.

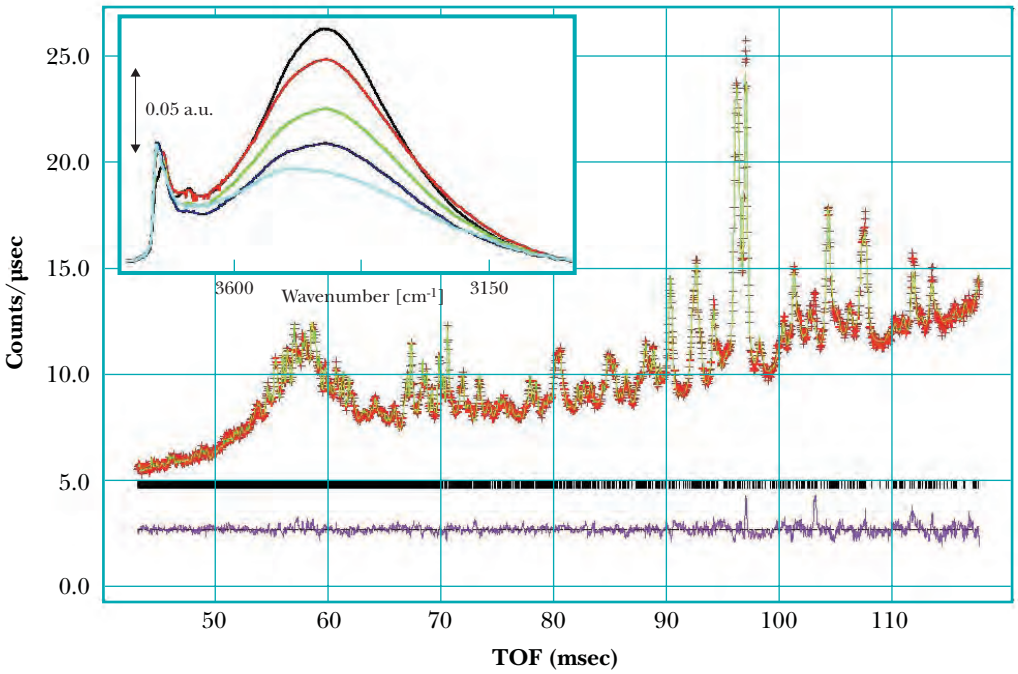

Fig. H5.2. Observed (red crosses), calculated (green line) and difference (purple line) powder diffraction patterns of TS-1 sample collected with the HRPD 168° detector bank. The inset reports the IR spectra, in the OH stretching region, of (from top to bottom) TS-1 samples with increasing Ti content, from 0 (silicalite black line) to 2.64 atoms per unit cell (pale blue line).

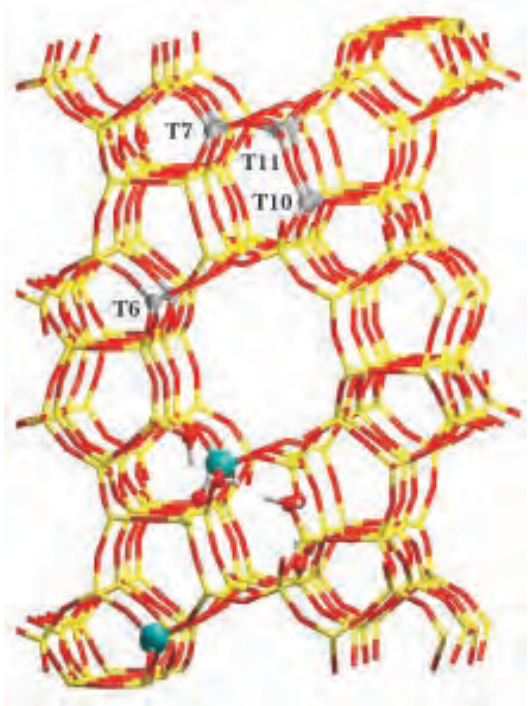

Fig. H5.3. Schematic representation of the preferential location of Ti atoms and Si vacancies in the MFI framework (upper part) and their interplay (lower part). Yellow and red sticks represent Si and O of the regular MFI lattice; green spheres refer to Ti, while red and white spheres refer to O and H of defective internal OH groups, respectively.

The hydrophobic and hydrophilic behaviour of methanol in water

'Hydrophobic', polar molecules and headgroups in aqueous solution tend to form aggregates, with the water excluded from between them. In fact, this effect is due to water being unable to form hydrogen bonds with such entities, and so forming a loosely hydrogen-bonded net around the hydrophobic molecule or headgroup. This hydrophobic effect is thought to be a fundamental factor in the folding or unfolding of biological macromolecules in solution. Recent investigations on SANDALS of the structure of methanol in solution have provided insights into the effects of hydrophobic and hydrophilic headgroups on the structure of biological molecules.

S Dixit, J Crain (Edinburgh), J Finney (UCL), A Soper (ISIS)

The effect of hydrophobic molecules on water is usually to *raise* the freezing point. At 150 bar, the atomic concentration of methane dissolved in water is about 1%, yet this solution freezes at +14 °C. Pure water at this pressure freezes at -3 °C. In contrast, so-called water-loving (hydrophilic) solutes such as ionic salts, sugars and the lower alcohols, usually suppress the melting point. Thus we have the intriguing fact that so-called 'water fearing' solutes actually enhance water structure, whereas 'water-loving' solutes tend to break down the hydrogen bonded structure.

Traditionally, hydrophobic effects are associated with solutes with low solubility in water. It might thus seem strange that methanol, overall a great water-lover, should be used to study the hydrophobic effect. In fact, methanol exhibits both hydrophobic and hydrophilic character. It has an —OH radical which can bond readily with the surrounding water molecules. It also has a methyl radical which cannot bond and is hydrophobic. Both headgroups are sufficiently simple in structure to be interpretable in a diffraction experiment at the atomic level.

Pioneering work some years ago at ISIS demonstrated the arrangement of the water molecules around methanol (Fig. H6.1). The methanol molecule polarises the local water arrangement, but in a manner which is consistent with preserving the water hydrogen-bond network. It also allows the water to be fully hydrogen bonded with the —OH radical while forming the expected hydrogen-bonded net around the methyl radical.

The most recent work on this system arose out of earlier Raman measurements of methanol-water mixtures over a wide range of concentrations. These indicated that, at high methanol concentrations, water was bonding preferentially to the —OH radical, causing a rapid breakdown of the hydrogen-bonded chains characteristic of pure methanol. This

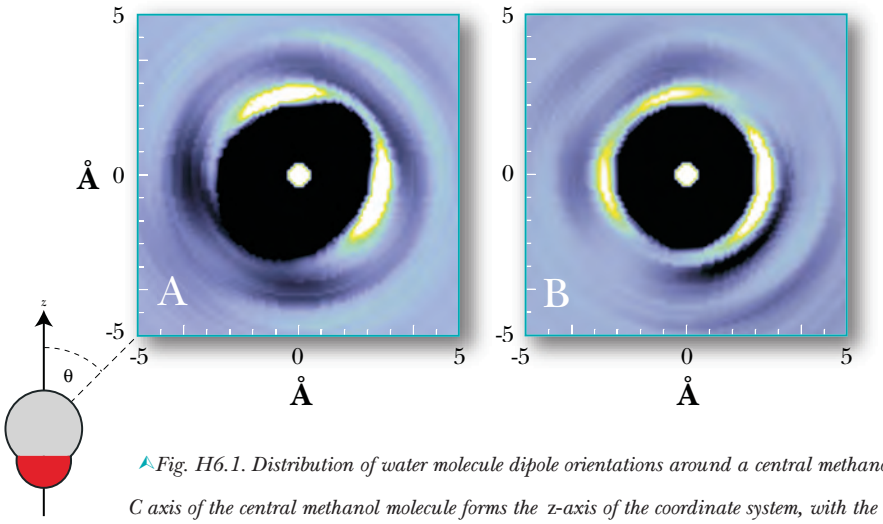

Fig. H6.1. Distribution of water molecule dipole orientations around a central methanol molecule. The O-C axis of the central methanol molecule forms the z-axis of the coordinate system, with the carbon atom at the origin. The plots show the distribution of water molecule dipole orientations at different angles relative to this axis (A) 45°, and (B) 135°. The brightness of the lobes indicates the density of water molecules with that orientation. In (A) we see that the dipole prefers to lie roughly tangential to the carbon-water direction. In (B) it is orientated so that either one of the OH vectors on the water molecule points directly towards the methanol oxygen.

present neutron diffraction study of the system has allowed this structural change to be mapped out in detail.

Fig. H6.2 shows the distribution of methanol chain lengths in pure methanol

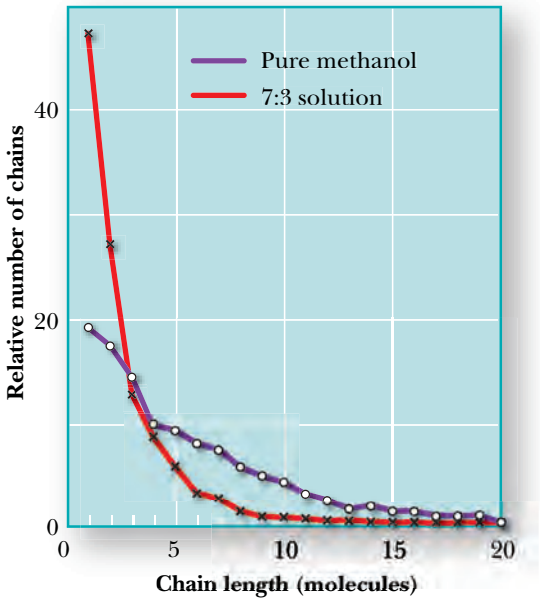

compared with that in a 7:3 solution of methanol in water, estimated from diffraction data. Adding even this small amount of water has a drastic effect on the ability of methanol to form chains in solution. In pure methanol the average chain length is 5.9 molecules per chain, but in a 7:3 solution this number drops to 2.9. At the much lower 1:19 concentration there were effectively no methanol-methanol chains observed.

Coinciding with this change in bonding between the —OH groups on methanol molecules, more subtle changes were seen. For example, at the 7:3 concentration the methyl-methyl nearest neighbour distance *shrinks* compared to pure methanol. At the 1:19 composition this distance was slightly longer than in pure methanol, but the methyl-methyl coordination was still substantial. Comparing the distribution of methanol molecules around a central molecule in the 1:19 solution with that in the pure liquid shows clearly the tendency for methyl-methyl association in the solution, which is not nearly so pronounced in the pure liquid (Fig. H6.3). Another feature of the dilute solution is the fact that there are small but significant changes in the *second* shell of water around a central water molecule, equivalent to the structural changes seen on raising the temperature of water slightly. These changes are a clue to why methanol is able to lower the freezing point of water substantially.

In conclusion therefore, it is clear that methanol exhibits a rich assortment of properties in the presence of water. It shows both hydrophobic and hydrophilic behaviour, in that the methyl headgroups become drawn together, while the hydroxyl radical forms strong hydrogen bonds with the surrounding water. Real biological macromolecules of course consist of a range of both hydrophobic and hydrophilic headgroups, and the relative abundance and nature of these will vary considerably. On the basis of the present results, it is clear that both hydrophobic and hydrophilic headgroups will have a significant influence on the conditions required to cause the molecule to fold or unfold. Indeed, it may be that subtle differences in the details of the aqueous environments of a macromolecule may determine the difference between folding and misfolding. What is certainly clear however is that both types of headgroups are involved in the process — molecular folding cannot be thought of as driven purely by hydrophobic effects.

Fig. H6.2. Distribution of number of molecules as a function of chain length in pure methanol and 7:3 methanol-water solution. It can be seen that the effect of the water is drastically to reduce the average chain length.

Fig. H6.3. Distribution of methanol molecules around a central methanol in (A) pure methanol, and (B) in a 1:19 solution of methanol in water. The same coordinate system as in Fig. H6.1 is used here. It can be seen that in the solution there is a considerable reduction in the number of methanol-methanol associations via their hydroxyl groups.

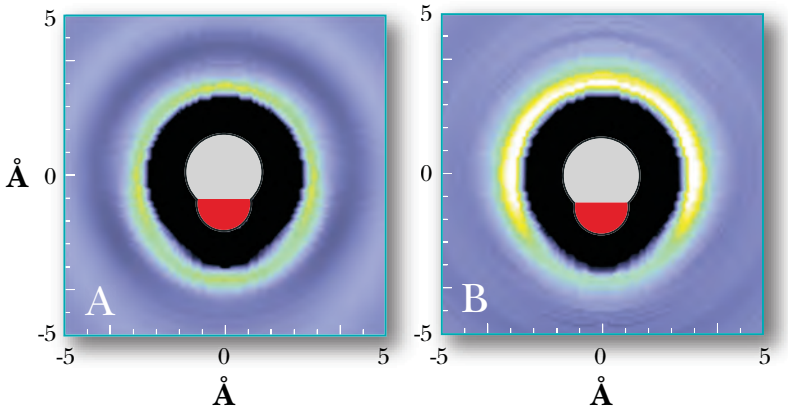

Room temperature ionic liquids

Interest in the properties of room-temperature ionic liquids is rapidly expanding. Although there have been numerous studies concerning their preparation, their use as a reaction medium and their physical properties, little is known about the packing of the ions within the liquid phase and how this relates to the available crystal structures. We have used SANDALS to examine the liquid structure and discovered a close relationship between local ordering in the solid and liquid phases.

C Hardacre, K Seddon, J McGrath (Queens University Belfast)

Room temperature ionic liquids consist solely of ions. However, unlike conventional molten salts (for example, molten sodium chloride), these materials often melt below 100 °C. This is achieved by incorporating a bulky asymmetric cation into the structure to stop the ions packing easily. Since the melting points are low, ionic liquids can act as solvents in which reactions can be performed, and because the liquid is made of ions rather than molecules, such reactions often give distinct selectivities and reactivity when compared with conventional organic solvents.

Room-temperature ionic liquids have been utilised as clean solvents and catalysts for green chemistry and as electrolytes for batteries, photochemistry and electrosynthesis. They have no significant vapour pressure and thus create no volatile organic components. They also allow for easy separation of organic molecules by direct distillation without loss of the ionic liquid. Their liquid range can be as large as 300 °C allowing for large reaction kinetic control, which, coupled with their good solvent properties, allows small reactor volumes to be utilised. Salts based upon poor nucleophilic anions such as $[BF_4]^-$, $[PF_6]^-$, $[CF_3CO_2]^-$, $[CF_3SO_3]^-$, etc, are water and air insensitive and possess remarkably high thermal stability. Many of these materials are based around the imidazolium cation, 1-alkyl-3-methylimidazolium (Fig. H7.1). By changing the anion or the alkyl chain on the cation, a wide variation in properties such as hydrophobicity, viscosity, density and solvation can be obtained. For example, they will dissolve a wide range of organic molecules to an appreciable extent, the solubility being controlled by the nature of the counter anion.

Although there has been much work performed on their use as a reactive medium, little is known about the structure of these liquids, particularly of liquids in which one or both of the ions is highly *non-spherical* leading to a corresponding non-spherical charge distribution around each ion. To try and understand the liquid structure, experiments were performed using SANDALS on dimethylimidazolium chloride, which melts at 128 °C and represents the simplest cation-anion pair for the structural study. In addition the crystal structure of this material is also known, and so can be compared with the observed liquid structure.

A simple measure of the degree of charge ordering in this system is the radial distribution of cations around cations, and anions around cations. These are measured from the centre of the imidazolium ring (Fig. H7.1). The radial distributions are calculated from a computer simulation of the liquid where the forces between atoms, and hence the positions of the ions, are refined to give the best possible fit to the diffraction data. In the case of imidazolium chloride, diffraction measurements were made with different hydrogen isotope substitutions, deuteron for

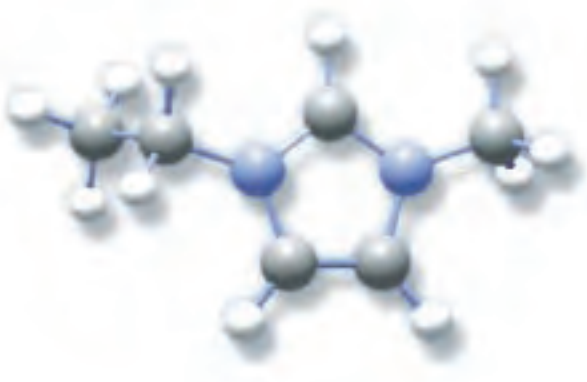

Fig. H7.1 Schematic of the 1-ethyl-3-methyl imidazolium cation.

proton, on the imidazolium ion. Selective substitution in this way helps to determine specific correlations between the selected atoms on the molecule and its surroundings.

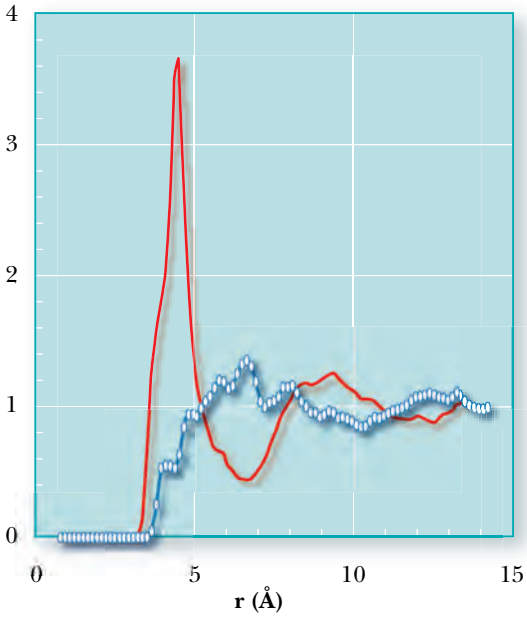

Fig. H7.2 shows the estimated anion-cation and cation-cation radial distribution functions derived from this structure refinement process. It will be seen that the first peak in the anion-cation distribution is well defined and at a much shorter distance than that of the cation-cation distribution. Furthermore at greater distances the pronounced oscillations in the cation-anion distribution are out of phase with the weaker oscillations in the cation-cation distribution. This therefore shows clearly the charge ordering that is taking place in this fluid. The chloride ion is sited at distances of approximately 4.0 Å and 8.0 Å from the centre of the imidazolium ring and the cation ring-cation ring spacing is approximately 6.0 Å. This compares with the crystal structure where the shortest contact between the chloride ion and the centre of the imidazolium ring is at ~3.5 Å.

The crystal structure also shows that the shortest contact between the cations is a methyl hydrogen-methyl hydrogen contact at ~2.5 Å. This is shown also in the simulation of the liquid diffraction data, where the only short contacts of significance between cations are the methyl hydrogen contacts which result in a broad peak between 2 and 5 Å. Changes in near-neighbours distances are naturally expected on melting due to the expansion of the lattice, but there are nonetheless strong overall similarities between the crystal structure and the liquid arrangement.

The point is further exemplified in Fig. H7.3, which shows the arrangement of both the chloride anions and imidazolium cations around a central imidazolium molecule. At short distances the anion is mainly found to be associated with the ring hydrogens, *i.e.* it tends to avoid the methyl groups. This is also consistent with the crystal structure where all the short contacts are found between the chloride ions and the ring hydrogens.

In conclusion, we have shown that there is significant order within the liquid state of a model room temperature ionic liquid even with very short alkyl chains. The close relationship between the crystal and liquid structures implies that the molecular packing in the first two or three coordination shells is similar in form for both the crystal and the liquid, although the absolute distances are obviously altered on melting. This work shows that the liquid structure of these complex molecules may be elucidated and opens up the possibility of understanding the solvation and reactive properties of room temperature ionic liquids.

Fig. H7.2. Radial distribution of chloride around imidazolium ions (red) and imidazolium about imidazolium (blue) in the molecular ionic liquid, dimethylimidazolium chloride.

Fig. H7.3. Three-dimensional realisation of the data of Fig. H7.2. The imidazolium ion is shown at the centre of the coordinate axes. On the left is shown the distribution of chlorine ions around the central imidazolium molecule, and on the right is shown the distribution of imidazolium ions. Note how the chloride ions associate primarily with the central ring of the imidazolium ion.

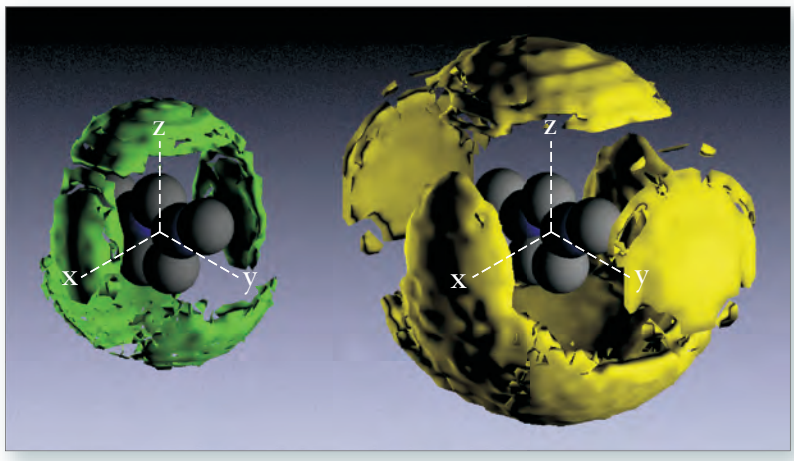

Making models of membranes

In the native state, the phospholipid membrane is difficult to study. Not only are the natural systems often too complex for the current understanding of lipid bilayer behaviour, but cells and vesicles are not in a state where they can be easily manipulated for investigation. There is therefore great interest in the development of artificial model lipid membranes with controlled composition, which are localised on a solid support so that they may be easily investigated. A method for establishing such bilayers has been developed, and neutron reflectivity measurements coupled with fitting from quasi-molecular models have confirmed the validity of the approach.

S Roser, A Hughes
(University of Bath)

A number of approaches to solving the problem of phospholipid membrane study have been proposed, and various fabrication schemes have been used, including Langmuir-Blodgett (LB) techniques, spontaneous fusion of uni-lamellar vesicles on un- or pre-coated surfaces, and self-assembled, tethered bilayers. However, the common flaw of these approaches is that in being localised on the substrate surface, the component lipids essentially become fixed and their freedom within the plane of the membrane is limited. A natural bio-membrane is a dynamic, fluid system, where the component molecules have considerable translational freedom. This fluidity is central to the behaviour of the membrane.

In multi-lamellar vesicles, it is well known that adjacent bilayers associate with each other through electrostatic and Van der Waals forces, but are prevented from sticking together by a balancing repulsive entropic pressure. That is, if the bilayers were to adhere directly to each other, their natural fluctuations would be suppressed, leading to a decrease in their overall entropy. This requirement of maximal entropy is manifested as a repulsive interaction between the bilayers such that each bilayer unit is separated from the next by an extensive (30 – 40 Å) layer of water. Our approach to reconciling the contradictory requirements of a supported yet unconstrained bilayer is to produce a system which mimics this balance of forces, so that the bilayer is associated with the substrate, but separated from it by an extensive water layer, leading to a system which is fully hydrated on both sides.

Our system is fabricated by a combination of Langmuir-Blodgett, Langmuir-Schaeffer (LS) and self assembly (SA) techniques. A silicon substrate is first coated with a self-assembled monolayer of Octadecyl-trichlorosilane (OTS), and two LB layers of phospholipid are deposited onto this. A final phospholipid layer is deposited using a horizontal LS deposition, resulting in the structure shown in Fig. H8.1.

We have extensively characterised this system by neutron reflectivity using the CRISP reflectometer. Generally, reflectivity from such systems is analysed using so called 'box' models, where the structure is parsed into a number of individual layers. However, due to the phase problem, it is not possible to simply convert the reflectivity data directly into a scattering length density (SLD) profile, since no direct unique solution exists. Rather, the independent parameters for each layer must be varied using standard minimisation techniques until a correspondence between simulation and experiment is obtained. The

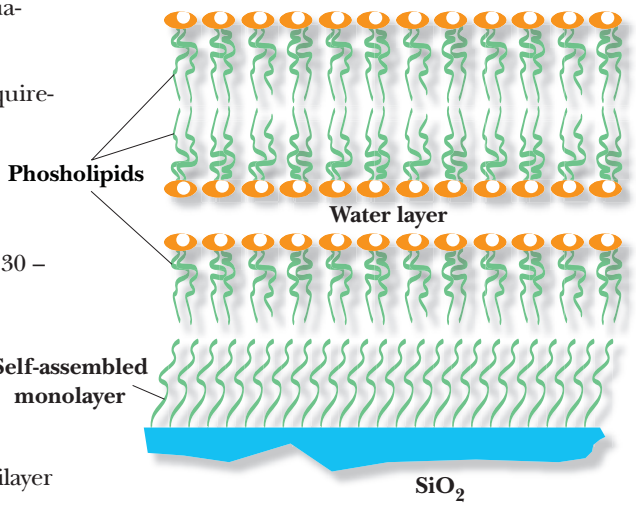

Fig. H8.1. The model membrane system, comprising a SAM of OTS on Silicon; two Langmuir-Blodgett layers of phospholipid, and a final Langmuir-Scaeffer phospholipid layer. The upper two layers form the fully hydrated model bilayer.

minimisation is sensitive to the total form of the SLD profile irrespective of how this is formed from its constituent boxes, and many combinations of parameters from individual boxes may lead to the same general SLD profile. For this reason, directly identifying a given box with a particular molecular fragment is extremely dubious, and the individual boxes themselves may not have any true physical meaning in a structural sense.

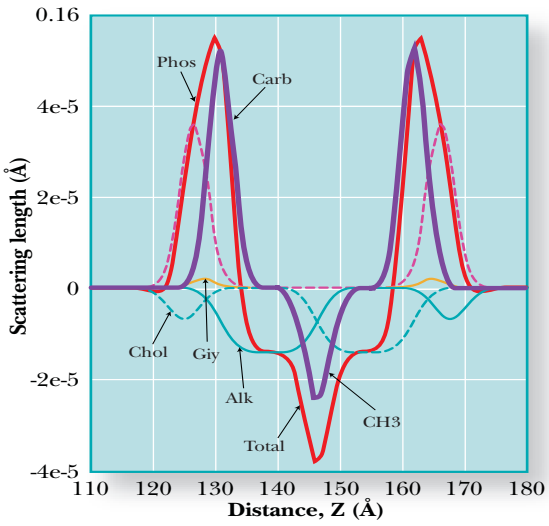

To understand the interaction of the model bilayer with biological agents, it is necessary to be able to fit the reflectivity data using models which maintain a close link with the real molecular structure. In our approach, the scattering length density profile of the bilayer is described in terms of Gaussian distribution functions rather than slabs, where each Gaussian represents the contribution of a particular molecular fragment to the total SLD profile. The Gaussians are arranged along the interface according to real molecular considerations, so that a clear and unambiguous picture of the structure of the bilayer is obtained. The structure of a DMPC bilayer in this system is shown schematically in Fig. H8.2, and simultaneous fits to three reflectivity profiles under three water contrasts are shown in Fig. H8.3. As can be seen, the reflectivity data are described very well by the quasi-molecular model.

The quasi-molecular approach allows the structure of the bilayer to be easily compared to others, such as those in multi-lamellar vesicles. Specifically, in going from the low temperature crystalline gel phase to the high temperature fluid phase, the thickness of the bilayer in vesicles decreases as chain melting occurs, and the area per molecule increases to accommodate the more diffuse chains. Also, the separation of the bilayers decreases as their fluctuations increase in amplitude. The bilayer thickness and area per molecule obtained from fitting of the quasi-molecular model to the CRISP data are in good agreement with the vesicle parameters. In addition, the same trend of decreasing repeat distance is observed in both cases, although the actual values are somewhat larger (i.e. slightly greater thickness of the inter-layer water film) in the supported bilayer case, due to differences in the confinement regime.

In summary, we have succeeded in producing a model bilayer system that is supported, but remains separated from the substrate by a substantial layer of water. Using the CRISP reflectometer, we have been able to characterise the phase behaviour of this bilayer system in detail, and have shown that the structural parameters of the bilayer change as they should across the 'main' bilayer transition. This means that the bilayer is minimally constrained, and therefore a realistic system for studying the interaction of biological agents with phospholipid bilayers.

Fig. H8.2. Quasi-molecular representation of the upper bilayer. The phospholipid head groups are parsed into Choline, Phospho, Glycerol and Carbonyl fragments, whilst the alkyl chain regions are split into methyl and methylene distributions. The SAM and lower layers (not shown) are represented by a standard 'box model' approach.

Fig. H8.3. Experimental (points) and simulated (lines) reflectivity profiles of the model bilayer at 15 °C under three water contrasts; D_2O (upper curve), 1:1 D_2O/H_2O (central curve) and H_2O (lower curve).

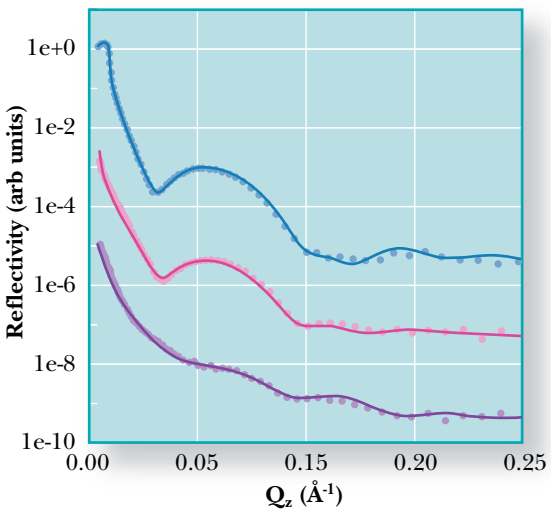

Ordering of surfactant mesophases at interfaces

Understanding the surface and near-surface structure in concentrated surfactant mesophases is essential for the optimisation of their extensive domestic, industrial and technological applications. Specular and off-specular neutron reflectivity measurements on CRISP and SURF have been used to show the rich surface behaviour that can exist in such systems. This has been demonstrated using two different di-alkyl chain surfactants, the anionic surfactant sodium bis(2-ethylhexyl) sulfosuccinate (Aerosol-OT, AOT), and the cationic surfactant di-dodecyltrimethyl ammonium bromide (DDAB).

R K Thomas, Z X Li, D McGillivray (University of Oxford), J Penfold (ISIS)

Concentrated mesophases are commonly present in the formulation of surfactants. The bulk phase behaviour in such systems is usually well established, but very little is known about their structure at interfaces. Previous work has shown that surface, interface and confined geometries can have a profound effect on the phase behaviour in such systems. The nature of the surface or near-surface structure is of central importance to understanding the role of the surface interaction in the widespread domestic, industrial and technological applications of detergents.

At low surfactant concentrations the phase diagram for AOT consists of an isotropic region (L_1, consisting of small spherical micelles). At higher concentrations there is a phase boundary between the L_1 region and an isotropic plus lamellar (L_1+Lα) phase. Small angle scattering, SANS, results show also that in the (L_1+Lα) phase the lamellar d-spacing decreases with increasing temperature. For 5 wt % AOT the lamellar spacing changes from 370 Å at 5 °C to 115 Å at 65 °C. This is contrary to expectation, where a lamellar phase swollen and stabilised by Helfrich undulations would give rise to an increase in d-spacing with increasing temperature. Although the electrolyte has a small effect on the structure (the d-spacing increases slightly with added electrolyte), the observed spacings are such that they must be stabilised by steric repulsion rather than double layer repulsion forces.

A similar structure is seen at the air-solution and liquid-solid (hydrophilic silica-solution) interfaces by specular neutron reflectivity. The specular reflectivity corresponds to a series of well-defined Bragg peaks (Fig. H9.1), characteristic of an ordered lamellar structure extending from the surface into the bulk fluid. The data correspond to a damped periodic function, extending ~ 0.5 microns from the interface into the bulk solution (see inset). The variation of the d-spacing at the interface with temperature is similar to that observed in the solution, except that it is slightly smaller, consistent with the interface partially suppressing fluctuations. The surface structure is more pronounced with increasing temperature: at lower temperatures the amplitude of the periodic function is smaller and the damping more profound, consistent with increased inter-layer roughness. A significant difference between the interface and solution behaviour is that the electrolyte has a much more dramatic effect on the ordering; the addition of 0.1M

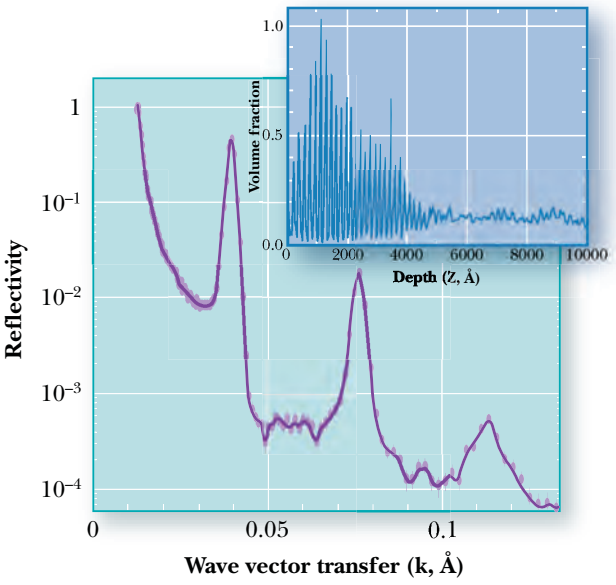

Fig. H9.1. The specular reflectivity for 2% h-AOT / D_2O at the hydrophilic silica/ solution interface at 35 °C. The solid line is a fit to the volume fraction distribution shown in the inset.

NaBr completely suppresses the surface structure, but only has a marginal effect on the solution structure.

Associated with the specular reflectivity is some pronounced off-specular scattering (Fig. H9.2). Whereas the specular reflectivity arises from structure perpendicular to the plane (q_z), the off-specular scattering arises from structural correlations in the plane (q_x). The strong off-specular features at constant $q_z \sim 0.04$ Å^{-1} and 0.08 Å^{-1}, and which are coincident with the specular Bragg peaks, are characteristic of conformal roughness. That is, they are associated with coherent in-plane fluctuations of the lamellae that are conformal from layer to layer. The curvature associated with the off-specular scattering at $q_z \sim 0.04$ Å^{-1} is due to refraction effects. Analysis of the off-specular data provides an estimate of the correlation length of the in-plane fluctuations. The correlation length is of the order of microns, and increases with increasing temperature. The additional off-specular scattering, emanating from the first order Bragg peak, comes from an effect analogous to Newton's interference fringes, arising from scattering from irregularities at the upper surface of a thin film with a smooth lower surface.

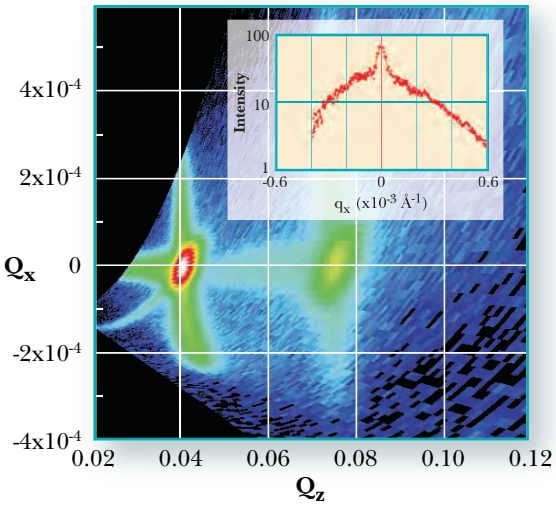

Fig. H9.2. Off-specular scattering (q_x-q_z) for 2% h-AOT in D_2O at the air-solution interface at 25 °C and for q of 0.8°. The inset shows the scattered intensity verses q_x for a 2% h-AOT in D_2O at the liquid-solid interface at a q_z of 0.07 Å^{-1}.

A change in the internal structure with increasing temperature can qualitatively explain the trends observed in both the specular and off-specular reflectivity. At low concentrations of AOT the L_1 and Lα phases coexist, becoming a pure Lα phase at higher concentrations. A change in the headgroup conformation with increasing temperature and a progressive dehydration of the headgroup (as reported elsewhere) will result in a decrease in the area/headgroup and a reduction in curvature. This will increase the Lα fraction and result in a reduction in the d-spacing. Such conformational changes are also consistent with an increase in the membrane rigidity and a decrease in steric repulsion; further enhancing the likelihood of a decrease in the d-spacing. This is consistent with the increased structural order, and the increase in the in-plane correlation lengths that are observed with increasing temperature.

Some preliminary results from DDAB provide an interesting contrast to the results from AOT. At low surfactant concentrations DDAB has a complex phase behaviour and a tendency spontaneously to form spherulites, or multi-lamellar vesicles. This gives rise to a rather different pattern in the specular and off-specular reflectivities compared to AOT (see Fig. H9.3). The characteristic features of the scattering show the same temperature dependence as AOT. The specular reflectivity consists of a complex series of interference fringes, which have a characteristic length scale ~ 1000 Å. It is attributed to the adsorption of spherulites at the interface. The off-specular scattering occurs at values of constant q_z, as observed with AOT, and is attributed to fluctuations within the multi-lamellae.

Fig. H9.3. Specular and off-specular scattering (λ, q) for 1% h-DDAB / D_2O at the hydrophilic silica-solution interface at 60 °C and q of 0.35°.

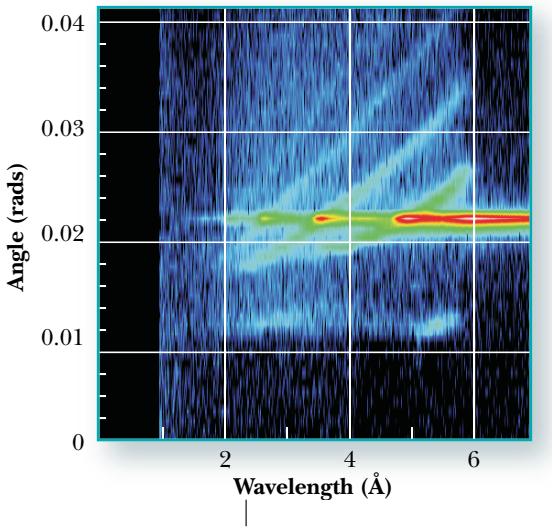

Vector magnetometry in spin-engineered double superlattices

Exchange bias refers to the unidirectional magnetic anisotropy that manifests itself as a hysteresis loop that is not centred around zero field for a coupled ferromagnetic (F) - antiferromagnetic (AF) bilayer system. This useful property is extensively used in magneto-resistive recording heads but is still not completely understood – in spite of the fact that it was first discovered in the mid 1950's. Artificially created ferromagnets and antiferromagnets have enabled the study of the magnetic configuration in a controlled manner using neutron reflectometry and polarisation analysis.

C H Marrows, M Ali, A T Hindmarch, B J Hickey (University of Leeds) S Langridge, S Foster, R Dalgliesh (ISIS)

Since the earliest observation of exchange bias by Meiklejohn and Bean in 1956, there has been much experimental and theoretical interest in understanding its origin, particularly in the past few years owing to its central position in magnetic recording technology. This unidirectional anisotropy relies on the interfacial coupling between a ferromagnet (FM) and an antiferromagnet (AF). This was first observed in the particulate system of the naturally occurring ferromagnet Co and the anti-ferromagnet CoO. The exchange bias then arises from the competition between the Zeeman energy and exchange coupling across the AF-FM interface. It is such a coupling in ultrathin FM/AF spin engineered bilayers that provides the magnetic pinning in the latest generation of spin valve heads in computer hard disks. A significant experimental difficulty in unraveling the exchange bias problem is the inability to examine in detail the spin structure in the AF layer, in particular at the buried interface.

Simple models overestimate the magnitude of the exchange bias by one to two orders of magnitude and do not reproduce the enhancement of the coercivity of the FM layer that commonly accompanies the loop shift. To explain this discrepancy requires the introduction of domain walls either perpendicular or parallel to the surface. In the former, defects at the interface produce a random field which breaks the AF layer into domains. In the latter, the exchange energy is spread through the anti-ferromagnet in an analogous fashion to an exchange spring.

To address this second idea we have produced artificial superlattices of Co and Ru: the sign and magnitude of the exchange coupling between neighbouring Co layers can be tuned by selecting the correct Ru thickness. Our sample comprises an antiferromagnetically ordered block of ten Co layers coupled ferromagnetically to a ferromagnetically ordered block of another 10 Co layers. We have created an artificial model exchange bias system that can be probed internally using neutron reflectometry. The inset to Fig. H10.1 shows the nominal superlattice structure of the form Si(001)/Ta(75Å)/[Co(35Å)/Ru(15Å)]$_{10}$/Co(35Å)/[Co(60Å)/Ru(10Å)]$_{10}$/Co(60Å)/Ta(25Å) along with the room temperature magnetisation loop. Individually the AF and FM components of the superlattice exhibit good coupling. The repeat distances of the individual multilayer blocks have been chosen to yield Bragg peaks at different points in reciprocal space. This

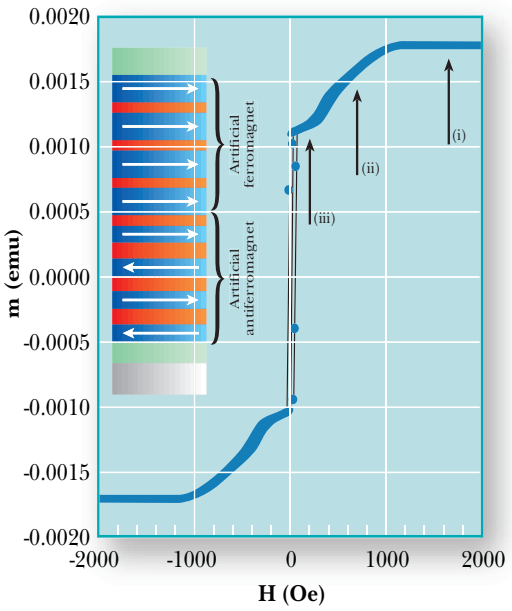

Fig. H10.1. The room temperature magnetisation loop for the Co/Ru superlattice. The inset shows the superlattice structure and the F and AF magnetic components of the Co layers indicated by the arrows.

structure is then directly analogous to exchange biased bilayers consisting of natural AF and FM materials with layers of Co taking the place of atomic planes of spins.

To understand the magnetic coupling in this system we have performed polarised neutron reflectivity measurements with polarisation analysis (PNR-PA) of the reflected beam. Components of the sample magnetisation collinear with the incident

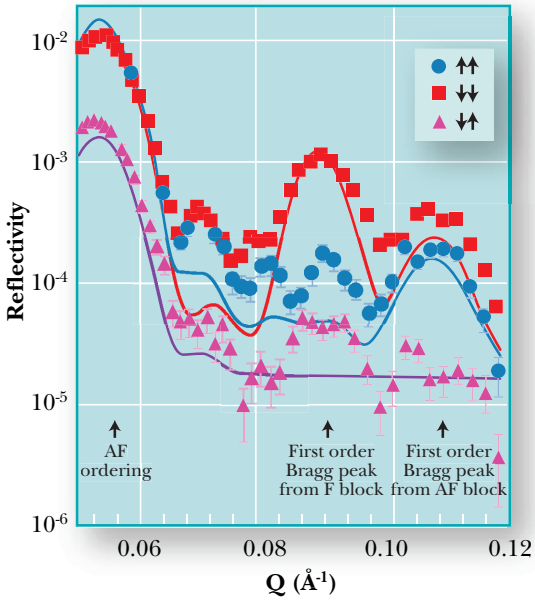

neutron spin do not alter the spin eigenstate of the neutron after scattering, i.e. non-spin flip scattering, whilst perpendicular components can flip the scattered neutron spin i.e. spin flip scattering. For such systems, analysing the spin of the scattered neutron beam as a function of momentum transfer Q provides the microscopic in-plane vector magnetisation depth profile and allows us directly to study the depth dependence of the magnetic coupling.

With reference to the magnetisation loop, there are three clearly identifiable phases as indicated by the vertical arrows. Using PNR-PA we have investigated the magnetisation process as a function of applied field. Clearly, for fields close to point (i), there is a saturation of both the FM and AF blocks of the multilayer. As the field is reduced towards point (ii) the AF block exhibits a spin-flop phase in which the moments are focused around the applied field direction. On a further reduction of the field, a new phase is visible, where it is necessary to connect the spin-flopped AF and saturated FM blocks with a bilinear coupling, leading to a twist in the magnetic structure spread over several layers The spin dependent polarised neutron reflectivity is shown in Fig. H10.2 for an applied field of 150 Oe. Noticeably, there are AF components for both the spin flipped and non-spin flipped contributions. Such a situation would arise for a twisted, or spring-like magnetic configuration. This is the equivalent of an in-plane domain wall in a natural AF/FM system.

To aid in the analysis of the neutron data we have performed energy minimisation calculations of the magnetic structure. These calculations are in excellent qualitative agreement with the observed magnetisation loops. By using these magnetic configurations and the structural parameters determined by X-ray reflectivity measurements as input for the neutron simulation we are able to identify the spin flop phase and the parallel domain wall as shown in Fig. H10.3. This represents the first observation of such a parallel domain wall in an artificial system. Such a wall reduces the interfacial energy by spreading the exchange energy through the AF layer. In no field region does the spring extend significantly into the FM region.

To extend these measurements, we propose to artificially control the in-plane anisotropy, which in the samples reported here is small, to investigate its influence on the exchange bias and the magnetic configuration.

Fig. H10.2. The observed polarised neutron reflectivity with polarisation analysis. The arrows indicate the orientation of the neutron eigenstate relative to the applied magnetic field. For clarity only one of the spin flip channels is plotted. The solid lines are simulations for the spring state described in the text.

Fig. H10.3. The calculated magnetic configurations for applied fields of 600 Oe (A) and 130 Oe (B). The spin flop and spring phases are clearly identifiable. (C) is a view o f (B) from above.

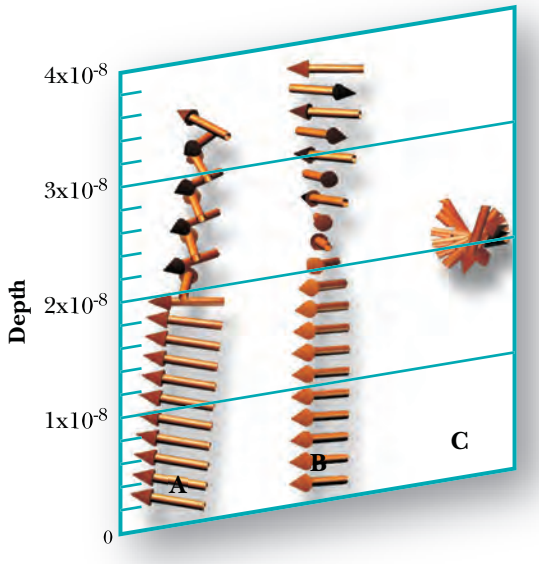

Polarization analysis of off-specular neutron scattering from magnetic domains and rough interfaces

Specular neutron reflectivity is commonly used as a powerful tool in determining the transversal scattering length density (SLD) profile near the surface of thin films. Lateral fluctuations in the SLD, such as the presence of magnetic domains and rough interfaces between layers, can be studied by the off-specular scattering of neutrons. The CRISP reflectometer was used to perform specular and off-specular polarized neutron reflectometry experiments on FeCoV/TiZr multilayers to obtain a detailed description of the orientations of the magnetic moments inside the FeCoV layers and at the FeCoV/TiZr interfaces.

RWE van de Kruijs, ***H Fredrikze***, ***MTh Rekveldt*** *(Delft University of Technology)* ***VA Ul'yanov***, ***NK Pleshanov***, ***VM Pusenkov***, ***AF Schebetov***, ***VG Syromyatnikov***, *(Petersburg Nuclear Physics Institute, Russia),* ***S Langridge*** *(ISIS)*

A high amount of off-specular neutron scattering was recently observed in FeCoV/TiZr multilayers. The origin of the scattering was attributed to the presence of magnetic domains and rough interfaces. The experiments described here focus on the polarization analysis of the off-specular scattering to obtain information on the orientations of the domains and on the orientations of the interfacial moments (magnetic roughness).

At an applied field of H=7 kA/m, close to the coercive field observed in the hysteresis loop, the non-spin-flipped specular reflectivity curves for both incident beam polarization directions are similar and no spin-flipped reflectivities are detected. These observations are explained by the fact that the neutrons effectively probe a structure with net magnetization close to zero. Off-specular reflectivity data predominantly consists of a diffuse band of scattering without any pronounced Bragg enhancements, showing that no correlations exist between the domain orientations throughout the multilayer stacking. The polarization analysis of the diffuse scattering shows a complete depolarization for all neutron wavelengths, indicating an isotropic distribution of domain orientations.

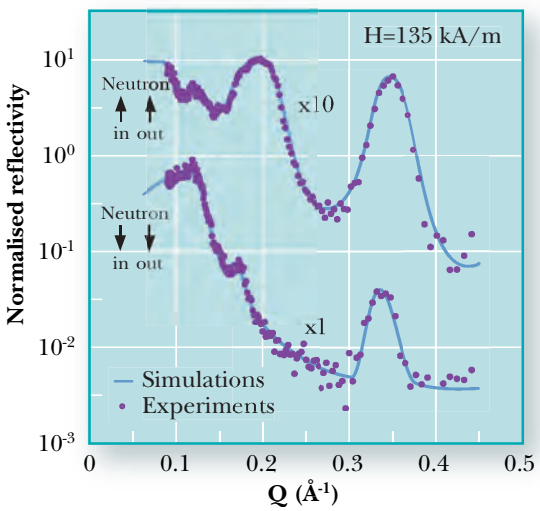

Fig H11.1. Experimental and simulated specular reflectivity curves at saturation.

Fig. H11.1 shows the specular reflectivity curves obtained for a field where the hysteresis loop was completely saturated. The absence of any spin-flip data, together with the absence of the diffuse scattering from domains (see Fig. H11.2), confirms the parallel alignment of all layer magnetizations at saturation. The data are analyzed by fitting reflectivity calculations, obtained by a standard matrix formalism, to the experimental data. When assuming equal shapes for the FeCoV/TiZr and TiZr/FeCoV intermixing regions, no good quality fit could be obtained. The calculations shown in Fig. H11.1 (solid lines) were obtained by using a more detailed description of the intermixing regions in the model calculations, including a nonmagnetic interfacial layer of approximately 1.0 nm and unequal r.m.s. heights of the intermixing regions: σ(FeCoV/TiZr) = 3.0 nm, σ(TiZr/FeCoV) = 2.0 nm.

Although the dimensions of the intermixing regions are readily obtained by fitting the specular reflectivities, no information is obtained about the lateral properties of the interfaces. By studying the off-specular scattering of neutrons, information about the in-plane correlation lengths and fractal dimensionalities of the rough interfaces becomes available. Fig. H11.2 shows the off-specular spectra for the saturated sample, exhibiting clear lines of enhanced scattering. The ↑↑ and ↓↓ spectra can be reproduced by model calculations of interfacial scattering using a Distorted Wave Born Approximation, including dynamic multilayer effects. Fig.

H11.3(a) shows simulations using a Gaussian surface roughness (fractal dimensionality = 0.5) and an in-plane correlation length of 5 µm. The thickness, roughness and SLD of all layers were taken from the analysis of the specular data. The roughness of all layers is assumed to be correlated by a perfect vertical reproduction of the roughness. An uncorrelated roughness (Fig. H11.3(b)) shows no distinct lines of enhanced scattering in the model calculations.

From the polarization analysis of the spectra at saturation, it was found that spin-flipped off-specular scattering could still be observed at saturation. The non-zero spin-flip scattering indicates the presence of magnetic moments that are not fully aligned with the applied field. The fact that the spin-flip scattering is enhanced along the lines identified with interfacial scattering suggests that the unaligned moments are situated at the chemically rough interfaces and that their orientations are correlated throughout the multilayer stacking. The in-plane correlation length of this magnetic roughness is comparable in size to that of the chemical roughness.

In summary, we have performed a full polarization analysis of the off-specular scattering from FeCoV/TiZr multilayers. Measurements close to the coercive field show completely depolarized diffuse scattering spectra that are linked to the presence of magnetic domains with no preferred orientations and no correlations throughout the multilayer stacking. At saturation, enhancement of the off-specular scattering along specific lines is caused by chemically rough interfaces, correlated over large vertical distances in the multilayer. The presence of spin-flip scattering along these lines is attributed to a correlated magnetic roughness.

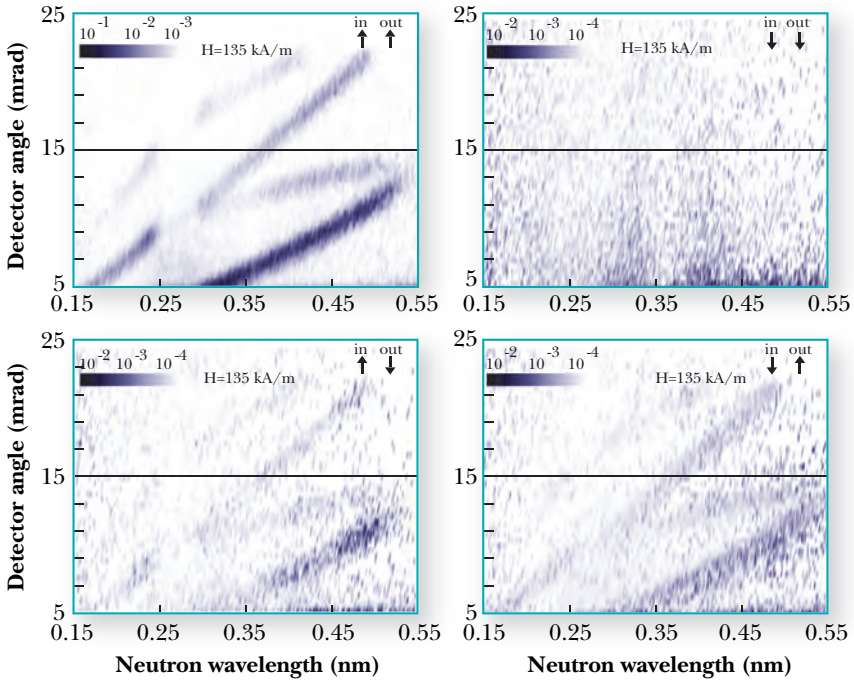

Fig. H11.3. Model calculations of off-specular neutron reflectometry from correlated (A) and uncorrelated (B) interfaces.

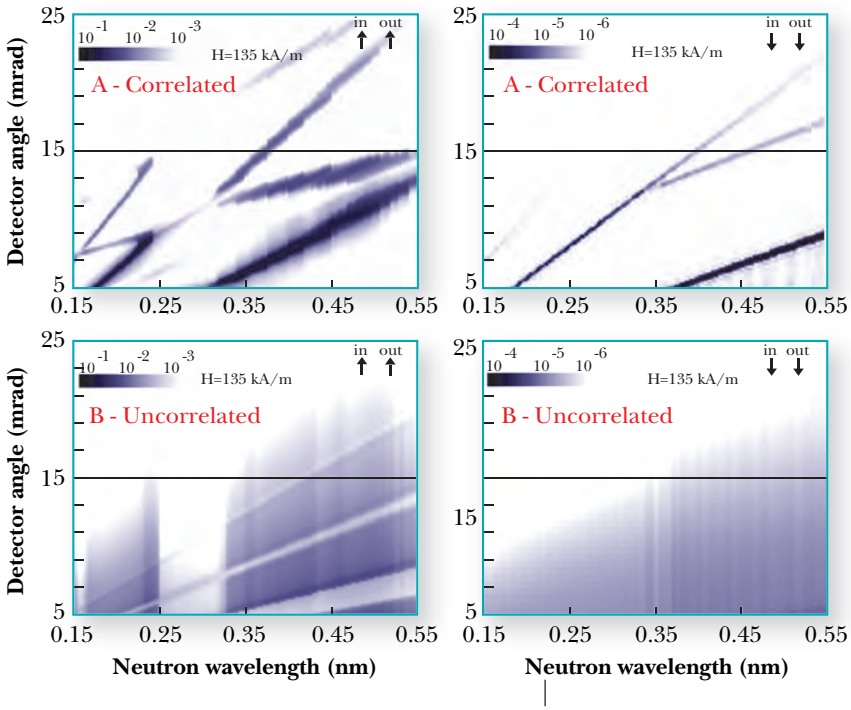

Fig. H11.2. Off-specular neutron reflectivity spectra for the saturated multilayer.

Mixed surfactant microemulsions

Mixed surfactants are commonly used to enhance the performance of products. To understand their behaviour, knowledge of their composition at different interfaces is required. The structure and composition of mixed surfactant, water in oil microemulsion droplets has been studied by small angle neutron scattering using four different contrast schemes. The results shed light on surfactant behaviour in real-life situations.

J Eastoe, A Bumajdad (Bristol), R K Heenan (ISIS)

Surfactant mixtures often give rise to enhanced performance over their individual components, and so surfactant blends are employed in a wide variety of practical applications. To understand the molecular origins of 'surfactant synergism' it is necessary to measure directly the interfacial composition at different types of interface, particularly air/water, oil/water and liquid/solid. Neutron reflectivity has been employed at ISIS to study surfactant mixtures at an air/water interface, but little is known about the corresponding oil-water systems. Small angle neutron scattering (SANS) is able to achieve this goal, for curved interfaces, using neutron contrast variation. Model systems are used in these studies, which are microemulsions of well defined nanometre sized water droplets in an alkane (heptane) solvent. The stabilising layers were surfactant mixtures with a carefully controlled composition. SANS measurements were carried out on LOQ at ISIS (and also at the ILL) along with complementary measurements of phase diagrams, NMR diffusion coefficients, and electrical conductivity.

The mixed surfactants used were chosen to have the same dodecyl hydrophobic group ($C_{12}H_{25}$ chains) but different hydrophilic head groups. Starting with the twin tailed DDAB (didodecyldimethylammonium bromide) the effects of adding different single tailed surfactants, DTAB (dodecyltrimethylammonium bromide), SDS (sodium dodecylsulphate) and $C_{12}E_5$ (pentaethylene glycol monododecyl ether) were investigated. The amount of water taken up in mixed surfactant microemulsion droplets is shown in Fig. H12.1 where w_{max} is the maximum number of water molecules per surfactant molecule. With 20-

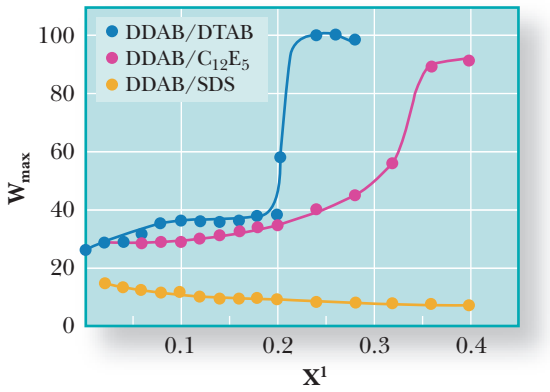

Fig. H12.1. Effect of mixing different single chain surfactants with di-chain DDAB on maximum water uptake for water-in-heptane microemulsions. X^1 is the mole fraction of single chain and the total surfactant concentration is always 0.1M.

30% of single chain surfactant in the mixture w_{max} is greatly enhanced for DTAB and $C_{12}E_5$, a synergistic effect which might be of benefit for practical uses, whilst for SDS there is an antagonistic effect and w_{max} decreases. Direct measures of the surfactant film composition and droplet sizes are required to discover whether the droplets truly have a mixed surfactant film and whether 'ideal mixing' occurs. In the ideal case the composition of the film is the same as the actual mixing ratio in the bulk. Alternatively there might be separate populations of droplets containing the individual surfactants and/or some surfactant remaining as dry micelles.

Using deuterated DDAB, these key questions may be answered by SANS using two different 'shell contrast' microemulsions, and fitting data simultaneously with 'core' and/or 'drop' contrasts as illustrated in Fig. H12.2. With D_2O, and d-heptane and both surfactants all hydrogenous, the microemulsion has 'shell-A' contrast. The SANS signal has a characteristic weak oscillation at high Q caused by

interference in the diffraction pattern between the inner and outer radii of the surfactant shell. In shell-B contrast the only deuterated component is DDAB which is mixed with the hydrogenous second surfactant. The signal is comparable to that from 'shell-A' contrast but is particularly sensitive to the film composition. The 'core' contrast shows scattering from the water cores alone, whilst 'drop' contrast that from the whole water plus surfactant droplet. Taken all together the absolute intensities of the fitted scattering patterns are sensitive to the film composition and to the nature of the mixing. Some results are shown in Fig. H12.3.

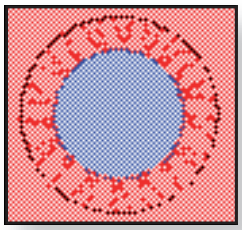

Core contrast

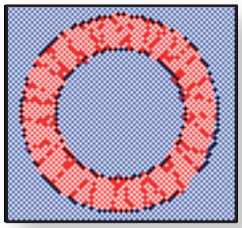

Shell A

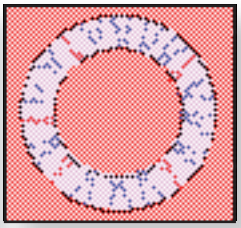

Shell B

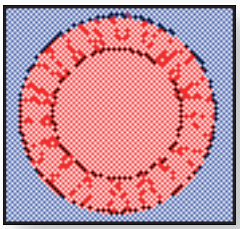

Drop

Not only is considerable care required in sample preparation but the bulk density of the surfactant film needs to be known. Using the value measured for molten DDAB (0.87 g.cm^{-3}) and assuming ideal mixing gives good agreement with the SANS experiments for DDAB with DTAB or $C_{12}E_5$; whilst the 0.85 g.cm^{-3} from an extrapolation of density measurements of DDAB microemulsions gives a line slightly lower. (The dotted lines in Fig. H12.3 give wider limits of 0.9 and 0.8 g.cm^{-3}.) Thus the SANS results confirm a model of ideal mixing for the two surfactants which exhibits a synergistic effect, an increasing w_{max} in Fig. H12.1. For $C_{12}E_5$ one would normally expect a rather high critical microemulsion concentration below which it prefers to dissolve as monomer in the heptane solvent. The composition of the film determined here suggests that all the $C_{12}E_5$ is in the mixed surfactant film and very little free in the solvent.

With higher fractions of DTAB mixed with DDAB ($X^1 > 0.2$) the SANS signals are not easily fitted to a model of spherical droplets, but with supporting evidence from electrical conductivity and NMR diffusion coefficients the system appears to form a bicontinuous structure, which is giving rise to the very high values of w_{max} in Fig. H12.1.

With SDS the head group has opposite charge to that of DDAB, so would be expected to closely associate with each other. A reduced repulsion between the head groups favours a lower droplet radius and hence lower w_{max}. With composition $X^1 \sim 0.2$ the SANS signal indeed shows a decrease in mean core radius from 35 Å to 20 Å.

SANS is a powerful tool to reveal not just the structure but also composition of quite complex colloidal systems, using neutron contrast variation. The confirmation of ideal mixing in typical mixed surfactant microemulsion systems is an important result, as well as the realisation that more complex bicontinuous structures may form in some cases. The findings provide new insight into stabilisation of practical systems such as emulsions and foams where surfactant mixtures are widely used.

Fig. H12.2. Schematic view of the contrast variation scheme used for mixed surfactant microemulsion droplets; red regions are hydrogenous, blue are deuterated. In the 'shell-B' case the shell (pink) is a mixture of deuterated and hydrogenous surfactants.

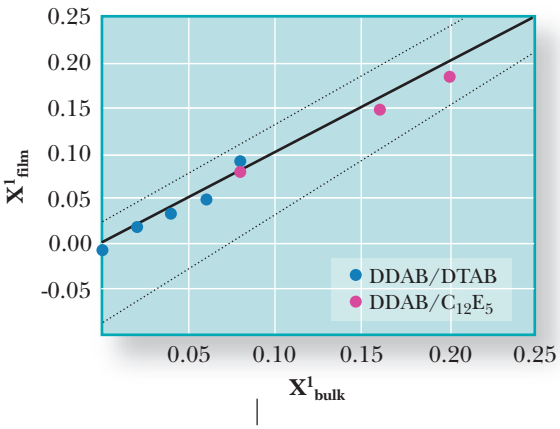

Fig. H12.3. Composition of mixed surfactant films in microemulsion droplets (from simultaneous fits to SANS contrast variation data) versus known bulk composition. Solid line assumes ideal mixing and a film density of 0.87 g.cm^{-3} whilst the dotted lines are for 0.90 (upper) and 0.80 (lower).

Influence of flow on polymer crystallisation

The physical properties of polymer-based products rely as much on the detail of the processing conditions as they do on the ingenuity of the chemist. In the case of semi-crystalline polymers the processing conditions strongly influence the morphology of the final product and so define the physical properties. This can lead to a wide variety of applications for a single material. Polyethylene (-$[CH_2]_n$-) for example, with sales of some 50 Mtonnes/ year, has applications ranging from high modulus ropes used in space through greenhouse cladding, electrical cabling and water piping to replacement hip-joints. The development of a quantitative understanding of the processes of flow and crystallisation remain amongst the key challenges facing polymer physics.

J J Holt, G R Mitchell *(University of Reading),* ***C K Chai, B P Lavera*** *(France)*

In product processing, a polymer melt may be subject to a flow field immediately before crystallisation, induced by cooling, takes place. In many instances the flow history has no effect on the crystallisation process. However, recent work has shown that the presence of a small proportion of very long polymer chains in the melt can have quite dramatic effects. This is significant because commercially produced polymers have broad molecular weight (MW) distributions; the 'longest' molecule may contain over a million CH_2 units (giving it a 'contour length' of over 100 mm) even though most of the polymer molecules may be many hundreds of times shorter.

Fig. H13.1a shows a transmission electron micrograph (TEM) of a medium MW polyethylene sample which was subjected to shear flow and then crystallised. The micrograph shows a classic spherulitic structure with no evidence of the flow history. In contrast, the addition of a small fraction (~10% w/w) of a linear polyethylene with a high MW to a similar sample results in a highly anisotropic morphology (Fig. H13.1b); the effect could not be more striking.

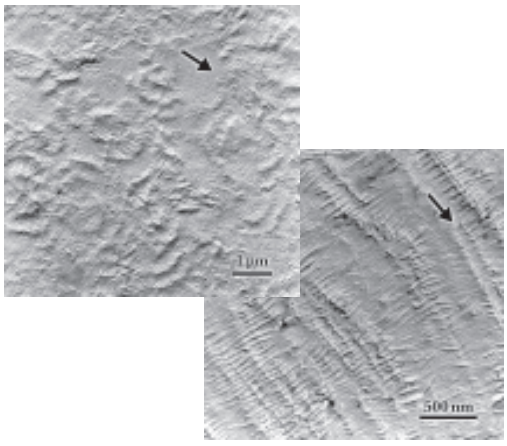

Fig. H13.1. Top: TEM of a crystallised branched polyethylene material following the imposition of shear flow ($g=10\ s^{-1}$). The arrow indicates the flow direction. Bottom: As for top image but with 10% w/w of a higher MW linear polyethylene.

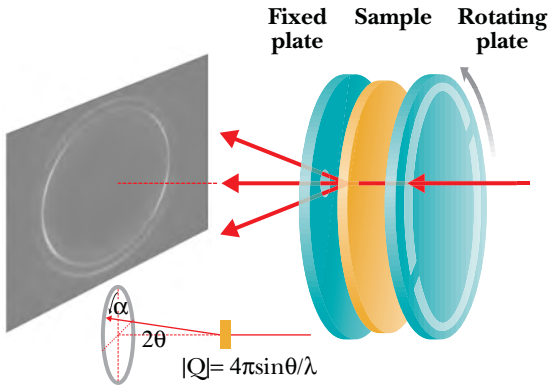

Fig.H13.2. A schematic of the shear flow cell.

It is thought that the very long polymer chains may act as nucleating sites for the development of a preferred crystal orientation. Since the longest chains will have the most interactions, it is highly likely that they will be preferentially extended.

A collaboration between the University of Reading and BP Chemicals has utilised in-situ, time-resolved wide-angle X-ray (WAXS) scattering measurements to provide quantitative parameters that describe the crystal growth process, and in-situ small-angle neutron scattering (SANS) on isotopically labelled polymer mixtures under shear flow to measure the degree of chain extension and orientation in the melt. Coupled with ex-situ TEM, these techniques have provided new insights into the flow and crystallisation processes.

Fig. H13.2 shows a schematic of the shear flow cell developed for these complementary X-ray and neutron scattering measurements. It operates in the temperature range 20 – 300 °C, can cool at ~50 °C min^{-1}, and generate shear rates between 10^{-3} - 10^{3} s^{-1}.

Measurements performed on Station 16.1 at the Daresbury SRS have provided data with a time resolution of ~1 second. They reveal that the crystal growth mechanism has a strong dependence on the shear strain (shear rate x time) applied before the sample is quenched to the isothermal crystallisation temperature. Fig. H13.3 shows two wide-angle X-ray scattering patterns from different stages in the crystallisation process.

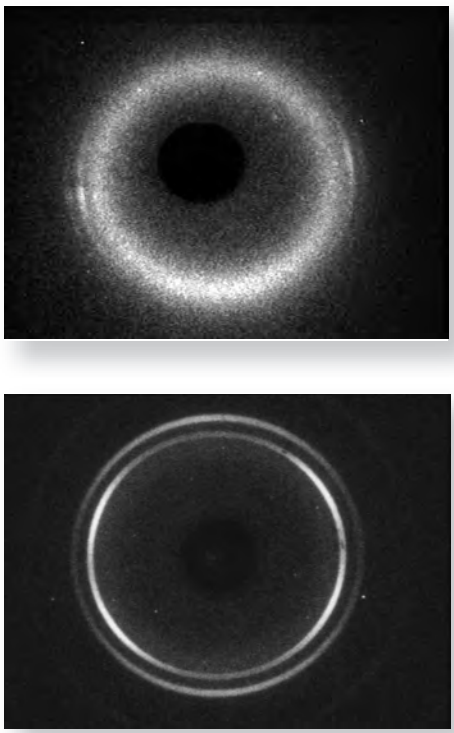

Fig.H13.3. WAXS patterns showing the 110 and 200 reflections for polyethylene during crystallisation after a shear rate of $1s^{-1}$.

The first few crystals that form show a fibre-like texture, whereas subsequent crystallisation involves a different crystal texture with tilted or twisted lamellae. The final pattern shows no evidence of the initial fraction of crystals; however, an observation which underlines the value and importance of the time-resolved measurements. Systematic studies of the crystal growth process show that it is largely independent of the shear rate but strongly dependent on the shear strain. In fact there appears to be a critical shear strain required for anisotropic crystal growth.

SANS measurements on LOQ were used to evaluate the extent of molecular anisotropy during shear flow that leads to the dramatic effects shown above. Fig. H13.4 shows the scattering patterns from a mixture of deuterated (medium MW with short-chain branching) and hydrogenated (linear high MW) polyethylene prior to, and during, shear. The degree of anisotropy in the scattering is clearly very weak, but the level of preferred crystal orientation that results is very high.

These patterns have been analysed in terms of a series of spherical harmonic functions $I_{2n}(Q)$, where n=1,2,3…. These provide a sensitive test of the degree of anisotropy. If the scattering is isotropic, terms for n > 0 are zero. A particular feature of such analyses is the largely Q-independent nature of the anisotropy. Molecular modelling shows that this type of anisotropy can only come from chains, or clusters of chains, which have been substantially extended in the flow direction. In fact, the magnitude of $I_2(Q)$ can be related to the fraction of extended chains. Significantly, it is found that as the fraction of high MW linear polyethylene in the blend is increased, the degree of preferred orientation of the crystals that grow on cooling from the anisotropic melt also increases.

These observations are the first of a series which it is hoped will enable models to predict the final structure and properties of polymer melts and blends on the basis of the MW distribution, the chemical topology and the flow conditions.

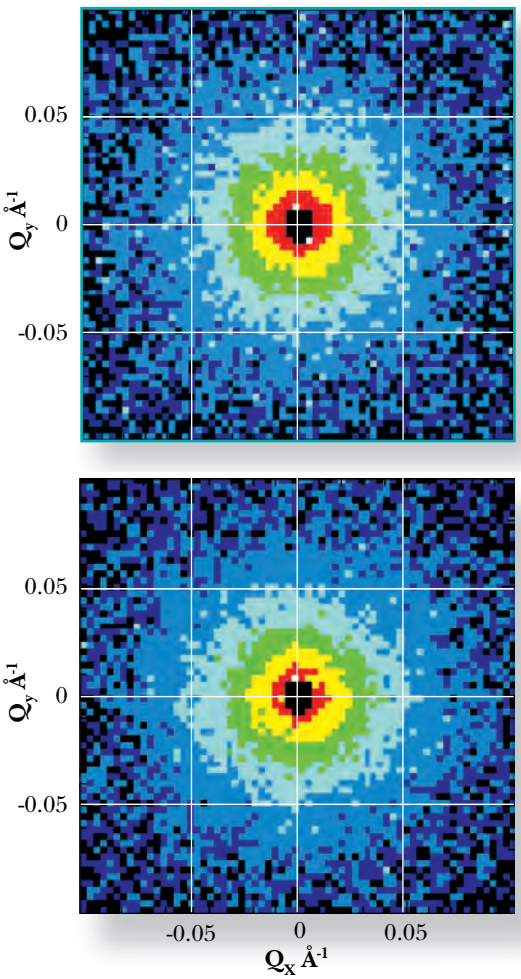

Fig. H13.4. SANS from a mixture 90% branched (deuterated) and 10% linear high MW (hydrogenated) polyethylene at 156 °C. Upper: no shear. Lower: g=1 s.

Exploring the standard model of rare earths through the investigation of the p-T phase diagram for erbium

The importance of magnetoelastic coupling in the physics of rare earth metals is well established. Recent developments in neutron scattering have been an essential element in the refinement of the standard model describing magnetism and magnetic excitations in the pure rare earth metals. Diffraction studies of the pressure-temperature phase diagram of erbium on PRISMA in combination with high pressure resistivity measurements have revealed a change of phase at 5 kbar that can only be explained by a change in the Fermi-surface topology. Our studies have been extended to investigate the relationship of the conical phase to the cycloidal phases found in erbium.

M Ellerby *(University College London),* ***M J Bull*** *(ISIS),* ***J Jensen*** *(Niels Bohr Institute, Denmark),* ***K A McEwen*** *(University College London)*

In recent years erbium has attracted considerable attention due to its complex magnetic phase diagram. Neutron diffraction has revealed three basic types of magnetic structures at atmospheric pressure. Below T_c = 18 K the structure is *conical* with moments ordered antiferromagnetically in the basal plane and ferromagnetically parallel to the *c*-axis with an ordering wave vector *of* $Q = 5/21\,c^*$. For 18 K < T < 52 K the moments are constrained to the *a-c* plane and ordered antiferro-magnetically along both axes. This elliptically polarised *cycloidal structure* locks to the lattice period in a number of commensurable phases. Between 52 K and 85 K the magnetic structure is *c-axis modulated* with the moments constrained to the *c*-axis and the size of the moment varying sinusoidally from one basal plane to the next with an ordering wave vector close to $Q = 2/7\,c^*$. Early magnetostriction studies revealed sharp changes in the values of the lattice constants at T_c. This behaviour of the strain parameters has been used to predict that the magnetoelastic energy would cause the cone structure to become unstable under a hydrostatic pressure of approximately 2.5 kbar.

Fig. H14.1(a) shows the measured and calculated (standard model) electrical resistivity at T = 4.5 K as a function of hydrostatic pressure. To explain why the change in the resistivity between the two magnetic phases is twice that observed at T_c and ambient pressure, it was tentatively proposed that the pressure-induced alteration of the magnetic structure is accompanied by an abrupt change of the ordering wave vector from $Q = 5/21\,c^*$ in the cone to the value of $2/7\,c^*$ above 5 kbar.

In Fig. H14.1(b) the pressure dependence of Q shows a number of features.

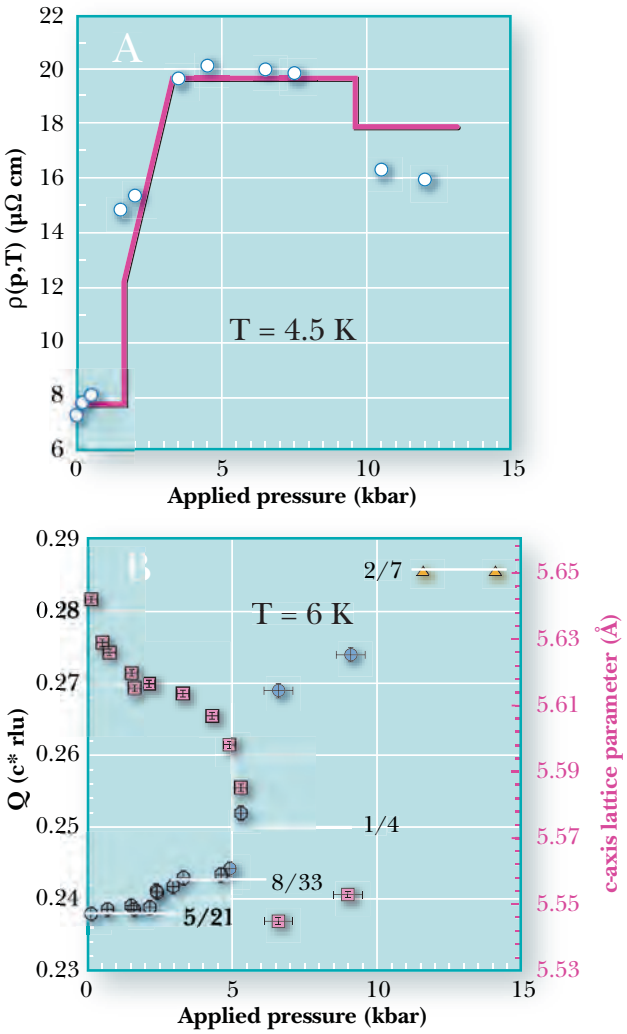

Fig. H14.1. (A) The pressure dependence of the resistivity at 4.5 K. Measured (circles) and calculated (solid line) for increasing pressure. (B) The wave vector Q *at T = 6 K (circles) including previous measurements (triangles) and the* c*-axis lattice parameter (squares). The horizontal lines indicate the positions of commensurate magnetic structures.*

Between 1.5 kbar and 3 kbar there is a smooth transition to a novel commensurate phase with $Q = 8/33\,c^*$, which persists until p = 4.8 kbar; above which there is a rapid increase. The Bragg intensities decrease sharply above p=4.8 kbar signifying the collapse of the

ferromagnetic cone to the cycloidal structure in a first-order transition. This is in contrast to the resistivity which is strongly modified already at 1 kbar. The reason for this difference is not clear but a non-uniform distribution of strains in the sample near the transition may cause a large increase of the resistivity while the bulk of the material is still in the cone phase. The present study shows that the change of the ordering wave vector between ambient pressure and 5 kbar is small. Clearly, the doubling of the resistivity change at the transition at 4.5 K in Fig. H14.1a, in comparison with that observed at T_c, is not caused by a large change of the ordering wave vector. Alternatively the Fermi-surface topology could become modified due to changes in the lattice constants. Analysis of the lattice parameter with pressure at 6 K (Fig. H14.1(b)) reveals an overall decrease in the c-axis parameter by approximately 1% between 1 bar and 5 kbar. This implies that effects on the Fermi surface due to the variation of the ordering wave vector away from $Q = 2/7c^*$ are no longer active after the strain-induced modification of the Fermi surface.

To investigate further the phase diagram (Fig. H14.2) we made a series of temperature sweeps at constant pressure. Fig. H14.3(a) shows the results for 3.5 kbar. At $T = 13$ K the position of these magnetic satellites increased rapidly, 'locking' to a value of $Q = 1/4c^*$ until $T = 22$ K where it increases abruptly. The c-axis lattice parameter also shows a sharp decrease at 13 K after which it remained fixed; the decrease corresponds to the collapse of the ferromagnetic phase. Measurements made at $p = 6.5$ kbar (Fig. H14.3(b)) did not show the sharp changes observed at lower pressures. The smooth change suggests an incommensurate behaviour. The c-axis parameter decreases, with no marked changes at $T = 21$ K.

In conclusion we have found that the ferromagnetic phase is more robust to hydrostatic pressure than expected and that changes in the crystal lattice are more potent, influencing changes in the Fermi surface and stabilising a new antiferromagnetic magnetic phase in erbium that was previously unknown.

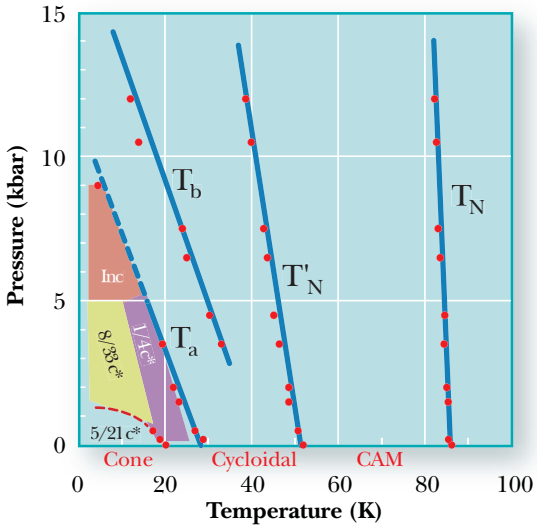

Fig. H14.2. The p-T phase diagram for erbium. The solid black circles represent data taken from resistivity measurements; the three coloured regions are described as commensurate $Q = 8/33c^*$ (yellow), incommensurate 'Inc.' (red), and commensurate $Q = 1/4c^*$ (purple). The fractions represent the period of antiferromagnetic order. The thin dashed line rising at $T \sim 18$ K and reaching a value of $p \sim 1.5$ kbar represents the earlier prediction of ferromagnetic collapse. Other lines are guides to the eye.

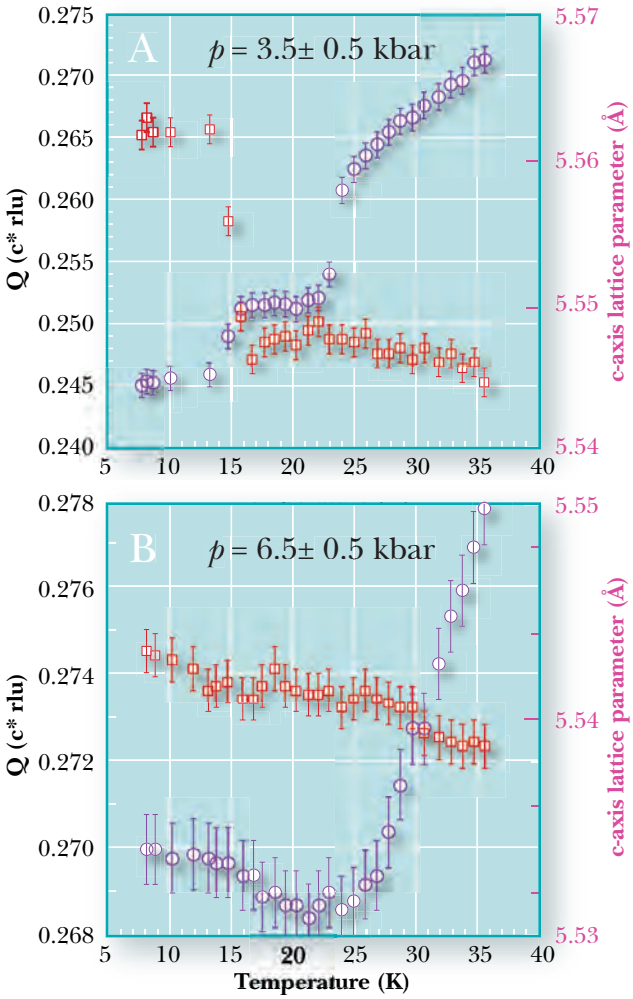

Fig. H14.3. (a) Temperature dependence of the magnetic satellites, Q, (open circles) and c-axis lattice parameter (open squares) for $p = 3.5$ kbar and (b) the temperature dependence of the magnetic satellites, Q, (circles) and c-axis lattice parameter (squares) for $p = 6.5$ kbar.

Dispersive excitations in different forms of SiO_2

Features which appear to show dispersion have been seen in inelastic neutron scattering measurements on vitreous silica. Their origin has been the source of much speculation, including claims that they are a direct observation of fast sound. Similar forms have now also been seen in scattering experiments on the crystalline analogues of the glass: α–cristobalite and α–quartz, making it likely that such 'dispersion' is in fact due to the short range order of the SiO_4 tetrahedra rather than some long-range collective mode.

M Arai, M Nakamura, T Otomo, Y Inamura (KEK, Japan), S M Bennington (ISIS)

Glassy or disordered materials have universal properties that are linked to their low energy dynamics, including a specific heat capacity that is larger than would be expected from a Debye model and a plateau in the thermal conductivity. A large number of measurements have been performed over the last few years in an attempt to understand these universal properties. Recent measurements on crystalline and amorphous forms of SiO_2 using the MARI spectrometer have observed features that appear to show dispersion (Fig. H15.1); a highly surprising and controversial result given the lack of periodicity in the amorphous forms.

These 'dispersive' features are resolved when the data is transformed into a generalised density of states G(Q,ω).

The scattering from α–cristobalite is very similar to that from the glass, much more so than that from α–quartz. This is reflected in the similarities in their densities (2.33 g/cm3 for α–cristobalite and 2.20 g/cm3 for the glass) compared to that of α–quartz (2.65 g/cm3) and the fact that first sharp diffraction peak of the glass corresponds very well with the strong (101) Bragg peak in α–cristobalite. Despite this, 'dispersive' features are seen in all three polymorphs implying that they are related to the one common feature of the three materials, namely the SiO_4 tetrahedral unit. This is reinforced by the observation that the 'dispersion' is unrelated to the first sharp diffraction peak in the glass, which we know is related to the materials medium to long-range order.

The low energy scattering from the three materials also highlights the similarity between the α–cristobalite and the glass (Fig. H15.2). In α–cristobalite the peak at 5 meV corresponds to a flattened transverse acoustic mode.

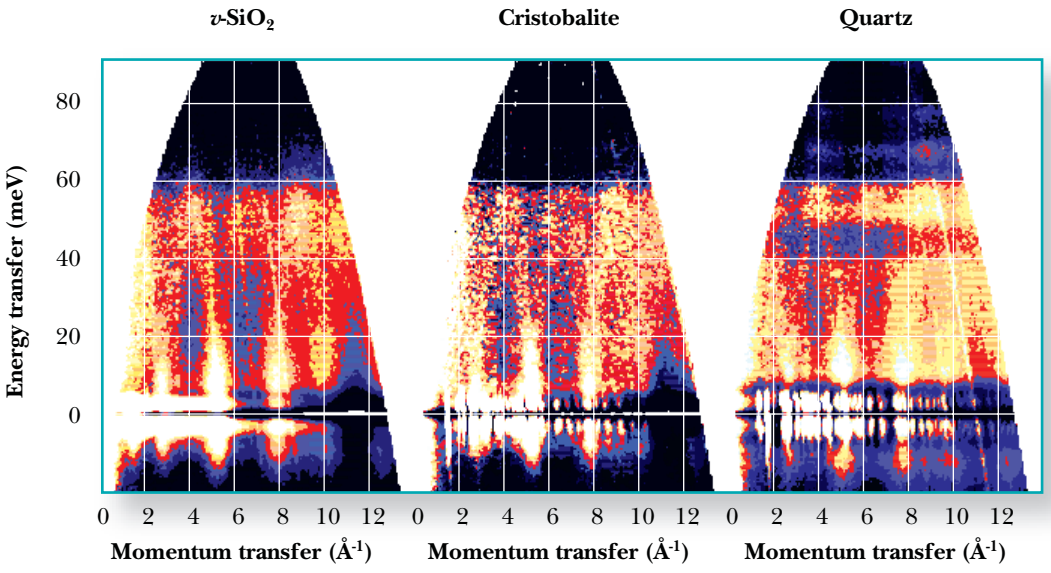

Fig. H15.1. An approximation to the generalised density of states for the three silica polymorphs: the glass, polycrystalline α-cristobalite, and polycrystalline α-quartz. The measurements were made on the MARI spectrometer with an incident energy of 100 meV.

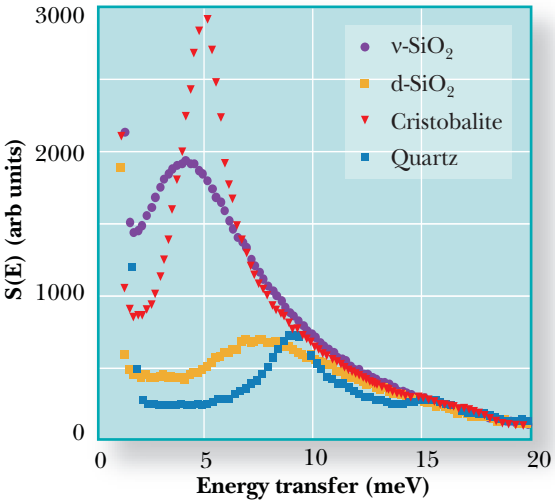

The peak in the glass appears at the same energy and exhibits the same form as a function of momentum transfer. Given that there are no optic modes in this region, this implies that the two modes are related. The major difference is that the peak in the glass is broader and extends to lower energies; an observation which may be crucial to the understanding of the universal properties of glasses.

Temperature dependent measurements (Fig H15.3) show effects localised at around 5 meV and a momentum transfer of 1.5 Å^{-1}, which also happens to be the position of the first sharp diffraction peak. This effect becomes more pronounced at low temperatures, and it is possible that this is related to quantum excitations, such as a tunnelling modes. This could be the basis of the two-level models that are often employed to explain the specific heat measurements and memory effects that are universal to amorphous systems.

In conclusion we believe that the observed 'dispersive' features are unlikely to be due to long-range collective excitations and are more closely related to the dynamics of a cluster of SiO_4 tetrahedra. We also observe temperature dependent scattering, which could be a trace of the tunnelling modes that are needed to explain many of the unusual properties of glasses.

Fig. H15.2. S(E) for the four silica polymorphs: the glass, α-cristobalite and α-quartz. The measurements were made on the MARI spectrometer with an incident energy of 25meV.

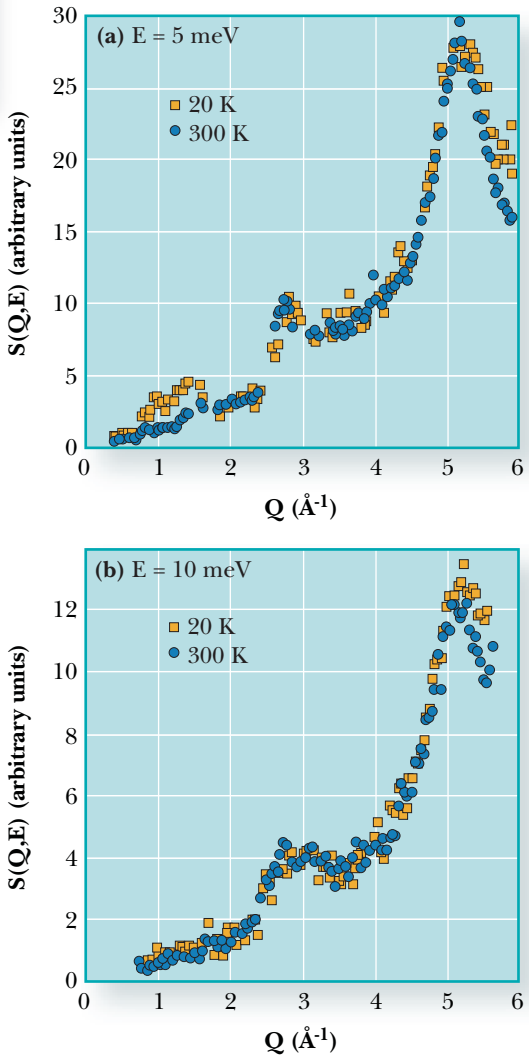

Fig. H15.3. The temperature dependence of the scattering from glassy SiO_2. A peak appears at 5 meV and 1.5 Å^{-1} at low temperatures. This may be related to tunnelling modes between different structural configurations.

Making MAPS of magnetism

MAPS is the first chopper spectrometer optimised to measure coherent excitations in single crystals. The scientific programme on MAPS started in August 2000, and since then magnetic and non-magnetic systems in one, two and three dimensions have been studied. This article reviews the motivation to build MAPS and the breadth of science performed on the spectrometer, and highlights the importance of information technology in its success.

T G Perring, C D Frost (ISIS)

The wavevector and frequency dependent excitation spectra in single crystals provide the most exacting tests of models for the inter-atomic interactions. For example the generalised magnetic susceptibility, $\chi''(\boldsymbol{Q}, \omega)$, contains the full information of the magnetic interactions, and is directly measured by neutron scattering. The past decade has seen an increasingly large number of single crystal measurements on the chopper spectrometers HET and MARI which take advantage of the low background, good energy resolution and incident energies greater than 100 meV. MAPS builds on the experience gained on these instruments to be a spectrometer optimised for measurements of magnetic excitations in single crystals.

At the heart of the design of MAPS is control of resolution, in both momentum and energy. This is achieved by using a 16 m^2 position sensitive detector array, 6 m from the sample, based on ^{3}He resistive wire technology with electronics developed at ISIS. This detector system provides 160,000 detector pixels over an almost continuous coverage in the forward angle direction and an additional narrower strip of detectors in the horizontal plane (so that the instrument can be used to measure lattice excitations). It provides MAPS with a wide range of energy resolution/flux options, and the ability to retain fine momentum transfer resolution.

The key element in the philosophy of the MAPS design is the flexibility that the pixellated detector array gives the experimenter. High speed visualisation and analysis software plays a vital role in the exploitation of MAPS data. Time-of-flight and pixel position of the scattered neutrons is stored in an array of 10^8 pixels, from which the scattering function is constructed, in software, in a volume of reciprocal space of typically 10^7 volume elements. Through the graphical user interface of the visualisation software MSLICE, the user has complete freedom to view slices from the data as a function of any two variables from the four components of momentum and energy transfer $(\boldsymbol{Q}, \omega)$. Model fitting can be performed in TOBYFIT, which convolutes the full 4D resolution function with models for the scattering and performs least-squares fits simultaneously to any number of 1D cuts and 2D slices from several runs.

Since the user programme started in August 2000, experiments in 1D, 2D and 3D systems have been performed, which include realisations of model magnetic systems, high temperature superconductors, colossal magnetoresistive manganites and transition metals. Two examples are described fully as science highlights ('Dimensional Crossover in the Strongly Fluctuating Antiferromagnet $KCuF_3$' and 'Phonon dispersion and strong

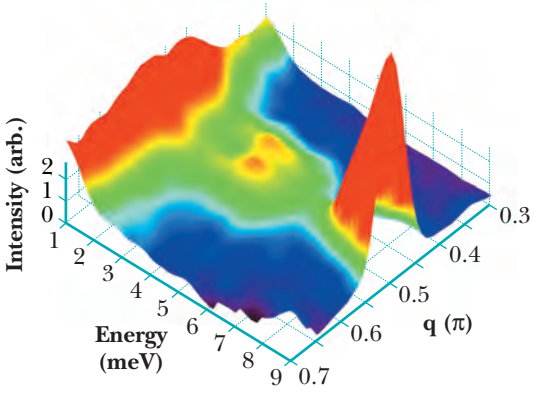

Fig. H16.1. The low energy excitation spectrum of $Y_{2-x}Ca_xBaNiO_5$ with x=4%, obtained in 19.8 hrs on MAPS with a 6.7 g sample. The spin-polaron modes at 4 meV are symmetric about $Q/\pi = 0.5$, and the triplet excitations start at 8 meV.

electronic anisotropy in the plane of $YBa_2Cu_3O_{7-x}$') but to give an idea of the capabilities of MAPS three others are briefly described below.

Model magnetic systems are important to study because they are a testing ground for our fundamental understanding of magnetism.

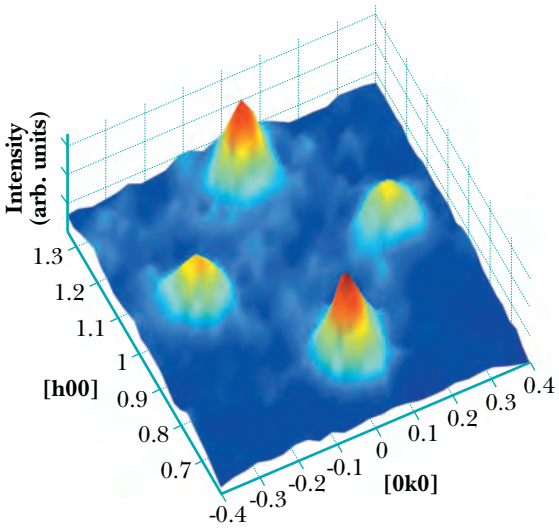

The chain of spin S=1 moments in Y_2BaNiO_5 form a spin liquid: a coherent quantum ground state that lacks static order. The main feature of the excitations of a S=1 spin liquid is a triplet band separated from the singlet ground state. The energy gap of ~8 meV and the full triplet dispersion with peak at 65 meV was observed on MAPS in one instrument setting. When holes are introduced onto the chains by partial substitution of Ca^{2+} for Y^{3+}, there are qualitative changes in spin dynamics (Fig. H16.1). Inelastic scattering appears below the triplet band reflecting the internal structure of the spin polarons created by truncating the chains. The high sensitivity, low background, and broad dynamic range of MAPS were all important factors that enabled an unprecedented view of dilute spin polarons in a quantum magnet.

Hole-doped transition metal oxides can have intriguing properties such as high temperature superconductivity or colossal magnetoresistance. An important recent concept in the field of high temperature superconductivity is the tendency of doped holes to form narrow stripes whose dynamical fluctuations have now been incorporated into a number of theories of superconductivity. A prototype for further experimental understanding of stripes is $La_{2-x}Sr_xNiO_4$, in which they seem to be more stable. Fig. H16.2 shows data from a survey of the dynamics for the case x=0.2 that has just started on MAPS. Many images like Fig. H16.2 covering a range of energy transfers are obtained from just one run, allowing a complete picture of the spin dynamics.

The transition metal ferromagnets iron, nickel and cobalt are the canonical examples of itinerant electron ferromagnets. The low energy excitations can be understood as spin wave modes, but at energies 0.1 - 0.5 eV they become damped due to interactions with the Stoner continuum, and interband resonances ('optic' spin waves) appear in the excitation spectrum. At these energies control of momentum resolution is paramount in order to resolve features in the excitation spectra. MAPS measurements on nickel have revealed the presence of previously unknown diffuse scattering around the zone boundary, at energies well above those of the phonons, extending to at least 200 meV. MAPS uniquely is able to take images of the spin correlation function like Fig. H16.3 which reveal these new excitations.

In its first year of operation, MAPS has already proved itself a valuable new tool to investigate the dynamics in single crystals.

Fig. H16.2. Plot of scattered intensity from $La_{1.8}Sr_{0.2}NiO_4$ in the plane of the Ni-O sheets taken with incident neutron energy 150 meV. The four peaks correspond to the incommensurate antiferromagnetic periodicity perpendicular to the stripes.

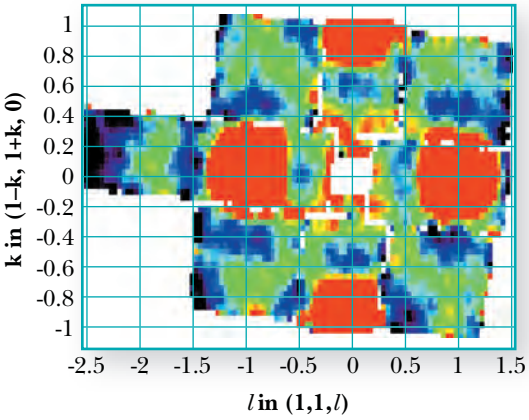

Fig. H16.3. Scattering intensity at an excitation energy of 90 meV, taken with incident neutron energy 200 meV. The four circles show the spin waves centred around the (2,0,0), (0,2,0) and (1,1,±1) reciprocal lattice points. Additional scattering due to the new modes appears along the zone boundaries. Note that Ni has the fcc structure. (Data taken with 400 g ^{60}Ni sample in 25 hrs.)

Dimensional crossover in the strongly fluctuating antiferromagnet $KCuF_3$

Understanding strongly fluctuating quantum systems and predicting their ground and excited states is a challenging and topical problem. At quantum critical points (QCPs), such systems become incoherent in time and their correlation lengths diverge to infinity. The one-dimensional Luttinger liquid is the most famous quantum critical phase. It describes the physics in systems as diverse as quantum wires, 'stripes' in high transition temperature cuprate superconductors, electron-positron gases and spin chains. This article discusses neutron scattering measurements on the quasi-one-dimensional (quasi-1D), spin (S)=1/2 antiferromagnetic compound, $KCuF_3$.

D A Tennant (Oxford and ISIS), B Lake, S E Nagler (Oak Ridge National Laboratory, U.S.A), C D Frost (ISIS)

Although $KCuF_3$ lies close to the one-dimensional Luttinger spin liquid, weak interchain coupling drives it away from perfect criticality and causes spontaneous long-range antiferromagnetic order below the Nèel temperature. Thus this compound demonstrates aspects of both the conventional magnetism of a 3D system (long-range order and spin-wave excitations) and the quantum magnetism of a 1D system (fluctuating ground state and spinon excitations). Here we investigate the Luttinger spin liquid state (characteristic of a 1D, S=1/2 antiferromagnetic with no interchain coupling) and its crossover to convention 3D magnetism.

$KCuF_3$ consists of parallel, S=½ Heisenberg antiferromagnetic chains coupled together into a square lattice. The intrachain coupling has size J=-34 meV while the interchain coupling is ferromagnetic and much weaker J'=1.6 meV. Long-range antiferromagnetic order is observed below the Nèel temperature T_N=39 K, with a saturated moment of only 0.5 μ_B at 4 K. The suppressed ordering temperature and moment reduction of 50% show that even though long-ranged order is achieved, $KCuF_3$ exhibits strong quantum fluctuations and is in the vicinity of a QCP. Fig. H17.1 shows its magnetic response measured on MAPS. At 50 K the scattering is spread out between upper and lower boundaries, and we are observing the spinon continuum that is characteristic of the 1D, S=½ antiferromagnet. Below T_N at 6 K the continuum is still observed at high energies but at low energies the excitations sharpen at the lower boundary and form the spin-waves characteristic of a 3D magnet.

Using this data and previous data from the HB1 spectrometer at Oak Ridge National Laboratory we have been able to construct the magnetic phase diagram of $KCuF_3$ (Fig. H17.2). Below 39 K where $KCuF_3$ orders antiferromagnetically, the chains see the staggered field of their neighbours, providing a confining potential between spinons. At energies below the perpendicular zone boundary energy *D* the spinons are tightly

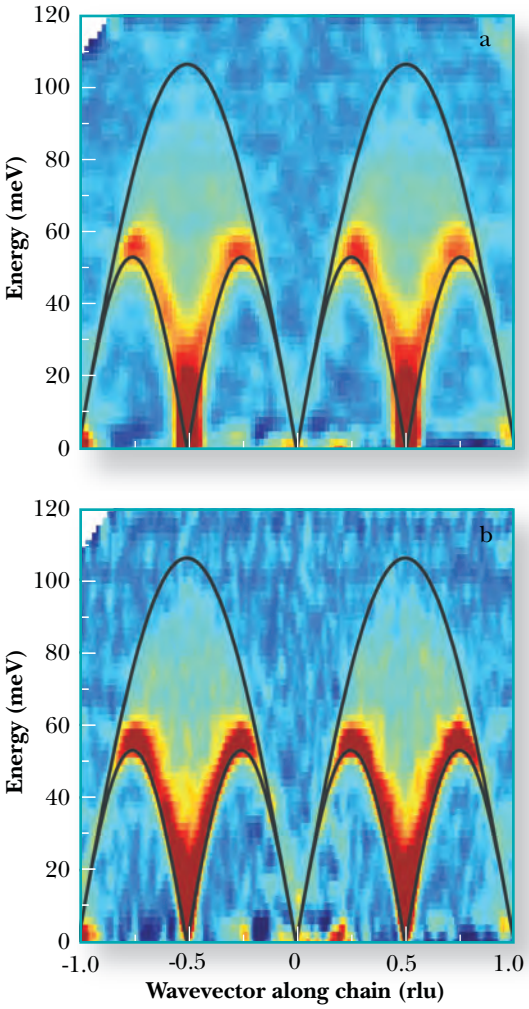

Fig. H17.1. The magnetic response of $KCuF_3$ measured on MAPS. Upper: neutron scattering at 50 K, above the transition temperature. The colours give the relative scattering intensity. Lower: the signal well below the transition temperature at 6K.

bound and the field renormalizes to a semi-classical 3D non-linear sigma model (3D NLσM). At energies greater than 2*D* the correlations are rapidly fluctuating and the spinons appear free both above and below the T_N. In this region the correlations should be that of a Luttinger liquid. Between the 3D NLσM and the quantum critical region is a non-universal crossover region where the strongly fluctuating Hamiltonian is influenced by the three-dimensionality. In such a region new effects can arise, and in the case of $KCuF_3$ a novel longitudinal mode is observed at 17 meV around the antiferromagnetic point below T_N. Above the Curie-Weiss temperature T_{CW}=200 K thermal fluctuations invalidate the continuum description and the correlations are expected to depart from Luttinger liquid behaviour.

The Luttinger liquid phase is characterized by some exceptional physics. The spinons themselves are unusual in that they are fractional particles carrying spin value of S=½, and they therefore have to be created in pairs in order to change the total spin moment by integer amounts. A theoretical prediction for the Luttinger liquid region is that it should demonstrate universal E/T scaling at the antiferromagnetic zone centre (i.e. at wavevectors q=±1 r.l.u.), which implies that the physics depends only on the ratio of energy (or frequency ω) and temperature rather than these two quantities individually. To test the scaling hypothesis, cuts were taken from the MAPS data sets (e.g.Fig. H17.1) over a small wavevector range around the antiferromagnetic zone centre. Each data set was measured at a different temperature from 6 K to 300 K. Above 80 meV, scaling was found to break down indicating that lattice effects become important at this energy. Data below 25 meV were also discarded because they lie in the non-universal crossover or 3D NLσM regions. The cuts from 6 K to 200 K were scaled by temperature and plotted as a function of energy in Fig. H17.3. They are seen to agree within error to the proposed universal scaling form and confirm the scaling hypothesis within the Luttinger liquid region.

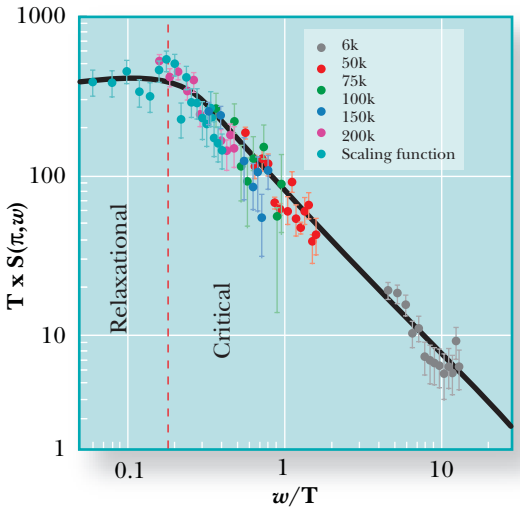

Fig. H17.3. Data measured in the Luttinger liquid phase are scaled as described in the text. The universal scaling form is also given (solid line).

In conclusion we have investigated the temperature, wavevector and energy dependence of the magnetic response in the strongly fluctuating quantum magnet $KCuF_3$. A phase diagram of the system has been constructed as a function of energy and temperature and shows a crossover from a 3D NLσM phase characterized by spin-wave excitations to 1D Luttinger liquid behaviour characterized by a spinon continuum. The Luttinger liquid phase was probed using the MAPS spectrometer at ISIS and was found to show the predicted E/T scaling behaviour.

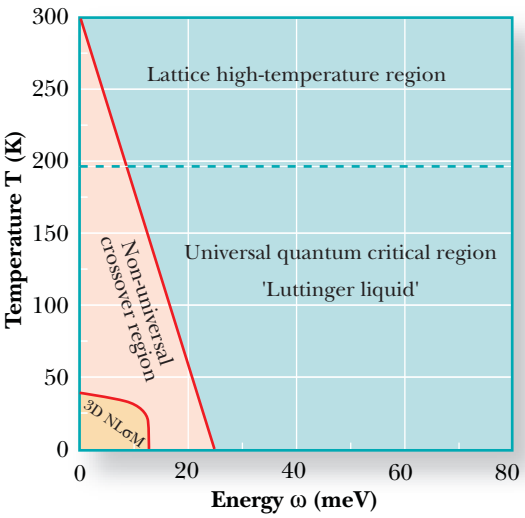

Fig. H17.2. The magnetic phase diagram of $KCuF_3$ showing the crossover from 3D to 1D behaviour. The correlations follow universal scaling in the Luttinger liquid phase whereas in the 3D NLσ M region semi-classical spin-waves predominate.

Phonon dispersion and strong electronic anisotropy in the plane of $YBa_2Cu_3O_{7-x}$

The phonon dispersion in $YBa_2Cu_3O_{6.95}$ observed by MAPS has led to a discovery of strong anisotropy in dielectric response in the CuO_2 plane. Such anisotropy implies anisotropy in the underlying electronic structure that could result from the charge-spin stripes. The results indicate strong interaction of electrons with the Cu-O bond-stretching phonons, with the possibility of electronic overscreening. This observation brings the phonons, which have long been considered to be irrelevant to high-temperature superconductivity, under a spotlight.

T Egami, J-H Chung, Y Petrov *(University of Pennsylvania),* ***R J McQueeney*** *(Los Alamos),* ***M Yethiraj, H A Mook*** *(Oak Ridge),* ***M Arai, Y Inamura,*** *(KEK),* ***Y Endoh*** *(Tohoku University),* ***S Tajima*** *(ISTEC),* ***C D Frost*** *(ISIS),* ***F Dogan*** *(University of Washington)*

MAPS is equipped with a large two-dimensional array of position-sensitive detectors in the forward scattering position to study magnetic excitations, and an extended high-angle arm up to 60° to capture the scattering from phonons. This detector coverage has proved invaluable in the study of phonon dispersion in superconducting cuprates.

Measurements were made of the phonons with a large twinned crystal of $YBa_2Cu_3O_{6.95}$. MAPS is crucial for this experiment because the pixellated detector array allows measurements of the dynamic structure factor $S(\boldsymbol{Q},\omega)$ in three dimensions (energy and momentum transfer vector in two-dimensions). This three dimensional data volume can then be projected on to a multitude of two-dimensional planes for analysis.

A constant-energy cut (41 meV) at 7 K is shown in Fig. H18.1. Two spots of magnetic resonance are seen around $Q = (h, k, l) = (0.5, \pm 0.5, l)$, in the units of the reciprocal lattice vectors. In order to see the longitudinal optic (LO) phonons a h-ω cut at $k = 0$ was made (Fig. H18.2). Since the neutron scattering intensity is proportional to $(\boldsymbol{Q}.\boldsymbol{e})^2$, where $\boldsymbol{e}$ is the phonon polarization vector, only the LO phonons are seen here. In this projection l is also changing with ω, but this was neglected, since the l dependence is weak in YBCO due to its layered structure. We focused on the Cu-O bond-stretching mode because this promotes charge transfer between Cu and O and is expected to interact strongly with charge. It was found that there are two branches of this mode, at 68 meV and 72 meV at the zone centre, in agreement with Raman results. Actually, the maximum of the dispersion is slightly shifted from the zone-centre, by about 1 % to the left (68 meV mode) and right (72 meV mode). This is due to the orthorhombic distortion of the lattice, while we assumed the tetragonal lattice in the average due to twinning. This revealed the 68 meV to be polarized along the b-axis (parallel to the chain) and the 72 meV polarized along a. We then made cuts along k to determine the dispersion of the transverse modes (Fig. H18.3).

The phonon dispersion of the in-plane modes revealed unexpectedly strong anisot-

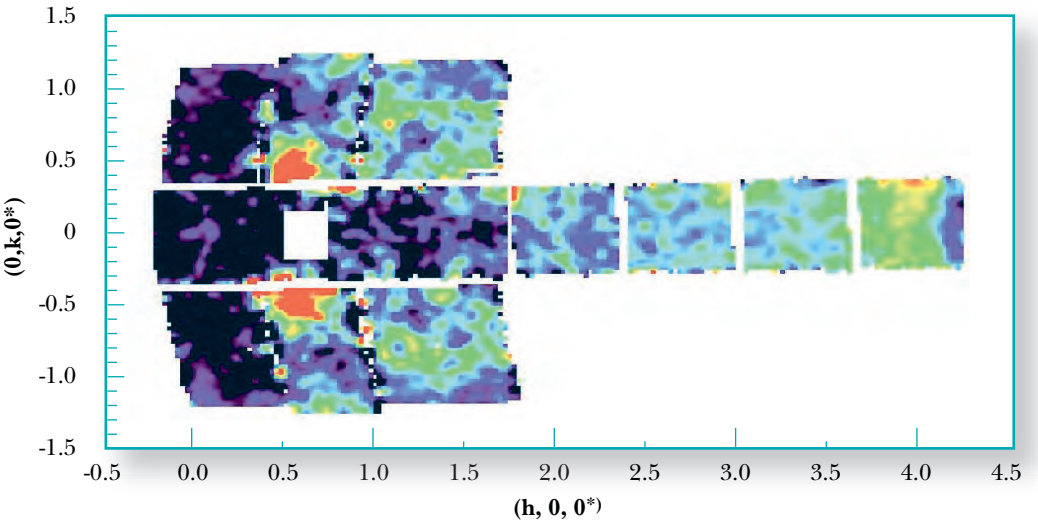

Fig. H18.1. Constant energy (h-k) *cut, at 41 meV, of the dynamic structure factor* S(Q, ω) *for* $YBa_2Cu_3O_{6.95}$ *at T= 7 K..*

ropy. The frequencies of the LO and transverse optic (TO) modes are nearly degenerate for the *b*-axis polarized mode, suggesting metallic screening of the phonon polarization, but for the *a*-axis mode they are different except for $q = 0$. This implies that electronic screening is weak in the *a*-axis direction of the CuO_2 plane, as in a semi-metal. This is consistent with the spin-charge stripe model, if we assume that the charge stripes are along the chain in YBCO as suggested recently by the neutron measurement of Mook et al.

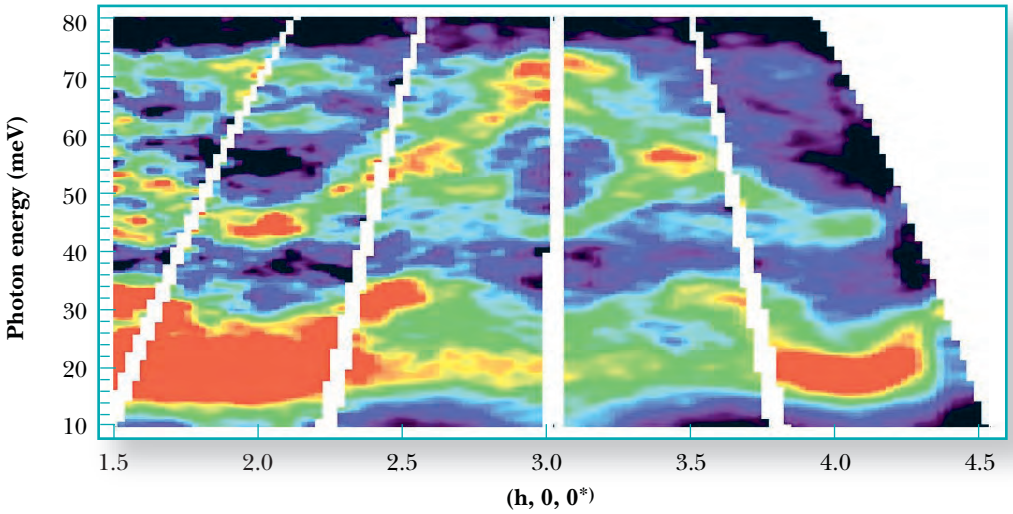

Fig. H18.2. Constant k *(*h*-ω) cut of* S(Q, ω) *divided by* Q^2*, showing LO phonon dispersions for* $YBa_2Cu_3O_{6.95}$ *at* $T = 110$ *K.*

The observed incomplete screening in the *a*-direction implies that long-range polar interaction may survive, resulting in strong electron-phonon interaction. It is noteworthy that the TO frequency is *higher* than the LO frequency for the *a*-axis polarized mode. This is highly unusual in the light of the Lyddane-Sachs-Teller (LST) relationship. The inverted LST relationship means the electric fields created by the neighbouring dipoles are opposite in direction to the polarization, or the negative dielectric constant. Such a situation can be due to overscreening, as was predicted by Tachiki and Takahashi, and suggests very strong interaction between phonons and electrons.

The anisotropy in dispersion was found to be temperature dependent. The *b*-axis polarized mode is continuous above T_C, but below T_C it becomes gapped just as the *a*-axis polarized mode. The order parameter of this change was determined earlier with the triple-axis-spectrometer at HFIR of Oak Ridge National Laboratory, and found to be very similar to that of superconductivity.

This observation of the strong in-plane anisotropy in the electronic structure, dielectric interaction and overscreening in the *a*-direction, and temperature dependent phonon dispersion, challenges the existing theories of high-temperature superconductivity, with serious consideration of the lattice degrees of freedom required. The unique perspective that MAPS provides has succeeded in bringing the phonons, which have long been considered irrelevant to high-temperature superconductivity, under the spotlight.

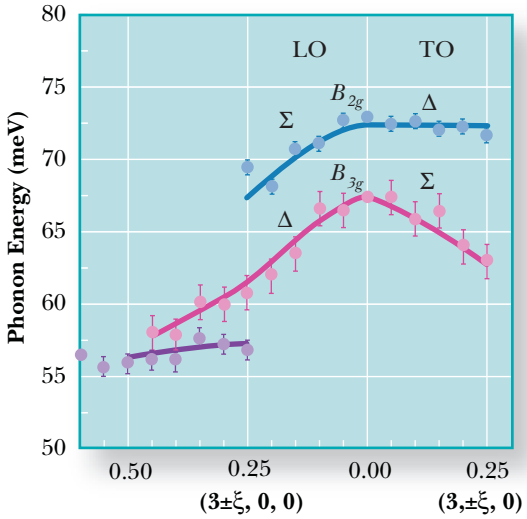

Fig. H18.3. Dispersion of the Cu-O bond-stretching modes determined for $YBa_2Cu_3O_{6.95}$ *at* $T = 110$ *K. The left-hand side denotes the LO modes for the* a*-axis polarized mode (denoted as* B_{2g} *at the zone-centre) and for the* b*-axis mode (*B_{3g}*).*

Testing the double exchange model in bilayer manganites

The cubic manganese perovskites $RE_{1-x}A_xMnO_3$ (RE=La, Nd, Pr, A=Sr, Ca, Pb, for example) have attracted attention because of their rich and fascinating physical properties. These can include not only changes in resistivity of several orders of magnitude in an applied field of a few Tesla, but also magnetic field, electric field-, photon- and strain- induced insulator-to-metal phase transitions. Here we test the ability of the venerable double exchange model for the manganites to explain the spin dynamics in naturally layered two dimensional analogues.

T G Perring, D T Adroja, G Chaboussant (ISIS), G Aeppli (NEC Research Institute, USA), T Kimura, Y Tokura (JRCAT, Japan)

The starting point to understand the manganites is double exchange theory, in which electrons in partially filled d-bands with e.g. character (i.e. $d_{3z^2-r^2}$ and $d_{x^2-y^2}$ orbitals) hop between adjacent Mn ions, each of which has a spin S=3/2 magnetic moment arising from local t_{2g} (i.e. d_{xz}, d_{yz}, d_{xz}) occupancy. As a band electron hops from site to site, strong intrasite exchange aligns the electron spin with the local Mn moment, thereby favouring ferromagnetism and metallic conductivity. Double exchange alone cannot explain the physics of the manganites, however, and there is a wealth of evidence pointing towards lattice distortions which localise carriers to form polarons in the paramagnetic phase.

Naturally layered manganites allow the influence of dimensionality to be explored in the manganites, and provide the venue for an object not found elsewhere in nature, namely a two-dimensional, fully spin-polarised electron liquid. $La_{2-2x}Sr_{1+2x}Mn_2O_7$ consists of bilayer slices of MnO_6 octahedra taken from the cubic compound, separated by insulating $(La,Sr)_2O_2$ layers that serve largely to decouple the bilayers (Fig. H19.1(a)). The questions addressed here are (i) to what extent does the double exchange model explain the spin dynamics in the ordered state, and (ii) what is the effect of the hole doping per Mn site, x, on the magnetism.

We performed inelastic neutron experiments on the HET and MARI spectrometers for x in the range 0.30 to 0.40, for which the Mn moments within a bilayer order ferromagnetically (the inter-bilayer coupling is ~100 times smaller than that within the bilayers, and is too weak to measure here). Fig. H19.2 shows part of the measured spin wave dispersion relations for x=0.35 and 0.40. Because of the bilayer structure, two branches exist, labelled by analogy with phonon modes as 'acoustic' and 'optic'. Features to note are that the energy scale is similar to equivalently doped cubic manganites, and that the branches are well described by those for a bilayered Heisenberg ferromagnet (solid lines). Only the optic branches near the zone boundary show a small deviation. This is in marked contrast to most cubic manganites, where the spin waves soften dramatically near

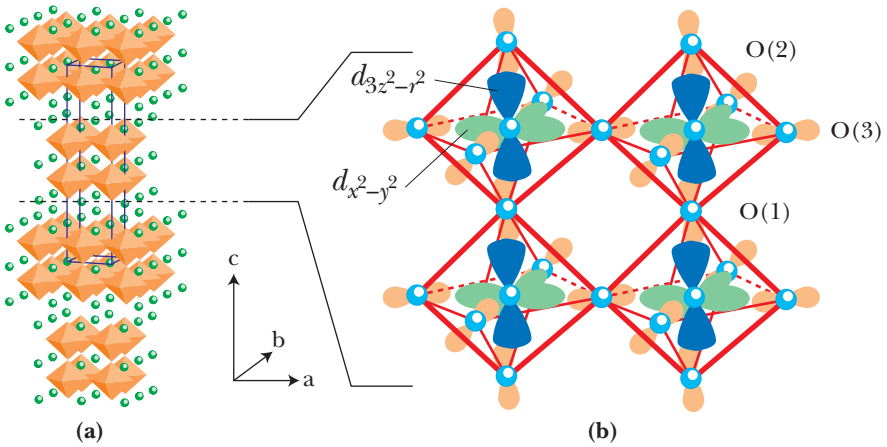

Fig. H19.1 (a) Crystal structure of $La_{2-2x}Sr_{1+2x}Mn_2O_7$. The Mn ions are at the centre of the MnO_6 octahedra. Circles denote La and Sr. (b) Expanded view of MnO_6 octahedra in a single bilayer, showing the Mn $d_{3z^2-r^2}$ and $d_{x^2-y^2}$ orbitals.

the zone boundary. In fact, recent theory that goes beyond linear spin wave theory in the double exchange model enables us to estimate the zone boundary energy as 25-40 meV, in

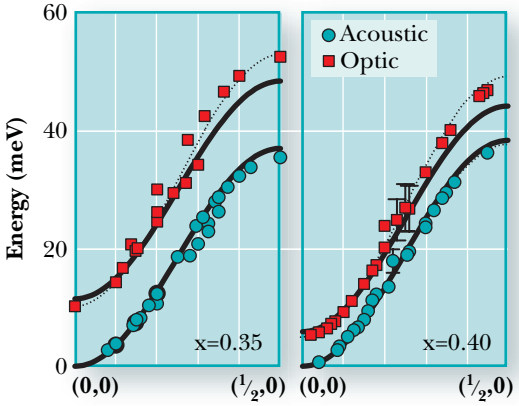

reasonable accord with the data, and shows that the dispersion relation is nearly that for the Heisenberg ferromagnet.

Fig. H19.3 shows the inverse lifetimes, γ, of the spin waves for x=0.40 as a function of excitation energy, ħω. The main features for both acoustic and optic modes are (i), γ is approximately linear in ħw, with γ/ħω = 0.33±0.02 and 0.46±0.02 respectively (ii) no sudden jumps are seen where the spin wave branches cross an optic phonon mode at ~20 meV. We saw similar results with x=0.35. The large ratio γ/ħω is hard to understand both theoretically and experimentally for a Heisenberg ferromagnet, and the absence of anomalies at phonon energies or of softening of the dispersion contrasts with theories that have strong coupling with lattice or orbital degrees of freedom. A natural explanation for the anomalous large damping comes from the double exchange model: the same calculations referred to above yield γ/ħω as high as 0.15 on the zone boundary at zero temperature. Given the sensitivity of the ratio to details of the band structure this appears to offer a plausible explanation of the data. Remarkably, the double exchange model appears to offer a full explanation of the spin dynamics.

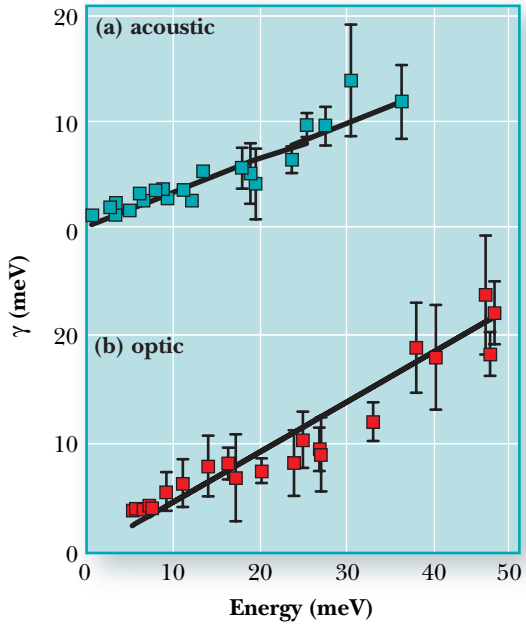

Fig. H19.3. Energy dependence for x=0.40 of the inverse spin wave lifetime, γ, for (a) acoustic (b) optic spin waves.

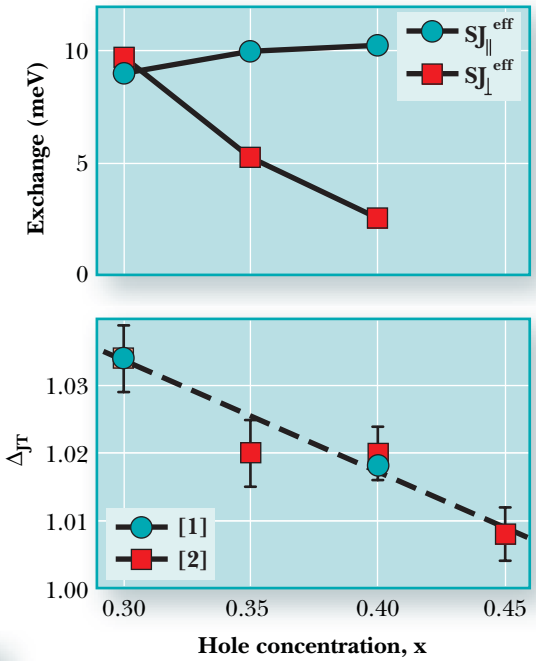

Fig. H19.4. (a) $J_{\parallel}$ and $J_{\perp}$ derived from fitting to the Heisenberg ferromagnet Hamiltonian with nearest neighbour exchange only. (b) Distortion of the MnO_6 octahedra, where $\Delta_{JT} = \frac{1}{2}(d_{Mn\text{-}O(1)+} d_{Mn\text{-}O(2)})/d_{Mn\text{-}O(3)}$.

Figure H19.4(a) shows the doping dependence of the in-plane and inter-plane (but still intra-bilayer) magnetic coupling constants. The figure reveals the changing e.g. orbital character as hole doping, x, decreases, or equivalently as the electron occupancy increases. While the in-plane coupling $J_{\parallel}$ barely changes, the interplane coupling $J_{\perp}$ changes from $0.25J_{\parallel}$ to $1.1J_{\parallel}$. This directly demonstrates that the extra electrons enter the Mn $d_{3z^2-r^2}$ orbitals, which link the two planes via O^{2-} p orbitals (Fig. H19.1(b)), rather than the $d_{x^2-y^2}$ orbitals, which link Mn ions via O^{2-} within the planes.

Hydrocarbons: testing molecular theory

Hydrocarbons provide an enormous series of homologous compounds. The vibrational spectroscopy of saturated hydrocarbons, the alkanes and cycloalkanes, has been extensively studied by infrared and Raman optical methods. However, high-resolution inelastic neutron scattering spectra as provided by TFXA and TOSCA give a number of advantages , including significant intensity in modes that are silent by optical methods and the ability to test theoretical descriptions of the vibrations of these species. This is illustrated with the n-alkanes and dodecahedrane.

B S Hudson (Syracuse University), T Yildirim (NIST), S F Parker, J Tomkinson (ISIS)

The low frequency vibrational spectroscopy of the linear n-alkanes has a long and interesting history. The most famous series of low-frequency modes of these compounds are the longitudinal acoustic modes or 'LAMs'. C-C-C angle bending is the major coordinate involved in LAM motion but there may be some contribution of the C-C stretch. The TOSCA spectra of pure, polycrystalline n-alkanes such an n-hexadecane exhibit these LAM modes as a series of features ranging up to 525 cm^{-1} (Fig. H20.1). There are, in addition, transverse bending modes at low frequency, overlapping the low-frequency LAM modes.

The vibrational frequencies and normal mode eigenvectors of n-alkanes can be computed with a variety of methods including ab initio and DFT techniques. From the eigenvectors the spectra intensities can be calculated. A comparison of the calculated and observed spectra is a test of the computation. In this case it is observed that the LAM modes are well described by an isolated molecule calculation but that the transverse modes are not well described. This is presumably due to intermolecular interactions.

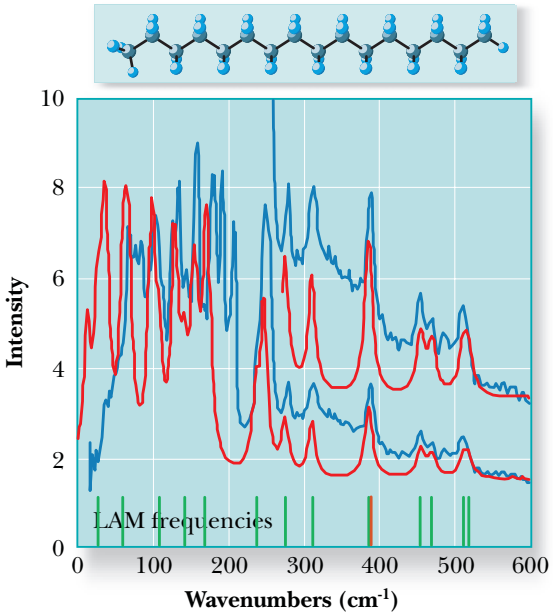

Fig. H20.1. The INS spectrum of n-hexadecane (structure shown at the top) obtained with TFXA (blue) compared with the results of a DFT calculation (red). The vertical green and red lines are the computed LAM mode frequencies

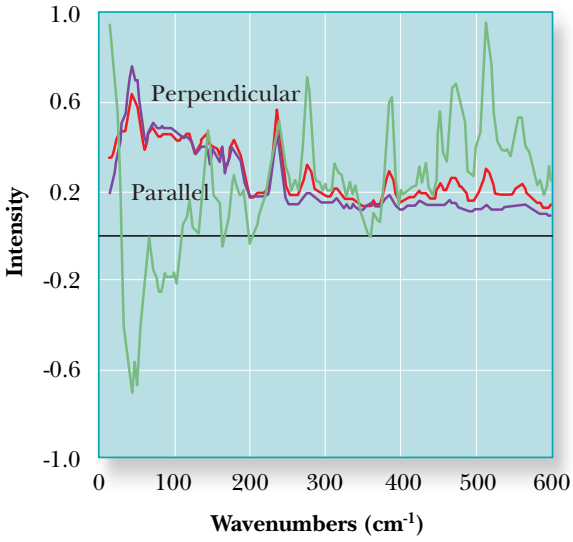

Fig. F20.2. The spectrum of n-hexadecane in deuterated urea inclusion complexes. The spectrum with the crystals oriented parallel to the bean is in blue, perpendicular is in red and the difference, parallel minus perpendicular, is in green. Positive excursions of the difference spectrum indicate parallel (LAM) modes.

The LAM vibrational normal modes involve the motion of the n-alkane atoms along the molecular axis of the fully extended chain. This aspect of the LAM motion can be demonstrated by preparation of oriented n-alkane chains. This is difficult using the pure materials but can be achieved using urea inclusion complexes. These macroscopically hexagonal compounds can be easily oriented with respect to the neutron beam. The resulting dichroism permits classification of the normal modes of the n-alkanes into longitudinal and transverse (see Fig. H20.2).

For an n-alkane with N carbon atoms there are N-2 LAM modes. These LAMs may be classified in terms of the phase difference, ϕ, between the motions of the adjacent translationally equivalent CH_2-CH_2 groups. The LAM modes for a given molecule exhibit a smooth dispersion behaviour when plotted as a function of ϕ. The longest wavelength mode that occurs with finite frequency is the 'accordion' mode in which all of the bond angles contract or expand. This mode is active in the Raman spectra of the n-alkanes but the higher order LAM modes are not. Thus INS permitting a more detailed test of theory for this type of vibrational mode.

The dispersion behaviour observed for all of the assigned LAM modes for the n-alkanes with 5 to 25 carbons can be compared with expectations for an infinite chain model that involves only C-C-C angle bending (see Fig. H20.3A). The general behaviour of the experimental results is captured by the infinite chain model but there are clear deviations due to end effects. The corresponding comparison of the theoretical results with the infinite chain model shows similar deviations (see Fig. H20.3B). Direct comparison of the observed and calculated LAM frequencies shows close agreement (Fig. H20.3C). When DFT methods are used the calculations need no scaling to give this level of agreement.

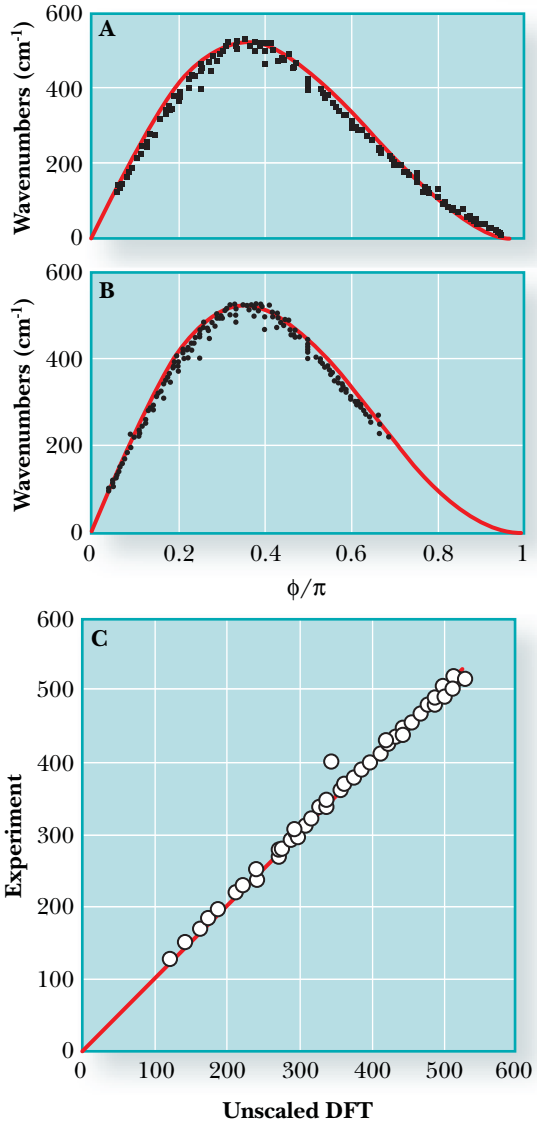

Fig. H20.3. Classification of the LAM modes on the n-alkanes according to phase angle between units. A: experimental. B: computed. C: direct comparison of the calculated and observed modes.

Alkanes come in many sizes and shapes. The most symmetric of these is the icosahedron as realized in the molecule $C_{20}H_{20}$ known as dodecahedrane (see Fig. H20.4). The I_h symmetry of this molecule results in 19 of the 30 normal modes being forbidden in both infrared and Raman spectroscopy. All modes are active in the INS spectra. In this case a detailed comparison of the observed spectrum with the results of computation has been initiated. In particular it is now possible to perform DFT calculations on solids with inclusion of periodic boundary conditions. This goes beyond the isolated molecule approximation. Preliminary results show that these calculations capture the major effects of the crystal lattice on the molecular vibrations.

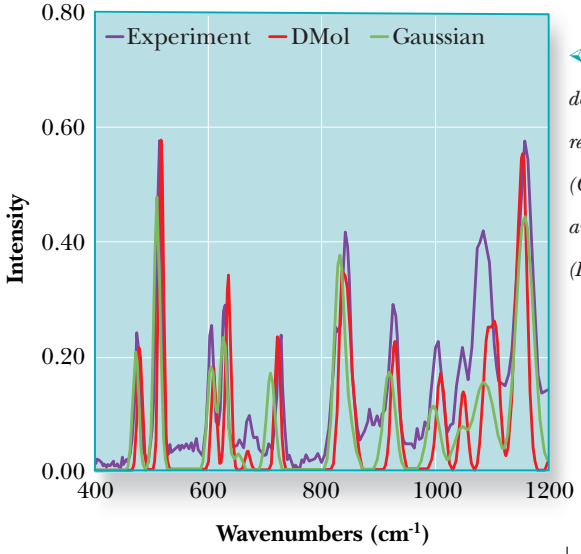

Fig. H20.4. The INS spectrum of dodecahedrane compared with the results of an isolated molecule (GAUSSIAN) calculation (green) and a periodic lattice calculation (DMol³).

An incoherent QENS study on the dynamic processes occurring in chemical hydrogels based on poly(vinyl alcohol)

Dynamic behaviour of water in hydrogels is a major issue for understanding how a polymeric matrix can function as drug delivery system (DDS).
It is known that hydrogen bonded liquids confined in mesoscopic domains display significant modifications of their structural and dynamic bulk properties. Surely water embedding a polymeric matrix, i.e any hydrogel used as drug delivery device, has to be regarded under this aspect as the release properties of the system will strictly depend on diffusive behaviour of the caged water.

G Paradossi, A Turtu', F Cavalieri, E Chiessi (University of Rome'Tor Vergata'), M T F Telling (ISIS)

In recent years pharmacological research has considered that the problem of the bioavailability, and therefore of the release of drugs by the carrier, is as important as the synthesis of pharmacologically-active new molecules. Moreover, some innovative therapeutic approaches, for instance gene therapy, are now abandoning the use of 'small molecular weight molecule' drugs, pursuing treatments with 'high molecular weight molecule' drugs, i.e. macromolecular species as nucleotide chains or active peptides. This poses some basic problems as the state of the medium (basically water) confined in heterogeneous (bio)systems, often hydrogels, used as drug carriers.

A versatile biocompatible material eligible for DDS is poly(vinyl alcohol), PVA, one of the few biocompatible synthetic polymers. PVA is known to form thermoreversible (physical) hydrogels upon freeze-thaw cycles. Also, chemical hydrogels based on PVA can be obtained by adding suitable bifunctional short molecules able to cross-link PVA chains and consequently to form a network. For the last few years we have focused on obtaining a family of chemical hydrogels with enhanced physical and chemical stability, without introducing cross-linkers chemically different from PVA. This is an important aspect of the final product as a biocompatibility comparable to that of the starting PVA is required.

Our method for obtaining PVA chemical hydrogels is based on the presence in a PVA chain of a small but measurable amount of sequence defects. Generally, repeating units are regularly spaced in 'head-to-tail' sequences along the chain, and a 'head-to-head' kink seldom occurs. The amount of such defects can vary depending on the polymerization conditions of PVA. We developed a convenient way of determining the number of the 'head-to-head' sequences contained in the starting

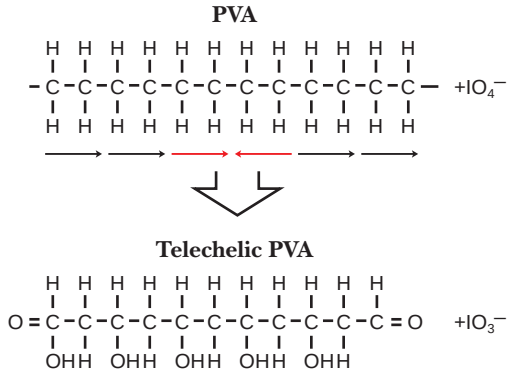

The number of → ← sequences is determined with a microcalorimetric experiment:

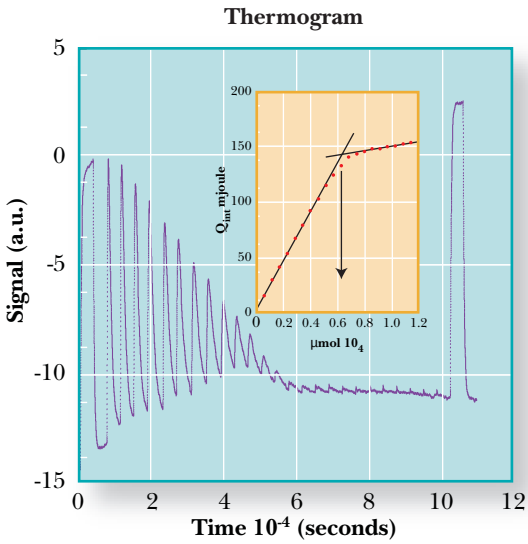

Fig. H21.1. Obtainment of telechelic *PVA is based on the specific splitting of the 'head-to-head' sequences (red arrows) from the 'head-to-tail' sequences (black arrows). The amount of the 'head-to-head' sequences is determined by a microcalorimetric titration and corresponds to the end point of the titration (shown by the vertical arrow in the inset).*

PVA chains by a microcalorimetric titration, as shown in Fig. H21.1.

The PVA network is obtained by splitting the 'head-to-head' sequences by a selective oxidizing agent (periodate) and producing the macromer cross-linking agent, i.e. the *telechelic* PVA. In a second step the cross-linking reaction between the terminal functional group and the 'head-to-tail' glycolic sequences is allowed, yielding a network that can be schematically represented in Fig. H21.2. Water acting as reaction medium is confined inside the gel as a consequence of the network formation. Its dynamic behaviour is modified by the confinement according to QENS experiments carried out at the IRIS beamline.

We carried out incoherent QENS experiments on telechelic PVA hydrogels in water and in D_2O at different temperatures and cross-linking degrees. The change of solvent was necessary in order to separate as much as possible water and polymer proton contributions to the observed incoherent scattering functions, therefore gaining insight into the dynamic behaviour of both components. Owing to the difference in the incoherent cross-section between protons and deuterons, PVA hydrogels containing water were mainly dominated from the diffusive motions of water protons, whereas incoherent QENS measurements carried out in D_2O were dominated by the incoherent scattering of the non-exchangeable protons contained in the polymer moiety. In Fig. H21.3 the observed dynamic structural factor, S(q,ω), obtained for the same hydrogel embedded in H_2O and in D_2O at a scattering vector q of 1.222 $Å^{-1}$ and at 303 K is shown. The spectra were analyzed as a convolution of the instrument resolution with a linear combination of lorentzians with different line broadening factors.

Parameters of the diffusive processes taking place in the hydrogels can be extracted from these measurements with the aid of appropriate models, i.e random jump diffusion, allowing for a diffusion coefficient and a residence time between consecutive jumps. The results show that water behaves as a supercooled liquid when it is confined within these matrices. These features are common to other bi- and tridimensional matrices containing hydrogen bonded liquids.

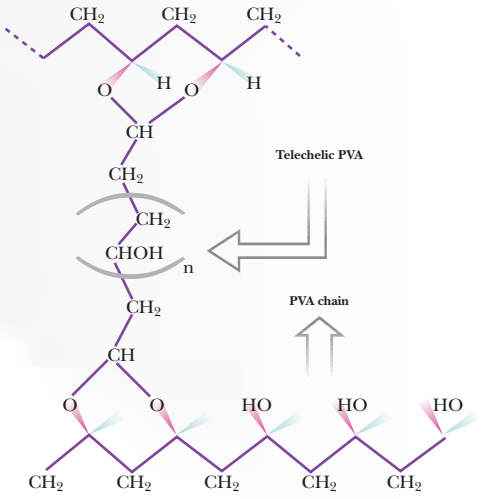

Fig. H21.2. Schematic representation of the chemical hydrogel based on telechelic *PVA.*

The experiments carried out in D_2O allowed an evaluation of the dynamics of the PVA polymer chains between two cross-linking points. One dynamic feature was an average characteristic displacement of the chains of about 10 Å. Comparable values are usually detected in polymer melts above the glass transition temperature.

In conclusion, QENS has proved to be a valuable approach for the study of water and polymer moieties in confined systems. In PVA matrices dynamics of water are characterized by an enhanced supercooled behaviour. On the other hand PVA polymer networks feature a confined chain diffusion due to the presence of chemical cross-links. Dynamics of the two components are strongly influenced by the confinement. These findings compare with the results obtained with other very different mesoscopic systems, which suggests a common behaviour of water considered as a confined hydrogen-bonded liquid.

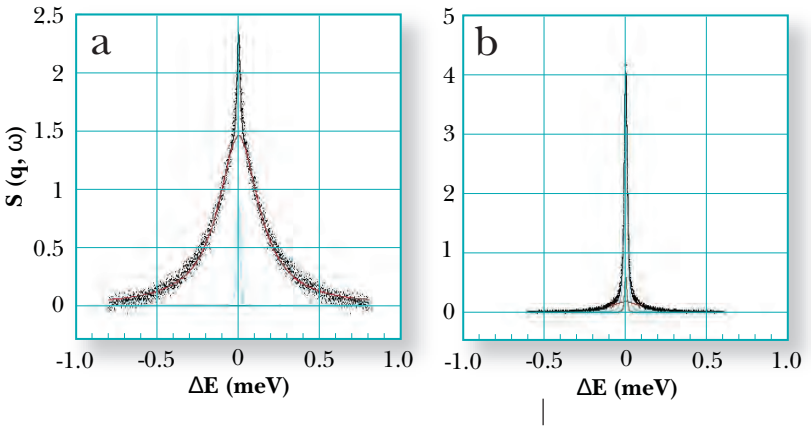

Fig. H21.3. Change in the lineshape of the scattering function of the telechelic *PVA hydrogels in water (a) and in D_2O (b).*

Single particle kinetic energy in solid and dense liquid ^{3}He

Solid ^{3}He at low temperature is a quantum crystal in which the effects of both atomic localization and strong anharmonicity result in a large excess of single-particle kinetic energy. Deep Inelastic Neutron Scattering (DINS) measurements using eVS have provided the first experimental determination of the single-particle mean kinetic energy of this system in the solid hcp and bcc phases, and in the high density liquid near the melting transition.

R Senesi *(INFM, Italy),* ***C Andreani*** *(University of Rome 'Tor Vergata' and INFM, Italy),* ***D Colognesi*** *(CNR, Italy, and ISIS)*

For many years the dense phases of the light helium isotope have attracted the interest of both theoretical and experimental physicists, it being a prototype system for the understanding of quantum many body physics. Indeed, thanks to the accurate knowledge of the inter-particle potential, and to the non-relativistic dynamical regime involved, a detailed, quantitative comparison can be made between theory and experiment which is not generally feasible for other quantum many-body systems. Despite this advantage, ^{3}He still appears to challenge the efforts of theoreticians, because of the intrinsic difficulty in dealing with a many-body anti-symmetric wave-function in computer simulations. From the experimental point of view the study of ^{3}He dynamics by thermal neutron spectroscopy has been limited by the large neutron absorption cross section which results in a striking lack of experimental data. However, recently we have been able to overcome this experimental constraint by using epithermal neutrons with energy in excess of 1 eV and to derive, for the first time, unique information on single-particle mean kinetic energies, $\langle E_k \rangle$, in the solid and high density liquid phases of ^{3}He. The results of this experimental work have been successfully compared with the most advanced ground-state simulation techniques. It is worth noticing that the single-particle mean kinetic energy is a quantity which strongly characterises dense quantum systems, being substantially different according to the system investigated and/or the approximations adopted (e.g. the classical Maxwellian regime, the quantum Boltzmann liquid regime, the Debye-like anharmonic crystal , the Bose condensates, the Fermi liquids etc.). Furthermore, epithermal neutron scattering has proved to be the only reliable technique providing direct access to its determination. The experiment was performed on the eVS spectrometer, where an intense flux of incident neutrons in the 1-100 eV spectral range and high momentum transfer, 90-140 Å^{-1}, are available. In this scattering regime the Impulse approximation (IA) can be invoked and the dynamical structure factor $S(q,\omega)$, is simply related to the single particle momentum distribution. The experiment was performed at a constant temperature T=2 K varying the applied pressure in order to obtain a high density liquid sample (molar volume v = 23.8 cm^3/mole), a body centred cubic (bcc) sample (molar volume v = 20.1 cm^3/mole) and a hexagonal close packed (hcp) sample (molar volume v = 18.8 cm^3/mole) of ^{3}He. In order to

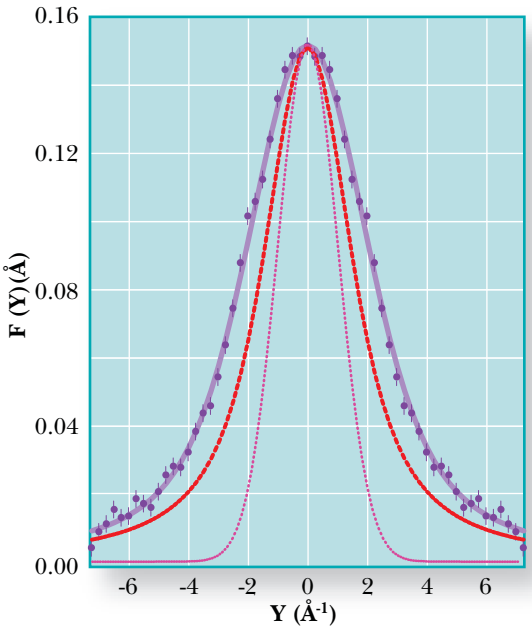

Fig. H22.1 Scaling scattering function F(y) for the bcc solid sample. Data (full circles); best fit (purple line); resolution function of eVS (red line); simulated resolution function expected for VESUVIO (pink line).

minimise the absorption of the sample it was vital to perform the experiment using the highest available incident neutron energies. The inelastic neutron spectrum has been determined using the filter difference technique measuring the time of flight of the neutrons absorbed by the 4.908 eV resonance of the Au foil filter. Under this experimental condition the average ratio between the sample absorption and scattering cross section was about 30, to be compared with a ratio of about 1000 for thermal neutrons.

Within the IA, the dynamic response of the sample, S(q,ω), can be expressed in terms of the single particle momentum distribution of the initial state, n(p), (i.e. the state of each particle before the collision with the incident neutron),

$$S(\vec{q},\omega) = \int n(\vec{p})\delta\ (\omega - \frac{q^2}{2M} - \frac{\vec{q}\cdot\vec{p}}{M})d\vec{p}$$

The dynamic response function in the IA can also be described in terms of a scaling function $F(y)=q/M\ S(q,\omega)$, where

$$y = \frac{M}{q}\ (\omega - \frac{q^2}{2M})$$

and M is the ^{3}He mass. The second moment of $F(y)$ is proportional to the single particle mean kinetic energy and, due to the scaling properties, a single response function resulting from an average over all the 32 detectors was derived. An example of the scaling function is reported in Fig. H22.1 for the bcc sample. The values of $<E_k>$ were obtained from this function assuming a Gaussian function for the helium momentum distribution, n(p), and exploiting the second moment sum rule.

In Fig. H22.2 the molar volume dependence of $<E_k>$ derived from the DINS experiment is plotted together with the same quantity evaluated by both Diffusion Monte Carlo (DMC) calculations and by the self-consistent phonon method. We observe that the experimental values of $<E_k>$ are in remarkable agreement with the DMC calculations for both liquid and solid phases. It has to be stressed that, among theoretical models, the DMC simulations seem to provide the most accurate results. Such a broad-band agreement has been attributed to the use of a recent ab initio interatomic potential which also includes three-body terms. As shown in Fig. H22.1, values of the single particle mean kinetic energy obtained through the self-consistent phonon calculation lie systematically lower than the experimental results. Indeed in this theoretical approach the anharmonic contributions to $<E_k>$ are only approximately accounted for through the introduction of a cubic anharmonic term. These results represent the first experimental determination of $<E_k>$ in solid ^{3}He and the demonstration that epithermal neutron scattering is the ideal quantitative probe for the study of single particle dynamic properties.

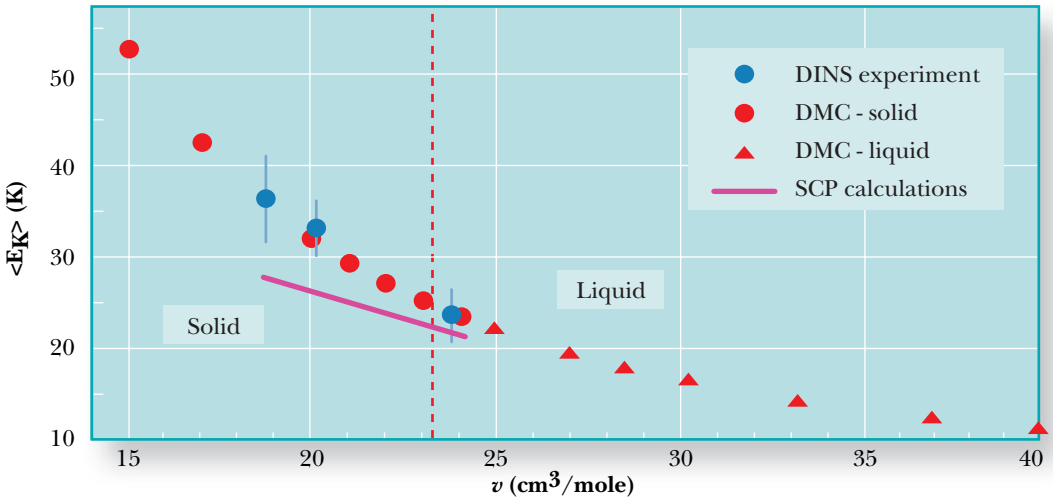

Fig. H22.2 Molar volume dependence of $<E_k>$: present DINS measurements (blue circles); Diffusion Monte Carlo calculations for the solid phase by Moroni et al. (red circles): Diffusion Monte Carlo calculations for the liquid phase by Casulleras et al. (red triangles): Self- Consistent Phonon calculations by Moleko et al. (continuous line); the vertical line represents the solid-liquid boundary at T=2 K.

Mapping exotic spin correlations by muon spin relaxation measurements.

Implanted positive muons can be used to investigate spin fluctuations in magnetic materials. Traditionally, the spin lattice relaxation time of a muon in a magnetic environment is interpreted using the concept of spin correlation time. However in some situations, no correlation time can be assigned to the spins, and a different interpretation is required. We have developed a model for such cases, using ISIS μSR data from a spin glass system as a test.

A Keren, G Bazalitsky (Technion), I Campbell (Orsay), J Lord (ISIS)

In a muon measurement with applied field parallel to the initial muon polarisation direction, one determines the time t it takes the polarization $P(H,t)$ to reach thermal equilibrium with the system under investigation, from an initial non-equilibrium state. The muon flip rate $(1/T_1)$ depends on how popular the Larmor frequency ($\omega_L=\gamma_\mu H$) is among the atomic spin fluctuations, since in order for the muon to flip from up to down states it must absorb (or release, depending on the field direction) the energy $\hbar w_L$ to the lattice. In other words, T_1 will be short if the Fourier transform of the spin-spin correlation function $q(t)=<S(t)S(0)>$ at ω_L is large, and vice versa.

It is customary to assume that the correlation function decays exponentially with some correlation time τ and therefore the Fourier transform of $q(t)$ is a Lorentzian in terms of the field H. Thus, at asymptotically high fields we expect T_1 proportional to H^2, and the muon polarization $P(H,t)$ should be a function of the ratio t/H^2. This conclusion holds even if instead of having a single correlation time in the system there is a distribution of τ's. However, the assumption that there is a correlation time could be incorrect to start with, and in many complex systems $q(t)$ can be strongly non-exponential, with time scale invariance or hierarchical relaxation. Here we demonstrate the presence of non-exponential correlation functions in nature by performing μSR measurements on the Heisenberg spin glass AgMn(0.5 at. %). We chose this system since numerical work on glasses indicates the presence of 'exotic' correlation functions. We also show how to determine the functional form of $q(t)$ using the field dependent muon depolarization measurements.

Fig. H23.1 shows representative data sets of the muon asymmetry $A(H,t)$, which is proportional to $P(H,t)$, at T=2.9 K (above T_g=2.8K) and at various fields. Note the break in the time axis. Clearly, H affects the muon polarization very strongly over more than two orders of magnitude in a magnetic field. In order to test whether either a single correlation time or a distribution of times could describe this system, we normalize the time t by the field to some power. We found that for high fields, the muon polarization is a function of t/H and not t/H^2 (Fig. H23.2). Thus, an exponential relaxation function or even a sum of exponential relaxations cannot account for these data. One must search for a correlation function whose Fourier transform falls off as 1/ω at high frequencies. This requirement

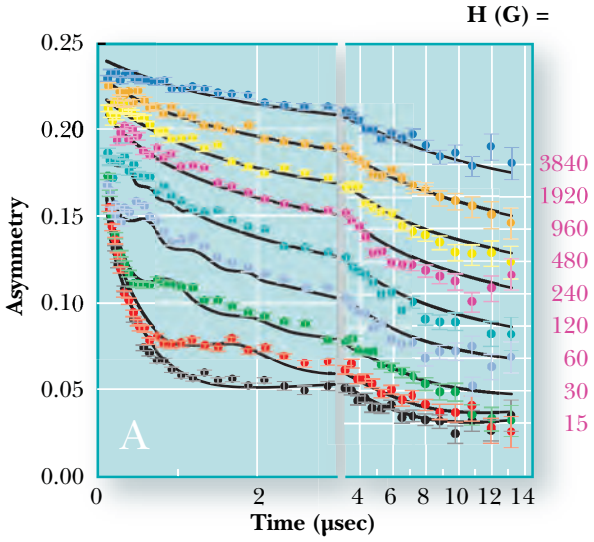

Fig.H23.1 Asymmetry versus time in the spin glass AgMn (0.5 atomic %) at T>T_g for various longitudinal magnetic fields. The solid lines are fits to a model relating T_1 to a cut off power law correlation function (as described in the text).

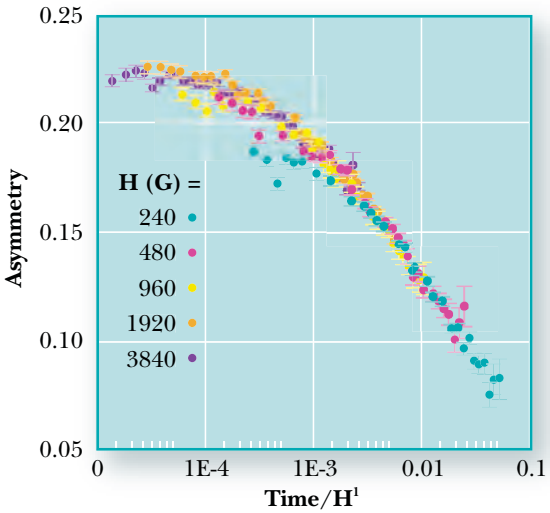

determines the behaviour of the correlation function at early times.

For low values of H, clear wiggles are observed in the beginning of the data (Fig. H23.1). The source of the wiggles are those muons for which a local transverse magnetic field B_T, has not relaxed abruptly during the time of one rotation. These muons will oscillate around the vector sum of both internal and external fields at a frequency $\omega=\gamma_\mu(H^2+B_T^2)^{1/2}$. Since at $T>T_g$ there is a distribution of B_T with zero average, the contribution of the local internal fields will show up as a relaxation of the wiggles, while the frequency of the wiggles will be at ω_L, the Larmour frequency. However, if there is a cutoff time τ, then by the time $t > \tau$ abrupt field relaxation occurs for all muons. In this case, a wiggle pattern will not be seen for longer times. As a result, the observation of a wiggle pattern up to time t is the proof that there are local fields that do not relax abruptly within time t. Thus the observation of wiggles gives us a model independent estimate of τ.

The combination of the asymptotic field dependence shown in Fig. H23.2 and the wiggles observed in Fig. H23.1 forces us to consider a cut off power law correlation function of the form $q(t)=t^{*}exp(-t/\tau)$ where x is a dynamical power. This, in fact, is the function used to analyze most of the molecular dynamic numerical work on spin glasses, and we have demonstrated that this function can be introduced into the general theory of spin-lattice relaxation. The fits shown in Fig. H23.1 are obtained using this theory; they capture the long time behaviour and the frequency of the wiggles very well. However, the account for the relaxation of the wiggles is not perfect.

We have performed these measurements at different temperatures above T_g, and determined the value of x at each temperature. As the temperature decreases x decreases (Fig. H23.3). In fact, our analysis shows that x is the only temperature-dependent parameter. It is therefore the stretching out of the power law part (decreasing x) that reveals the slowing down of spin fluctuation upon cooling.

Fig. H23.2. The asymmetry from Fig. H23.1 plotted as a function of t/H *for fields higher than 240 G. The fact that the asymmetry is a function of* t/H *and not* t/H² *rules out the possibility of describing the spin correlation function with one or many correlation times.*

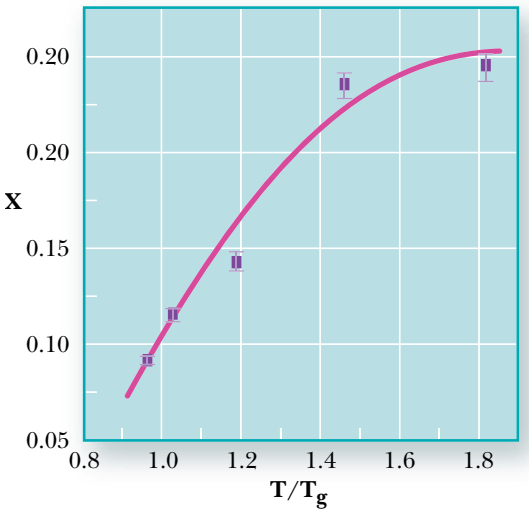

Fig. H23.3. The dynamic power x plotted versus temperature. The slowing down of spin fluctuations is manifested in the decrease of x upon cooling.

Dynamics in the nematic liquid crystal 5-CB studied with μSR

Liquid crystals are widely used as displays. An important property to be optimised for a liquid crystal to be useful in such an application is the speed at which it can be switched. Here we demonstrate for the first time how the muon spin depolarization technique can be used to measure the dynamical properties of liquid crystals.

BW Lovett, SJ Blundell (Oxford), F L Pratt (ISIS)

The uniaxial nematic (N) mesophase of a liquid crystal is a state of matter which exhibits symmetry properties intermediate between those of a solid (S) and an isotropic liquid (I). In the N-phase, molecules have translational freedom and orientate preferentially along one particular axis, which is defined by a unit vector called the director. This orientationally ordered phase arises due to packing constraints of the rod-like molecules. The N-phase has been investigated by a variety of experimental techniques, particularly NMR, and there has been significant theoretical interest in the nature of the molecular dynamics. The usefulness of the positive muon, an alternative local magnetic probe, has recently been established in dynamical studies of small organic molecules, but this technique has not until now been applied to liquid crystals.

We present the results of muon measurements carried out on probably the most widely used nematic compound 4'-n-pentyl-4-cyanobiphenyl (5CB). It has a S-N transition at 24 °C and a N-I transition at 35 °C. In 5CB, we expect muonium (Mu = μ^+e^-) to form by electron capture soon after muon implantation. Mu behaves as a light isotope of hydrogen and so reacts with unsaturated bonds forming a muonated radical. Since 5CB is a relatively large molecule, we implicitly assume that the radical formed has the same dynamical properties as the parent 5CB. The unpaired electronic spin density couples to the muon spin through the isotropic Fermi contact interaction and the anisotropic magnetic dipole-dipole interaction.

At high magnetic fields applied transverse to the muon spin direction, two muonium precession frequencies are observed from which can be extracted the isotropic muon hyperfine constant. In the liquid phase, where the anisotropic component of the hyperfine tensor is averaged out, we identify four pairs of pairs of Mu precession signals (see Fig. H24.1) due to the four possible inequivalent sites for Mu addition to the 5CB molecule. The obtained values agree with predictions based on empirical rules for muon addition to substituted benzene molecules.

In magnetic fields applied parallel to the muon polarisation direction, relaxation in the muon polarization can only occur if there is a time varying fluctuation in the magnetic environment. This spin-lattice relaxation allows us to extract dynamical information on 5CB. We show specimen depolarization curves, taken in the S, N and I phases, and the temperature dependence of the relaxation rate, in Fig. H24.2. The relaxation in the N phase is clearly much greater than that in the S phase, a fact which may be attributed to a

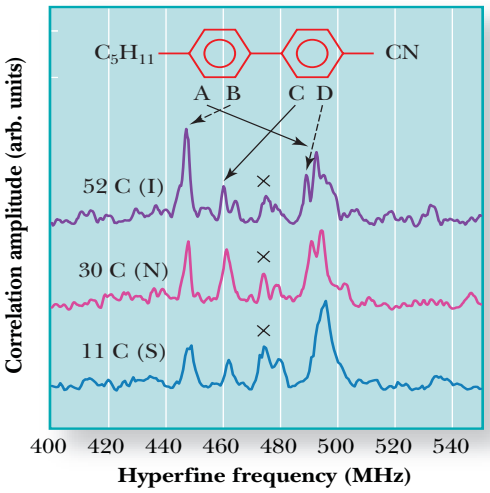

Fig. H24.1. Structure of 5CB showing four muon positions and corresponding correlation amplitudes obtained from a transverse field experiment. The cross marks an artifact peak.

greater fluctuation rate of the dipolar part of the hyperfine interaction between the muon and the electronic spin density. The relaxation becomes slower at higher temperatures, indicating faster fluctuations and stronger motional narrowing effects.

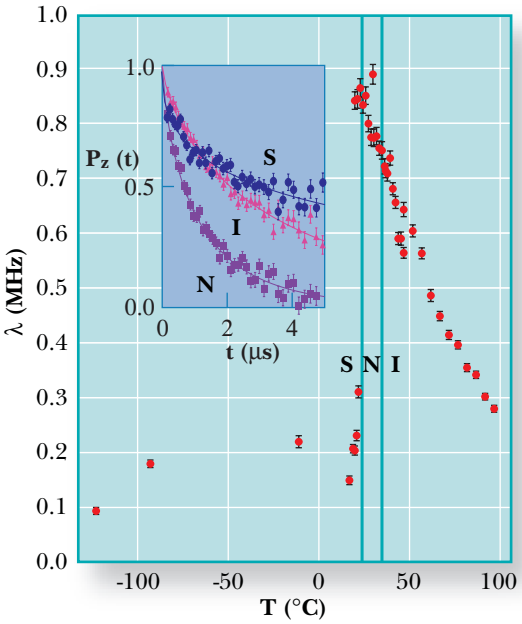

The relaxation could be dominated by a modulation of the contact term which would occur through intramolecular modes, i.e. changes in internal vibrational or torsional states (but this would not be effective at zero field, in contrast to our results) or due to whole molecule reorientation, through modulation of the dipolar part of the interaction.

Modelling of the muon depolarisation allows extraction of the fluctuation rate (Fig. H24.3). There is a large increase in its value at the S-N transition as the molecules become free to move around. The fluctuation rate then progressively increases as the temperature is raised, and is well fitted by an activated dependence with energy barrier 159(3) meV.

The absolute values of the fluctuation rate and the size of the energy barrier are in reasonable agreement with deuterium nuclear quadrupole resonance results. Since the relaxation does not disappear in zero field and is well described by the changing dipolar field and not so well by a fluctuating Fermi contact term, it could be that we are seeing a rotation of the ring as part of rotation of the whole molecule, and not an internal torsional mode. The lack of discontinuity in the relaxation rate at the N-I transition suggests we are seeing motion not intrinsic to the liquid crystal phase, i.e. that director fluctuations are not important. This would be consistent with a rotation of the whole molecule about its long axis, which is not a collective phenomenon. The large dynamic range observable by muons when used in organic radicals enables observation of both the slower collective dynamical properties of 5CB and also the faster individual molecular motions.

The muon technique has several advantages over NMR. NMR results can be complicated by the effect of dipolar coupling of the aromatic protons of interest with the methyl protons at the ends of the aliphatic chain. Muons do not couple strongly to protons at such a large distance because the muon will naturally select sites of unsaturation and the radical spin is then located on the aromatic ring, precisely the parts of the molecule which give rise to mesogenic behaviour. This to some extent circumvents the need for selective deuteration which is required for NMR studies in liquid crystals.

Fig. H24.2. Main figure: muon relaxation rate as a function of temperature at 50 mT. Inset: muon depolarization at 50 mT for the S, N and I-phases.

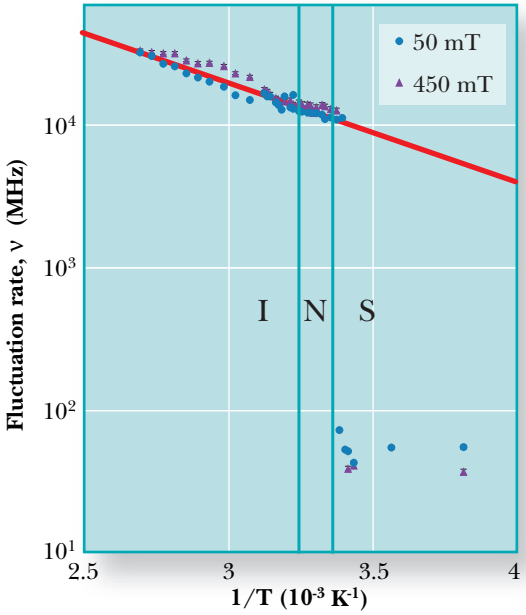

Fig. H24.3. Molecular fluctuation rate as a function of temperature at 50 and 450 mT.

Engineering applications of Bragg edge neutron transmission

Analysis of Bragg edges in the transmitted neutron beam of polycrystalline materials is providing novel solutions in the engineering use of neutrons. A new 10 x 10 pixellated detector enables fast and accurate strain imaging, but can also be used to monitor quantities such as texture and phase fraction. Using the $\sin^2\psi$ method, maps of the unstressed lattice parameter can be produced, vital information for the determination of stress in complex engineering components. The large total detector area (400mm^2) provides extremely high rates of data acquisition and has allowed the study of in situ phase transformations in bulk steel with a time resolution better than 10s.

J R Santisteban, M E Fitzpatrick, L Edwards (Open University), A Steuwer, PJ Withers (Manchester Materials Science Centre), M R Daymond, NJ Rhodes, E M Schooneveld (ISIS)

Neutron diffraction can provide unique insights into stress fields deep within engineering components. It has become an increasingly important engineering tool leading to improved manufacturing processes and structural integrity lifing procedures. However, the determination of unstressed lattice parameters (a_0) from which elastic strains can be calculated is still problematic, particularly if compositional variations exist.

A new solution to this problem uses the Bragg edges appearing in time of flight (TOF) spectra of *transmitted* neutrons (Fig. H25.1). The transmission spectrum contains a wealth of information about texture, crystalline states, constituent phases etc. in the sample as it is due to all the available processes scattering neutrons from the beam. Each Bragg edge corresponds to a particular crystal lattice spacing; changes in their position thus enable the determination of strain parallel to the beam. An edge profile function of the Bragg edges observed at ISIS has been implemented in specially developed software for multiple edge refinements, enabling inter-planar distances to be determined to $\Delta d/d=10^{-5}$.

The transmission geometry enables a pixellated detector to produce an 'image' of the lattice parameter variation in the sample. However, as the measurement is an average over the path through the sample, it is useful mainly for examining 2D objects. A new 10 x 10 array of 2 x 2 mm^2 scintillator pixels has been built and installed on ENGIN. Fig H25.2 presents the strain around a cold expanded hole in steel plate. Cold expansion increases the fatigue lives of fastener holes. Fatigue life predictions rely critically on estimates of the residual stress distribution about the hole.

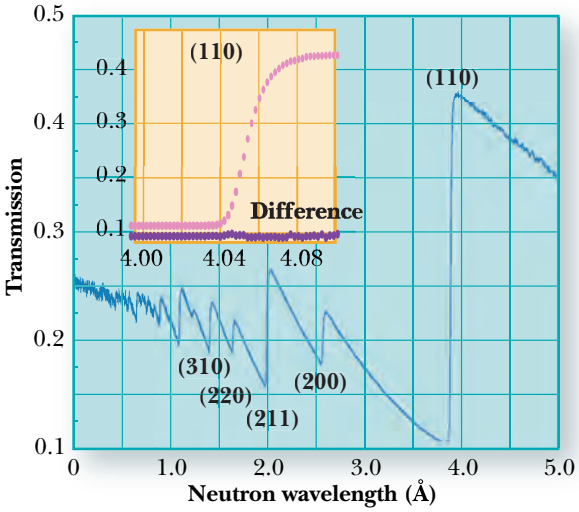

Fig. H25.1. Neutron transmission of Fe powder displaying characteristic Bragg edges. A least-squares refinement of the (110) edge is shown in the inset.

The technique can also be used to produce a map of the stress free lattice parameter using the $sin^2\psi$ technique. For a biaxial (plane) stress field, the unstressed

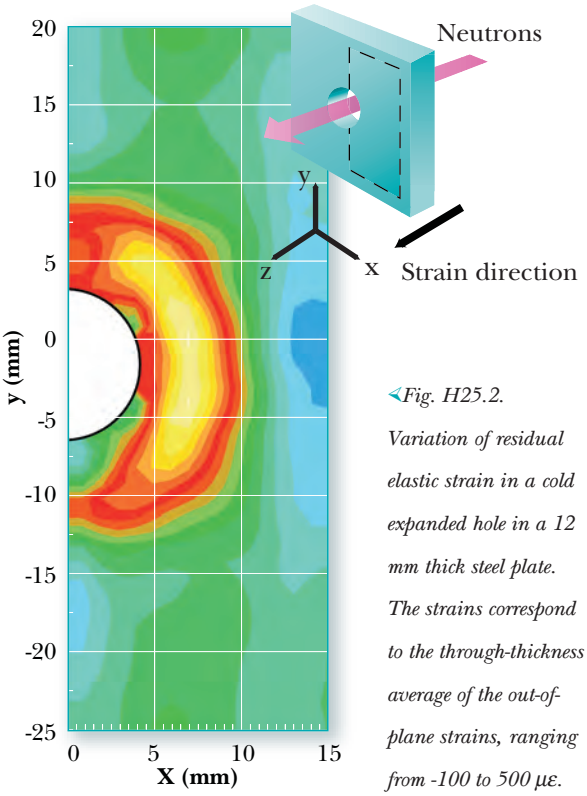

Fig. H25.2. Variation of residual elastic strain in a cold expanded hole in a 12 mm thick steel plate. The strains correspond to the through-thickness average of the out-of-plane strains, ranging from -100 to 500 με.

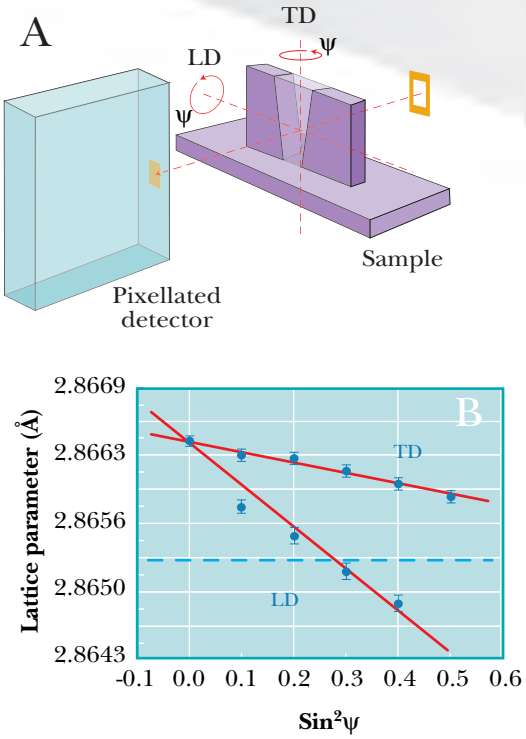

Fig. H25.3. Determination of the unstressed lattice parameter a_0 by transmission: (a) Experimental set-up, indicating the angle of tilt ψ , (b) Value of a_0 (dotted blue line) determined from the linear dependence of a on $\sin^2\psi$ for two orthogonal directions (c). Macrograph of the ferritic weld sample, (d) a_0 map for the white rectangle shown in (c).

lattice parameter can be defined as the sample is tilted around two perpendicular axes (TD, LD in Fig. H25.3a). The linear dependence of the lattice parameter on $\sin^2\psi$ and the material's properties define the unstressed lattice parameter a_0, indicated by the dotted blue line in Fig. H25.3b. The method has been applied to produce a map of the a_0 variation for a ferritic steel weld round robin sample in the VAMAS TWA 20 program to develop an international standard for residual stress measurements by neutron diffraction. A 3 mm thin slice from the weld was tilted along two perpendicular axes producing a graph similar to Fig. H25.3b for each pixel of the detector. The imaged area is shown in Fig. H25.3c and the resulting map of the unstressed lattice parameter shown as pseudo-strain relative to the parent material is given in Fig. H25.3d. The distribution of a_0 mirrors the weld and its associated heat-affected zone.

The very high counting rate obtained on summing all the detector pixels opens new possibilities in studying phase transformations in situ. Moreover, the technique is insensitive to the sample location along the beam giving flexibility and simple sample environments. A recent experiment has studied the isothermal decomposition from Austenite (fcc or γ-Fe) to Bainite (bcc α-Fe + carbides) in steel, using two tubular furnaces aligned with the neutron beam. Fig. H25.4 shows part of the total cross section measured at four different times.

These examples, from EPSRC sponsored research, show that unique information can be relatively easily obtained from the transmitted neutron beam. In particular, the use of a pixellated detector opens up a whole new range of imaging applications.

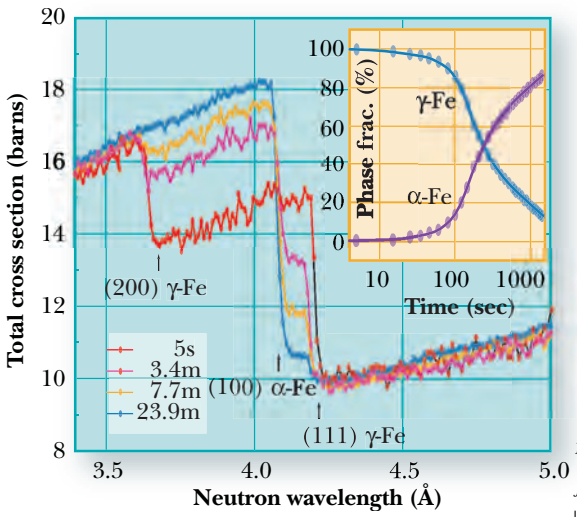

Fig. FH25.4. Total cross section of EN24 steel at 380 °C after austenisation at 830 °C. The times are measured from sample insertion in the furnace. The inset shows the phase evolution of γ and α obtained from Rietveld analysis of spectra.

The ISIS neutron and muon production targets

The performance of the neutron and muon target assemblies is crucial to ISIS being a high-intensity, reliable source. Described here are developments of the neutron target which have resulted in flux increases to instruments using the hydrogen moderator, and construction of a new muon target assembly to enable operation at a proton current of 300μA.

T A Broome, J Hogston (ISIS)

Neutron targets

Depleted uranium was the original choice for the ISIS neutron target material. While this proved reasonably satisfactory up to about 100 μA proton current, it became clear that the lifetime of such a target was too short to be practical at currents much above this. This eventuality had been considered, so a tantalum target, geometrically identical to the uranium design, had been made as a backup. The four tantalum targets which have been used since have given very few operational problems.

It is well known that tungsten is a better target material than tantalum in two main respects. First it produces more neutrons per proton, and secondly the heat produced from the induced activity in tungsten is about one third that of tantalum. However, tungsten is a more difficult metal to machine and is subject to corrosion by water.

A development programme was put in place to establish fabrication methods to construct a target made from tungsten plates clad in tantalum. The cooling system design was optimised to minimise the number of cooling channels in the target and simplify the complex cooling manifold design required for uranium targets and used on the tantalum ones. A schematic of the target design is shown in Fig. H26.1.

Calculations showed that the overall increase in neutron production from this new target would be 15% greater than that from tantalum. A study was also performed to calculate the fluxes from the ISIS moderators as a function of target position along the proton beam direction, keeping the moderators in their present position. The results of these calculations are shown in Fig. H26.2.

The new target was installed at the start of the 2001 run year. After consultation with the ISIS Instrument Scientists it was decided to position it 5 cm downstream of the old target position. This has the result that the fluxes from the upstream moderators are un-

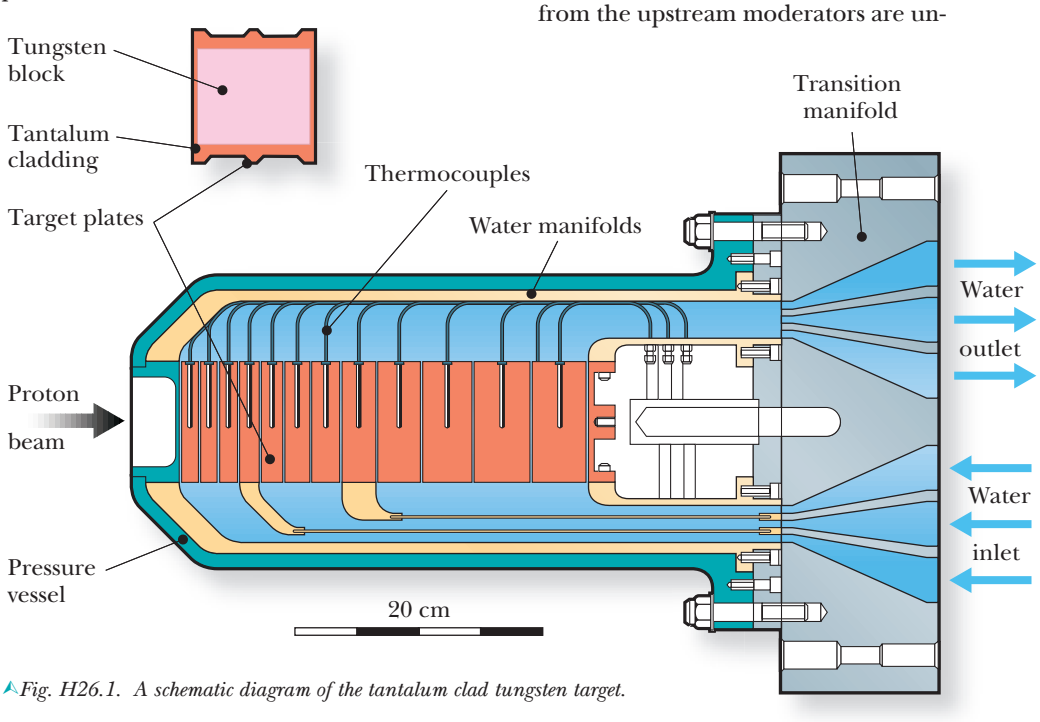

Fig. H26.1. A schematic diagram of the tantalum clad tungsten target.

changed, but the hydrogen moderator flux - affecting SURF, CRISP and LOQ - was calculated to increase by about 28%. In operation this gain has been measured to be 25%.

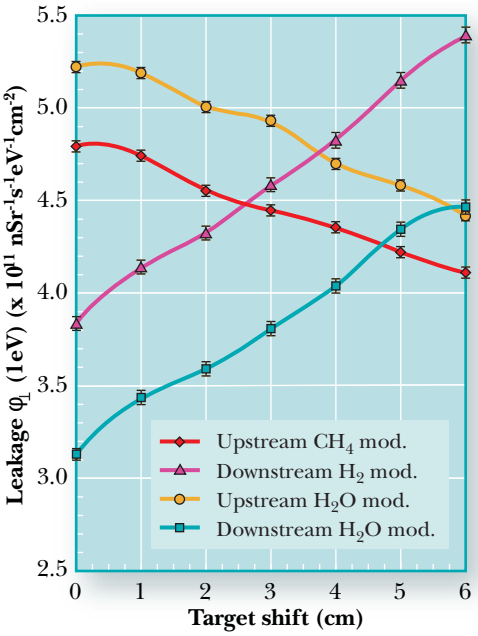

Muon target upgrade

The muon transmission target is positioned part way along the extracted proton beam line and services three muon beamlines on the south side of the ISIS hall and the Japanese RIKEN-RAL facility on the north side. The present target consists of a thin (0.5-0.7 cm) pyrolytic graphite slab (5 x 5 cm in area) brazed to a water-cooled copper disc. It has been decided that this design will not be able to cope with the power dissipated in the target when ISIS is upgraded to a beam of 300 μA.

To improve the cooling and the brazed joint between the dissimilar materials, a cone shaped joint (cone angle of 20°) has been used to produce new targets, rather than the flat butt joint of the old design. Also, instead of brazing, diffusion bonding, using an interlayer of pure aluminium foil 0.25mm thick, was found to be successful in producing a robust uniform bond (Fig. H26.3). The diffusion bonding is achieved in a vacuum furnace with a loading of 1 tonne at a temperature of about

Fig. H26.3. A section through the diffusion bonded carbon/ carbon composite cone.

550°C. A new clamp assembly has also been developed to support the target which will make remote handling easier (Fig. H26.4).

The intention is to use a 9 mm thick target which will absorb about 2 kW of beam power. It was decided to abandon the pyrolitic graphite in favour of a carbon/carbon fibre composite, because the cone joint requires uniform thermal properties and the larger thickness is difficult to obtain. The composite also has a higher thermal conductivity than ordinary graphite.

Fig. H26.2. The variation of the fluxes from the ISIS moderators with target position.

Thermal tests of the target assembly were carried out using a 60 kV electron beam at AEA, Culham. They indicated that the target will run reliably at lower temperatures than the present target. A target temperature of 1300 °C was recorded at 1.5 kW dissipation. These measurements accorded well with finite element analysis ANSYS calculations. It is hoped to install the new target assembly in 2002.

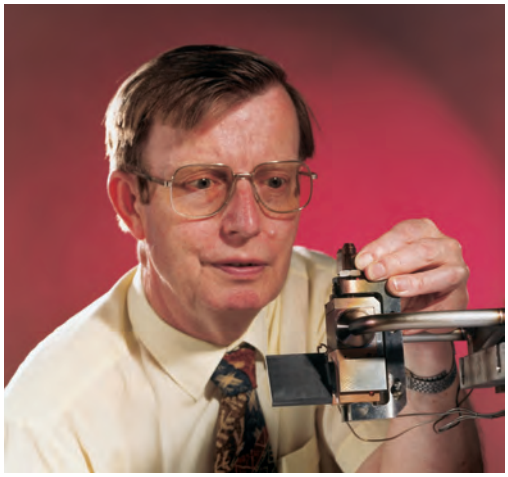

Fig. H26.4. John Hogston adjusts the new muon target in its water-cooled clamp assembly.

Beam stability in the ISIS synchrotron

Beam stability is an important issue in circular accelerators; any small effect which tends to 'blow up' the beam is repeated many times and may result in disastrous loss to the walls. The mechanisms for these losses are often complicated and may be a function of many parameters. Hence, the design of the synchrotron and its components is crucial if it is to run at high intensity with little beam loss, and requires considerable skill on the part of the accelerator designers.

ISIS operates at high beam currents, which are set by beam loss levels that allow 'hands-on' maintenance of components in the ring with acceptable levels of radiation. A typical operating level is 2.5×10^{13} protons per pulse (ppp) at 50 Hz. A maximum coasting beam of 4×10^{13} ppp has been obtained at the injection energy of 70 MeV (with the limit set by the performance of the linac injector at the time of the experiment).

ISIS is at the cutting edge of this science and the beam stability results are somewhat controversial among some accelerator physicists. There are five beam stability issues of concern, which are elaborated below. Of these, the first and fifth are not observed in ISIS and the second not in normal operation; the third and fourth are found but are cured by programming the vertical and horizontal betatron tune values, particularly the former.

1.The interaction of the longitudinal electromagnetic fields of a coasting beam with the longitudinal impedance of the vacuum chamber (longitudinal coasting beam resistive wall effect). Perturbations in the line density of a coasting beam give rise to longitudinal space charge fields. Dangerous mode frequencies are in the range 100 to 3000 MHz. Such components exist in the ISIS injected beam due to the residue of the linac bunch structure at 202.5 MHz and its harmonics. Experiments on ISIS show rapid damping of the linac bunch structure residue instead of the predicted antidamping. Initial concern over this feature has thus disappeared.

2. The interaction of the longitudinal fields of a bunched beam with the longitudinal impedance of the chamber, particularly the rf cavities (longitudinal bunched beam instability). The

Fig. H27.1. The ISIS synchrotron.

G H Rees *(ISIS)*

most important effects are the interaction of the bunched beam with the fundamental and parasitic modes of the six rf cavities. Feed-forward beam compensation is used at the start of acceleration to reduce the effect of the heavy fundamental beam loading. The feed-forward is needed for all intensities above 10% of the normal operating level. Without feed-forward, there are large modulations of the cavity fields, with resultant beam loss. After 2 ms, the feed-forward control is gradually removed.

Envelope mode oscillations may develop towards the end of the 10 ms acceleration cycle. The source is again the fundamental cavity mode, but correct reactive tuning of the cavity removes the oscillations.

The cavities have been designed to reduce the number of parasitic higher modes. There is only one mode in the range of frequencies of the beam spectrum and the interaction with this mode is insufficient to cause instability.

3.The interaction of the transverse fields of a coasting beam with the transverse impedance of the chamber (transverse coasting beam resistive wall effect). An unstable coasting beam mode is observed at $4x10^{13}$ ppp and 70 MeV if the vertical betatron tune is > 3.7. The instability is removed by lowering the vertical betatron tune. Chromatic tune spreads are small compared to the space charge tune shifts and spreads, and are less than the values predicted as necessary for stability. However, there is no evidence for any growth during ISIS injection when some beam bunching disturbs the development of any coasting beam mode.

4.The interaction of the transverse fields of a bunched beam with the transverse impedance of the chamber and the influence of the ring chromaticity (the bunched beam head-tail instability). The two proton bunches in ISIS may exhibit some coherent vertical growth during the 2 to 4 ms interval of the 0 to 10 ms acceleration period. The growth is suppressed almost entirely with the ring at its natural chromaticity if the vertical betatron tune is ramped down during the 2 to 4 ms stage. There is no instability observed in the periods 0 to 2 and 4 to 10 ms.

The unstable pattern is that of a single displacement node for the coherent motion at each bunch centre, as shown in Fig. H27.2 . The nodes are traditionally assumed to arise due to the cancellations between the coherent betatron motions of the positive and negative off-momentum bunch particles. Excitation forces arise due to the differential currents in the resistive walls. It is speculated for ISIS that the central node is caused by a cancellation between the coherent motions of small and large synchrotron amplitude particles.

5. The ionisation of the residual gas in the machine by the circulating beam and its subsequent interaction with the ionised electrons and the secondary electrons created at the chamber walls (the electron-proton or electron cloud instability). A residual gas, electron-proton instability is not observed in ISIS, for either a coasting or a bunched beam, in contrast to the limiting situation in the PSR at LANL. ISIS beam densities are lower in the case of bunched beams, but higher densities have been achieved for coasting beams. The observations are of much interest for the design of next generation, more intense, neutron sources.

Fig. H27.2. The Head-tail Instability. The amplitude of the beam is prevented from increasing between 2-4 ms by ramping the quadrupole magnet fields in the ring. The average vertical amplitude of the particles in the bunch is shown as the particles rotate in the synchrotron.

Instrument Developments 3

Development at ISIS is a continuous process, driven both in response to the changing needs of the user community and to maintain the facility as a world-class neutron and muon source. Evolution and development of existing instruments, and design and construction of new ones, open up fresh opportunities for condensed matter investigations. Some of the major improvements over the past year are described here.

The development of new instruments has been a constant process since ISIS began operations. The scarcity of neutron beam ports now requires existing instruments to be taken off-line for new ones to take their place. Described in this chapter are the ongoing, major instrument developments over the past year.

GEM

The first phase of the construction of the GEM detector was completed in June, with the installation of the low-angle bank (Bank I, ~5°-15°). The low-Q information provided by these new detectors (d-spacing up to 30 Å in the first wavelength frame) will provide GEM with enhanced capabilities in the field of magnetic structures and disordered materials. A new EPSRC grant for the completion of the GEM detector has been approved for funding. The construction of the new detectors, starting from the 65 degree (Bank 4) modules, will commence immediately, and new modules will be installed progressively for the next year and a half. Final completion is expected in early 2003.

On the sample environment side, a major milestone was reached in late July, with the delivery of the GEM oscillating radial collimator (ORC, Fig. 3.1). This device, to be installed during the October shutdown, is designed to suppress the scattering from sample environment, which, in most cases, is the dominant source of background. With the ORC in place, measurements of milligram-size samples inside cryostats, furnaces and the cryomagnet will become possible for the first time. The GEM-ORC, developed in collaboration with EuroCollimators Ltd., is unique in the world because of its size (it must collimate *all* the GEM detectors simultaneously) and its oscillation mechanism, designed to operate in a $1x10^{-4}$ mbar vacuum.

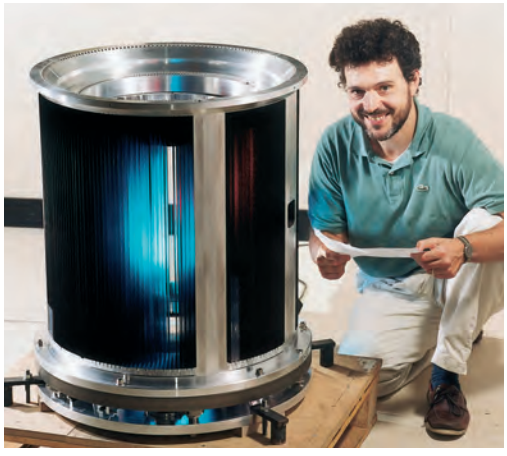

Fig. 3.1. Paolo Radaelli (ISIS) with the GEM oscillating radial collimator (01RC3465).

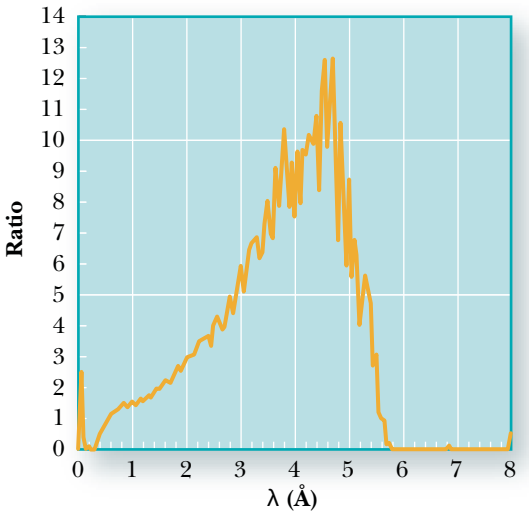

Fig. 3.2. Flux gains on Prisma measured with standard vanadium sample and diffraction detector.

PRISMA

During the April 2000 shutdown, Phase I of the Prisma Neutron Guide Project was completed. The major reconstruction of the PRISMA primary spectrometer includes the installation of two metres of supermirror guide in the shutter, two supermirror-on-silicon frame-overlap filters, a new disc chopper, a modified nimonic chopper, the diverging guide steelwork, and a modular nose section housing two sets of collimators, two incident beam monitors, and a set of jaws. In addition, the spectrometer was almost entirely recabled. Software for the control of the jaws and the collimators has been completed and installed on the LabVIEW system control PC, and the two programs now run simultaneously.

First neutrons were received on July 4th, followed by a commissioning period, and successful user experiments using both the diffraction and the analyser modules took place up until the October shutdown. Phase II installation took place during this period. The existing collimation within the target wall has been removed and the second two metre

length of supermirror guide has been added. Additionally, supermirrors have been installed in the diverging steelwork located downstream from the chopper positions.

After Phase II of the installation, the flux gains on the sample are between 2 and 10 depending upon the wavelength (Fig. 3.2).

OSIRIS

OSIRIS is presently scheduled for diffraction experiments whilst it awaits the installation of its inelastic analyser bank, which was delayed due to the failure of a major vacuum component. However, the crystal analyser is assembled and installation is planned for the first half of 2002, together with a large collimator. The 25 meV analyser involves a 40cm high array of graphite crystals, which will be cooled to about 20 K. In the meantime the diffractometer section of the instrument has been fully commissioned and, by way of comparison, OSIRIS produces the same count rate as GEM for the same resolution but not, of course, over the same Q-range.

Polarisation analysis on OSIRIS will be performed using a ^{3}He spin-filter. Advantage will be taken of the new ISIS polarisation laboratory that is now equipped to develop a continuously pumped circulating system. This is expected to improve levels of ^{3}He polarisation and avoid problems associated with polarisation time-dependence. It is expected to be running under laboratory conditions during the coming year.

ENGIN-X

Work on ENGIN-X, the new high resolution diffractometer optimised for engineering measurements, continues apace. ENGIN-X will be situated on a fifty metre flight path, sharing the same primary shutter as HRPD. It will include facilities to handle very large components, as well as to carry out *in situ* thermomechanical loading. The new building which will house the guide and experimental area has been completed ready for installation of the various beamline components during the long shutdown starting at the end of 2001.

A number of innovations have been incorporated in the design, including variable incident resolution and a new high spatial resolution scintillator detector design. A prototype for the new detector, which is based on a 3 mm pitch, rather than the 5 mm pitch found on other powder diffractometers at ISIS, has been successfully tested. ENGIN-X is expected to be operational for summer 2002.

TOSCA

Installation and commissioning of the final phase of TOSCA took place this year. The project has required a complete rebuild of the beamline from the biological shield to the beamstop. A background and frame overlap chopper was installed with the instrument at 17 m from the source (TFXA and TOSCA-I were at 12 m). This resulted in a major gain in resolution, which is now comparable to that of routine infrared and Raman spectra. The other major differences from its predecessors are that detectors are located in both forward and backscattering directions, and there is provision for diffraction detectors at scattering angles of 45° and 135° in addition to those at

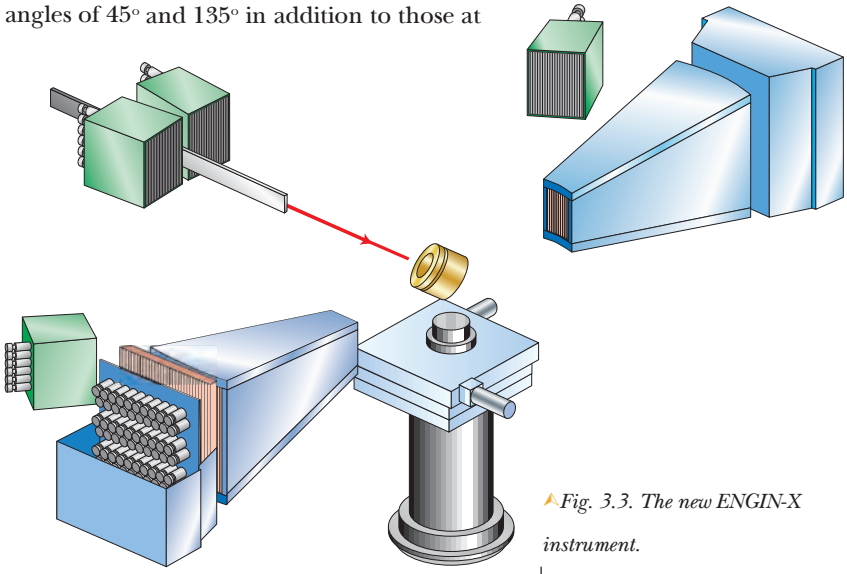

Fig. 3.3. The new ENGIN-X instrument.

Fig. 3.4. One of the two banks of seven modules comprising the new HRPD 90° bank (00RC5523).

180°. The diffraction detectors at 180° will be installed in the autumn 2001 shutdown and those at 45° and 135° during 2002. A second instrument position at 22 m was also created and it is intended that this should be used for the installation of INES, a diffractometer provided by the Italian CNR.

HRPD

The uniquely high resolution available on the HRPD instrument for powder diffraction studies ($\Delta d/d$ of ~4.10^{-4}) has been extended further by the latest upgrade: the installation and technical commissioning of new, much larger detector arrays at ±90°. The installation of the 14 GEM type detector modules increases the solid angle by a factor of 10 and the enhancement provides an order of magnitude gain in count rate over the previous 90° bank, with essentially unchanged resolution of $\Delta d/d \sim 2.10^{-3}$. The high count-rate, high resolution 90° bank is now an ideal, well-matched complement to the ultra-high resolution backscattering bank, helping to maintain the world-leading capabilities of HRPD. The project was funded by a grant from EPSRC through the Chemistry multi-project research equipment science programme following wide support from the User Community.

SXD

The new SXD instrument, funded by EPSRC, is now installed and beginning operation, having taken its first neutrons on 11 May 2001. This new instrument is completely reconfigured, with 11 PSDs in the detector array. The fabrication of the 11 detector modules by an external manufacturer led to completion of the construction phase well inside the original schedule. The array now offers more than 2π solid angle coverage. Following the basic installation of the sample and detector array, work has begun on the incident beam optics. These will include adjustable beam-defining jaws - many of the samples on SXD will have dimensions of order 1 mm - and laser alignment facilities.

VESUVIO

eVS has undergone a major upgrade over the past year, with the installation of the EEC funded VESUVIO modifications. These modifications will considerably improve the resolution for measurements at backscattering, particularly for studies of quantum fluids. The new sample tank and filter-cooling device is now installed in the VESUVIO blockhouse. The new filter consists of six 60° segments each containing either a thick, thin or no uranium foil. By oscillating the device ± 60°

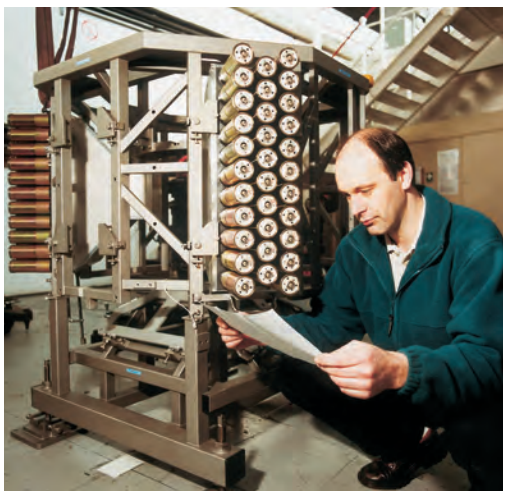

Fig. 3.5. Ashley Lester (ISIS) with the new SXD detector array (01RC1575).

about the vertical position, each detector at backscattering is covered by one of these options and the double difference technique is then used to eliminate the Lorentzian tails in the old eVS resolution function. Further improvement in resolution is obtained by cooling the foils to 30 K, thereby eliminating thermal broadening of the uranium resonance line-shape, which defines the resolution function. The device has been tested using the original eVS detector modules at back-scattering and has performed according to expectations. The first 60° segment of the new ^{6}Li doped glass scintillator backscattering detector, with optimised geometry, will be installed during August 2001 and should lead to a further improvement in resolution and also in count rate.

MERLIN

Much work has gone into the design of a new instrument, MERLIN, optimised for high count rate and medium resolution to complement MARI and MAPS. The principle design features include:

- A detector bank which will provide an eight-fold increase in solid angle over HET. The high solid angle (π sr) will reduce counting times and provide unrivalled coverage of momentum transfer-energy transfer (Q,ω).
- Position sensitive detectors, divided into approximately 50000 pixels to provide exceptional flexibility.
- A supermirror guide will enhance the flux on the sample for thermal and cold neutrons by up to a factor of 8.
- An oscillating collimator will be available to reduce dramatically the background scattering from sample environment equipment.

Provision has been made for the installation of polarising filters in both the incident and scattered beams when the technology becomes sufficiently advanced. It will also offer the capability to operate with advanced sample environment equipment.

MERLIN's improved flux and solid angle compared with existing instruments will make a real impact on many areas of condensed matter science. Signs are promising regarding funding, and it would be planned to have the spectrometer ready for general use by the end of 2004.

Muons

Development of the radio-frequency μSR technique has continued this year. RF-μSR is ideally suited to a pulsed muon source such as ISIS, and the work has resulted in the award of an EPSRC grant to enable detailed investigations of molecular, gas-phase, ion-conducting and semiconducting systems. It is clear that RF-μSR, together with more conventional μSR investigations, would benefit from rate and applied field improvements, and plans are ongoing to develop a new muon instrument with an order of magnitude increase in field and rate over those available now.

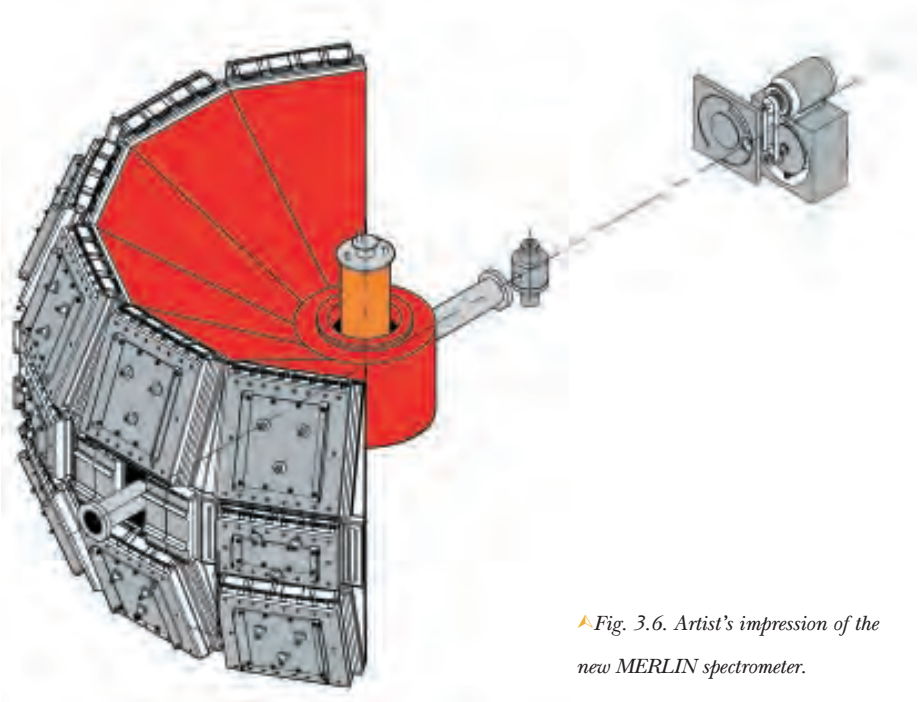

Fig. 3.6. Artist's impression of the new MERLIN spectrometer.

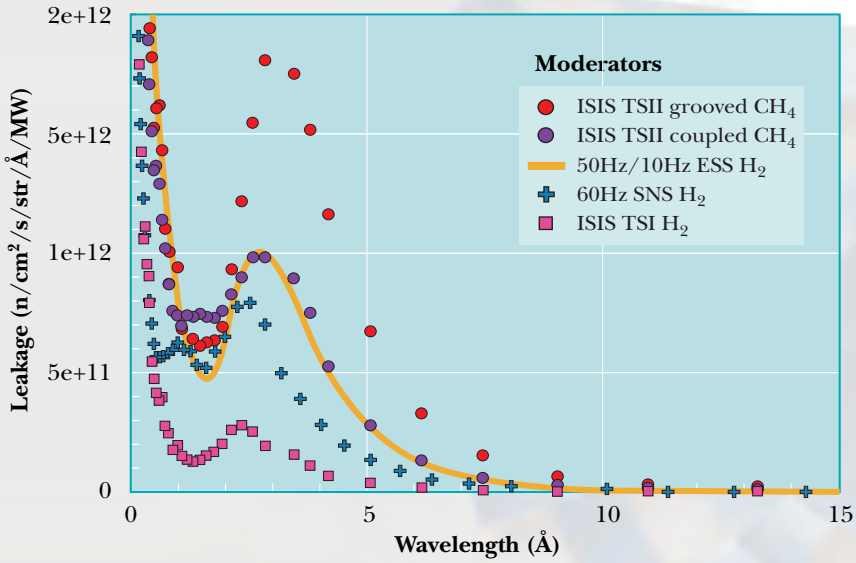

Fig. 3.7. The flux, per megawatt, from the coupled solid-methane moderator (from both the back of the groove and the flat face) compared to that from the existing hydrogen moderator and two of the planned coupled hydrogen moderators at the American SNS and the European Spallation Source.

Second Target Station

The Second Target Station at ISIS will not only double the size of the facility, it will host a range of new generation instrumentation that will offer unrivalled potential for structural and dynamical studies of matter. The design of a spallation neutron target station always involves some compromise due to the need to service a broad user programme. However, the building of a Second Target Station will enable creation of more specialised instrumentation that is better optimised for particular scientific fields. The addition of extra RF-cavities in the synchrotron will increase its proton current by 50% to a total of 300 micro-amps. Diverting one pulse in five will supply 48 kW at 10 Hz to the new target. This gives the opportunity to match the moderators with their instruments more closely and to use many of the new ideas and technologies that have been developed since ISIS was first built. The new target will have space for 18 instruments or guide bundles, doubling the size of the facility. The low repetition rate immediately orientates the target station towards long-wavelength and/or high-resolution applications, such as small-angle neutron scattering, reflectivity, high-resolution diffraction and spectroscopy. This would free the existing high repetition rate target for high/medium energy spectroscopy and high intensity diffraction and S(Q) measurements.

The design of the new target station is still evolving, but currently it consists of a 6 cm diameter tantalum-clad tungsten target cooled from its surface using D_2O. Two moderators are positioned above and below the target. One will be a coupled solid-methane moderator with two open faces. One of the faces has a single deep groove, which supplies an integrated, *per proton*, flux 15-20 times that from hydrogen moderator at the expense of a much broader pulse width. For individual instruments the expected gains, when moving from the existing to the new target, will depend on their respective repetition rates, but overall we are expecting an order of magnitude improvement in instrument performance. The other moderator will be de-coupled and poisoned, that is it will have lower flux but a much narrower pulse shape. One of the faces will be designed to have a narrow pulse shape similar to the existing methane moderator, and one will have a slightly broader pulse shape similar to the existing hydrogen moderator. Although the gains over the existing target station are more modest, the flux from the moderator will be cooler and will benefit applications needing long-wavelength neutrons.

The Second Target Station is an exciting development for ISIS. It will keep the facility at the forefront of neutron scattering research for many years to come, and positions us well for future developments such as a one megawatt upgrade.

Fig. 3.8. A cut-away schematic of the target station assembly.

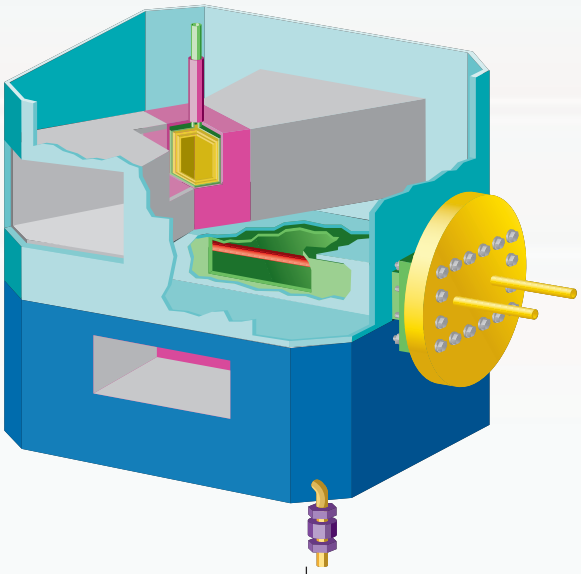

Accelerator and Target 4

Studies of the accelerator and target characteristics, and modifications to the accelerator equipment, enable continual improvements to be made to the proton beam intensity and stability. This chapter outlines the performance of the accelerator and target over the past year, and describes some of the main developments designed to improve the machine reliability and performance.

ISIS Beam Statistics 2000 - 2001

ISIS continues to be the world's most intense pulsed spallation neutron source. A total of 687 mA-hrs of proton beam was delivered to the muon and neutron targets at an average current of 165 µA during scheduled user operating cycles, for the year 2000-2001.

Table 4.1 gives beam statistics for the individual cycles in the year; for comparison, the statistics since 1994 are given in Table 4.2. Fig. 4.1 shows the total integrated current and Fig. 4.2 shows the distribution of days according to the amount of beam delivered. Over 90% of days are delivered with a total current of 3 or more mA-hrs.

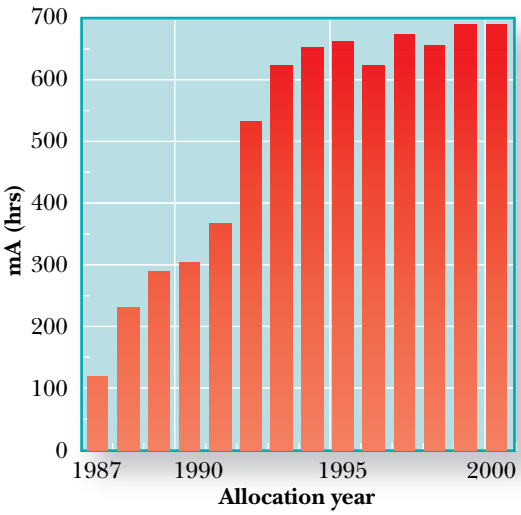

Fig. 4.1. Yearly integrated proton current, 1987 - 2000.

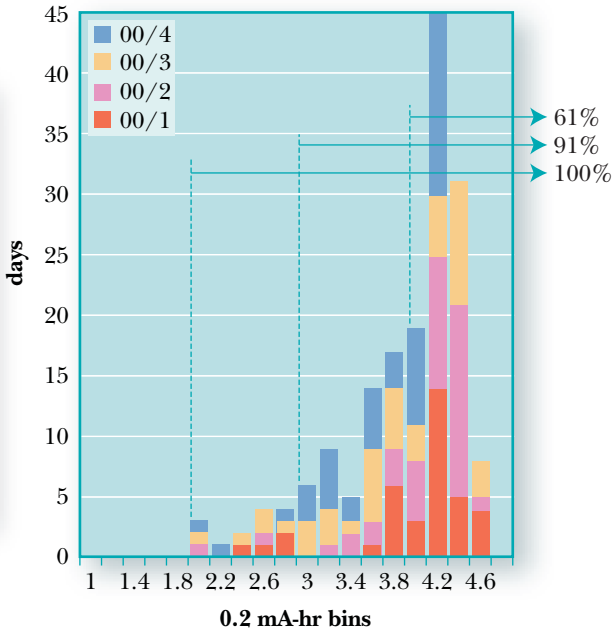

Fig. 4.2. Frequency plot of beam delivery for the 2000 - 2001 year.

Cycle	00/1	00/2	00/3	00/4
Beam on target (hrs)	931	937	876	938
Total beam current (mA.hrs)	176	177	166	168
Average beam current on target(µA)	189	189	189	177
Peak beam current (µA, averaged over 24 hrs)	194	193	192	182
Current averaged over cycle (µA)	168	169	162	161
Average beam trips per day	25	53	24	30

Year	1994	1995	1996	1997	1998	1999	2000
Total scheduled user time (days)	168	168	168	168	175	168	168
Total time on target (days)	155	151	152	153	160	153	154
Total integrated current (mA.hrs)	653	661	621	672	656	687	687
Average current on target (µA)	176	182	171	183	171	187	186
Peak current (24 hr average, µA)	184	201	204	197	193	198	194
Current averaged over year (µA)	145	162	153	167	156	171	165
µA.hrs per trip	59	80	115	81	72	106	120
Total power consumption (GWh)	50	46	47	47	42	52	46
Energy efficiency (mA.hr/GWh)	13.1	14.4	13.1	14.9	14.9	13.2	14.9

Top: Table 4.1. ISIS operational statistics for the year 2000 - 2001. Bottom: Table 4.2. ISIS performance year-on-year.

Accelerator and Target Developments

Efforts are continually made to maintain and advance the ISIS accelerator and target reliability. Old and obsolete equipment is being replaced and systems improved to maintain ISIS at the forefront of pulsed neutron sources. Significant progress has been made in a number of areas including muon and neutron targets, RFQ developments, the 300 μA upgrade and component replacement in straight 1.

Injector Group

The Injector Group is responsible for the H^- ion source, the 665 keV pre-injector and the 70 MeV drift tube linear accelerator (linac). Good reliability has been maintained over the year, with the ion source, in particular, continuing to attract attention throughout the accelerator world for the excellence of its operation.

New pulsed power supplies for the drift tube quadrupole magnets in linac Tank 1 have replaced obsolescent units. Progress has continued on the test stand for the 665 keV, 202.5 MHz, 4-rod RFQ accelerator, intended as a replacement for the present pre-injector.

Commissioning of the ion source development facility is largely complete. The rig will be used both to optimise ISIS ion sources off line and to upgrade ion sources towards ESS specifications. Also for the ESS, a 2.5 MeV, 280 MHz, 4-rod RFQ accelerator has been designed. A representative full-scale model has been built and its RF characteristics proved (Fig. 4.3).

Fig. 4.3. Alan Letchford adjusting the model 4-rod RFQ (01RC3458).

Fig. 4.4. Terry Weston assembles a second harmonic cavity for the 300 μA upgrade (01RC2224).

Synchrotron and Electrical Engineering Group

Group activities concentrate on refurbishing, redesigning and replacing equipment to achieve optimum performance. Support is also given to other groups within ISIS, particularly electrical design and installation services.

A major project of design and procurement to replace ageing components for superperiod 1 is complete. These components are highly active, requiring careful planning for installation, which is scheduled to start in January 2002 with completion by June.

The ISIS 300 μA upgrade is now funded and a programme is underway to install two dual harmonic cavities in the 2002 shutdown and a further two cavities in 2003 (Fig. 4.4).

The pulsed power supplies for the extraction kicker magnets consist of fast switching thyratrons discharging pulse-forming networks (PFNs). The work of standardising the thyratron chests is complete, reducing the need for a diversity of components. The PFN

➢*Fig. 4.5. Adrian Hooper surveys a quadrupole magnet for alignment on its stand (01RC2249).*

chests contain large numbers of capacitors, which are charged and discharged to 42 kV every 20 ms, resulting in occasional failures. To improve reliability, new higher voltage capacitors will be installed in 2002 with the addition of clamping diodes to reduce voltage over-swing.

A tripartite collaboration on future RF systems for high intensity proton beams continues with KEK, Japan and ANL, USA. Also, significant contributions have been made to the ESS, possible future 1 MW and 5 MW upgrades of ISIS, and to accelerator-based projects around the world.

Operations and Installations Group

The Group is responsible for providing a Facility-wide service through its mechanical, electrical, ancillary plant and vacuum sections. It is also responsible for the correct operation of the Facility during user cycles. In addition to participation in a wide range of activities involving other groups, the Group has its own programmes, which include upgrading the machine interlock systems.

During beam injection into the synchrotron, negative hydrogen ions from the linac are stripped of electrons by passage through a thin foil in the synchrotron injection straight. These delicate aluminium oxide foils (122 mm x 40 mm and 50 mg/cm^2 thick) were specially developed at ISIS and are now produced by the vacuum section. They are made by anodising aluminium to the required thickness, then dissolving away the unwanted metal. A thin aluminium coating is evaporated onto the foil to eliminate charge build-up during irradiation. Fig. 4.6 shows 2 foils being removed from the vacuum coating plant. Great care and patience are necessary at every stage of the fabrication procedure, which takes approximately 4 days. In the early days of ISIS, installed foils were lasting on average 10 mA hrs before failure. Improvements in quality control, together with improved installation techniques, have increased this average to 300 mA-hrs - almost two operational cycles; one foil has lasted 850 mA-hrs – a whole operational year.

Target Group

The Group has been responsible for installation of a new tantalum clad tungsten neutron target (see page 68), resulting in a hydrogen moderator flux increase of 25%. Work has also continued on irradiation experiments at the CARE reactor of Imperial College London to assess the effect of chemical scavengers in reducing the build-up of high-mass hydrocarbons in the methane moderator. The results show that they will not increase the operational lifetime. However, changes in the remote handling procedures have reduced the

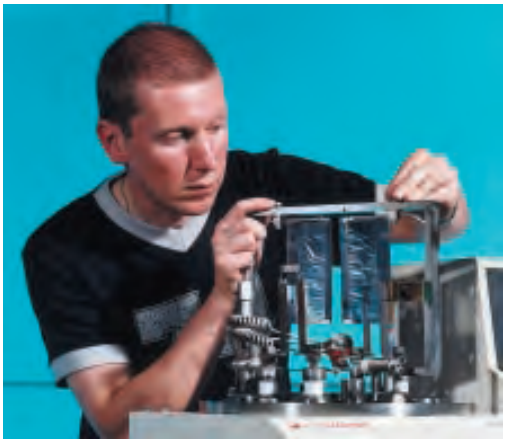

➢*Fig. 4.6. Geoff Matthews removing two foils from the coating plant (01RC3059).*

time taken to replace a moderator from 21 to 14 days, relieving some of the constraints on the ISIS operating schedule.

Work on the control systems has continued, with the control computer being replaced by the new VISTA system together with replacement of all the valve control hardware.

A major extension to the R55 experimental hall has been built to provide a new lorry access to the hall. This released space for a fourth muon beam line on the RIKEN-RAL Muon Facility.

The proposal for a Second Target Station is proceeding through the Gateway process required for major government funded projects, with approval for construction hopefully to be given in Autumn 2001 (Fig. 4.7).

Project Engineering Group

The PE Group provide support to the running of ISIS in areas such as sample environment equipment and improvements aimed at increasing reliability. Projects over the past year have included designs for a complete new extraction straight (super-period 1), with the aim of creating a fully modularised system. The new septum magnet, vacuum vessels, monitors and scintillator will accept the larger beam of the 300 μA ISIS upgrade. Work on the design and build of 4 new 2nd harmonic accelerating cavities is proceeding (Fig. 4.4). The RFQ linac, which is to replace the present injector, has been completed in collaboration with Frankfurt University. A new, improved muon target system, including full target change cell, is being designed (page 68).

With the completion of the GEM detector array, the Group has been designing new instruments: ENGIN-X, which incorporates a supermirror vacuum neutron guide, and Vesuvio, with its novel detectors. The proposed instrument MERLIN has been designed and costed.

ISIS Theory and Future Projects Group

Besides the present commitment to ISIS, much of the work of the Group involves future projects at RAL and laboratories abroad. The main activity has been a study of a 4 MW proton driver for a neutrino factory. Two designs have been produced, based on an H^- linac followed by a system of booster and main synchrotrons, with final beam energies of 5 GeV at 50 Hz or 15 GeV at 25 Hz. The design delivers very short (1 ns) pulses to produce the required neutrino flux. The group has also contributed to a parallel study at CERN based on a 2.2 GeV superconducting linac.

Work has also been carried out in connection with the ESS (beam chopper, superconducting linac option, re-design of the transfer lines and H^- injection studies). Members of the Group continue to act as consultants for the US spallation neutron source. In addition, the group provides

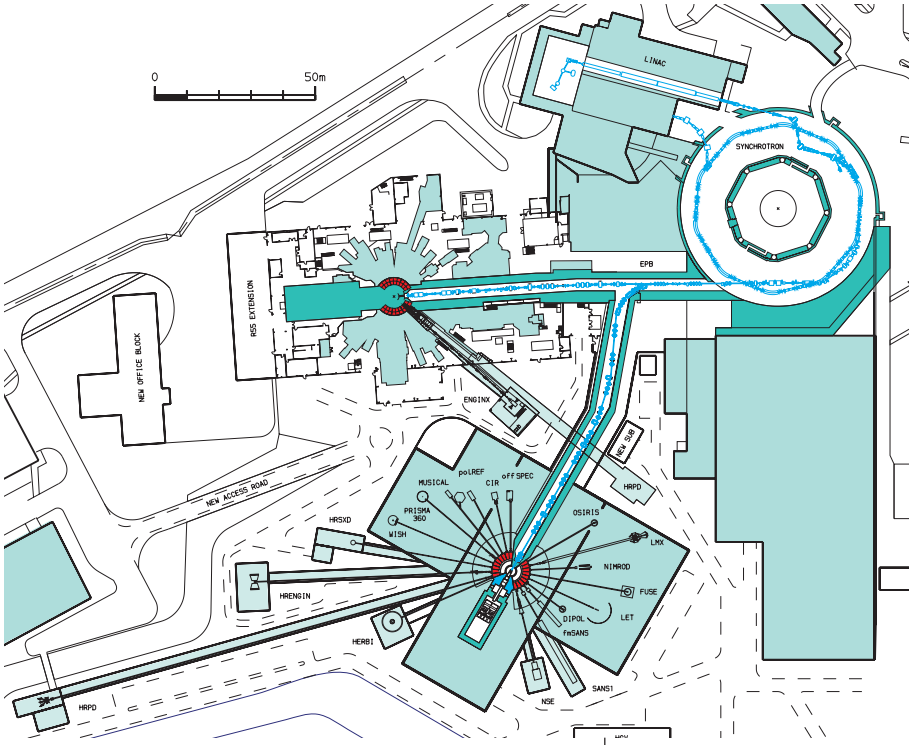

Fig. 4.7. Plan view of the ISIS Facility showing the planned Second Target Station. The neutron instruments and beam lines are shown only for illustrative purposes.

Fig. 4.8. The ISIS accelerator control room is constantly staffed by a team of three during ISIS running. Some of the ISIS crew members are shown here (01RC1503).

representatives for various organising committees, including CERN Accelerator Schools, EPAC conferences and the ICFA workshops, and the editorial board of the journal *Particle Accelerators*.

Controls Group

The Group provides computer control and monitoring for accelerator and target systems using the Vsystem package, and a variety of custom and industrial control hardware. Much of its work involves integrating new equipment, as obsolescent components are replaced, and working towards the retirement of its own ageing GEC systems.

Controls Standard STEbus (CSS) control and data acquisition systems have been designed, manufactured, commissioned and are being used on the 2nd Harmonic RF, RFQ, and ion source development projects. An upgrade of the Vsystem software enables the future development of a heterogeneous control system.

Communications software has been developed to allow LabVIEW software running on National Instruments PXI based systems to be integrated with the control system. Separate projects provide an interface to networked Omron and Modicon programmable logic controllers (PLC).

The control and monitoring of the target Saunders valves and pumps were converted from a GPMPX to an Omron PLC system; a similar replacement for the target Fisher control valves is in progress. Synchrotron RF control via the new system has been developed and cloned to provide test environments for the 2nd Harmonic RF project.

Ongoing work includes the transfer of the synchrotron timing and the ISIS radiation monitoring systems to the new control system and development of a replacement high energy drift space chopper control system.

Ion Beams Group

Studies of solid targets for a proposed neutrino factory have concentrated on the problems of material strength and fatigue associated with the thermal shock wave induced by repeated proton pulses. Finite element modelling has shown that intense high power electron beams can simulate the conditions. Experiments on candidate materials are about to commence in a commercial welding facility.

Investigations of the Particle Physics Test Beam suggest that an ample number of energetic muons should be available to perform a cooling experiment for the neutrino factory. Also, the production of an intense beam of muons from an extracted proton beam has been studied. This would provide a powerful test bed for experiments on targets, capture and cooling for the neutrino factory.

The theoretical and experimental (at ISOLDE, CERN) analysis of the release of particles from thin tantalum foil targets for radioactive ion beams has progressed. Participation in the development of an ion source for highly charged radioactive ions is continuing at Daresbury as part of a European research programme. This work will be of significant importance for the proposed CASIM Facility at the Daresbury Laboratory.

User Interaction and Support 5

Essential for the successful operation of ISIS are the specialised teams responsible for maintaining and developing experimental and computing facilities. The technical support given by these groups is complemented by the organisational and administrative services provided by the User Office, which oversees the arrangements for the 1600 scientists who visit annually.

Organisation and User Interaction

The ISIS User Office is responsible for the travel and accommodation arrangements for the 1600 researchers who visit the Facility annually. The Office also collates and records the 1000 or so proposals for beamtime on ISIS instruments received annually. These proposals are reviewed by international scientists who make up the Instrument Scheduling Panels.

There are two calls for experimental proposals each year in April and October, and these are followed in June and December by meetings of the Instrument Scheduling Panels (ISPs). The seven ISPs comprise ~70 international scientists (see Table 5.1) who have the job of assessing the scientific quality and timeliness of submitted proposals, and to advise on the allocation of beamtime.

User Liaison

The ISIS User Office plays a central role in user reception and programme organisation. The information entered into the ISIS integrated database system by the ISIS User Office forms the first stage in the scheduling of the instruments and the sample environment equipment which is carried out by the instrument scientists and the user support group.

Information about ISIS, the ISIS instruments and how to apply for beamtime at ISIS is available on the World Wide Web (http://www.isis.rl.ac.uk), including electronic versions of the ISIS beamtime application forms. Nearly 90% of the applications during the year were by electronic submission.

ISIS User Committee

The ISIS user community is represented by the ISIS User Committee (IUC) which draws its membership from the seven ISIS Instrument User Groups. The chairman from each group plus an elected representative attend, together with the Division Heads of the ISIS Science Divisions and the Leader of the User Support Group. The committee reports to the Director of ISIS. The present committee membership is shown in Table 5.2. The Chairman of the committee can act as Ombudsman in cases of unresolved disagreement between ISIS and members of the community. The group meets twice a year following the ISIS Scheduling Panel meetings. Its terms of reference are: to address all aspects of user satisfaction at the facility, including scientific and technical support, source reliability, instruments and sample environment, detectors, electronics, data acquisition and control, computing and

ISP-1	ISP-2	ISP-3	ISP-4	ISP-5	ISP-6	ISP-7
Diffraction	**Liquids**	**Large Scale Struct.**	**Excitations**	**Mol. Spectroscopy**	**Muons**	**Engineering**
P Attfield	P Madden	RM Richarson	KA McEwen	J Z Larese	S Blundell	P Withers
A Albinati	MCBellissent-Funel	N Clarke	AT Boothroyd	JP Bradshaw	P Carretta	P J Bouchard
G Artioli	H Fisher	T Cosgrove	D Edwards	D Haddleton	J Campos Gil	ME Fitzpatrick
W Clegg	N Greaves	P Grundy	J M F Gunn	A Navarro Rascon	A Keren	M Johnson
M Estermann	T Otomo	J Lawrence	S Julian	D M O'Hare	RL Lichti	T Lorentzen
J A Hriljac	K Seddon	FAM Leermakers	K Kakurai	K Prassides	P Mitchell	DJ Smith
T Kamiyama	N Skipper	B Newling	M Loewenhaupt	R O Simmons	N Nishida	
A Powell	M E Smith	A R Rennie	T Mason	D Timms	B D Rainford	
G D Price		S M Thompson	D Noreus	B Winkler	I Reid	
P R Raithby		R Triolo		M Zoppi		
C Ritter		J W White				
M Weller						
RM Ibberson	D Bowron	JRP Webster	TG Perring	J Mayers	SP Cottrell	J Dann
CC Wilson	AK Soper	J Penfold	R S Eccleston	J Tomkinson	PJC King	M Daymond

Table 5.1. Instrument Scheduling Panel Membership.

data analysis, safety and security, food, accommodation, and transport and claims; to provide input and advice on development of instruments, and sample environment and associated equipment; to coordinate user groups and user meetings; to recommend specific training courses for the community.

User satisfaction

ISIS values the opinions of its users, and all visiting scientists are asked to complete a satisfaction survey after each experiment. The facility scores consistently highly in areas of scientific and technical support, and instrument performance (Fig. 5.1). Areas where improvements are needed are acted upon – as an example, last year's efforts to improve processing and payment of claims are having a significant impact.

Chairman	RJ Stewart (IUG 3)	University of Reading
IUG1 Crystallography	P Battle	University of Oxford
	RJ Nelmes	University of Edinburgh
IUG2 Liquids and Amorphous	A Barnes	University of Bristol
	N Skipper	University College London
IUG3 Large Scale Structures	RJ Stewart	University of Reading
	RK Thomas	University of Oxford
IUG4 Excitations	D McK Paul	University of Warwick
IUG5 Molecular Science	DK Ross	University of Salford
	V Arrighi	Heriot Watt University
IUG6 Muons	UA Jayasooriya	University of East Anglia
	S Kilcoyne	University of Leeds
IUG7 Engineering	G Swallowe	Open University
	M Fitzpatrick	Open University
AD Taylor	Director, ISIS	
J Green	EPSRC	
U Steigenberger	ISIS Spectroscopy and Support Division Head	
J Tomkinson	ISIS User Office Co-ordinator	
R S Eccleston	ISIS Instrumentation Division Head	
WG Williams	ISIS Diffraction and Muon Division Head	
Z A Bowden	ISIS User Support Group Leader	
V Fox	ISIS IUC Secretary	

Table 5.2. ISIS User Committee Membership.

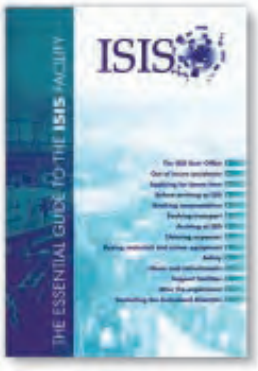

The Essential Guide to ISIS . . . everything a facility user needs to know.

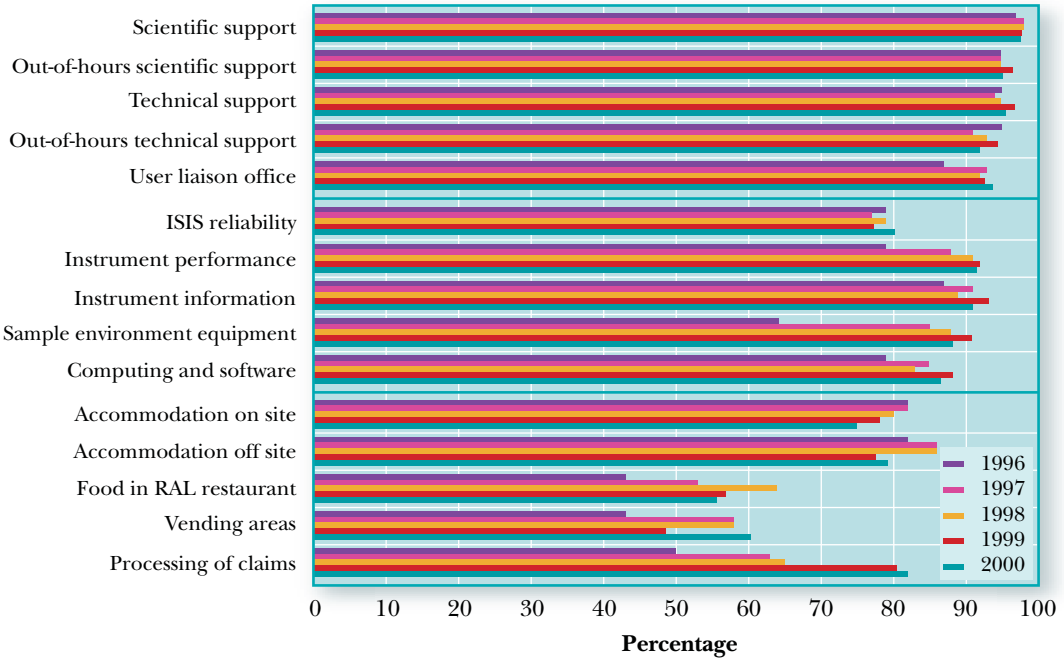

Fig. 5.1. ISIS user survey results 1997 - 2000.

News and Events

A round-up of news and events from the Facility, including the signing of the second ten year agreement with the Japanese RIKEN facility, ISIS' involvement with the European Spallation Source and how ISIS science is being promoted to schools.

The RIKEN-RAL muon collaboration

Ten years ago the first large-scale scientific partnership between the UK and Japan was initiated: a collaboration between the Japanese RIKEN Facility and the Rutherford Appleton Laboratory to develop and exploit a world-class muon facility at the ISIS pulsed neutron and muon source. The fruits of this partnership, an intense muon source used for fundamental and applied investigations of matter, has resulted in the renewal of the collaboration for a further ten years together with plans to continue the source development and expansion.

The RIKEN muon facility at ISIS enables intense muon beams to be produced for studies of materials and of energy production through muon catalysed fusion. The present facility represents an investment by RIKEN at ISIS of tens of millions of pounds. The signing of a new agreement between RIKEN and CCLRC will ensure the source continues to be exploited for world-class scientific research. A further £2m investment will see expansion of the muon source for the development of new techniques aimed at increasing the effectiveness of muons for analysis of matter.

Quinquennial Review

In February the Government published the report of stage one of the Quinquennial Review on CCLRC which addresses the question 'Is CCLRC's current organisation and status right for science?'.

The report concluded that research undertaken using the UK's national large-scale facilities has been of the highest calibre, and international evidence submitted to the review furthermore underlined the world class quality of the facilities themselves, particularly ISIS. A major contribution to the scientific excellence of the CCLRC derives from the international standing of its staff and the quality of its facilities.

ISIS regularly takes work experience students from local schools. Andrew Franklin joined us for two weeks over the summer from King Alfred's School, Wantage (00RC3584).

The report also highlighted a need to change the operation of CCLRC, particularly its financial basis and its relationship with the grant-awarding research councils. It recommends that CCLRC becomes a limited company under the joint ownership of these particular research councils, whilst remaining a Non Departmental Public Body (NDPB). The implications of this, and of the other recommendations, now go forward to stage two of the review process. The full report is available on the web at http://www.cclrc.ac.uk/QReview/.

Progress with the ESS

The European Spallation Source (ESS) project continues to make good progress. Under the leadership of Peter Tindemans, the chairman

of the ESS council, and Kurt Clausen, the project director, a number of critical questions have been addressed this year. For the user community one of the most important issues is the choice for the target stations for the ESS. This question was at the centre of the discussions at a workshop at Engelsberg in Switzerland organised by the Scientific Advisory Committee of the ESS and attended by over 70 neutron scientists from all over Europe. The largest demand was for a sharp pulsed 50 Hz target, providing high intensity and high resolution. The workshop further recommended that the second ESS target station should be long pulsed, operating at 16⅔ Hz, at a power level of 4 – 6 MW. The view was that such a station could potentially offer substantial gains in instrument performance for instruments where the pulse structure is of little relevance, e.g. neutron spin echo and small angle scattering. In order to realise the anticipated performance the development teams are now addressing the specific technical and neutronic requirements for a long pulse target.

So far the instrumentation teams, under the stewardship of Feri Mezei (HMI) and Roger Eccleston (ISIS), have concentrated their efforts on defining and modelling a generic suite of instruments. These activities have already produced some interesting results that could be tested and exploited in future developments of the ISIS instrument suite.

Detailed reports on the teams' work can be obtained from the ESS instrumentation Web page http://www.ess-europe.de.

Work on the accelerator is also progressing well. Under the guidance of the task leader Ian Gardner (ISIS) the design has been refined, in particular the linac front end, and detailed costing has been produced for the normal conducting version of the accelerator complex. The next steps will be to undertake a cost / benefit analysis of the development and operation of a superconducting option.

ISIS users and staff continue to play an active part in the ESS project, as members of the ESS Scientific Advisory Committee, in the R&D activities and through their active involvement in many associated projects, in particular instrumentation issues.

EU access to ISIS neutrons and muons

ISIS has been awarded contracts with the EU to provide access to both ISIS neutrons and muons under Framework Programme 5 – Investing in Human Potential. The Facility is particularly keen to attract new users, groups, or research teams wishing to apply neutron scattering or muon implantation techniques to novel scientific areas. Scientists working in EU Member States or Associated States other than the UK can apply for beam time for any of the ISIS neutron and muon instruments. Applications to the EU sponsored programme are handled at the same time and in much the same way as the other ISIS proposals. After submission at the two regular deadlines of 16th April and 16th October, the proposals are reviewed by international expert panels. A list of successful proposals is then selected and submitted to Brussels for approval. Following this final approval, researchers will be informed of the outcome and be contacted for beam time scheduling. In the case of a

A-Level students attending the Particle Physics Master Class are given a tour of the ISIS synchrotron (01RC1915).

➢ *The 'Living in a Materials World' interactive demonstration - available from the ISIS web pages soon.*

successful application, travel and subsistence will be paid for up to two people participating in the experiment.

Magnetic Resonance of Defects in Materials Meeting

The Institute of Physics was host to a successful 1-day meeting organised by the ISIS muon group on the Magnetic Resonance of Defects in Materials in April. Some 30 participants heard talks on ESR and μSR spectroscopy of fullerenes and zeolites, together with descriptions of μSR investigations of shallow donor states in wide band gap semiconductors, dynamics in liquid crystals and other molecular species, and free radicals involved in catalysis. The ten oral presentations were accompanied by sixteen posters contributions; over lunch, parallel business meetings of the ISIS muon user group and the AGM of the new BRSG Magnetic Resonance Group of the IOP took place.

Living in a Materials World

Martyn Bull and Christopher Frost (ISIS) have been awarded an EPSRC PPA (Partnerships

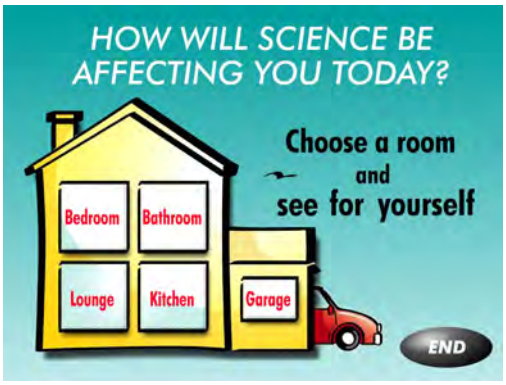

for Public Awareness) grant for the 'Living in a Materials World' project. This project aims to make links with surrounding schools enabling today's teachers to better inspire tomorrow's scientists and to extend knowledge of the excitement of ISIS science to a wider audience.

During a Teachers Day next spring, ISIS scientists will demonstrate the many facets of contemporary scientific research at ISIS whilst also having the opportunity to learn from teachers how better to communicate their science to visiting school groups. Another aspect of the project, which builds on a CD-ROM developed for the Oxfordshire museum in Woodstock explaining the relevance of ISIS research to everyday life, will produce a CD-ROM resource for teaching A-Level students. Discussions during the Teachers Day will form part of the process of content selection to ensure that it remains relevant to school requirements and the CD-ROM should be available next summer.

CCLRC Science Centres

One of the principal initiatives over the past year within CLRC has been the creation of a number of interdepartmental Research Centres that are based principally upon CLRC facilities. Proposals have been sought for setting up these Research Centres, which will act as a focus for the interdisciplinary and inter-facility opportunities made possible by scientists within CCLRC working in close collaboration with external university and

➢ *Biomolecular technology MSc postgraduates from Nottingham University on their annual visit to ISIS to learn about neutron scattering (01RC1520).*

industrial researchers. The underlying principle is that these Centres will enable users of CLRC facilities to exploit the full range of these world-class facilities in cutting-edge scientific applications. The spirit of collaboration is strongly emphasised within the remit of these Centres. Each will have significant membership from a broad base within CLRC laboratories and from strong partnerships with University colleagues. From an initial call for proposals, the following Centres have been selected to be taken forward to the final assessment stage:

Centre for Materials Science
Molecular Science Centre
Fundamental Physics Centre

ISIS staff and users are expected to play a substantial role particularly in the Centre for Materials Science and the Molecular Science Centre, alongside colleagues from SRS, the Central Laser Facility and the Computational Science and Engineering Department.

Science for art's sake

The June / July image from the ISIS 2000 calendar ('Nanodali'), rendered by Alastair Florence from the University of Strathclyde, has won 2nd place in the 'Art with Small Molecules' competition, run by the Small Molecule Special Interest Group of the ACA. A full list of entries can be seen at http://www.bernstein-plus-sons.com/wow-2000. The 'Superconductor' image from the previous ISIS Calendar had a real moment of fame earlier this year when it appeared as part of the 'Beyond Appearances : Imagery in Science at the Millennium' exhibition at the PaineWebber Art Gallery in New York.

ISIS People

ISIS has welcomed several new faces this year: Francis Pratt and Adrian Hillier (Muons), Rob Dalgleish and Stephen Holt (Large Scale Structures), Michael Hoffmann and Matthias Guttmann (Crystallography), Stephen Wakefield (Head of the Programme Support Section), Michael Brind (Chopper support) and Ben Eltham (Electrical technician). Other new arrivals include James, born to Chris and Karen Moreton-Smith; and Ben, born to Mark and Harriet Harris. Fond farewells were bid to Michele Sferazza, who took up a post at Surrey University, and to Allan Smith from the control room, who retired after 36 years service.

Congratulations to Dave Keen on his award of an EPSRC 5-year Fellowship. Congratulations also to Mike Johnson, formerly Head of the ISIS Instrumentation Division, who has been appointed Director of the CCLRC Instrumentation Department, and to Roger Eccleston who has taken his place within ISIS; also to Jeff Penfold who was appointed as a Visiting Professor at the University of Bristol and to Philip King on becoming Group Leader of the ISIS Muon Group.

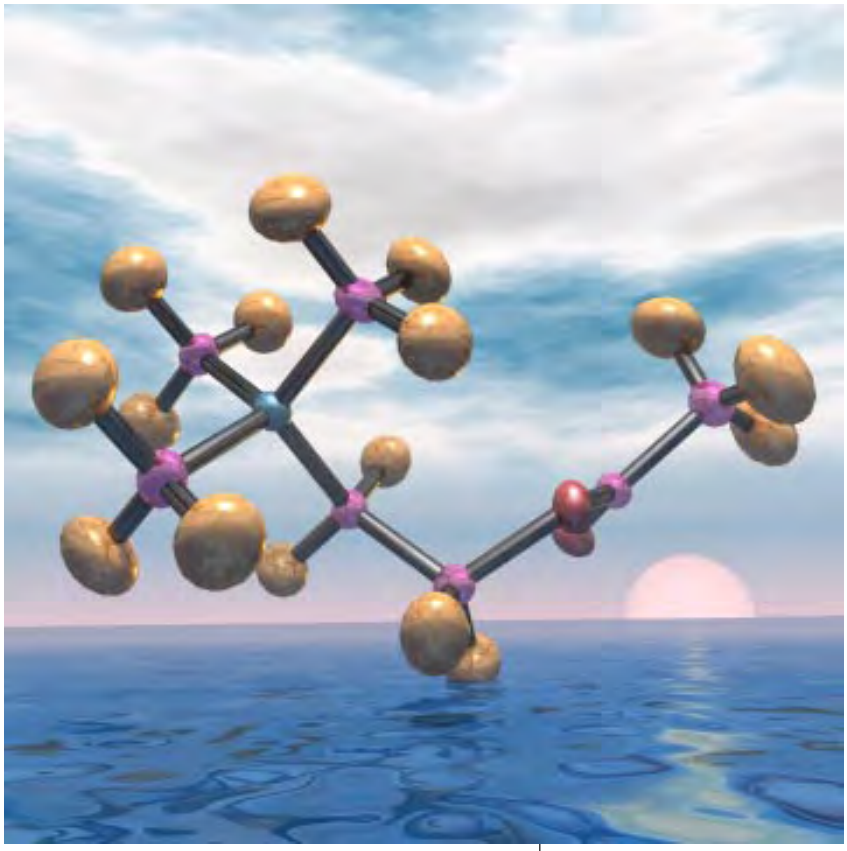

'Nanodali', from the ISIS 2000 calendar.

Experimental Support

The activities of the Sample Environment, Computing, Electronics and Detector Groups can be divided into three areas: support of the experimental programme; delivery of hardware and software for new projects; and the development of new technologies and capabilities.

Sample Environment

The current year saw the completion of spend on the £600k EPSRC Advanced Sample Environment Grant. The four final projects (out of 13 in total) were completed this year: the 10 K - 600 K hot-stage CCR unit, the 1.5 kbar SANS high-pressure cell, the in-situ chemical reaction system and the catalysis system for the Molecular Science Group.

The Group's other main development projects have been a 4 K CCR-based exchange-gas cryostat for HET, complete with a new design Omega centre-stick with resolution of 0.005°. A high-precision rotation stage with an angular resolution of 0.001° has also been provided for the Kelvinox dilution fridge insert.

The GEM 10-position sample changer built by Salford University has now been put into service. The LabVIEW-controlled stage enables samples to be changed in ~8 s!

The high-pressure section has acquired a new 10 kbar PLC-controlled helium intensifier, and in anticipation of an increasing number of hydrogen experiments a 3 kbar hydrogen-compatible pump has been ordered. To extend further the range of science accessible using the cryomagnet a Beryllium-copper alloy 10 kbar clamped cell was purchased from the ILL.

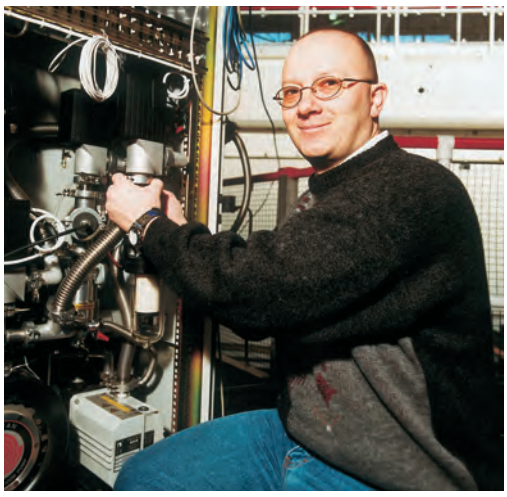

Richard Down preparing the muon sorption cryostat pumping rack (01RC1589).

A continuous flow ^{3}He insert to be used with 100 mm Orange cryostats has been ordered to replace the ageing single shot ^{3}He sorption cryostat which over the last few years has been used almost exclusively for condensed helium experiments.

Notable successes during the year have been our support of the first combined high pressure and cryomagnet experiment at ISIS and the first experiment combining the Kelvinox dilution insert and cryomagnet. Requests for the cryomagnet have now reached a level where it is in almost continuous use during each cycle.

The interests of both the cryomagnet and high pressure user communities are now being represented at two working groups, comprised of both SE Group staff and instrument scientists.

Electronics

The support aspect of the Electronics Group activities is centred on the operation of DAE-I, including the integration of detector upgrades. This year new detectors on OSIRIS, TOSCA, ROTAX, VESUVIO and ENGIN were all supplied with new detector input modules, and a DAE-I interface was built and commissioned for the new LOQ detector. ENGIN has also been equipped with a new interface which allows the ENGIN stress rig / Eurotherm combination to control the DAE-I data

The size of data sets from new instruments requires thinking about data collection and manipulation in new ways. Here , Don McKenzie-Paul (Warwick) and Simon Levett (ILL) are analysing their MAPS data (01RC1634).

acquisition process. The group has supplied detector electronics for the HRPD detector upgrade and for GEM, and detector cards for SXD-II are being produced.

The major project within the Electronics group is the development of the next generation data acquisition electronics, DAE-II. DAE-II has been running on MAPS since the instrument started operating last autumn, and GEM and SXD will run DAE-II from the autumn of 2001. As experience is gained on the instruments' performance, the system will be developed and additional functionality, such as on-board time focusing, will be integrated. A roll-out programme for DAE-II on to existing instruments will begin in October.

The planned move from VMS to Windows based software for instrument control has the potential to allow faster data transfer rates, and the technologies to exploit this are being evaluated.

The production of DAE-II components such as detector cards has been hampered in the past by the delivery of substandard PCBs from suppliers and time-consuming testing. A small group of reliable suppliers has been identified and will be used in future. Developments which are currently underway make use of standard off-the-shelf components where possible, reducing staff time required for development, assembly and support, and reducing the risks of delays. In addition test rigs and procedures have been developed which will reduce testing time. Large instrument projects such as MERLIN and the rollout of DAE-II to the whole ISIS instrument suite and possibly Second Target Station instruments, mean that short, reliable production times will become increasingly important.

Computing

During the last year ISIS instruments collected 170 Gbytes of data, an increase of 70% on last year's figure. On individual instruments such as SXD, GEM and MAPS, the commissioning of large, pixellated detector arrays means that raw data files are getting larger. This puts pressure on the performance, storage capacity and data transfer rates for the instrument control computers, requiring computer upgrades and improved archiver performance.

Data acquisition developments, performed in conjunction with the Electronics Group, have now produced an order of magnitude reduction in the time taken to begin a run on MAPS with DAE-II. We are also looking to reduce the END and UPDATE times for these instruments with large detector arrays.

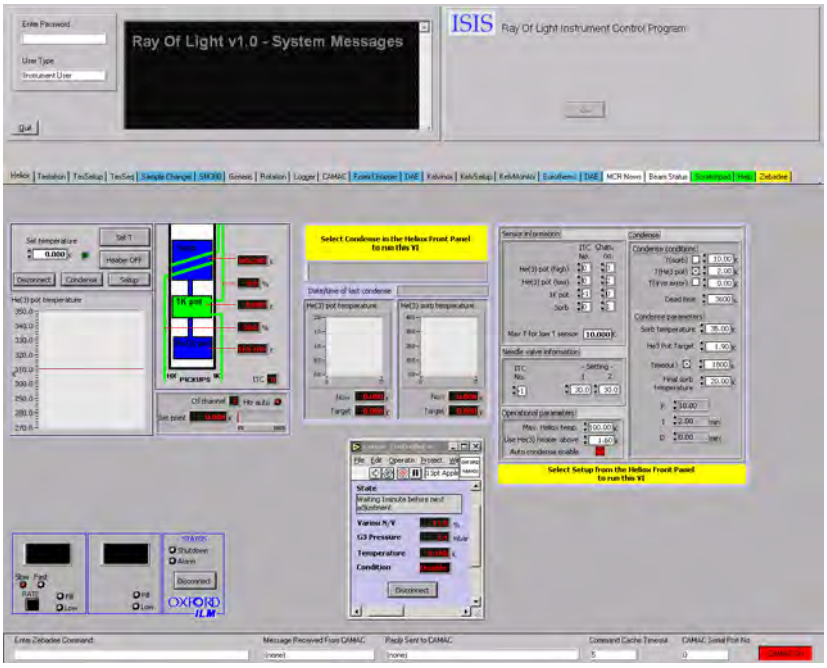

The display panel of the 'Ray Of Light' control program for a Heliox sorbtion cryostat.

Installation of the new LOQ detectors (01RC2182).

Work to implement the combined neutron, X-ray and muon data format NeXus has continued. OpenGENIE can already write NeXus files (NeXus is based on HDF, which can be read by commercial packages such as IDL and MATLAB) and a dictionary of terms for each instrument is being compiled across different sources. This fits in well with GRID activities, which will allow better access to data from different sources and availability of increased computer power in the future.

A full, PC-based control system combining both data acquisition and control devices is being developed. LabVIEW-based control workstations are now available on all instruments and more control devices have been integrated with the system, including filters on eVS, GEM and TOSCA, sample changers, and the cryomagnet. A communication link between a PC and the DAE has been developed and will be tested on an ISIS beamline in the autumn. The instrument control and data acquisition functions will then be integrated. The first instrument to operate in this way will be ENGIN-X, with a steady rollout to other instruments beginning in the middle of next year.

Another development is the use of web interfaces to data analysis software. In association with MAPS scientists it is hoped to make the MATLAB based analysis programs available to its users. It is intended that interfaces to other IDL and OpenGENIE based packages will also be produced.

Detectors

Major detector upgrades to SXD, HRPD and TOSCA have all been completed this year in addition to a number of other systems. The design of new detectors continues, while the research and development programme has provided stimulating results.

The SXD detector upgrade has been completed, with 11 modules produced and installed in May 2001. Each module is a fibre optically coded ZnS/^{6}Li scintillation detector with 4096 pixels of 3 mm x 3 mm resolution. This upgrade provides SXD with more than 45000 pixels covering 50% of the neutron scattering solid angle.

Fourteen HRPD 90° detector modules were finished and successfully commissioned on the instrument in November 2000. They provide 1680 new detector elements and increase the count rate in the 90° region by an order of magnitude. Two GEM 1 bank detectors comprising of 330 detector elements have also been completed, tested, installed and are awaiting commissioning.

Dominic Duxbury and Addrian Marxh (Instrumentation Department) testing pin detectors on ROTAX (01RC1439).

The TOSCA detector system has been rebuilt using new gas detectors to provide a factor of three increase in available detector area. This new system now comprises both forward and backscattering detector arrays and was operational in September 2000.

The 100-element transmission detector for ENGIN was ready for its first experiment on 12 October 2000. This detector makes use of new position sensitive photomultiplier tubes and has an independent counting chain associated with each detector pixel enabling very high data rates. By the end of the first experiment the advantages of such a system were clearly evident in the short run times required to generate high quality data sets. This bodes well for the MARI transmission detector system, which is based on a similar design and is now under development.

Monte Carlo studies have been carried out to model detector characteristics of a linear ZnS/^{6}Li scintillation detector with 3 mm resolution for ENGIN-X. This work generated two possible scintillator/reflector configurations. A prototype detector of each configuration has been manufactured and tested: while it is clear that both types of detector can be made to satisfy the ENGIN-X detector requirements the new Venetian scintillator geometry provides somewhat superior detector characteristics. It is this geometry that has been adopted for ENGIN-X .

Design of a new backscattering detector for VESUVIO has been completed. An 8-channel prototype has been shown to work successfully and the first 44 channel module is almost ready. A 42 channel gas detector system and associated electronics have been constructed for the OSIRIS inelastic analyser and successfully tested. It is awaiting a new vacuum vessel prior to installation. Designs of new detectors to complete both GEM and ENGIN-X are well advanced and requirements for MERLIN now being considered.

John Bones wiring a new sensor on to a closed-cycle refrigerator (01RC2671).

Collaboration with the Milan and Rome groups under the TECHNI network to develop a detector sensitive to 100 eV neutrons is progressing well. In a mammoth experiment in July 2001, a variety of solid state and scintillation detectors were evaluated on eVS and analysis of the results continues.

In conjunction with MSI, Gd Borate scintillator strips have been incorporated into an HRPD 90° type detector and tested on HRPD. Preliminary results are promising. The detector has now been fully populated and equipped with new electronics before more rigorous tests are carried out in the summer. The Gd Borate scintillator offers much higher pulse pair resolution than the ZnS/^{6}Li scintillator.

The two-dimensional position sensitive silicon beam monitor has been run on PRISMA providing valuable information on the performance of the guide and beam line collimator components. In collaboration with the Instrumentation Department a pin detector has been successfully tested on ROTAX and offers the potential of a high rate, pixelated gas detector.

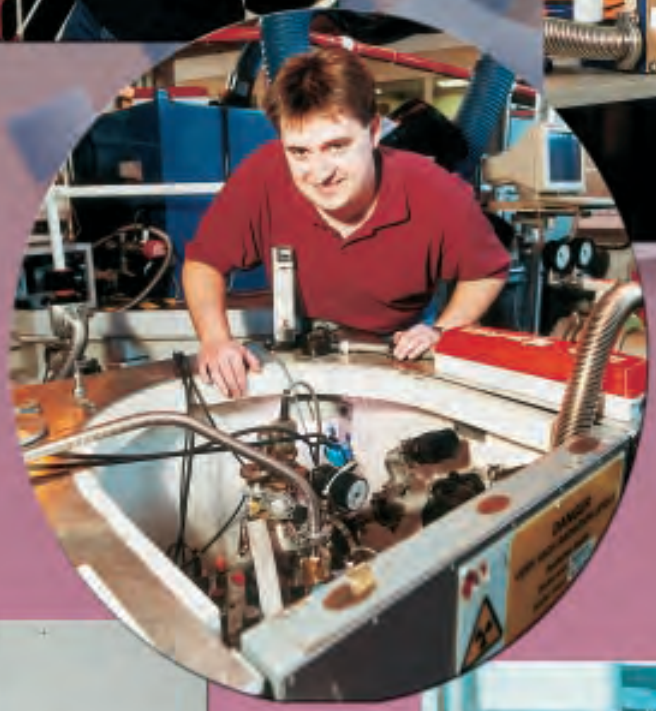

Above: Mike Charlton and Phil Donnelly using muons on EMU to investigate hydrogen spillover on heterogenous catalysts (01RC1544). Middle: Mark Lumsden (Oak Ridge National Laboratory) studying magnetic excitations in $K_2V_3O_8$ on IRIS (01RC1603). Below: Je-geun Park and Ji-yong So (Korea) using HET to investigate non fermi liquid behaviour in Cerium compounds (01RC1463).

Above: Jonathan Wasse and Helen Thompson (University College London) looking at the structure of alkali metal - ammonia solutions on SANDALS (01RC1600). Below: Richard Harvey (Kings College London) studying Langmuir-Blodgett films on CRISP (01RC1615).

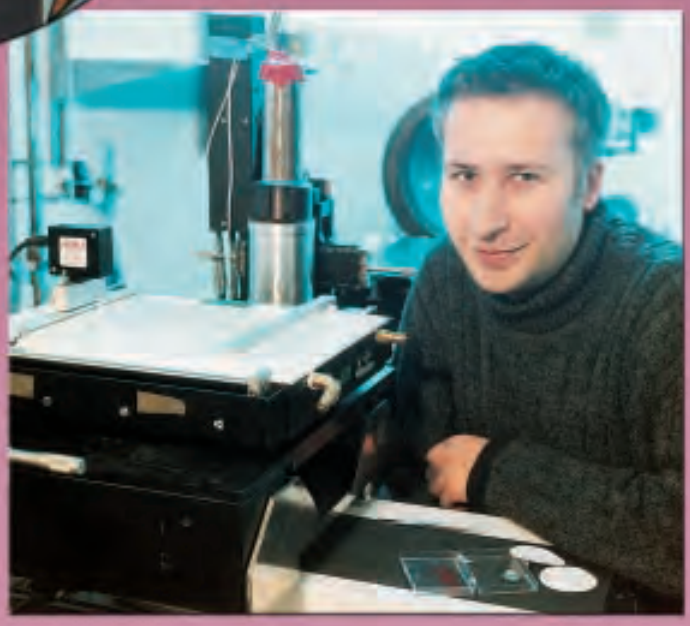

Publications 6

Publications relate to all work carried out at ISIS. In addition, work performed elsewhere by ISIS staff is included where relevant. 448 publications resulting from ISIS work were reported this year; a futher 75 are updated from those which were 'in press' at the time of last year's report.

ISIS Publications 2000 - 2001

I Abrahams, F Krok, M Malys, A J Bush
Defect structure and ionic conductivity as a function of thermal history in BIMGVOX solid electrolytes
J Mater Sci (in press 2001)

M A Adams
Superfluid ^{4}He - A very novel material
Neutron scattering in Novel Materials. Proc 8th Summer School on Neutron Scattering, Ed A Furrer (World Scientific) p289 (2000)

C P Adams, T E Mason, E Fawcett, A Z Menshikov, C D Frost, J B Forsyth, T G Perring, T M Holden
High-energy magnetic excitations and anomalous spin-wave damping in $FeGe_2$
J Phys:Condens Matter **12** 8487 (2000)

M A Adams, W S Howells, M T F Telling
The IRIS User Guide - 2nd Edition
RAL-TR-2001-002 (2001)

D T Adroja, J G M Armitage, P C Riedi, M R Lees, O A Petrenko
The cross-over from the low dimension to three dimension ferromagnetism in $CePd_{1-x}Pt_xSb$ alloys
Phys Rev **B61** 1232 (2000)

C Ager, F Y Ogrin, S L Lee, C M Aegerter, S Romer, H Keller et al
Angular dependent muon-spin rotation and torque magnetometry on the mixed state of the high temperature superconductor $YBa_2Cu_3O_{7-\delta}$
Phys Rev **B62** 3528 (2000)

P W Albers, A Karl, J Mathias, D K Ross, S F Parker
INS-, SIMS- and XPS-investigations on the controlled postoxidation of pigment blacks - identification of different species of strongly adsorbed water
Carbon (in press 2001)

P W Albers, E Auer, K Ruth, S F Parker
Inelastic neutron scattering investigation of the nature of surface sites occupied by hydrogen on highly dispersed platinum on commercial carbon black supports
J Catalysis **196** 174 (2000)

P W Albers, J Pietsch, S F Parker
Poisoning and deactivation of palladium catalysts
J Mol Catal A: Chemical, Special issue: Catalysis with Supported Palladium Metal at the Turn of the 20th Century, Eds B Corain, M Kralik (in press 2001)

P W Albers, S Bosing, D K Ross, S F Parker
Inelastic neutron scattering study on the influence of after-treatments on different technical cokes of varying impurity level and sl2/sp3 character
Carbon (in press 2001)

P A Alekseev, J-M Mignot, R Kahn, A Ochiai, E S Clementyev, V N Lazukov, E V Nefeodova, I P Sadikov, P Fabi
Neutron scattering study of the magnetic excitation spectra in mixed valence Sm_3Te_4
J Phys:Condens Matter **12** 2725 (2000)

K H Andersen, D Martin, M Barlow
OSIRIS: The polarisation analysis spectrometer and diffractometer at ISIS: New Developments and ^{3}He Spin-Filter Polarisation Analysis
Proc ICANS XV, KEK Report 2000-22 (2000)

D Andersson, C Svanberg, J Swenson, W S Howells, L Borjesson
Diffusive dynamics in polymer gel electrolytes investigated by quasi-elastic neutron scattering
Physica B **301** 44 (2001)

C Andreani, D Colognesi, R Senesi
Single particle mean kinetic energy in low density supercritical ^{4}He
Europhys Lett **50** 202 (2000)

C Andreani, E Degiorgi, R Senesi, F Cilloco, D Colognesi, J Mayers, M Nardone, E Pace
Single particle dynamics in fluid and solid hydrogen sulphide: an inelastic neutron scattering study
J Chem Phys **114** 387 (2001)

Y Andreev, P G Bruce
Using crystallography to understand polymer electrodes
J Phys:Condens Matter (in press 2001)

R J Angel, U Bismayer, W G Marshall
Renormalisation of the phase transition in lead phosphate, $Pb_3(PO_4)_2$
J Phys:Condens Matter (in press 2001)

M Arai, Y Endoh, S Tajima, S M Bennington
Local lattice distortion and charge-spin stripe structure of superconducting $YBa_2Cu_3O_{6+x}$
Physics in local lattice distortions, Eds H Oyanagi, A Bianconi (American Institute of Physics) (2001)

J Arai, T Ishiguro, M Hirai, H Shinmen, J Yokoyama, I Watanabe, K Nagamine
Zn-induced magnetic order detected by μSR around x= 1/8 in $La_{2x}Sr_xCu_{1y}Zn_yO_4$
Physica B **289-290** 347 (2000)

V Arrighi, R Ferguson, R E Lechner, M T F Telling, A Triolo
Local dynamics of atactic polyproplene across the glass transition
Physica B **301** 35 (2001)

E Balcar, S W Lovesey
Neutron-electron spectroscopy
Notizario, Neutroni e Luce di Sincrotrone p18 (2000)

D J Barlow, M J Lawrence, P A Timmins
Molecular modelling of surfactant vesicles
Nonionic Surfactant Vesicles, Ed I Uchegbu (Harwood Academic Press) (in press 2000)

I O Bashkin, A I Kolesnikov, M A Adams
Pressure effect on the hydrogen vibrations in γ-TiH and γ-ZrH
J Phys: Condens Matter **12** 4757 (2000)

I O Bashkin, V E Antonov, A I Kolesnikov, E G Ponyatovsky, J Mayers, S F Parker, J Tomkinson, A P Moravsky, Y M Shulga
Hydrogen in the vibrational spectra of high-pressure hydrofullerite
Molecular Materials **13** 251 (2000)

M Becker, M Jansen
Synthese und Charakterisierung von Quecksilbercyanamid
Z Anorg Allg Chem **626** 1639 (2000)

M Bee, D Djurado, J Combet, M T F Telling, P Rannou, A Pron, J-P Travers
Dynamics of camphor sulfonic acid in polyaniline (PAni-CSA): a QENS study
Physica B **301** 49 (2001)

C J Benmore, B L Tomberli
The structure of carbon dioxide around naphthalene investigated using H/D substitution in neutron diffraction
J Eng Chem Res **39** 4491 (2000)

S M Bennington, S I Campbell, T A Broome
Target Station II: Pulse shapes and moderator efficiency
Target Station Report TS2TF-P8-00 (2001)

S M Bennington, S I Campbell, T A Broome, D J Picton, T D Beynon
Target Station II: Parameterisaton of the Monte-Carlo output
Target Station Report TS2TF-P9-00 (2001)

W Bensch, B Sander, R K Kremer, W Kockelmann
Unexpected spin-glass behaviour of the mixed sulfide-selenide chalcogenides $TlCr_5S_{8-y}Se_y$ mediated by the nonmagnetic sublattice
J Solid State Chemistry **158** 198 (2001)

P S Berdonosov, D O Charkin, A M Kusainova, C H Hervoches, V A Dolgikh, P Lightfoot
The crystal structures of $BiTeO_3I$, $NdTeO_3X$ (X = Cl, Br) and $Bi_5TeO_{8.5}I_2$: some crystal chemistry peculiarities of layered Bi(Ln)-Te oxyhalides
Solid State Sciences **2** 553 (2000)

C Bilton, J A K Howard, N N L Madhavi, A Nangia, G R Desiraju, F H Allen, C C Wilson
Crystal engineering in the gem-alkynol family. Synthon repetitivity and topological similarity in diphenylethynylmethanols: structures that lack O-H...O hydrogen bonds
Acta Cryst **B56** 1071 (2000)

C Bilton, J A K Howard, N N l Madhavi, G R Desiraju, A Nangia, A H Allen, D A Keen, C C Wilson
Crystal engineering in the gem-alkynol family. The key role of water in the structure of 2,3,5,6-tetrabromo-trans-1,4-diethynyl-cyclohexa-2,5-diene-1,4-doil monohydrate
Acta Cryst (in press 2001)

S J Blundell, S F J Cox
Longitudinal muon spin relaxation in metals and semimetals
J Phys:Condens Matter **13** 2163 (2001)

S J Blundell, F L Pratt, I M Marshall, A Husmann, W Hayes, R E Martin, A B Holmes
Muon-spin relaxation study of charge carrier dynamics in the conducting polymer PPV
Synthetic Metals **119** 205 (2001)

S Bordiga, I Roggero, P Ugliengo, A Zecchina, V Bolis, G Artioli, R Buzzoni, G L Marra
Characterization of defective silicalite
J Chem Soc, Dalton Trans 3921 (2000)

J Bowers, A Zarbakhsh, J R P Webster, L R Hutchings, R W Richards
Neutron reflectivity studies at liquid-liquid interfaces: Methodology and analysis
Langmuir **17** 140 (2001)

J Bowers, A Zarbakhsh, J R P Webster, L R Hutchings, R W Richards
Structure of a spread film of a polybutadiene-poly(ethylene oxide) linear diblock copolymer at the air-water interface as determined by neutron reflectometry
Langmuir **17** 131 (2001)

D T Bowron, A K Soper, J L Finney
Temperature dependence of the structure of a 0.06 mole fraction tertiary butanol-water solution
J Chem Phys **114** 6203 (2001)

D T Bowron, R Weigel, A Filipponi, M A Roberts, J L Finney
X-ray absorption spectroscopy investigations of the hydrophobic hydration of krypton at high pressure
Mol Phys **99** 761 (2001)

D K Breitinger, J Mohr, D Colognesi, S F Parker, H Schukow, R G Schwab
Vibrational spectra of Augelites $Al_2(OH)_3(XO_4)$ (X=P, As, V)
J Mol Struct **563/4** 377 (2001)

C K Broder, J A K Howard, D A Keen, C C Wilson, F H Allen, R K R Jetti, A Nangia, G R Desiraju
Halogen trimer synthons in crystal engineering: low-temperature X-ray and neutron diffraction study of the 1:1 complex of 2,4,6-tris(4-chlorophenoxy)-1,3,5-triazine with tribromobenzene
Acta Cryst **B56** 1080 (2000)

W Bronger, T Sommer, G Auffermann, P Muller, H Schilder
Na_3OsH_7, Synthese, Struktur und magnetische Eigenschaften sowie Untersuchungen zur Existenz einer analogen Rutheniumverbindung
Z anorg allg Chem **627** 426 (2001)

W Bronger, T Sommer, G Auffermann, P Muller
New alkali metal osmium- and rutheniumhydrides
J Alloys Compounds (in press 2001)

D J Bull, D K Ross
Monte Carlo simulations of quasi-elastic neutron scattering from lattice gas systems
Physica B **301** 54 (2001)

F J Burghart, W Potzel, G M Kalvius, E Schreier, G Frosse, D R Noakes, W Schäfer, W Kockelmann, S J Campbell et al
Magnetism of crystalline and nanostructured $ZnFe_2O_4$
Physica B (in press 2001)

V Butun, S P Armes, N C Billingham, Z Tuzar, A Rankin, J Eastoe, R K Heenan
The remarkable 'Flip-Flop' self-assembly of a diblock copolymer in aqueous solution
Macromolecules **34** 1503 (2001)

E Bychkov, A C Hannon, A Lapp
Short- and intermediate-range order in MI-As_2Se_3 glasses (M=Ag, Cu): A neutron diffraction and small-angle neutron scattering study
Proc ICG XIX, Edinburgh (in press 2001)

E Bychkov, D L Price, A C Hannon, C J Benmore
Ion transport regimes in chalcogenide glasses: From the host to the cation-related network connectivity
Proc SSI 2001, Cairns (in press 2001)

E Bychkov, D L Price, A Lapp
Universal trend of the Haven ratio in glasses: Origin and structural evidence from neutron diffraction and small-angle neutron scattering
J Non-Cryst Solids (in press 2001)

E Bychkov, D L Price, A Lapp, C J Benmore
Ionic transport and structural features of silver and copper chalcogenide glasses studied by neutron diffraction
Proc ESRF workshop on the structure and dynamics of the liquid and glassy states p40 (2000)

C Cabrillo, F J Bermejo, M Jimenez-Ruiz, M T Fernandez-Diaz, M A Ganzalez, D Martin
Partial ordering of supercooled liquid ethanol into a rotator-phase crystal as an entropy-driven transition
Phys Rev **B64** 064206 (2001)

J M Cadogan, Suharyana, D H Ryan, O Moze, W Kockelmann
Neutron diffraction and Mössbauer study of the magnetic structure of $HoFe_6Sn_6$
45th Annual Conference on Magnetism and Magnetic Materials, MMM'2000 J Appl Phys (in press 2001)

N J Calos, E Graham, D R Cousens, P Christodoulou, C H L Kennard, L K Bekessy, S F Parker
Mode of boron solubility in ferrous alloys
Materials Transactions **42** 496 (2001)

S I Campbell, M T F Telling, C J Carlile
The new IRIS pyrolytic graphite analyser
Physica B **276-278** 207 (2000)

S J Campbell, W A Kaczmarek, M Hofmann
Mossbauer insight - metallurgy; Materials science and engineering
Hyp Int **126** 175 (2000)

L Capogna, P G Radaelli, S W Cheong et al
Charge, orbital and magnetic ordering in $La_{0.333}Ca_{0.667}MnO_3$
Mat Sci Forum **321-323** 818 (2000)

P Carlsson, R Zorn, D Andersson, B Farago, W S Howells, L Borjesson
The segmental dynamics of a polymer electrolyte investigated by coherent quasi-elastic neutron scattering
J Chem Phys **114** 9645 (2001)

M Celli, D Colognesi, M Zoppi
The experimental determination of the translational kinetic energy of liquid and solid hydrogen
Europ Phys Jour B **14** 239 (2000)

B C Choi, A Samad, C A F Vaz, J A C Bland, S Langridge, J Penfold
Layer selective determination of magnetization vector configurations in an epitaxial double spin valve structure:
Si(001)/Cu/Co/Cu/FeNi/Cu/Co/Cu
Appl Phys Lett **77** 892 (2000)

H Choo, M A M Bourke, M R Daymond
A finite element analysis of the inelastic relaxation of thermal residual stress in continuous fibre reinforced composites
Composites Science and Technology 61 1757 (2001)

M T Clavaguera-Mora, J Rodriguez-Viejo, D Jacovkis, J L Touron, N Clavaguera, W S Howells
Neutron diffraction and calorimetric study on Al-based metallic glasses
J Non-Cryst Solids (in press 2001)

N J Clayden, U A Jayasooriya, J A Stride, P J C King
Dynamics of polyurethane elastomers by muon spin rotation
Polymer **41** 3455 (2000)

R Coldea, S M Hayden, G Aeppli, T G Perring, C D Frost, T E Mason, S W Cheong, Z Fisk
Spin waves and electronic interactions in La_2CuO_4
Phys Rev Lett **86** 5377 (2001)

A I Coldea, L D Noailles, I M Marshall, S J Blundell, J Singleton, P D Battle, M J Rosseinsky
Enhancement of the magnetoresistence at the Curie temperature of the ferromagnetic insulator $La_{1.5}Sr_{0.5}MnRhO_6$
Phys Rev **B62** R6077 (2000)

R Coldea, D A Tennant, A M Tsvelik, Z Tylczynski
Experimental realization of a 2D fractional quantum spin liquid
Phys Rev Lett (in press 2001)

J M Cole, R J Newport, D T Bowron, R F Pettifer, G Mountjoy, T Brennan, G A Saunders
A rare-earth K-edge EXAFS study of rare-earth phosphate glasses, $(R_2O_3)_x(P_2O_5)_{1-x}$, x=0.187-0.239, R=La, Nd, Sm, Eu, Gd, Dy, Er
J Phys:Condens Matter **13** 6659 (2001)

J M Cole, C C Wilson, J A K Howard
Rationalising the SHG response in DCNP through anomalous atomic thermal motion
J Non-Linear Optics **25** 265 (2001)

S Collins, S K Peace, R W Richards, W A MacDonald, P Mills, S M King
Transesterification in polyethylene terephthalate-polyethylene naphthalene-2,6-dicarboxylate mixtures: a comparison of small-angle neutron scattering with NMR
Polymer **42** 7695 (2001)

D Colognesi, E Degiorgi, E Pace
Deep inelastic neutron scattering from freely rotating molecules
Physica B **293** 317 (2001)

L Cormier, G Calas, P H Gaskell
Cationic environment in silicate glasses studied by neutron diffraction with isotopic substitution
Chemical Geology **174** 349 (2001)

L Cormier, D R Neuville, G Calas
Structure and properties of low-silica calcium aluminosilicate glasses
J Non-Cryst Solids **274** 110 (2000)

S P Cottrell, J S Lord, W G Williams
Proton sites and dynamics in divalent metal hydroxides probed by muon spin relaxation
J Phys Chem Solids (in press 2001)

S F J Cox, M Charlton, P Donnelly, A Amato, A Schenk
The neutral fraction of muonium in silicon at high temperatures
J Phys:Condens Matter **13** 2155 (2001)

S F J Cox, E A Davis, S P Cottrell, P J C King, J S Lord, J M Gil, H V Alberto, R C Vilao et al
Experimental confirmation of the predicted shallow donor hydrogen state in zinc oxide
Phys Rev Lett **86** 2601 (2001)

S F J Cox, E A Davis, P J C King, J M Gil, H V Alberto, R C Vilao, J Piroto Duarte, N Ayres de Campos, R L Lichti et al
Shallow versus deep hydrogen states in ZnO and HgO
J Phys:Condens Matter (in press 2001)

S F J Cox, S P Cottrell, M Charlton, P A Donnelly, C Ewels, M Heggie, B Hourahine
A molecular radical model for hydrogen and muonium in graphite
J Phys:Condens Matter **13** 2169 (2001)

E P K Currie, M Wagemaker, M A Cohen Stuart, A A van Well
Structure of grafted polymers, investigated with neutron reflectometry
Physica B **283** 17 (2000)

E P K Currie, M Wagemaker, M Cohen Stuart, A A van Well
Structure of monodisperse and bimodal brushes
Macromolecules **32** 9041 (1999)

E Daly, N Hatto, S M King, T Cosgrove, B R Saunders
A small-angle neutron scattering study of responsive poly(n-isopropylacrylamide) microgel particles
Macromolecules (in press 2001)

R M Daniel, J L Finney, V Reat, R Dunn, M Ferrand, J C Smith
Enzyme dynamics and activity: timescale dependence of dynamical transitions in glutamate dehydrogenase solution
Biophysical Journal **77** 2184 (1999)

J A Dann, A D Hillier, J G M Armitage, R Cywinski
A μSR study of the magnetic properties of $CeAgSb_2$
Physica B **289-290** 38 (2000)

P Day
The Bakerian Lecture, 1999 - The molecular chemistry of magnets and superconductors
Phil Trans Roy Soc London A **357** 3163 (1999)

P Day
Setting the GEM
Mater World **8** 25 (2000)

P Day
Lustrous GEM
Chemistry in Britain 36 24 (2000)

M R Daymond
Determination of intergranular anisotropy strain from analysis of single diffraction peaks
Proc 6th Int Conf on Residual Stress (Institute of Materials, Oxford) p1357 (2000)

M R Daymond, A M Korsunsky
Determination of macroscopic plastic strain by analysis of multiple diffraction peaks
J Phys Soc Japan **70A** 545 (2001)

M R Daymond, M W Johnson
Determination of a stress free lattice parameter without a stress free material using elastic anisotropy
J Appl Cryst **34** 263 (2001)

M R Daymond, J Schreiber, Yu V Taran
Mechanical characterisation of fatigued austenitic stainless steel under applied loads by in situ neutron diffraction
J N Res (in press 2001)

M R Daymond, M W Johnson
The determination of d_0 without a reference material
J N Res (in press 2001)

M R Daymond, M W Johnson
Optimisation of the design of a neutron diffractometer for strain measurement
Proc ICANS XV, Vol 1 p499, KEK report 2000-22 (2000)

M R Daymond
The blurring in strains measured at a pulsed neutron source introduced by use of a detector with a large angular coverage
Physica B **301** 221(2001)

R De Renzi, S Fanesi
Longitudinal muon relaxation in spin glasses: from the concentrated to the diluted case
Physica B **289** 209 (2000)

R De Renzi, G Allodi, G Amoretti, M Cestelli Guidi, S Fanesi, G Guidi, F Licci, A Caneiro, F Prado et al
Phase diagram of low doping manganites
Physica B **289** 85 (2000)

B Derby, R T Edwards, J R P Webster
Reactions at active braze-ceramic interfaces studied by neutron reflection spectroscopy
Advanced Brazing and Soldering Technologies, Eds P T Vianco, M Singh (ASM, Materials Park, USA) p257 (2000)

A M Donald, K L Kato, P A Perry, T A Waigh
Scattering studies of the internal structure of starch granules
Starke (in press 2001)

A M Donald
Plasticisation and self-assembly in the starch granule
Cereal Chem (in press 2001)

A M Donald
Unravelling starch granule structure with small angle scattering
Fibre Diffraction Review **8** 31 (1999)

A M Donald, P A Perry, T A Waigh
The impact of internal granule structure on processing and properties
Starch 2000: Structure and Properties, Eds A M Donald, P J Frazier, T Barmsby (RSC) (in press 2001)

M T Dove, K O Trachenko, M G Tucker, D A Keen
Rigid unit modes in framework structures: Theory, experiment and applications
Reviews in Mineralogy **39** 1 (2000)

M T Dove, K D Hammonds, M J Harris, V Heine, D A Keen, A K A Pryde, K Trachenko, M C Warren
Amorphous silica from the rigid unit mode approach
Min Mag **64** 377 (2000)

C A C Dreismann, T Abdul-Redah, J Sperling
Sub-femtosecond dynamics and dissociation of C-H bonds in the condensed phase: Effects of entangled protonic states
J Chem Phys **113** 2784 (2000)

M Dutta, G Bruno, L Edwards, M E Fitzpatrick
Internal stress changes measured by neutron diffraction in a metal matrix composite after mechanical and thermal treatments
Proc 6th Int Conf on Composite Engineering, Ed D Hui, p195 (1999)

D Dye, S M Roberts, P J Withers, R C Reed
The determination of residual strains and stresses in a TIG-welded sheet of IN718 superalloy using neutron diffraction
J Strain Anal **35** 247 (2000)

J Eastoe, A Paul, S Nave, D C Steytler, B H Robinson, E Rumsey, M Thorpe, R K Heenan
Micellisation of hydrocarbon surfactants in supercritical carbon dioxide
J Am Chem Soc **123** 988 (2001)

J Eastoe, S Nave, R K Heenan, D C Steytler, I Grillo
What is so special about Aerosol-OT? Part 2: microemulsion systems
Langmuir **16** 8741 (2000)

J Eastoe, A Downer, A Paul, D C Steytler, E Rumsey, J Penfold, R K Heenan
Fluoro surfactants at the air-water and water-CO_2 interfaces
Phys Chem Chem Phys **2** 5235 (2000)

J Eastoe, M Summers, R K Heenan
Control over phase curvature using mixtures of polymerizable surfactants
Chemistry of Materials **12** 3533 (2000)

L Edwards, P J Withers, M R Daymond
ENGIN-X - A neutron stress diffractometer for the 21st Century
Proc 6th Int Conf on Residual Stress (Institute of Materials, Oxford) p1116 (2000)

Y Endoh, T Fukuda, S Wakimoto, M Arai, K Yamada, S M Bennington
Dynamical magnetic susceptibility in the optimum doped LSCO with T_c= 37K
J Phys Soc Japan **69** 16 (2000)

S Engelberg, U Beck, W Freyland
Study of electrical conductivity and microscopic structure in the transition range from ionic to metallic behaviour
J Phys Chem B (in press 2001)

S Enzo, F Delogu, R Frattini, A Primavera, A Trovarelli
Structural characterization of ceria-zirconia powder catalysts prepared by high-energy mechanical milling: a neutron diffraction study
J Mater Res **15** 1538 (2000)

S Enzo, R Frattini, P Canton, M Monagheddu, F Delogu
Neutron diffraction study of mechanically alloyed and in situ annealed $Al_{75}Mo_{25}$ powders
J App Phys **87** 2753 (2000)

J S O Evans, P A Harrison, R M Ibberson, U Kameswari, N Duan, A W Sleight
Negative thermal expansion and oxygen migration in $ZrW_{2-x}Mo_xO_8$
J Amer Chem Soc **122** 8694 (2000)

D Filges, R-D Neef, K Nunighoff, C Pohl, B Haft, S M Bennington
Detailed Monte Carlo simulations on the neutronic performance of different moderators for the ESS
ESS-SAC-Mod-No:3 (2001)

D Filges, B Haft, R-D Neef, C Pohl, H Tietze-Jaensch, S M Bennington
A first attempt to estimate the performance of the ESS moderators for the short pulse target station.
ESS-SAC-Mod-No:1 (2001)

D Filges, R-D Neef, K Nunighoff, C Pohl, B Haft, S M Bennington
H_2 and H_2O moderator neutron performance Monte Carlo simulations for the ESS reference target-moderator-reflector system
ESS-SAC-Mod-No:2 (2001)

F Fillaux, C Cachet, S F Parker, J Tomkinson, A Quivy, L T Yu
Inelastic neutron scattering studies of the proton dynamics in Bi-doped manganese oxides
J Electrochem Soc **147** 4184 (2000)

F Fillaux
Hydrogen bonding and quantum dynamics in the solid state
Int Rev in Phys Chem **19** 533 (2000)

J L Finney
The structural basis of the hydrophobic interaction
Hydration Processes in Biology, Ed M-C Bellissent-Funel (IOS Press) p115 (1999)

J Q Fonseca, M R Daymond, P Mummery
Internal strains in high volume fraction composites
J Advanced Materials (in press 2001)

G C Forbes, A R Kennedy, R E Mulvey, R B Rowlings, W Clegg, S T Liddle, C C Wilson
'Inverse crown ether' complexes extended to group 12 through the syntheses of $[Na_2Zn_2(HMDS)_4(O)]$ and $[\{K_2Zn_2(HMDS)_4(O_2)_x(O)_y\}_n]$
Chem Comm 1759 (2000)

M A Fox, A E Goeta, J A K Howard, A K Hughes, A K Johnson, D A Keen, K Wade, C C Wilson
The molecular structure of $(PSH^+)(nido\text{-}7,8\text{-}C_2B_9H_{12})$ determined by neutron diffraction (PS = proton sponge, 1,8-bis(dimethylamino)naphthalene)
Inorg Chem **40** 173 (2001)

G Fragneto, T J Su, J R Lu, R K Thomas, A R Rennie
Adsorption of proteins from aqueous solutions on hydrophobic surfaces studied by neutron reflection
Phys Chem Chem Phys **2** 5214 (2000)

C S Frampton, K S Knight, N Shankland, K Shankland
Single-crystal X-ray diffraction analysis of pyrene II at 93K
J Mol Struct **29** 520 (2000)

J Frunzke, T Hansen, A Harrison, J S Lord, G S Oakley, D Visser, A S Wills
Magnetic ordering in diluted Kagome antiferromagnets
J Materials Chemistry **11** 179 (2001)

Z Gadjourova, D Martin, K H Andersen, Y G Andreev, P G Bruce
Structure of the polymer electrolyte complexes PEO_6:$LiXF_6$ (X=P,Sb), determined from neutron powder diffraction data
Chemistry of Materials **13** 1282 (2001)

S Gagliardi, V Arrighi, R Ferguson, M T F Telling
Restricted dynamics in polymer-filler systems
Physica B **301** 110 (2001)

L Galoisy, L Cormier, S Rossano, A Ramos, G Calas, P H Gaskell, M Le Grand
Cationic ordering in oxide glasses: the example of transition elements
Min Mag **64** 409 (2000)

D Gatteschi, P Carretta, A Lascialfari
Molecular magnets and magnetic nanoparticles: new opportunities for μSR
Physica B **289-290** 94 (2000)

N Gidopoulos, S W Lovesey
The Legacy of Leon van Hove, Ed A Giovannini (World Scientific Singapore) p15 (2000)

J M Gil, H V Alberto, R C Vilao, J Piroto Duarte, N Ayres de Campos, A Weidinger, J Krauser, E A Davis, S P Cottrell, S F J Cox
Shallow donor muonium states in II-VI semiconductor compounds
Phys Rev B (in press 2001)

J M Gil, H V Alberto, R C Vilao, J Piroto Duarte, N Ayres de Campos, A Weidinger, E A Davis, S F J Cox
Muonium states in HgO
J Phys:Condens Matter **13** L613 (2001)

R J C Gilbert, O Byron
The application of neutron scattering to the action of a pore forming toxin
Notiziaro Neutroni e Luce di Sincrotrone **4** 12 (1999)

G A Gilchrist, J R Lu, J L Keddie, E Staples, P Garrett
The adsorption of pentaethylene glycol monododecyl ether at the solid poly(methyl methacrylate)-water interface: a spectroscopic ellipsometry study
Langmuir **16** 740 (2000)

E Gilioli, P G Radaelli, A Gauzzi et al
Structure and superconductivity of $YSr_2Cu_3O_{7-\delta}$
Physica C **341** 605 (2000)

M Giustini, G Palazzo, A Ceglie, J Eastoe, A Bumajdad, R K Heenan
Studies of cationic and non-ionic surfactant mixed microemulsions by small-angle neutron scattering and pulsed field gradient NMR
Prog Colloid Polym Sci **115** 25 (2000)

A E Goeta, C C Wilson, J C Autino, J Ellena, G Punte
Hydrogen bonding in nitroanilines: neutron diffraction study of m-nitroaniline at 100K
Chem Mat **12** 3342 (2000)

M A Green, K Prassides, P Day, D A Neumann
Structure of the n=2 and n=infinity member of the Ruddlesden-Popper series, $Sr_{(n+1)}Sn_{(n)}O_{3(n+1)}$
Int J Inorg Mater **2** 35 (2000)

R J Green, T J Su, J R Lu
Removal of pre-adsorbed lysozyme by cationic surfactants
J Phys Chem B (in press 2001)

R J Green, T J Su, H Joy, J R Lu
Interaction of lysozyme and sodium dodecyl sulphate at the air-water interface
Langmuir **16** 5797 (2000)

D H Gregory, A Bowman, C F Baker, D P Weston
Dicalcium nitride, Ca_2N - a 2D 'excess electron' compound; synthetic routes and crystal chemistry
J Mater Chem **10** 1635 (2000)

B A Grguric, A Putnis
Rapid exsolution behaviour in the bornite-digenite series and implications for natural ore assemblages
Min Mag **63** 1 (1999)

P C Griffiths, B L Bates, A M Howe, A R Pitt, J A Roe
A spin-probe study of the modification of the hydration of SDS micelles by insertion of sugar-based nonionic surfactant molecules
J Phys Chem B **104** 264 (2000)

P C Griffiths, P Teerapornchaisit, I A Fallis, I Grillo
Hydrophobically modified gelatin and its interaction with SDS
Langmuir (in press 2001)

P C Griffiths
Neutron scattering and nuclear magnetic resonance investigations of cycle polymers
Cyclic Polymers, Ed A J Semlyen, Kluwer Academic Publishers (2000) ISBN 0-412-83090-6

P C Griffiths, J A Roe, A M Howe, A R Pitt, B L Bates
Fluorescence probe studies of gelatin-SDS interactions
Langmuir **16** 8248 (2000)

P C Griffiths, J A Roe, R L Jenkins, J Reeve, A Y F Cheumg, D G Hall, A R Pitt, A M Howe
Micellisation of sodium dodecyl sulphate with a series of nonionic n-alkyl malano-bis-N-methylglucamides in the presence and absence of gelatin
Langmuir **16** 9983 (2000)

M A Hamilton, A C Barnes, U Beck, P Buchanan, W S Howells
A neutron diffraction and isotopic substitution measurement of the structure of liquid Cu_2Se
J Phys:Condens Matter **12** 9525 (2000)

M A Hamilton, A C Barnes, W S Howells, H E Fischer
Ag^+ dynamics in the superionic and liquid phases of Ag_2Se and Ag_2Te by coherent quasi-elastic neutron scattering
J Phys:Condens Matter **13** 2425 (2001)

R J Harrison, U Becker, S A T Redfern
Thermodynamics of the R3bar to R3barc phase transition in the ilmenite-hematitie solid solution
Am Mineral **85** 1694 (2000)

R J Harrison, S A T Redfern
An in situ neutron diffraction study of short- and long-range ordering in the ilmenite-hematite solid solution
Phys Chem Minerals (in press 2001)

A Harrison, K M Kojima, A S Wills, Y Fudamato, M I Larkin, G M Luke, B Nachumi, Y J Uemura, D Visser, J S Lord
μSR studies of the kagome antiferromagnet $(H_3O)Fe_3(OH)_6(SO_4)_2$
Physica B **289-290** 217 (2000)

A L Hector, M F Thomas, M T Weller
Structural and Mossbauer studies of Sr_2FeO_3 (X=F, Cl, Br) and the magnetic structure of Sr_2FeO_3F
J Mater Chem **11** 527 (2001)

S Hemmersbach, B Zibrowius, W Kockelmann, U Ruschewitz
Ternary alkali metal transition metal acetylides A_2MC_2 (A=Na, K; M=Pd, Pt)
Chem Eur J **7** 1952 (2001)

R Hempelmann
Quasielastic neutron scattering and Solid State Diffusion (book)
Oxford Series on Neutron Scattering in Condensed Matter (Clarendon Press, Oxford) Vol 13 (2000)

C M B Henderson, S A T Redfern, R I Smith, K S Knight, J M Charnock
Composition and temperature dependence of cation ordering in Ni-Mg olivine solid solutions: a time-of-flight neutron powder diffraction and EXAFS study
Am Mineral (in press 2001)

P F Henry, M T Weller, C C Wilson
Using isotopes in neutron diffraction: detailed structural analysis at the metal-insulator transition in $SmNiO_3$
M R S (in press 2001)

P F Henry, M T Weller, R W Hughes
A nickel phosphate based zeotype, $RbNiPO_4$
Inorg Chem **39** 5420 (2000)

P F Henry, M T Weller, C C Wilson
Multiple data set Rietveld analysis using isotopes in powder neutron diffraction. 1. Accurate measurement of the doping level in the ternary system $Ni_xMg_{1-x}O$
J Appl Cryst **34** 42 (2001)

C H Hervoches, P Lightfoot
Cation disorder in 3-layer Aurivillius phases: structural studies of $Bi_{2-x}Sr_xTi_{1-x}Nb_{2+x}O_{12}$ ($0<x<0.8$) and $Bi_{4-x}La_xTi_3O_{12}$ (x=1 and 2)
J Solid State Chem **153** 66 (2000)

W Higemoto, I Watanabe, K Nagamine, S Kuroda, K Takita
Investigation of the effect of electric current on the dynamics of flux-line lattice
Physica B **289-290** 400 (2000)

W Higemoto, H Tanaka, I Watanabe, S Ohira, A Fukaya, K Nagamine
Anomalous magnetic field dependence of muon spin relaxation in S=1/2 double-chain system $KCuCl_3$ and $TlCuCl_3$
Physica B **289-290** 172 (2000)

S A Holt, P A Reynolds, J W White
Growth of silicated films at the solid/liquid interface
Phys Chem Chem Phys **2** 5667 (2000)

S A Holt, J W White
The molecular structure of the surface of commercial cow's milk
Phys Chem Chem Phys **1** 5139 (1999)

U Hoppe, H Ebendorff-Heidepriem, J Neuefeind, D T Bowron
A neutron and x-ray diffraction study of the structure of Nd phosphate glasses
Z Naturforsch **56a** (in press 2001)

U Hoppe, R Kranold, A Barz, D Stachel, J Neuefeind, D A Keen
Combined neutron and X-ray scattering study of oxide glasses
J Non-Cryst Solids (in press 2001)

C J Howard, K S Knight, B J Kennedy, E H Kisi
The structural phase transitions in strontium zirconate revisited
J Phys:Condens Matter **12** L677 (2000)

W S Howells, U Dahlborg, M Calvo-Dahlborg, J M Dubois
Diffusive motions in a crystalline $Al_{50}Cu_{35}Ni_{15}$ alloy
Physica B **301** 78 (2001)

B S Hudson, J Tse, M Z Zgierski, S F Parker, D A Braden, C Middleton
The inelastic incoherent neutron spectrum of crystalline oxamide: experiment and simulation of a solid
Chem Phys **261** 249 (2000)

A Husmann, S J Blundell, T Jestadt, B W Lovett, I M Marshall, F L Pratt, L E Spring, P D Battle, M J Rosseinsky
Effect of dimensionality on the magnetic properties of Ruddlesden-Popper manganites
Physica B **289-290** 69 (2000)

L R Hutchings, R W Richards, R L Thompson
Small angle neutron scattering from single arm labelled polybutadiene star polymers in dilute solution
Macromolecules (in press 2001)

Y Inamura, M Arai, M Nakamura, T Otomo, N Kitamura, S M Bennington, A C Hannon, U Buchenau
Intermediate range structure and low energy dynamics of densified vitreous silica
J Non-Cryst Solids (in press 2001)

E Irran, K Kollisch, S Leoni, R Nesper, P F Henry, M T Weller, W Schnick
$Ce_4[Si_4O_4N_6]O$ - A hyperbolically layered oxonitridosilicate oxide with an ordered distribution of oxygen and nitrogen
Chemistry - A European Journal **6** 2714 (2000)

J T S Irvine, D J D Corcoran, P A Cull
Structure and ionic conduction in solids
Proc Nordic Energy Workshop, 37 (2000)

J T S Irvine, A J Feighery, D P Fagg, S Garcia-Martin
Structural studies on the optimisation of fast oxide ion transport
Solid State Ionics **136-137** 879 (2000)

H Jacobs, F Haarmann, W Kockelmann
Reorientational disorder of anions in the hydrogen sulfides of sodium and potassium (NaDS and KDS) investigated by neutron diffraction between T=4K and T=470K
J Chem Phys **113** 6788 (2000)

S Jenkins, I Morrison, D K Ross
Symmetry classification of the projected vibrational density of states in Ice VIII from ab initio methods
J Phys:Condens Matter **12** 815 (2000)

J Jeong, T M Briere, N Sahoo, T P Das, S Ohira, K Nishiyama, K Nagamine
Hartree-Fock investigation of muon trapping in the chemical ferromagnet 4-(p-chlorobenzylideneamino)-TEMPO
Physica B **289-290** 132 (2000)

T Jestadt, M Kurmoo, S J Blundell, F L Pratt, C J Kepert, K Prassides, B W Lovett
Muon-spin-rotation and magnetization study of metal-organic magnets based on the dicyanamide anion
J Phys:Condens Matter **13** 2263 (2001)

M W Johnson, M R Daymond
The Neutron Silicon Lens: An update of the thermal neutron lens results
Proc ICANS XV, Vol 1 p542, KEK report 2000-22 (2001)

M W Johnson, M R Daymond
An optimum design for a neutron diffractometer for measuring engineering stresses
J Appl Cryst (in press 2001)

M W Johnson, M R Daymond
Neutron Pulsed Source Instrumentation
Analysis of Residual Stress by Diffraction using Neutron and Synchrotron Radiation, Eds M E Fitzpatrick, A Lodini (Gordon & Breach Publishing) (2001)

G M Johnson, A Tripathi, J B Parise
Synthesis and structure of an aluminogermanate zeolite with the RHO topology
Microporous and Mesoporous Materials **28** 139 (1999)

F Juranyi, J-B Suck, O Petrenko
The order-disorder transition in supersaturated $Zr_{(100-x)}Al_{(x)}$ studied by inelastic neutron scattering
J Non-Cryst Solids (in press 2001)

R Kadono, W Higemoto, K Nagamine, F L Pratt
Muonium atom in the Bloch state
Physica B **289-290** 459 (2000)

C T Kaiser, V W J Verhoeven, P C M Gubbens, F M Mulder, I de Schepper, A Yaouanc, P Dalmas de Reotier, S P Cottrell et al
Li mobility in the battery cathode material $Li_x[Mn_{1.96}Li_{0.04}]O_4$ studied by muon-spin relaxation
Phys Rev **B62** R9236 (2000)

U Kameswari, J S O Evans, A W Sleight
Rapid synthesis of ZrW_2O_8 and related phases and structure refinement of $ZrWMoO_8$
Int J Inorganic Materials **2** 333 (2000)

E B Karlsson, S W Lovesey
Scattering by entangled spatial and spin degrees of freedom
Physica Scripta (in press 2001)

D A Keen, S Hull
Structural behaviour at the $\gamma - \beta$ phase transition of Ag_3SI
J Phys:Condens Matter **13** L343 (2001)

D A Keen, M T Dove
Total scattering studies of silica polymorphs: similarities in glass and disordered crystalline local structure
Min Mag **64** 447 (2000)

P F Kelly, A Soriano-Rama, P T Wood, I D Reid, T A Claxton, C J Rhodes, U A Jayasooriya
Muonium addition to sulphur-nitrogen chains
Mag Res in Chemistry **38** S65 (2000)

M Kemali, J E Totelici, D K Ross, I Morrison
Inelastic neutron scattering measurements and ab initio calculations of hydrogen in single crystal palladium
Phys Rev Lett **84** 1531 (2000)

E Kemner, I M de Schepper, G J Kearley, U A Jayasooriya
The vibrational spectrum of solid ferrocene by inelastic neutron scattering
J Chem Phys **112** 10926 (2000)

M Kenzelmann, R A Cowley, W J L Buyers, J S Gardner, R Coldea, S M Bennington, D F McMorrow
Spin-excitation spectrum in quasi one-dimensional spin-1 compound $CsNiCl_3$
Phys Rev Lett (in press 2001)

S H Kilcoyne, B Webster
Muonium radical formation in dextran and iron dextran complexes
Mag Res in Chemistry **38** 520 (2000)

S M King, P Griffiths, J Hone, T Cosgrove
SANS from adsorbed polymer layers
Macromol Symp (in press 2001)

P J C King, I Yonenaga
Low temperature muonium behaviour in Cz-Si and Cz-$Si_{0.91}Ge_{0.09}$
Physica B (in press 2001)

S M King, M Ellis, C Richardson, D Barrett
Field observations from some caves in Umphang district, Tak province, Thailand
Cave & Karst Science (in press 2001)

H Kisch, B Eisen, R Dinnebier, K Shankland, W I F David, F Knoch
Charge-transfer complexes of metal dithiolenes, part XXVII - Chiral metal-dithiolene/viologen ion pairs: Synthesis and electrical conductivity
Chemistry - a European Journal **7** 738 (2001)

C S Knee, M T Weller
A neutron powder diffraction study of the ferromagnetic superconductor $Gd_{1.3}Ce_{0.7}Sr_2Cu_2RuO_{10-d}$
MRS Symposium II Proc (in press 2001)

C S Knee, B D Rainford, M T Weller
Crystal structure of the ferromagnetic superconductor $RuSr_2(Gd_{1.3}Ce_{0.7})Cu_2O_{10-d}$ by powder neutron diffraction
J Mater Chem **10** 2445 (2000)

K S Knight
Powder neutron diffraction studies of $BaCe_{0.9}Y_{0.1}O_{2.95}$ and $BaCeO_3$ at 4.2K: a possible structural site for the proton
Solid State Ionics **43** 12 (2000)

K S Knight
Structural phase transitions, oxygen vacancy ordering and protonation in doped $BaCeO_3$: Results from time-of-flight neutron powder diffraction investigations
Solid State Ionics (in press 2001)

K S Knight
A high temperature structural phase transition in crocoite at 1068K: Crystal structure refinement at 1073K and thermal expansion tensor determination at 1000K
Min Mag **64** 225 (2000)

W Kockelmann, W Schäfer, A Kirfel, H Klapper, H Euler
Hydrogen positions in KCo, CsCo, CsNi and CsCu tutton salt compounds determined by neutron powder diffraction
Materials Science Forum (in press 2001)

C A Koh, R P Wisbey, X P Wu, R E Westacott, A K Soper
Water ordering around methane during hydrate formation
J Chem Phys **113** 6390 (2000)

A I Kolesnikov, M A Adams, I O Bashkin, E G Ponyatovsky
Hydrogen vibrations in γ-TiH and γ-ZrH under high pressure
High Pressure Research **17** 281 (2000)

A M Korsunsky, M R Daymond, K E Wells
The correlation between plastic strain and anisotropy strain in aluminium alloy polycrystals
Mat Sci Eng (in press 2001)

C Kranenberg, D Johrendt, A Mewis, W Kockelmann
Kristall- und elektronische Struktur von $LaAlSi_2$
Z Naturforsch (in press 2001)

V V Krishnamurthy, I Watanabe, K Nagamine, H Kuwahara, Y Tokura
Spin dynamics in $Nd_{1-x}Sr_xMnO_3$ with x=0.5
Physica B **289-290** 56 (2000)

V V Krishnamurthy, K Nagamine, I Watanabe, K Nishiyama, S Ohira, M Ishikawa, D H Eorn, T Ishikawa
Non-Fermi liquid behaviour in $CeCoGe_{3x}Si_x$ alloys
Physica B **289-290** 47 (2000)

A M Kusainova, S Yu Stefanovich, V A Dolgikh, A V Mosunov, C H Hervoches, P Lightfoot
Dielectric properties and structure of Bi_4NbO_8Cl and Bi_4TaO_8Cl
J Mater Chem (in press 2001)

S Langridge, S W Lovesey
Uses of neutron and X-ray beams to investigate magnetism
Radiation Physics & Chemistry - ISRP-8 (in press 2001)

S Langridge, J Schmalian, C H Marrows, D T Dekadjevi, B J Hickey
Quantification of magnetic domain disorder and correlations in antiferromagnetically coupled multilayers by neutron reflectometry
Phys Rev Lett **85** 4964 (2000)

S Langridge, S W Lovesey
Resonant magnetic X-ray diffraction
Scattering, Ed P Sabatier, E R Pike (Academic Press) Chap 2.7.4 (2001)

J Z Larese, D Martín, D S Sivia, C J Carlile
Tracking the evolution of interatomic potentials with high resolution inelastic neutron spectroscopy
Phys Rev Lett (in press 2001)

R Lauterbach, E Irran, P F Henry, M T Weller, W Schnick
High-temperature synthesis, single-crystal X-ray and neutron powder diffraction, and materials properties of $Sr_3Ln_{10}Si_{18}Al_{12}O_{16}N_{36}$ (Ln=Ce, Pr, Nd) - novel sialons with an ordered distribution of Si, Al, O and N
J Mater Chem **10** 1357 (2000)

J M Leger, J Haines, C Chateau, G Pocquillon, M W Schmidt, S Hull, F Gorelli, A Le Sauze, R Marchand
Phosphorous oxynitride PON, a silica analogue: structure and compression of the cristobalite-like phase; P-T phase diagram
Phys Chem Minerals (in press 2001)

H Lehnert, H Boysen, J Schneider et al
A powder diffraction study of the phase transition in $LaAlO_3$
Z Krist **215** 536 (2000)

D A Leigh, S F Parker, D Timpel, F Zerbetto
The inelastic neutron scattering of two benzylic amide [2]catenanes
J Chem Phys **114** 5006 (2001)

A Leineweber, H Jacobs, F Huning, H Lueken, W Kockelmann
Nitrogen ordering and ferromagnetic properties of ε-Fe_3N_{1+x} ($0.10<x<0.39$) and ε-$Fe_3(N_{0.8}C_{0.2}0)_{1.38}$
J Alloys Compounds **316** 21 (2001)

A Leineweber, R Niewa, H Jacobs, W Kockelmann
The manganese nitrides η-Mn_3N_2 and θ-Mn_6N_{5+x}: Nuclear and magnetic structures
J Mater Chem **10** 2827 (2000)

D Lennon, J McNamara, J R Phillips, R M Ibberson, S F Parker
An inelastic neutron scattering spectroscopic investigation of the adsorption of ethene and propene on carbon
Phys Chem Chem Phys **2** 4447 (2000)

R K Li, C Greaves
Magnetic structures of $Y_2SrCu_{0.6}Co_{1.4}O_{6.5}$ and $Y_2SrCuFeO_{6.5}$
Phys Rev **B62** 14149 (2000)

R K Li, C Greaves
A new double-layered ruthenate $Sr_3Ru_2O_7F_2$ formed by fluorine insertion into $Sr_3Ru_2O_7$
Phys Rev **B62** 3811 (2000)

R K Li, C Greaves
Synthesis and characterisation of the electron-doped single layer manganite $La_{1.2}Sr_{0.8}MnO_{4-d}$ and its oxidised phase $La_{1.2}Sr_{0.8}MnO_{4+d}$
J Solid State Chem **153** 34 (2000)

Y Li, R Xu, D M Bloor, J Penfold, J F Holzwarth, E Wyn-Jones
Moderation of the interactions between SDS and PVP using ninionic $C_{12}E_6$: an EMF, microcalorimetry and SANS study
Langmuir **16** 8677 (2000)

Y Li, D M Bloor, J Penfold, J Warr, J F Holzwarth, E Wyn-Jones
SANS studies of micellar SDS in supramolecular complexes involving poly(1,4-diaminobutane) dendrimers and of $C_{12}E_6$ micelles in the presence of the dendrimers
Langmuir **16** 7999 (2000)

Y Li, R Xu, S Couderc, D M Bloor, J Penfold, J F Holzwarth, E Wyn-Jones
The structure of complexes formed between SDS and a charged and uncharged ethoxylated polyethylene - small angle neutron scattering, EMF and ITC measurements
Langmuir (in press 2001)

Z X Li, J R Lu, R K Thomas, A Weller, J Penfold, J R P Webster, A R Rennie, D S Sivia
Conformal roughness in the adsorbed lamellar phase of aerosol-OT at the air/water and liquid/solid interface
Langmuir (in press 2001)

P Lightfoot, D A Woodcock, M J Maple, L A Villaescusa, P A Wright
The widespread occurrence of negative thermal expansion in zeolites
J Mater Chem **11** 212 (2001)

C M B Line, G J Kearley
An inelastic incoherent neutron scattering study of water in small-pored zeolites and other water-bearing minerals
J Chem Phys **112** 9058 (2000)

C Lobban, J L Finney, W F Kuhs
The structure and ordering of ices III and V
J Chem Phys **112** 7169 (2000)

J S Lord, W G Williams
Muon study of proton behaviour in rhenium oxide
Solid State Ionics (in press 2001)

J S Lord, S P Cottrell, P J C King, H V Alberto, N Ayres de Campos, J Gil, J Piroto Duarte, R C Vilao, R L Lichti et al
Probing the shallow donor muonium wavefunction in ZnO and CdS via transferred hyperfine couplings
Physica B (in press 2001)

S W Lovesey, K S Knight, D J Sivia
The orbital magnetization of a Mott insulator, V_2O_3, revealed by resonant X-ray Bragg diffraction
Phys Rev B (in press 2001)

S W Lovesey, K S Knight, E Balcar
Resonant (1s-3d) X-ray Bragg diffraction and structure factors for transition metal compounds
Phys Rev **B64** 054405 (2001)

S W Lovesey, K S Knight
Calculated x-ray dichroic signals and resonant Bragg diffraction structure factors for dysprosium borocarbide (DyB_2C_2)
Phys Rev B (in press 2001)

S W Lovesey, U Staub
Reply to Comment on Magneto-elastic model for relaxation of lanthanide ions in YBCO observed by neutron scattering
Phys Rev B (in press 2001)

S W Lovesey, K S Knight, D S Sivia
Orbital properties of vanadium ions in magnetically ordered V_2O_3
2nd Int Workshop on Electron Correlations and Materials Properties, Eds A Gonis, N Kioussis (Kluwer Acedemic/Plenum Publishers) (in press 2001)

S W Lovesey, S P Collins
X-ray birefringence and dichroism obtained from magnetic material
J Synchrotron Rad **8** 1065 (2001)

B W Lovett, J S Stiessberger, S J Blundell, A Ardavan, I M Marshall, F L Pratt, I D Reid
Director fluctuations in a nematic liquid crystal probed using ALC spectroscopy
Physica B **289-290** 612 (2000)

B W Lovett, S J Blundell, J Stiessberger, F L Pratt, T Jestadt, S P Cottrell, I D Reid
Molecular dynamics in a nematic liquid crystal probed by positive muons
Phys Rev **B63** 054204 (2001)

J R Lu
Neutron reflection study of globular protein adsorption at planar interfaces
Ann Rep Proc Chem C **95** 3 (1999)

J R Lu, T J Su, B Howlin
The effect of solution pH on the structural conformation of lysozyme layers adsorbed on the surface of water
J Phys Chem B **103** 5903 (1999)

J R Lu, T J Su, R K Thomas
Structural conformation of bovine serum albumin layers at the air-water interface studied by neutron reflection
J Colloid Interface Sci **213** 426 (1999)

S Magazu, C Branca, F Migliardo, P Migliardo, E Vorobieva, U Wanderlingh
QENS study of trehalose/water/acrylamide-acrylic acid
Physica B **301** 134 (2001)

S Magazu, V Villari, P Migliardo, G Maisano, M T F Telling, H D Middendorf
Quasielastic neutron scattering study of disaccharide aqueous solutions
Physica B **301** 130 (2001)

A P Maierhofer, M Brettreich, S Burghardt, O Vostrowsky, A Hirsch, S Langridge, T M Bayerl
Structure and electrostatic interaction properties of monolayers of amphiphilic molecules derived from C_{60}-fullerenes: A film balance, neutron-, and infrared reflection study
Langmuir **16** 8884 (2000)

D Mannix, S Coad, G H Lander, J Rebizant, P J Brown, J A Paixao, S Langridge, S Kawamata, Y Yamaguchi
Neutron and synchrotron diffraction study of UPtG
Phys Rev **B62** 3801 (2000)

M Marezio, E Gilioli, P G Radaelli et al
Mechanical against chemical pressure in the $Y(Ba_{1-x}Sr_x)_2Cu_3O_{7-d}$ system
Physica C **341** 375 (2000)

A J Markvardsen, W I F David, J C Johnson, K Shankland
A probabilistic approach to space-group determination from powder diffraction data
Acta Cryst A **57** 47 (2001)

C H Marrows, S Langridge, B J Hickey
Determination of equilibrium coupling angles in magnetic multilayers by polarized neutron reflectometry
Phys Rev **B62** 11340 (2000)

I M Marshall, S J Blundell, A Husmann, T Jestadt, B W Lovett, F L Pratt, J Lago, P D Battle, M J Rosseinsky
A μSR study of high oxidation state iron oxides displaying large magnetoresistance
Physica B **289-290** 89 (2000)

I M Marshall, F L Pratt, S J Blundell, A Husmann, W Hayes, T Sugano
A μSR study of the CDW in TTF-TCNQ
Synthetic Metals **120** 997 (2001)

R Marx, R M Ibberson
Powder diffraction study on solid ozone
Solid State Sciences **3** 195 (2000)

C Massobrio, F H M van Roon, A Pasquarello, S W De Leeuw
Breakdown of intermediate-range order in liquid $GeSe_2$ at high temperatures
J Phys:Condens Matter **12** L697 (2000)

M Matsuda, K Katsumata, R S Eccleston, S Brehmer, H-J Mikeska
Magnetic excitations and exchange interactions in the spin-1/2 two-leg ladder compound $La_6Ca_8Cu_{24}O_{41}$
Phys Rev **B62** 8903 (2000)

T Matsuzaki, K Ishida, I Watanabe, K Nagamine, G H Eaton, W G Williams
The RIKEN-RAL Pulsed Muon Facility
Nucl Instr Meth **A465** 365 (2001)

S Matthies, H G Priesmeyer, M R Daymond
On the diffractive determination of elastic single crystal constants using polycrystalline samples
J Appl Cryst (in press 2001)

D Mazza, W Kockelmann
Silica-free mullite structures in the Al_2O_3-B_2O_3-P_2O_5 ternary system
Chemistry of Minerals (in press 2001)

K A McEwen, M J Bull, A Martin-Martin
From localised moments to non-Fermi liquids in uranium intermetallics
J Phys Soc Japan **70** Suppl A 18 (2001)

D F McMorrow, K A McEwen, U Steigenberger, H M Ronnow, F Yakhou
X-ray resonant scattering study of the quadrupolar order in UPd_3
Phys Rev Lett **87** 057201 (2001)

M Mekata, K M Kojima, I Watanabe, K Nagamine, H Ikeda
Magnetic ordering and fluctuations in Ising spin nets $Rb_2Co_xMg_xF_4$
Physica B **289-290** 194 (2000)

P G Meredith, K S Knight, S A Boon, I G Wood
The microscopic origin of thermal cracking in rocks: An investigation by simultaneous time-of-flight neutron diffraction and acoustic emission monitoring
Geophysical Review Letters **28** 2105 (2001)

H W Meyer, S Marion, P Sondergeld, M A Carpenter, K S Knight, S A T Redfern, M T Dove
Displacive components of the low-temperature phase transitions in lawsonite
Am Mineral **86** 566 (2001)

F Migliardo, S Magazu, P Migliardo
Diffusive properties of Vitamin C aqueous solutions by quasielastic neutron scattering
Physica B **301** 141 (2001)

A F Miller, R W Richardson, J R P Webster
Well-defined graft copolymers at the air-water interface
Abstr Pap Am Chem Soc **218** 566 (1999)

A F Miller, R W Richardson, J R P Webster
Organization of well-defined amphiphilic graft copolymers at the air-water interface
Macromolecules **33** 7618 (2000)

R Mittal, S L Chaplot, R Parthasarathy, M J Bull, M J Harris
Lattice dynamics calculations and phonon dispersion measurements of zircon, $ZrSiO_4$
Phys Rev **B62** 12089 (2000)

Y Miyake, K Shimomura, Y Matsuda, R J Scheuermann, P Bakule, S Makimura, P Strasser et al
Construction of the experimental set-up for ultra slow muon generation by thermal Mu ionization method at RIKEN-RAL
Physica B **289-290** 666 (2000)

C A Moore, E J Cussen, P D Battle
Synthesis, structural chemistry and magnetic properties of $Ca_{3.1}Cu_{0.9}RuO_6$
J Solid State Chem **153** 254 (2000)

O Moze, W Kockelmann, F Canepa, P Manfrinetti, A Palenzona
Magnetic structure of $Nd_2Co_6Al_7$
J Alloys Compounds **317-318** 546 (2001)

T Muranaka, S Margadonna, I Maurin, K Brigatti, D Colognesi, K Prassides, Y Iwasa, M Arai, M Takata, J Akimitsu
Vibrational spectroscopy of superconducting MgB_2 by neutron inelastic scattering
J Phys Soc Japan **70** 1480 (2001)

E F Murphy, J R Lu, J Brewer, J Russell
Characterisation of protein adsorption at the phosphorylcholine incorporated polymer-water interface
Macromolecules **33** 4545 (2000)

K Nagamine, F L Pratt, S Ohira, I Watanabe, K Ishida, S N Nakamura, T Matsuzaki
Intra- and inter-molecular electron transfer in cytochrome-c and myoglobin observed by the muon spin relaxation method
Physica B **289-290** 631 (2000)

M Nakamura, M Arai, T Otomo, Y Inamura, S M Bennington
Dispersive excitations in different forms of SiO_2
J Non-Cryst Solids (in press 2001)

A Niemann, R Stahl, H Jacobs, W Kockelmann
Ungewohnliches Wasserstoffbruckenbindungsverhalten von Verbindungen mit allseitig eckenverknupften MO_4-Tetraedern bei tiefen Temperaturen
Z Kristallogr Suppl **16** 165 (1999)

C J Nuttall, S G Carling, P Day
Effect of organic cation A on the crystal structure and magnetisation of the layer molecular ferrimagnets $AFe^{(II)}Fe^{(III)}(C_2O_4)_3$
Mol Cryst Liq Cryst A **334** 615 (1999)

F Y Ogrin, S L Lee, C Ager, C M Aegerter, E M Forgan, S H Lloyd, P G Kealey, T Riseman, R Cubitt, G Wirth
Vortex studies in heavy-ion irradiated $Bi_{2.15}Sr_{1.85}CaCu_2O_{8+d}$ probed by μSR and small-angle neutron scattering
Physica B **289-290** 355 (2000)

S Ohira, T Ishida, T Nogami, I Watanabe, F L Pratt, K Nagamine
μSR studies on the organic radical magnet, 4-arylmethyleneamino-TEMPO
Physica B **289-290** 123 (2000)

E C Oliver, T Mori, P J Withers, M R Daymond
Measurement of interphase and intergranular strains in carbon steels by neutron diffraction
Proc 6th Int Conf on Residual Stress (Institute of Materials, Oxford) p98 (2000)

H M Palmer, C Greaves
Magnetic and nuclear structures of $Fe_{0.5}Cu_{0.5}Cr_2S_4$ and $FeCr_2S_4$
Physica B **276-278** 568 (2000)

C Panagopoulos, B D Rainford, J R Cooper, C A Scott
Antiferromagnetic correlations versus superfluid density in $La_{2-x}Sr_xCuO_4$
Physica C **341-348** 843 (2000)

C Panagopoulos, B D Rainford, T Xiang, C A Scott, M Kambara, I H Inoue
Penetration depth measurements in MgB_2: Evidence for unconventional superconductivity
Phys Rev (in press 2001)

J W L Pang, M Preuss, P J Withers, G J Baxter
The development of residual stresses in inertia friction welding of Ni superalloys
Proc 6th Int Conf on Residual Stress (Institute of Materials, Oxford) p1415 (2000)

J W L Pang, G Rauchs, P J Withers, N W Bonner, E S Twigg
Measurement and prediction of residual stresses in TiMMC rings
MECA SENS - Stress Evaluation by Neutron & Synchrotron Radiation (in press 2001)

G Paradossi, M T Di Bari, M T F Telling, F Cavalieri, A Turtu
Incoherent QENS study of chemical hydrogels based on poly (vinyl alcohol)
Physica B **301** 150 (2001)

S F Parker
Inelastic neutron scattering of polymers
Applications of neutrons to soft condensed matter, Eds B J Gabrys (Gordon and Breach, London) p26 (2000)

S F Parker, H Herman, A Zimmerman, K P J Williams
The vibrational spectrum of K_2PdCl_4: first detection of the silent mode ν_5
Chem Phys **261** 261 (2000)

S F Parker, C C Wilson, D A Keen, K Shankland, J Tomkinson, A J Ramirez-Cuesta, P C H Mitchell, A J Florence, N Shankland
Structure and dynamics of maleic anhydride
J Phys Chem A **105** 3064 (2001)

F Partal, M Fernandez Gomez, J J Lopez Gonzalez, A Navarro, G J Kearley
Vibrational analysis of the inelastic neutron scattering spectrum of pyridene
Chem Phys **261** 239 (2000)

A Pavese, G Ferraris, V Pischedda et al
Further study of the cation ordering in phengite 3T by neutron powder diffraction
Min Mag **64** 11 (2000)

J V Pearce, R T Azuah, B Fak, A R Sakhel, H R Glyde, W G Stirling
High-resolution measurements of excitations in superfluid ^{4}He beyond the roton
J Phys:Condens Matter **13** 4421 (2001)

D R Pederzolli, J P Attfield
High-temperature in situ neutron powder diffraction study of monoclinic $Tl_2Ba_2CuO_{6+d}$
Int J Inorg Mater **2** 533 (2000)

J Penfold, E Staples, I Tucker, L Thompson, R K Thomas
The adsorption of non-ionic mixtures at the air-water interface: the effect of temperature and electrolyte
J Coll Int Sci (in press 2001)

J Penfold
The structure of the surface of pure liquids
Rep Prog Phys (in press 2001)

J Penfold
The impact of neutron scattering techniques in polymer science
Phys Chem Chem Phys (in press 2001)

J Penfold, E Staples, I Tucker, L Soubiran, R K Thomas
A comparison of the co-adsorption of benzyl alcohol and phenyl ethanol with C_{16}TAB at the air-water interface
J Coll Int Sci (in press 2001)

T G Perring, D T Adroja, G Chaboussant, G A Aeppli, Y Tokura
Spin-wave measurements in $La_{2-2x}Sr_{1+2x}Mn_2O_7$ (x=0.35)
Proc ICM2000 (in press 2001)

P A Perry, A M Donald
A SANS study of the distribution of water within starch granules
Int J Biol Macromol **28** 31 (2000)

S Peter, J B Parise, R I Smith, H D Lutz
High-pressure neutron diffraction studies on laurionite-type Pb(OD)Br
J Phys Chem Solids **60** 1859 (1999)

P F Peterson, Th Proffen, I-K Jeong, S J L Billinge, K-S Choi, M G Kanatzidis, P G Radaelli
Local atomic strain in $ZnSe_{1-x}Te_x$ from high real space resolution neutron pair distribution function measurements
Phys Rev B (in press 2001)

D J Picton, T D Beynon, S M Bennington, T A Broome
Performance and heating studies for a grooved coupled moderator and decoupled moderator on the second target station
Target Station Report (2001)

D J Picton, T D Beynon, S M Bennington, T A Broome
Moderator heating and reflector optimisation studies for the second target station
Target Station Report (2001)

V P Plakhty, J Kulda, D Visser, E V Moskvin, J Wosnitza
Chiral critical exponents of the triangular-lattice antiferromagnet $CsMnBr_3$ as determined by polarized neutron scattering
Phys Rev Lett **85** 3942 (2000)

V P Plakhty, S V Maleyev, J Kulda, D Visser, J Woznitza, E V Moskvin, Th Bruckel, R K Kremer
Spin chirality and polarised neutron scattering
Physica B **297** 60 (2001)

M Plazanet, M R Johnson, J D Gale, T Yilderim, G J Kearley, M T Fernandez-Diaz, D Sanchez-Portal et al
The structure and dynamics of crystalline durene by neutron scattering and numerical modelling using density functional methods
Chem Phys **261** 189 (2000)

M Plazanet, M R Johnson, G J Kearley
Single-molecule dynamics in a molecular cluster - semi-empirical approach
Physica B **276-278** 228 (2000)

F L Pratt, A E Goeta, F Palacio, J M Rawson, J N B Smith
ZF μSR of an organic ferromagnet with T_c=35K
Physica B **289-290** 119 (2000)

F L Pratt
WIMDA: a muon data analysis program for the Windows PC
Physica B **289-290** 710 (2000)

F L Pratt, S L Lee, C M Aegerter, S H Lloyd, S J Blundell, F Y Ogrin, E M Forgan et al
μSR studies of the flux vortex phases in a BEDT-TTF superconductor
Synthetic Metals **120** 1015 (2001)

F L Pratt, S J Blundell, T Jestadt, B W Lovett, R M Macrae, W Hayes
Muon radical states in some electron donor and acceptor molecules
Mag Res in Chemistry **38** S27 (2000)

T E Quine, M J Duncan, A R Armstrong, A D Robertson, P G Bruce
Layered $Li_xMn_{1-x}Ni_yO_2$ intercalation electrodes
J Mater Chem **10** 2838 (2000)

A J Ramirez-Cuesta, P C H Mitchell, S F Parker
An inelastic neutron scattering study of the interaction of dihydrogen with the cobalt site of a cobalt aluminophosphate catalyst. Two-dimensional quantum rotation of adsorbed dihydrogen
J Mol Cat A: Chemical **167** 217 (2001)

A J Ramirez-Cuesta, P C H Mitchell, S F Parker, P A Barrett
Probing the internal structure of a cobalt aluminophosphate catalyst. An inelastic neutron scattering study of sorbed dihydrogen molecules behaving as one- and two-dimensional rotors
Chem Comm 1257 (2000)

S A T Redfern, G Artioli, R Rinaldi, B J Wood, C M B Henderson, K S Knight
Octahedral cation ordering in olivine at high temperature. II: in situ neutron powder diffraction study on synthetic $MgFeSiO_4$ (Fa50)
Phys Chem Minerals **27** 630 (2000)

J J Reece, S A T Redfern, M D Welch, C McCammon, C M B Henderson
Temperature dependent Mn partitioning in two manganogrunerites
Phys Chem Minerals (in press 2001)

P A Reynolds, E P Gilbert, J W White
High internal phase water-in-oil emulsions studied by small angle neutron scattering
J Phys Chem B **104** 7012 (2000)

R W Richards, R L Thompson, D G Bucknall
Partitioning of a heterotelechelic to separate interfaces of thin film bilayers
E Phys J (in press 2001)

R Rinaldi, G Artioli, S A T Redfern
High temperature behaviour of Mg-Fe olivine by in situ neutron diffraction
Proc 31st Int Geological Congress (Rio de Janeiro) (2000)

A D Roberston, A R Armstrong, A J Fowkes, P G Bruce
$Li_x(Mn_{1-x}Co_y)O_2$ intercalation compounds as electrodes for lithium batteries: influence of ion exchange on structure and performance
J Mater Chem **11** 113 (2001)

A D Robertson, A R Armstrong, P G Bruce
Influence of ion exchange conditions on the defect chemistry and performance of cobalt doped layered lithium manganese oxide based intercalation compounds
Chem Commun 1997 (2000)

A D Robertson, A R Armstrong, P G Bruce
Low temperature Co doped spinel intercalation electrodes
J Power Sources (in press 2001)

A D Robertson, A R Armstrong, P G Bruce
Layered $Li_xMn_yCo_{1-y}O_2$ intercalation electrodes - influence of ion exchange on capacity and structure upon cycling
Chemistry of Materials (in press 2001)

H M Ronnow, D F McMorrow, R Coldea, A Harrison, I D Youngson, T G Perring, G Aeppli, O Syljuåsen, K Lefmann, C Rischel
Spin dynamics of the 2D spin 1/2 quantum antiferromagnet copper deuteroformate tetradeuterate (CFTD)
Phys Rev Lett **87** 037202 (2001)

V Rossi-Albertini, D Colognesi, J Tomkinson
A study on the calibration of a time-focused Inelastic Neutron Scattering Spectrometer
J Neutron Research **8** 245 (2000)

J L Ruggles, S A Holt, P A Reynolds, J W White
Synthesis of silica films at the air/water interface: Effect of template chain length and ionic strength
Langmuir **16** 4613 (2000)

U Ruschewitz, P Muller, W Kockelmann
Zur Kristallstruktur von Rb_2C_2 und Cs_2C_2
Z Anorg Allg Chem **627** 513 (2001)

M-L Saboungi, D L Price
Dynamic disorder in crystalline intermetallic compounds
Intermetallic Compounds: Principles and Practice, Ed J H Westbrook, R L Fleischer (Wiley & Sons, Chichester) Vol 3 (2001)

J R Santisteban, L Edwards, A Steuwer, P J Withers, M R Daymond, M W Johnson
Strain imaging by Bragg edge neutron transmission
Nucl Inst Methods A (in press 2001)

P M Saville, J W White
Polymeric surfactant structure
Chinese Journal of Polymer Science **2** 135 (2001)

P Schobinger-Papamantellos, G Andre, J Rodriguez-Carvajal, O Moze, W Kockelmann, L D Tung, K H J Buschow
Magnetic ordering of $PrCoAl_4$. A neutron diffraction study
J Magn Magn Mater **231** 162 (2001)

P F Schofield, S J Covey-Crump, M R Daymond, K S Knight, I C Stretton
Accurate quantification of deformation induced strain partitioning within natural minerals from in situ neutron diffraction measurements
Eos, Trans Am Geophysical Union (in press 2001)

M Schreyer, M Jansen
Synthesis, structure and properties of Ag_2PdO_2
Solid State Sciences **30** 25 (2001)

A Schroder, G Aeppli, R Coldea, M A Adams, O Stockert, H von Lohneysen, E Bucher, R Ramazashvili, P Coleman
Onset of antiferromagnetism in heavy-fermion metals
Nature **407** 351 (2000)

N Scotti, W Kockelmann, J Senker, H Jacobs
Sn_3N_4-Syntheses und erste Kristallstrukturbestimmung einer binaren Zinn-Stickstoff-Verbindung
Z Kristallogr Suppl **16** 61 (1999)

R Senesi, C Andreani, D Colognesi, A Cunsolo, M Nardone
Deep Inelastic Neutron Scattering determination of the single particle kinetic energy in solid and liquid ^3He
Phys Rev Lett **86** 4584 (2001)

M Sferrazza, C Xiao, R A L Jones, J Penfold
Kinetics of formation of interfaces between immiscible polymers
Phil Mag **80** 561 (2000)

M Sferrazza, R A L Jones, D G Bucknall
The thermally driven collapse of a polymer brush in a polymer matrix
Phys Rev **E59** 4434 (1999)

S Shamoto, K Iizawa, T Koiwasaki, M Yasukawa, S Yamanaka, O Petrenko, S M Bennington et al
Pressure effect and neutron scattering study on A_xHfNCl (A; Alkali Metals and Organic Molecules)
Physica C **341-348** 747 (2000)

T Shiroka, C Bucci, R De Renzi, F Galli, G Guidi, G H Eaton, P J C King, C A Scott
Synchronous pulsed magnetic fields in muon spin rotation
Physica B **289-290** 684 (2000)

T Shiroka, C Bucci, R De Renzi, F Galli, G Guidi, G H Eaton, P J C King, C A Scott
Muon spin rotation with pulsed sources: Fundamental and application-oriented aspects of synchronous pulsed magnetic fields
Appl Mag Res **19** 431 2000

T Shiroka, C Bucci, R De Renzi, F Galli, G Guidi, G H Eaton, P J C King, C A Scott et al
Production of pulsed ultraslow muons and first mSR experiments on thin metallic and magnetic films
Appl Mag Res **19** 471 2000

R N Sinclair, C E Stone, A C Wright et al
Inelastic neutron scattering studies of superstructural units in borate glasses and crystalline phases
Phys Chem Glasses **41** 286 (2000)

P Sittner, P Lukas, D Neov, M R Daymond, V Novak, G M Swallowe
Stress induced martensitic transformation in CuAlZnMn polycrystals investigated by two in situ neutron diffraction techniques
Mat Sci Eng A (in press 2001)

E Sivaniah, M Sferrazza, R A L Jones, D G Bucknall
Chain confinement effects on interdiffusion in polymer multilayers
Phys Rev **E59** 885 (1999)

J M S Skakle, A M Coats, J Marr
The crystal structures of $Ba_2R_{2/3}V_2O_8$ (R=La, Nd) and $Sr_2La_{2/3}V_2O_8$; Palmierite derivatives
J Mater Sci **35** 3251 (2000)

P R Slater, J T S Irvine
Synthesis and structure of new perovskite phase in the La-Ti-Al-O system
J Solid State Chem **146** 437 (1999)

M V Smalley, H L M Hatharasinghe, I Osborne, J Swenson, S M King
Bridging flocculation in vermiculite-PEO mixtures
Langmuir **17** 3800 (2001)

L Smrcok, B Koppelhuber-Bitschnau, K Shankland, W I F David, D Tunega, R Resel
Decafluoroquarterphenyl - crystal and molecular structure solved from X-ray powder data
Zeitschrift Fur Kristallographie **216** 63 (2001)

I Sosnowska, R Przenioslo, W Schäfer, W Kockelmann, R Hempelmann, K Wysocki
Possible deuterium positions in the high temperature deuterated proton conductor $Ba_3Ca_{1+y}Nb_{2-y}O_{9-d}$ studied by neutron and X-ray powder diffraction
J Alloys Compounds (in press 2001)

I Sosnowska, W Schaefer, W Kockelmann, I O Troyanchuk
Neutron diffraction studies of the crystal and magnetic structures of $BiMn_xFe_{1-x}O_3$ solid solutions
Materials Science Forum (in press 2001)

T Steiner, I Majerz, C C Wilson
First geometrically symmetric O-H-N hydrogen bond obtained by thermally induced proton migration
Ang Chemie Int Ed Engl (in press 2001)

T Steiner, C C Wilson, I Majerz
Thermisch induzierte Wanderung des Protons in einer sehr starken N-H-O Wasserstoffebrucke beobachtet mit temperaturvariabler Neutronendiffraktion
Schriften des Forschungszentrums Julich, Matter and Materials **8** 23 (2001)

A Steuwer, G Bruno, P J Withers, L Edwards, M R Daymond, M W Johnson
Neutron transmission spectroscopy
Physica B (in press 2001)

A Steuwer, P J Withers, J R Santisteban, L Edwards, G Bruno, M E Fitzpatrick, M R Daymond, M W Johnson, D Q Wang
Bragg edge determination for accurate lattice parameter and elastic strain measurement
Physica A **185** 221 (2001)

A Steuwer, P J Withers, R Burguete
The d_0 distribution in Al-2024 friction stir welds
MECA SENS - Stress Evaluation by Neutron & Synchrotron Radiation (in press 2001)

J R Stewart, R Cywinski
Real-time kinetic neutron powder diffraction study of the α-Mn to β-Mn phase transition
J Phys:Condens Matter **11** 7095 (1999)

O Stockert, S M Hayden, T G Perring, G Aeppli
Magnetic fluctuations in paramagnetic chromium
Physica B **281** 701 (2000)

C E Stone, A C Wright, R N Sinclair, S A Feller et al
Structure of bismuth borate glasses
Phys Chem Glasses **41** 409 (2000)

V G Storchak, D G Eshchenko, J H Brewer, S P Cottrell, S F J Cox, E Karlsson, R W Wappling
Electron transport in cryocrystals
J Low Temp Phys (in press 2001)

V G Storchak, D G Eshchenko, J H Brewer, G D Morris, S P Cottrell, S F J Cox
Electron localization in a disordered insulating host
Phys Rev Lett **85** 166 (2001)

D A Styrkas, V Butun, J R Lu, J L Keddie, S P Armes
pH-controlled adsorption of polyelectrolyte diblock copolymers at the solid/liquid interface
Langmuir **16** 5980 (2000)

D A Styrkas, J L Keddie, J R Lu, T J Su, P A Zhdan
Structure of self-assembled layers on silicon: Combined use of spectroscopic variable angle ellipsometry, neutron reflection and atomic force microscopy
J Appl Phys **85** 1 (1999)

T J Su, J R Lu, Z F Cui, R K Thomas
Fouling of ceramic membranes by albumins under dynamic filtration conditions
J Membrane Sci **173** 167(2000)

T J Su, R J Green, Y Wang, E F Murphy, J R Lu, R Ivkov, S K Satija
Adsorption of lysozyme onto the silicon oxide surface chemically grafted with a monolayer of pentadecyl-1-ol
Langmuir **16** 4999 (2000)

J-B Suck
Dependence of the dynamics of metallic glasses on quenched-in density fluctuations and on temperature
J Non-Cryst Solids (in press 2001)

J Swenson, R Bergman, S Longeville, W S Howells
Dynamics of 2D-water as studied by quasi-elastic neutron scattering and neutron resonance spin echo
Physica B **301** 28 (2001)

A Szczygielska, A Burian, J C Dore
Paracrystalline structure of activated carbons
J Phys: Condens Matter **13** 5545 (2001)

M G Taylor, K Simkiss, S F Parker
Vibrational spectroscopy of phosphate biominerals: an inelastic neutron scattering study
Chemistry and Biology of Mineralized Tissues, Eds M Goldberg, A Boskey, C Robinson (American Academy of Orthopaedic Surgeons) p 443 (2000)

M G Taylor, S F Parker, K Simkiss, P C H Mitchell
Bone mineral: evidence for hydroxyl groups by inelastic neutron scattering
Phys Chem Chem Phys (in press 2001)

M T F Telling, S I Campbell, J Tomkinson, D D Abbley, Z A Bowden, M A Adams, C J Carlile
Performance of the new PG analyser on the IRIS Spectrometer at ISIS - preliminary results
RAL-TR-2001-001 (2001)

R I Todd, B Derby
Neutron diffraction study of correlation between reinforcement size, residual stress and microcracking in Alumina/SiCp composites
Proc 6th Int Conf on Residual Stresses (IOM, London) p57 (2000)

C N Tome, M R Daymond, M A M Bourke
Interpretation of experiments and modeling of internal strains in beryllium using a polycrystal model
Proc Int Conf on Residual Stress VI **2** 1349 (2000)

N Torikai, M Seki, Y Matsushita, M Takeda, K Soyama, N Metoki, S Langridge, D G Bucknall, J Penfold
Comparison between interfacial structures of a block copolymer and two-component homopolymers by neutron reflectivity measurement
J Phys Soc Japan **70** Suppl (in press 2001)

R Triolo, V Arrighi, P Migliardo, S Magazu, J B McClain, D Betts, J M DeSimone, H D Middendorf, A Triolo
QENS from polymeric micelles in supercritical CO_2
Nuclear and Condensed Matter Physics, Ed A Messina, p234 (2000)

F Triolo, A Triolo, J S Lin, G Lucido, F Lo Celso, R Triolo
Fractal approach in petrology: Combining ultra small angle (USANS) and small angle neutron scattering (SANS)
Nuclear and Condensed Matter Physics, Ed A Messina, p138 (2000)

F Triolo, A Triolo, D I Donato, J S Johnson Jr, F Lo Celso, R Triolo
Modelling small angle neutron scattering data from polymers in supercritical fluids
Nuclear and Condensed Matter Physics, Ed A Messina, p222 (2000)

M G Tucker, M P Squires, M T Dove, D A Keen
Dynamic structural disorder in cristobalite: neutron total scattering measurements and reverse Monte Carlo modelling
J Phys:Condens Matter **13** 403 (2001)

M G Tucker, M T Dove, D A Keen
Simultaneous analysis of changes in long-range and short-range structural order at the displacive phase transition in quartz
J Phys:Condens Matter **12** L723 (2000)

G V Vajenine, G Auffermann, Yu Prots, W Schnelle, R Kremer, A Simon, R Kniep
Preparation, crystal structure and properties of barium pernitride
Inorg Chem (in press 2001)

R W E van de Kruijs, H Fredrikze, M Th Rekveldt, A A van Well, Yu V Nikitenko, V G Syromyatnikov
Polarization analysis of neutron reflectometry on non-collinear magnetic media: polarized neutron reflectometry experiments on a thin cobalt film
Physica B **283** 189 (2000)

R W E van de Kruijs, V A Ul'yanov, M Th Rekveldt, H Fredrikze, N K Pleshanov, V M Pusenkov, V G Syromyatnikov, A F Schebetov, S Langridge
Probing magnetic structures by neutron reflectometry: Off-specular scattering from interfaces and domains in FeCoV/TiZr multilayers
Physica B **297** 180 (2001)

A A van Well, R Brinkhof
Protein adsorption at a static and expanding air-water interface: a neutron reflection study
Colloids and Surfaces A **175** 17 (2000)

P Vaquiero, A V Powell, S Hull, D A Keen
Pressure-induced phase transitions in chromium thiospinels
Phys Rev **B63** 064106 (2001)

V Villari, C Branca, A Faraone, S Magazu, G Maisano, F Migliardo, P Migliardo, M T F Telling
Diffusive dynamics in disaccharide aqueous solutions by QENS
J Phys Chem (in press 2001)

D Visser, A R Monteith, H R Ronnow, W J A Maaskant
Acoustic phonons in the hexagonal perovskite $CsNiCl_3$ around the gamma-point
Physica B **276-278** 302 (2000)

D Visser, R G Delaplane, W J A Maaskant
Structural study of the high-temperature phases of the hexagonal perovskite $KNiCl_3$
Physica B **276-278** 300 (2000)

L Vocadlo, K S Knight, G D Price, I G Wood
Thermal expansion and crystal structure of FeSi between 4K and 1173K determined by time-of-flight neutron powder diffraction
Phys Chem Minerals (in press 2001)

M Wagemaker, F J G Boerboom, H J Bos, A A van Well
Overflowing cylinder for neutron reflection research at expanding surfaces
Physica B **283** 278 (2000)

R I Walton, D O'Hare
Watching solids crystallise using in situ powder diffraction
Chem Comm 2283 (2000)

C Washington, M J Lawrence, D Barlow
Neutron scattering in pharmaceutical sciences: Applications of neutron scattering to soft condensed matter
Applications of neutrons to soft condensed matter, Ed B J Gabrys (Gordon & Breach) p361 (2000) ISBN 90-5699-300-3

J C Wasse, P S Salmon, R G Delaplane
Structure of molten trivalent metal bromides studied by using neutron diffraction: the systems $DyBr_3$, YBr_3, $HoBr_3$ and $ErBr_3$
J Phys:Condens Matter **12** 9539 (2000)

J C Wasse, I Petri, P S Salmon
Structure of glassy AsTe: the effect of adding a small quantity of Au or Ag
J Phys:Condens Matter **13** 6165 (2001)

I Watanabe, N Wada, K Awaga, S Ohira, K Nahamine
μSR study on dynamics of dimer spin in the 2D organic antiferromagnet, m-MPYNN·BF4, with S=1
Physica B **284** 1501 (2000)

I Watanabe, M Akoshima, Y Koike, S Ohira, W Higemoto, K Nagamine
μSR study on the '1/8 effect' in Zn-substituted Bi-2212 system
Physica B **284** 1071 (2000)

I D Watts, S G Carling, P Day, D Visser
Muon spin relaxation studies of magnetic ordering in the molecular-based ferrimagnets $PPh_4Mn^{II}Fe^{III}(C_2O_4)_3$ and $(n\text{-}C_4H_9)MnFe^{II}Fe^{III}(C_2O_4)_3$
J Phys:Condens Matter **13** 2225 (2001)

M T Weller, P F Henry, C C Wilson
An analysis of the thermal motion in the negative thermal expansion material $Sc_2(WO_4)_3$ using isotopes in neutron diffraction
J Phys Chem B **104** 12224 (2000)

M T Weller, A L Hector
The structure of the $Fe^{(IV)}O_4^{4-}$ ion
Angew Chem Int Ed **112** 4330 (2000)

P F Willemse, F M Mulder, W Wei, M Th Rekveldt, K S Knight
Residual stress measurements in an SiC continuous fibre reinforced Ti matrix composite
Scripta Mater **42** 775 (2000)

C C Wilson, K Shankland, N Shankland
Single-crystal neutron diffraction of urea-phosphoric acid: evidence for H-atom migration in a short hydrogen bond between 150K and 350K
Z Krist (in press 2001)

C C Wilson
Migration of the proton in the strong hydrogen bond in urea-phosphoric acid
Acta Cryst B (in press 2001)

P J Withers, M W Johnson, J S Wright
Neutron strain scanning using a radially collimated diffracted beam
Physica B **292** 273 (2000)

P J Withers, H K D H Bhadeshia
Residual stress. I - Measurement techniques
Mat Sci & Tech **17** 355 (2001)

P J Withers, M R Daymond, M W Johnson
The accuracy of diffraction peak location
J App Cryst (in press 2001)

P J Withers
Monitoring strain and damage by neutron and synchrotron beams
Mat Sci & Tech (in press 2001)

P J Withers, T M Holden
Diagnosing engineering problems with neutrons
MRS Bull **24** 17 (1999)

R L Witners, Y Tabira, J S O Evans, I J King
A new three-dimensionally modulated cubic phase in ZrP_2O_7 and its symmetry characterisation via temperature dependent electron diffraction
J Solid State Chem (in press 2001)

R A Wood, M H Lewis, G West, S M Bennington, M G Cain, N Kitamura
Transmission electron microscopy, electron diffraction and hardness studies of high-pressure and high-temperature treated C_{60}
J Phys:Condens Matter **12** 10411 (2000)

J P Wright, J P Attfield, W I F David, J B Forsyth
High-resolution powder neutron diffraction study of helimagnetic order in $CrP_{1-x}V_xO_4$ solid solutions
Phys Rev **B62** 992 (2000)

J P Wright, A C McLaughlin, J P Attfield
Partial frustration of magnetic order in synthetic angelellite, $Fe_4As_2O_{11}$
J Chem Soc, Dalton Trans 3663 (2000)

G Xu, C Broholm, D H Reich, M A Adams
Triplet waves in a quantum spin liquid
Phys Rev Lett **84** 4465 (2000)

G Xu, G Aeppli, P Bischer, C Broholm, J F DiTusa, C D Frost, T Ito, K Oka, H Takagi, M Treacy
Holes in a quantum spin liquid
Science **289** 419 (2000)

Y Yamamoto, Y Miyako, T Takeuchi, M Ocio, P Pari, H Jacques, I Watanabe, K Nagamine
μSR study on SDW transition in $Ce(Ru_{0.95}Rh_{0.05})_2Si_2$
Physica B **281-282** 351 (2000)

M Zoppi, M Celli, D Colognesi
Stato del progetto TOSCA: primi risultati sperimentali
Notiziario Neutroni e Luce di Sincrotrone 4 (1) (1999)

M Zoppi, D Colognesi, M Celli
Microscopic dynamics in liquid hydrogen
Europhys Lett **53** 34 (2001)

ISIS 2000 Update

St Adams, J Swenson
Investigations of migration pathways in Ag-based superionic glasses and crystals by the bond valence method
Phys Rev **B63** 054201 (2001)

D T Adroja, B D Rainford, K S Knight, P C Riedi
Neutron scattering studies of an antiferromagnetic Kondo lattice: $Ce_8Pd_{24}Ga$
J Phys:Condens Matter **13** 459 (2001)

P Ahlstrom, O Borodin, G Wahnstrom, E J W Wensink, P Carlsson, G D Smith
Molecular dynamics simulation of structural and conformational properties of poly(propylene oxide)
J Chem Phys **112** 10669 (2000)

D J Barlow, M J Lawrence, S Zuberi, T Zuberi, R K Heenan
Small angle neutron studies on the nature of the incorporation of polar oils in aggregates of N,N-dimethyl-dodecylamine-N-oxide
Langmuir **16** 10398 (2000)

D Barlow, A M Muslim, J R P Webster, J Penfold, C M Hollinshead, M J Lawrence
Molecular modelling of surfactant monolayers under constraints derived from neutron reflectance measurements
Phys Chem Chem Phys **2** 5208 (2000)

S J Blundell, A Husmann, T Jestadt, F L Pratt, I M Marshall, B W Lovett, M Kurmoo, T Sugano, W Hayes
Muon studies of molecular magnetism
Physica B **289-290** 115 (2000)

A N Burgess, K A Johnson, K A Mort, W S Howells
The liquid structure of halocarbons
Applications of neutrons to soft condensed matter, Ed B J Gabrys (Gordon & Breach) p61 (2000) ISBN 90-5699-300-3

F J Burghart, W Potzel, G M Kalvius, E Schreier, G Frosse, D R Noakes, W Schafer, W Kockelmann, S J Campbell et al
Magnetism of crystalline and nanostructured $ZnFe_2O_4$
Physica B **289-290** 286 (2000)

J M Cole, C C Wilson, J A K Howard, F R Cruikshank
Quantitative analysis of hydrogen-bonding and anomalous atomic thermal motion in the organic non-linear optical material DCNP using X-ray and neutron diffraction
Acta Cryst B **56** 1085 (2000)

S Collins, A M Kenwright, C Pawson, S K Peace, R W Richards
Transesterification in mixtures of polyethylene terephtalate and polyethylene naphthalene-2,6-dicarboxylate: an NMR study of kinetics and end group effects
Macromolecules **33** 2974 (2000)

S F J Cox, S P Cottrell, M Charlton, P Donnelly, S J Blundell, J L Smith, J C Cooley, W L Hults
Muon Korringa relaxation
Physica B **289-290** 594 (2000)

U Dahlborg, W S Howells, M Calvo-Dahlborg, J M Dubois
Diffusive motions in a crystalline $Al_{50}Cu_{35}Ni_{15}$ alloy
Mat Sci Eng A **294-296** 670 (2000)

P Dalmas de Reotier, A Yaouanc, R H Heffner, J L Smith, P C M Gubbens, C T Kaiser
Muon spin relaxation and rotation measurements on single crystals of the heavy fermion superconductor UBe_{13}
Phys Rev **B61** 6377 (2000)

P Dalmas de Reotier, A Yaouanc, P C M Gubbens, C T Kaiser, A M Mulders et al
Magnetism and superconductivity of UPt_3 by muon spin techniques
Physica B **289-290** 10 (2000)

M R Daymond, C N Tome, M A M Bourke
Intergranular strains in textured steel
Mat Sci Forum **347-349** 54 (2000)

J Eastoe, S Nave, J Penfold
What is so special about Aerosol-OT? Part 1: aqueous systems
Langmuir **16** 8733 (2000)

L Edwards, J R Santisteban, M E Fitzpatrick, A Steuwer, P J Withers, M R Daymond, M W Johnson
Neutron transmission spectroscopy: a solution to the d_0 problem?
Proc 6th Int Conf on Residual Stress (Institute of Materials, Oxford) p1239 (2000)

C Frontera, J L Garcia-Munoz, A Llobet, M Respaud, J M Broto, J S Lord, A Planes
Spin dynamics, phase coexistence, magnetic inhomogeneity and disorder in the charge ordered state of $Pr_{2/3}Ca_{1/3}MnO_3$
Phys Rev **B62** 3381 (2000)

H R Glyde, R T Azuah, W G Stirling
Condensate, momentum distribution and final-state effects in liquid ^4He
Phys Rev **B62** 14337 (2000)

S R Green, T J Su, J R Lu, J Penfold
The monolayer structure of the branched nonyl phenol oxyethylene glycols at the air-water interface
J Phys Chem B **104** 1507 (2000)

R J Green, T J Su, J R Lu, J R P Webster, J Penfold
Competitive adsorption of lysozine and $C_{12}E_5$ at the air/liquid interface
Phys Chem Chem Phys **2** 5222 (2000)

B A Grguric, R J Harrison, A Putnis
A revised phase diagram for the bornite-digenite join from in situ neutron diffraction and DSC experiments
Min Mag **64** 299 (2000)

U Hoppe, R Kranold, H-J Weber, J Neuefeind, A C Hannon
The structure of potassium germanate glasses - a combined X-ray and neutron diffraction study
J Non-Cryst Solids **278** 99 (2000)

U Hoppe, R Kranold, D Stachel, A Barz, A C Hannon
Variation in P-O bonding in phosphate glasses - a neutron diffraction study
Z Naturforsch **55a** 369 (2000)

G M Johnson, P J Mead, M T Weller
Synthesis of a range of gallium and germanium containing sodalites
Microporous and Mesoporous Materials **38** 445 (2000)

H Kagi, J B Parise, H Cho, G R Rossman, J S Loveday
Hydrogen bonding interactions in Phase A ($Mg_7Si_2O_8(OH)_6$) at ambient and high pressure
Phys Chem Minerals **27** 225 (2000)

M S Kalhoro, B J Gabrys, W Zajac, S M King, D G Peiffer
Small angle neutron scattering study of SPBT/PC blend
Polymer **42** 1679 (2001)

G M Kalvius, D R Noakes, G Grosse, W Schafer, W Kockelmann, S Fredo, I Halevy, J Gal
Magnets frustrated by competing exchange ($TbFe_6Al_6$ and $ErFe_6Al_6$)
Physica B **289-290** 225 (2000)

P J C King
Imaging and analysis of crystal defects using transmission channelling
MRS Bulletin **25** 21 (2000)

S M King, P C Griffiths, T Cosgrove
Using SANS to study adsorbed layers in colloidal dispersions
Applications of neutrons to soft condensed matter, Ed B J Gabrys (Gordon & Breach) (2000) ISBN 90-5699-300-3

W Kockelmann, E Pantos, A Kirfel
Neutron and synchrotron radiation studies of archaeological objects
Radiation in Art and Archaeometry, Eds D C Creagh, D A Bradley (Elsevier Science) p347 (2000) ISBN:0-444-50487-7

W Kockelmann, A Kirfel, E Hahnel
Non-destructive phase analysis of archaeologiocal ceramics using TOF neutron diffraction
J Archaeological Science **28** 213 (2001)

A I Kolesnikov, O I Barkalov, M Calvo-Dahlborg, U Dahlborg, W S Howells, E G Ponyatovsky
Neutron diffraction and reverse Monte Carlo study of bulk amorphous $Ga_{38}Sb_{38}Ge_{24}$ alloy
Phys Rev **B62** 9372 (2000)

A M Korsunsky, M R Daymond, K E Wells
The development of strain anisotropy during plastic deformation of an aluminium polycrystal
Mat Sci Forum **347-349** 492 (2000)

A M Korsunsky, K E Wells, B A Shaw
A comparative study of diffraction methods for strain measurement in a particulate MMC
Mat Sci Forum **347-349** 504 (2000)

A Llobet, J L Garcia-Munoz, C Frontera, M Respaud, L Pinsard, A Revcolevschi, C A Scott
Magnetism and orbital-ordering in $La_{7/8}Sr_{1/8}MnO_3$
Physica B **289-290** 77 (2000)

J S Loveday, R J Nelmes
Ammonia monohydrate VI - a hydrogen-bonded molecular alloy
Phys Rev Lett **83** 4329 (1999)

B W Lovett, S J Blundell, F L Pratt, T Jestadt, W Hayes, S Tagaki, M Kurmoo
Very low temperature muon relaxation in an organic spin-Peierls compound
Physica B **289-290** 145 (2000)

B W Lovett, S J Blundell, F L Pratt, T Jestadt, W Hayes, S Tagaki, M Kurmoo
Spin fluctuations in the spin-Peierls compound $MEM(TCNQ)_2$ studied using μSR
Phys Rev **B61** 12241 (2000)

G Ma, D J Barlow, M J Lawrence, R K Heenan, P A Timmins
Small angle neutron scattering studies of non-ionic surfactant vesicles
J Phys Chem B **104** 9081 (2000)

D F McCormack, W B Rowe, X Chen, A Bouzina, M E Fitzpatrick, L Edwards
Characterizing the onset of tensile residual stresses in ground components
Proc 6th Int Conf on Residual Stresses (Institute of Materials, Oxford) p225 (2000)

P C H Mitchell, D A Green, E Payen, S F J Cox, C A Scott
Modelling hydrogen transport in molybdenum disulfide catalysts with muon spin relaxation spectroscopy
Mag Res in Chemistry **38** 543 (2000)

B Paci, M S Deleuze, R Caciuffo, A Arduini, F Zerbetto
Molecular motion in C_{60}@Calix(8)arene
Mol Phys **98** 567 (2000)

J Penfold, E Staples, I Tucker, L Soubiran, A Creeth, J Hubbard
The adsorption of di-chain cationic and non-ionic surfactants at the air-water interface
Phys Chem Chem Phys **2** 5230 (2000)

J Penfold, E Staples, I Tucker, R K Thomas
The adsorption of mixed cationic and non-ionic surfactants at the hydrophilic silicon surface from aqueous solution: the effect of solution composition and concentrations
Langmuir **16** 8879 (2000)

F L Pratt, S J Blundell, A Husmann, I M Marshall, B W Lovett, W Hayes, S L Lee et al
BEDT-TTF superconductors studied by μSR
Physica B **289-290** 396 (2000)

F L Pratt, S J Blundell, T Jestadt, B W Lovett, A Husmann, I M Marshall, W Hayes, A Monkman et al
μSR of conducting and non-conducting polymers
Physica B **289-290** 625 (2000)

P Rangaswamy, M B Prime, M R Daymond, M A M Bourke, B Clausen, H Choo, N Jayaraman
Comparison of residual strains measured by X-ray and neutron diffraction in a titanium matrix composite
Mat Sci Eng A **31** 889 (2000)

S A T Redfern, R J Harrison
Order-disorder phase transitions in silicates and oxides: recent observations of strain coupling
Ferroelectrics **236** 293 (2000)

J J Reece, S A T Redfern, M D Welch, C M B Henderson
Mn-Mg disordering in cummingtonite: a high-temperature neutron powder diffraction study
Min Mag **64** 255 (2000)

R Rinaldi, G Artioli, C C Wilson, G McIntyre
Octahedral cation ordering in olivine at high temperature. I: in situ neutron single crystal diffraction studies on natural mantle olivines (Fa12 and Fa10)
Phys Chem Minerals **27** 623 (2000)

P F Schofield, C C Wilson, K S Knight, I C Stretton
Temperature related structural variation of the hydrous components in gypsum
Z Krist **215** 707 (2000)

N Shankland, A J Florence, C C Wilson, K Shankland
Molecular structures determined by neutron diffraction
Applications of Neutrons to Soft Condensed Matter, Ed B J Gabrys (Gordon & Breach) Ch 2 p27 (2001)

T Shiroka, C Bucci, R De Renzi, F Galli, G Guidi, G H Eaton, P J C King, C A Scott
Muon spin rotation with pulsed sources: Fundamental and application-oriented aspects of synchronous pulsed magnetic fields
Appl Mag Res **19** 431 2000

T Shiroka, C Bucci, R De Renzi, F Galli, G Guidi, G H Eaton, P J C King, C A Scott, K Trager, A Breitruck, M D Trigo, A Grossmann, K Jungmann, J Merkel, P Neumayer, I Reinhard, R Santra, L Willmann, V Meyer, E Roduner, R Scheuermann, M C Charlton, P Donnelly
Production of pulsed ultraslow muons and first μSR experiments on thin metallic and magnetic films
Appl Mag Res **19** 471 2000

E Staples, I Tucker, J Penfold, N Warren, R K Thomas
The structure and composition of polymer-surfactant mixtures of SDS/$C_{12}E_6$ and poly-dmdaac at the air-water interface
J Phys:Condens Matter **12** 6023 (2000)

T Steiner, C C Wilson, I Majerz
Neutron diffraction study of a very short O-H...N hydrogen bond: crystalline adduct of 2-methylpyridine and pentachlorophenol
Chem Comm 1231 (2000)

J Strutwolf, A L Barker, M Gonsalves, D J Caruana, P R Unwin, D E Williams, J R P Webster
Probing liquid/liquid interfaces using neutron reflection measurements and scanning electrochemical microscopy
J Electroanal Chem **483** 163 (2000)

J Swenson, P Carlsson, L Borjesson, L M Torell, R L McGreevy, W S Howells
The application of reverse Monte Carlo modelling to a polymeric melt
Computational and Theoretical Polymer Science **10** 465 (2000)

J Swenson, A Matic, C Karlsson, L Borjesson, C Meneghini, W S Howells
Random distribution model: a structural approach to the mixed alkali effect in glasses
Phys Rev **B63** 132202 (2001)

J Swenson, R Bergman, W S Howells
Quasi-elastic neutron scattering of 2D-water in a vermiculite clay
J Chem Phys **113** 2873 (2000)

J Swenson, A Matic, L Borjesson, W S Howells
Experimental insight into the mixed mobile ion effect in glasses
Solid State Ionics **136-137** 1055 (2000)

M T F Telling, J A Dann, R Cywinski, J Bogner, M Reissner, W Steiner
Spin dynamics in the concentrated spin glass system $Y(Al_{1-x}Fe_x)_2$
Physica B **289-290** 213 (2000)

N Torikai, Y Matsushita, S Langridge, D G Bucknall, J Penfold, M Takeda
Interfacial structures of block and graft copolymers with lamellar microphase-separated structures
Physica B **283** 12 (2000)

C H Uffindell, A I Kolesnikov, J-C Li, J Mayers
Inelastic neutron scattering study of water in the sub- and super-critical region
Phys Rev **B62** 5492 (2000)

R R Urbano, C Rettori, S B Oseroff, G B Martins, Z Fisk, P G Pagliuso, J L Sarrao, R Caciuffo, R M Ibberson
Structural effects in the EPR spectra of Ni^{3+} in $La_2Ni_{0.5}Li_{0.5}O_4$
Phys Rev B (in press 2000)

M T Weller, A M Healey, G M Johnson
The synthesis and characterisation of JBW-type zeolites: Part A: sodium/potassium aluminosilicate $Na_2K[Al_3Si_3O_{12}]$-0.5H_20
Microporous and Mesoporous Materials **37** 153 (2000)

M T Weller, S J Skinner
Neutron and X-ray powder diffraction studies of the oxynitrides, $SrW(O,N)_3$, $Ba_3W_2(O,N)_8$ and $Ba_3Mo_2(O,N)_8$
Int J Inorg Materials **2** 463 (2000)

M T Weller, S E Dann, G M Johnson, P J Mead
Multinuclear MAS NMR studies of sodalitic framework materials
J Phys Chem B **104** 1454 (2000)

C C Wilson
Hydrogen atoms in acetylsalicylic acid (aspirin): the librating methyl group and probing the potential well in the hydrogen bonded dimer
Chem Phys Lett **335** 57 (2001)

C C Wilson
Temperature-dependent study of the crystal structure of paracetamol by single crystal neutron diffraction
Z Krist **215** 693 (2000)

C C Wilson, H Nowell
Methyl group librations in sterically hindered dimethylnaphthalene molecules: neutron diffraction studies of 1,8-dimethylnaphthalene between 50 and 200K
New J Chem **24** 1063 (2000)

C C Wilson
Refinement of two different crystal structures simultaneously from a multiple-crystal sample: neutron study of 3-deazauracil and lead hydrogen arsenate at 100K
J Mol Struct **560** 239 (2001)

T Yamaguchi
New horizons in hydrogen bonded clusters in solution
Pure Appl Chem **71** 174 (1999)

A Yaouanc, P Dalmas de Reotier, P C M Gubbens, A M Mulders, Y Isikawa
Zero and longitudinal field muon spin depolarization measurements of CeNiSn
Physica B **289-290** 28 (2000)

➢ *Bella Lake (Oak Ridge National Laboratory) taking time out from her PRISMA experiment. (01RC2665).*

◅ *Pavel Bakule (RIKEN-RAL muon facility) prepares a laser system for an experiment to produce 'slow' muons by muonium ionisastion (01RC2681).*

ISIS Seminars 2000 - 2001

Kristian Nielsen (Risø National Laboratory, Denmark)
Monte Carlo Simulations of Neutron Scattering Instruments Using McStas

John J Quinn (University of Tennessee, Knoxville, USA)
Pertinent Developments in Understanding Electrons in a Magnetic Field: Composite Fermions and their Remarkable Statistics

Marc Malfois (European Molecular Biology Laboratory, Hamburg)
The SasCIF Dictionary and Conversion Tools

Dmitri Svergun (European Molecular Biology Laboratory, Hamburg and Institute of Crystallography, Leninsky, Moscow, Russia)
Advanced Methods for Solution Scattering Data Analysis and Their Applications

Simon Billinge (Department of Physics and Astronomy, Michigan State University, USA)
Local Structure in Cuprates and Manganites by the PDF Method

Carlo Kaiser (Interfacultair Reactor Instituut, Delft University of Technology)
μSR on Monodisperse Nano-scale Pd Clusters

T Nakayama (Hokkaido University, Sapporo, Japan)
Glasses: Dynamics at THz Frequencies and Below

Mike Zhitomirsky (ETH, Zurich)
Excitonic Ferromagnetism: a New Paradigm for Itinerant Magnets

Andrew Millis (Rutgers University, USA)

Robert Papoular (Léon Brillouin Laboratory, CEN Saclay)
Neutron/ X-Ray Crystallographic Imaging of Disordered Molecular Solids using Maximum Entropy

Jorge Kohanoff (Atomistic Simulation Group, Queen's University Belfast)
The Status of the Low-Temperature Phase Diagram of Hydrogen at the Turn of the Century

Luigi Paolasini (European Synchrotron Radiation Facility, Grenoble, France)
Interplay Between Orbital and Magnetic Long Range Order by Resonant X-ray Scattering in Cr-doped V_2O_3

Donald Brown (Los Alamos National Laboratory)
A Neutron Diffraction and Self-Consistent Modelling Study of the Deformation of Beryllium

A Balagurov (JINR, Dubna, Russia)
Structural Studies of 'New Materials' at the IBR-2 pulsed Reactor

Ana Gaspar (University of Lisbon and The Technical University of Lisbon)
Investigations of the Structure and Dynamics of Aqueous ionic Solutions

V G Storchak (Russian Science Centre, Kurchatov Institute, Russia)
Electron Transport in Matter Studied via Muon Spin Relaxation Techniques

Denis Golosov (Department of Theoretical Physics, Oxford)
Spin Wave Theory of Double Exchange Magnets

John Tranquada (Brookhaven National Laboratory)
Stripe Phases in High Temperature Superconductors

Science Discussion Group Meetings

Informal meetings for the presentation and discussion of new ideas, latest results and recent developments

Bill David	*RAL Research Centres* 6 July 2000
John Webster	*The Liquid-Liquid Interface* 20 July 2000
Nikitas Gidopoulos	*Nuclear Potential Energy Surfaces in Molecules Beyond the Born-Oppenheimer Approximation* 3 August 2000
Anders Markvardsen	*Space Group Determination from Powder Diffraction Data* 7 September 2000
Steve Cox	*Anything Protons do, Muons do Better!* 21 September 2000
Stephen Lovesey	*Neutron Compton Scattering by Proton and Deuteron Systems with Entangled Spatial and Spin Degrees of Freedom* 15 February 2001
DT Adroja	*Neutron scattering study of Colossal Magnetoresistance Materials* 1 March 2001

How ISIS Works Lectures

A series of lectures describing how ISIS works, with an emphasis on the Accelerator and Target systems.

Tim Broome	*Target* 17 April 2000
Adrian Morris	*Synchrotron (electrical)* 26 May 2000
Uschi Steigenberger	*Neutron Experiments at ISIS* 15 June 2000
Bob Mannix	*ISIS Controls* 16 October 2000
Grahame Rees	*Accelerators Elsewhere* 8 November 2000
Peter Gear	*Operating ISIS* 23 November 2000
Chris Prior	*Beam dynamics* 15 December 2000
Philip King	*Muons* 8 March 2000